Oil & Natural Gas Technology

DOE Award No.: DE-FC26-01NT41248

Phase Behavior, Solid Organic Precipitation, and Mobility Characterization Studies in Support of Enhanced Heavy Oil Recovery on the Alaska North Slope

Submitted by:
Petroleum Development Laboratory
Institute of Northern Engineering
University of Alaska Fairbanks
P.O. Box 755880
Fairbanks, AK 99775-5880

Prepared for:
United States Department of Energy
National Energy Technology Laboratory

December 2008

Office of Fossil Energy

Phase Behavior, Solid Organic Precipitation, and Mobility Characterization Studies in Support of Enhanced Heavy Oil Recovery on the Alaska North Slope

Final Report

Submitted to

United States Department of Energy
National Energy Technology Laboratory
3610 Collins Ferry Road
P.O. Box 880
Morgantown, WV 26507-0880
Ph: 304-285-4764, Fax: 304-285-4403

Principal Authors

Shirish Patil
Abhijit Dandekar
Santanu Khataniar

Submitted by

Petroleum Development Laboratory
Institute of Northern Engineering
University of Alaska Fairbanks
P.O. Box 755880
Fairbanks, AK 99775-5880
Ph: 907-474-7734, Fax: 907-474-5912

University of Alaska Fairbanks
America's Arctic University

PDL

INE

INE

DISCLAIMER

ABSTRACT

The medium-heavy oil (viscous oil) resources in the Alaska North Slope are estimated at 20 to 25 billion barrels. These oils are viscous, flow sluggishly in the formations, and are difficult to recover. Recovery of this viscous oil requires carefully designed enhanced oil recovery processes. Success of these recovery processes is critically dependent on accurate knowledge of the phase behavior and fluid properties, especially viscosity, of these oils under variety of pressure and temperature conditions. This project focused on predicting phase behavior and viscosity of viscous oils using equations of state and semi-empirical correlations.

An experimental study was conducted to quantify the phase behavior and physical properties of viscous oils from the Alaska North Slope oil field. The oil samples were compositionally characterized by the simulated distillation technique. Constant composition expansion and differential liberation tests were conducted on viscous oil samples. Experiment results for phase behavior and reservoir fluid properties were used to tune the Peng-Robinson equation of state and predict the phase behavior accurately. A comprehensive literature search was carried out to compile available compositional viscosity models and their modifications, for application to heavy or viscous oils. With the help of meticulously amassed new medium-heavy oil viscosity data from experiments, a comparative study was conducted to evaluate the potential of various models. The widely used corresponding state viscosity model predictions deteriorate when applied to heavy oil systems. Hence, a semi-empirical approach (the Lindeloff model) was adopted for modeling the viscosity behavior. Based on the analysis, appropriate adjustments have been suggested: the major one is the division of the pressure-viscosity profile into three distinct regions. New modifications have improved the overall fit, including the saturated viscosities at low pressures. However, with the limited amount of geographically diverse data, it is not possible to develop a comprehensive predictive model. Based on the comprehensive phase behavior analysis of Alaska North Slope crude oil, a reservoir simulation study was carried out to evaluate the performance of a gas injection enhanced oil recovery technique for the West Sak reservoir. It was found that a definite increase in viscous oil production can be obtained by selecting the proper injectant gas and by optimizing reservoir operating parameters. A comparative analysis is provided, which helps in the decision-making process.

TABLE OF CONTENTS

LIST OF FIGURES

LIST OF TABLES

ACKNOWLEDGEMENT

The authors are highly thankful to the U.S. Department of Energy (USDoE) for their financial support to perform the presented work. Their support is highly appreciated.

EXECUTIVE SUMMARY

The medium-heavy oil (viscous oil) resources in the Alaska North Slope are estimated at 20 to 25 billion barrels. Most of the Alaska North Slope heavy oil resources lie in the West Sak, Milne Point, and Ugnu reservoirs, close to both the Prudhoe Bay oil field and the Trans Alaska Pipeline System, which serve as the necessary infrastructure for production facilities and transportation. At present, viscous oils from "West Sak-Schrader Bluff" formation are being developed. With conventional oil production on the Alaska North Slope projected to decline to 200,000 bbl/day to 400,000 bbl/day by 2015, there will be a critical need for pumping additional liquid to provide an adequate volume for economic operation of the Trans Alaska Pipeline System as well as for meeting growing demand. Production of heavy oil resources on the Alaska North Slope could supply the needed fluid volume if the oil could be produced economically and in sufficient quantity. These oils are viscous, flow sluggishly in the formations, and are difficult to recover. Recovery of this viscous oil requires carefully designed enhanced oil recovery processes. The principal technological issues and challenges in heavy oil recovery identified by Alaska North Slope operators are complex fluid phase behavior and lack of pressure-volume-temperature characterization data, phase behavior changes in the presence of a solvent, and unpredictable viscosity behavior and its influence on flow. Success of the enhanced oil recovery processes is critically dependent on accurate knowledge of phase behavior and fluid properties, especially viscosity, of these oils under variety of pressure and temperature conditions. This project focused on predicting phase behavior and viscosity of viscous oils using equations of state and semi-empirical correlations.

To address the issues related to Alaska North Slope heavy oil recovery, we conducted a comprehensive research program designed to develop a fundamental understanding of the fluid phase behavior, pressure-volume-temperature properties, and viscosity of Alaska North Slope heavy oils. The phase behavior and viscosity data can then be used as input for predicting Alaska North Slope heavy oil recovery through numerical reservoir simulation. Such a study is certainly needed for the successful future commercialization of heavy oil production technology in Alaska and other North American heavy oil resources.

The main objectives of this study were to quantify the phase behavior of the Alaska North Slope heavy oils experimentally, and through equation of state modeling in order to provide data for compositional reservoir simulation, evaluate the commonly used compositional viscosity models for predicting heavy oil viscosity and improve upon the performance of the selected model for better prediction of the viscosities of medium-heavy oils from the Alaska North Slope. Finally, the tuned equation of state model will be used to perform a compositional reservoir simulation to predict the performance of the West Sak reservoir for different gas injection schemes and a variety of injection gases.

The phase behavior and fluid properties of viscous oils from the Alaska North Slope were experimentally studied. Flashed heavy oil samples from the Alaska North Slope were recombined with methane at reservoir conditions to simulate live oils. Compositions of two representative heavy oil samples were determined using simulated distillation technique. Constant composition expansion, differential liberation, and viscosity measurement experiments were conducted on the oil samples for analyzing the phase behavior and fluid properties. Phase behavior was modeled by tuning the equation of state with measured data. The Peng-Robinson equation of state was successfully tuned and it provided satisfactory match of experimental data. Using a wide range of medium-

heavy oil viscosity data, a comparative study was conducted to evaluate the potential of various viscosity models. The widely used corresponding state viscosity model predictions deteriorate when applied to heavy oil systems. Hence, a semi-empirical approach (the Lindeloff model) was adopted for modeling the viscosity behavior of viscous oils. Based on the analysis, appropriate adjustments have been suggested: the major one being the division of the pressure-viscosity profile into three distinct regions. These new modifications to the Lindeloff model have improved the overall fit of experimental viscosity data, including the saturated viscosities at low pressures. However, with the limited amount of geographically diverse data, it is not possible to develop a universal predictive model. Based on this comprehensive phase behavior analysis of the Alaska North Slope crude oil, a compositional reservoir simulation study was carried out, with the tuned Peng-Robinson equation of state, to evaluate the implications of using gas injection as an enhance oil recovery technique for the West Sak reservoir. It was found that a definite increase in viscous oil production can be obtained with the proper selection of an injectant gas and optimized reservoir operating parameters. A comparative analysis of several enhanced oil recovery scenarios is provided.

Chapter 1 INTRODUCTION

United States' largest domestic deposits of heavy hydrocarbons are in Alaska, California, and Utah. Out of the total US heavy oil resources, about 20 to 25 billion barrels exist on the Alaska North Slope (ANS). The ANS heavy oils typically lie in what is called "A Class": medium-heavy oil (Figure 1.1). The A Class type oils are of moderate API gravity and relatively low downhole viscosity and hence are less problematic to produce than B or C Class oils. Most of the ANS heavy oil resources lie close to both the Prudhoe Bay oil fields and the Trans Alaska Pipeline System (TAPS), which serve as the necessary infrastructure for production facilities and easy transport. With conventional oil production on the ANS projected to decline to 200,000 to 400,000 bbl/day by 2015, there will be a critical need for pumping additional liquid to provide an adequate volume for economic operation of the TAPS. Production of heavy oil resources on the ANS could supply the needed fluid volume if the oil could be produced economically and in sufficient quantity. Blending heavy oil with light oil would provide sufficient viscosity reduction to support transportation through the TAPS. The ANS heavy oil resources are also low in sulfur, heavy metal content, and asphaltenes, thereby increasing suitability for refining. The heavy oil belt lies above existing ANS light oil fields where geologic description is well known saving associated exploration cost. Development of ANS heavy oil also offers other intangible benefits such as opportunities for carbon sequestration.

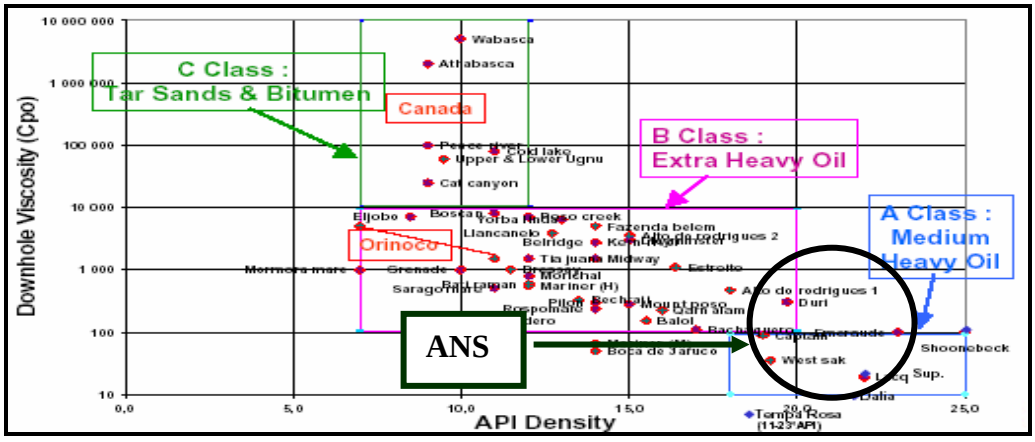

Figure 1.1 Classification of Heavy Oils (Francois, 2003)

1.1 Heavy Oil Potential of the Alaska North Slope

The Alaska North Slope contains vast resources of heavy oils primarily concentrated in the West Sak, Milne Point, and Ugnu reservoirs. There are currently five fields producing viscous oil in Alaska: Orion, Polaris, Schrader Bluff, Tabasco, and West Sak. The West Sak and Ugnu heavy oil deposits lie within the Kuparuk River Unit (KRU) while the Orion and Polaris heavy oil belts are classified under the Prudhoe Bay Unit. The Schrader Bluff viscous oil formation overlies the Kuparuk River formation and primarily comes under the Milne Point Unit. General delineation of these pools is shown in the Figure 1.2. At present, viscous oils from "West Sak-Schrader Bluff" formation are being developed.

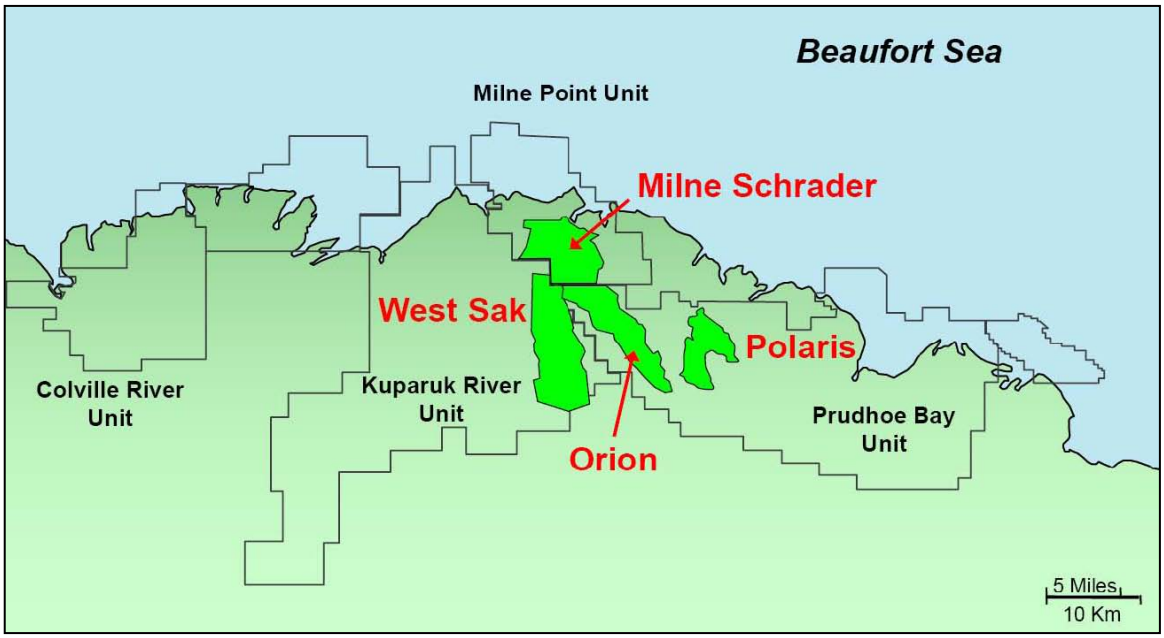

Figure 1.2 Alaska's Viscous Oil Reserves (Source: BP Exploration Alaska Inc. presentation to Alaska Department of Revenue, February 18, 2005)

The Ugnu formation overlies the West Sak formation under the Kuparuk River Unit. The estimated total oil in place within these reservoirs amounts to about 20-25 billion barrels, with about two-thirds of the heavy oil lying under the Kuparuk River Unit. (Targac et al., 2005). Figure 1.3 shows a cross-section of the various viscous oil formations in this heavy oil belt on the ANS.

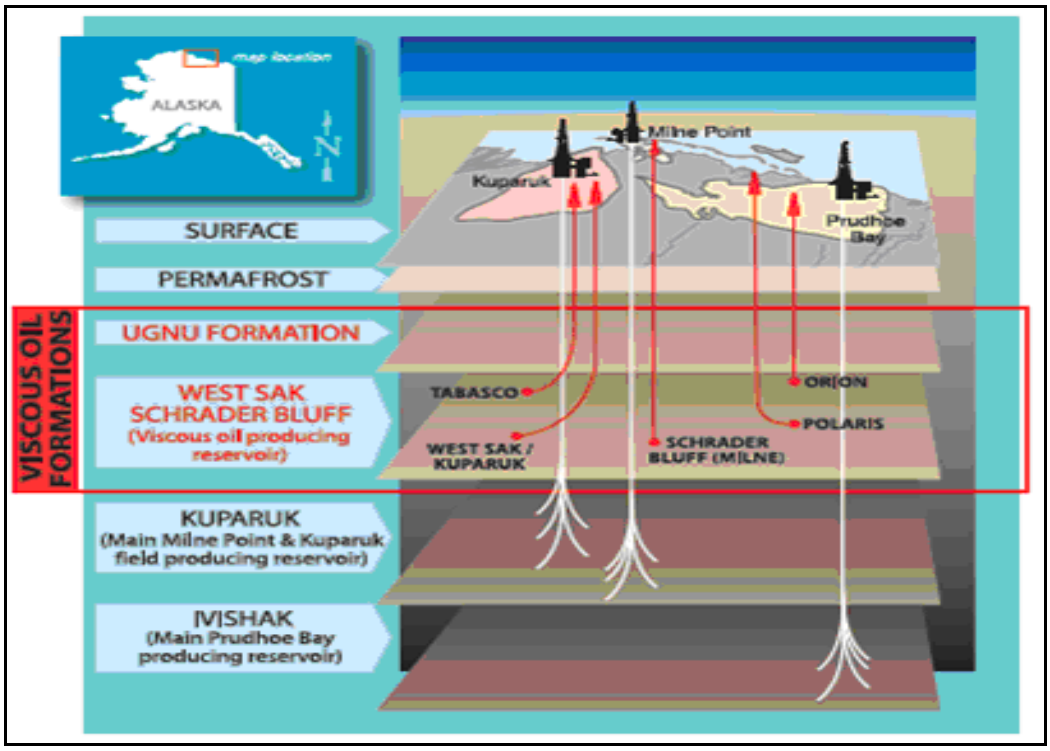

Figure 1.3 Cross Section of Alaska's Viscous Oil Deposits (Source: International Energy Agency, Resources to Reserves, November 2005, page 76)

Despite the large reserve of heavy oil on the ANS, production of heavy oil from the ANS has been very limited. Currently, only about 12,000 bbl/day of heavy oil is produced from the West Sak and Orion fields. Principal technological issues and challenges in heavy oil recovery identified by ANS operators are:

1. Complex fluid phase behavior and lack of pressure-volume-temperature (PVT) characterization data.
2. Phase behavior changes in the presence of a solvent.
3. Unpredictable viscosity behavior and its influence on flow.
4. Solids deposition in the pipeline and near-well bore regions.

These problems are all directly or indirectly related to a poor understanding of the PVT characteristics and fluid phase behavior of heavy oil systems containing co-solvents, gases, asphaltenes and waxes. Lack of good correlations for predicting heavy oil viscosity adds to the problem.

1.2 Heavy Oil Phase Behavior and Viscosity

Phase behavior investigations of hydrocarbons, hydrocarbon mixtures, and crude oils are indispensable in petroleum and allied industries. Primary production, enhance oil

recovery (EOR) processes, and treatment of petroleum crude oils require thorough knowledge of phase behavior. Fluid pressure-volume-temperature (PVT) properties play an important role throughout the life of a reservoir. Reliable predictions of fluid properties are essential for determination of in-place volumes and recovery factors through material balance equations. Reservoir fluid properties provide key input to simulators used to evaluate reservoir development strategy. Accurate PVT properties are required for interpretation of well test data and design of surface facilities and processing plants. Fluid characterization and distribution within the reservoir help in defining the continuity and communication within various zones (Nagarjan et. al., 2006). Both compositional and black oil simulators require input of fluid properties or models describing the fluid properties as function of pressure, temperature, and composition.

The phase behavior of heavy oil systems is complex and often exhibits unusual and completely unanticipated phenomena such as the appearance (or disappearance) of additional liquid and/or solid phases with changes in pressure or temperature (Abedi et al., 1998). Unless a comprehensive understanding of phase behavior and fluid properties of these heavy oils is obtained, effective development of these valuable resources will always be hindered. Addition of carbon dioxide, nitrogen, and light hydrocarbon gases to reservoir fluids as envisaged in a number of secondary recovery process schemes can induce complex and unusual phase and viscosity behavior over the ranges of pressure and temperature encountered (Nghiem et al., 2000).

Correct fluid property data is vital for reservoir modeling and facilities design. Similarly, it is also necessary to measure PVT phase-behavior as this data is typically useful for tuning compositional equations of state (EOS) for use in managing reservoir as well as offshore facilities design calculations. Viscosity is the primary fluid property targeted in most heavy oil recovery techniques. Additionally, viscosity is critical for calculating pressure loss and flow line sizing. Hence, viscosity data at a wide range of pressure and temperature conditions is needed for tuning viscosity correlations and testing viscosity models. Asphaltene precipitation from reservoir fluids during oil production can cause serious problems in the reservoir by permeability reduction and wettability alterations, the latter leading to either positive or negative effects on reservoir performance (Dandekar et al., 2000). However, if it takes place in the well bore or in the surface processing facilities, serious plugging problems and pressure losses will result (Ali, 1974). Asphaltene precipitation can occur during primary depletion of highly

undersaturated reservoirs or during miscible hydrocarbon gas or CO_2 injection. The injection of hydrocarbon gases or CO_2 for improved oil recovery (IOR) may promote asphaltene precipitation. However, this is primarily a function of pressure, temperature conditions, reservoir oil compositions, and more importantly the molecular weight or the 'richness' of the injection gas (Kokal and Sayegh S, 1995).

Fluid viscosity can be modeled in a number of ways. In the broader perspective, the models can be classified in the following ways: (1) theoretical models, (2) semi-theoretical models, and (3) empirical models (Mehrotra et al., 1996). Generally, the theoretical models are very accurate. However, at present, these are applicable only for simple fluid systems, viz. simple gas-mixtures. Additionally, these theoretical models are computationally exhaustive and require many intangible variables that are intractable. Since its inception, the oil industry has been largely dependent on empirical models. These models are generally simple to use and require easily available field-measured variables. At the same time, the results are within the acceptable margin of error.

Over the years these empirical models have served the oil industry very well, albeit limited to the light oil reservoirs. When these empirical models are extrapolated to the heavy oils, they are usually insufficient to predict viscosity behavior. Additionally, though the effect of temperature is very well captured by these models, the effect of a lesser-viscous solvent addition to reduce the viscosity, is difficult to estimate. In particular, the ANS heavy oil reservoirs have limitations for production strategies, due to the presence of permafrost. Here, the well-established thermal recovery methods cannot be applied. The main recovery methods could be Water-Alternating-Gas (WAG) or Vapor Extraction (VAPEX). For these methods to be applied, it is important to know the relationship between the amounts of solvent added versus a decrease in the viscosity. Considering the above scenario, semi-theoretical models could provide an ideal choice to model the viscosities. These methods consist primarily of compositional models.

Most of the compositional models are based on the principle of the corresponding states. The most famous compositional models are the Lohrenz-Bray-Clark (LBC) model (1964) and the Pedersen model (Pedersen et al., 1984; Pedersen and Fredenslund, 1987). These models are featured in most of the commercial reservoir modeling software available in the oil industry. They accurately predict the viscosities of the light oil systems; viscosities up to 10 cP. Because of their tremendous potential, numerous attempts have been made in the past few years to extend these models to heavy oils. A

comparative study to demonstrate the performance of various models for predicting medium-heavy oil viscosity is necessary and useful for evaluation of recovery potential of these oils. Because of its remarkable promise, the new generation Lindeloff model (Lindeloff et al., 2004) needs to be studied in detail.

1.3 Objectives of the Study

To address the issues related to ANS heavy oil recovery, we conducted a comprehensive research program designed to develop a fundamental understanding of the fluid phase behavior, PVT properties, and viscosity of ANS heavy oils in the presence of solvents and gases. The phase behavior and viscosity data can then be used as input for predicting ANS heavy oil recovery through numerical reservoir simulation. Such a study is certainly needed for the successful future commercialization of heavy oil production technology in Alaska and other North American heavy oil resources. The specific objectives of this project were:

- Quantify the phase behavior of the ANS heavy oils experimentally and, through EOS modeling, provide data for compositional reservoir simulation. The tuned EOS model forms the basis for reservoir scale simulations of EOR projects and various field development options. Tuned EOS are also required in compositional viscosity models.
- Measure live and dead crude oil viscosity under the variety of pressure and temperature conditions encountered in the reservoir for validation of compositional viscosity models for ANS heavy oils.
- Evaluate the commonly used compositional viscosity models and weigh their competence against each other based on the compiled medium-heavy oil viscosity data.
- Choose the best medium-heavy oil viscosity model for extended analysis. If possible, improve upon the performance of the selected model for better prediction of the viscosities of medium-heavy oils from ANS. The model will be validated by applying to the experimentally determined data sets representing the heavy oils from ANS, in addition to the data sets complied from other sources
- Develop a tuned EOS model for the West Sak oil using available experimental data from the previous steps.

- Use the tuned EOS model to carry out compositional reservoir simulation to predict performance of the West Sak reservoir for different gas injection schemes and a variety of injection gases.

Chapter 2 LITERATURE REVIEW

A review of literature pertinent to this study is presented in this chapter. This includes phase behavior experiments, phase behavior modeling, and oil viscosity prediction methods. Because phase behavior and viscosity prediction methods developed in this study were used to simulate viscous oil recovery from the West Sak reservoir, a background on the West Sak reservoir and enhanced oil recovery methods is also presented.

2.1 Phase Behavior Experiments

Reliable quantification of fluid phase behavior requires measurement of reservoir fluid properties at varying thermodynamic conditions of pressure and temperature. However, it is time consuming and expensive to measure the fluid phase properties at different conditions. Therefore, equations of state (EOS) are used to predict these properties. Predictions from EOS cannot be relied upon directly as they cannot accurately simulate the interactions between numerous hydrocarbon and non-hydrocarbon components present in petroleum crude oil. In order to have meaningful and accurate estimates of fluid properties and phase behavior, EOS require some amount of tuning to match with experimental data.

Phase behavior of any system is dictated by its pressure, temperature, and composition. Experimental phase behavior studies include measuring volumetric properties as a function of pressure and temperature. Constant composition expansion, differential liberation, and separator tests were conducted to analyze the volumetric properties of the heavy oils. Nagarajan et al. (2006) reviewed the entire process from fluid sampling to tuning EOS for all types of reservoir fluids. They also focused on the key laboratory fluid analyses for capturing the fluid phase behavior for different production strategies ranging from simple depletion to complex tertiary recovery.

Over the past few years studies have been conducted to understand the recovery mechanisms from heavy oil fields. Heavy oil reservoirs tend to be low pressure and low energy systems. Satik et al. (2004) carried out a study of Venezuelan heavy oil solution gas drive. This included PVT tests and depletion tests on live heavy oil samples. They concluded that for heavy oils non-equilibrium characteristics play a major role in interpreting depletion experiments and recommended non-conventional PVT tests like constant composition expansion without any external mixing and differential wait

interval between consecutive pressure steps. Several mechanisms have been suggested to explain the recovery in heavy oil fields. Sand co-production, foamy oil drive reservoir compaction, high critical gas saturation, and low gas mobility are some of the factors identified to be responsible for heavy oil recovery. High critical gas saturation (Whitson et al., 1983) and low gas mobility (Cenzig et al., 2004) are considered to be the primary mechanisms for high solution gas drive recovery.

Viscosity reduction is the primary task in improving heavy oil recovery. Thermal recovery processes are effective in reducing the oil viscosity by increasing the reservoir temperature. Though very effective, thermal recovery process is not suitable for many reservoirs, especially those with thin pay zones, environmental constraints, or depth issues. For moderately viscous oils (μ<1000 cP) non-thermal methods are more effective compared to thermal ones. Application of non-thermal processes requires reliable prediction of process performance which requires knowledge about mechanisms active in the process and contribution of each toward total oil recovery.

Non-thermal EOR of heavy oil involves solubilization of solvent into oil, mass transfer from vapor to liquid by diffusion, reduction of oil viscosity by solvent dilution, mixing of diluted and undiluted oil by mixing and diffusion, and upgrading of oil by asphaltene precipitation and deposition. This mechanistic study requires knowledge of solubility and viscosity behavior of the oil-solvent system. Ted et al. (2002) carried out PVT and viscosity measurements for Lloyminster-Aberfeldy heavy oils in the presence of solvents. A capillary viscometer was used online with a PVT cell to measure the oil viscosity for the solvent-oil mixtures. Methane, ethane, propane, and CO_2 were used as solvents and the phase behavior in the presence of each solvent was quantified. They also confirmed formation of asphaltene at high solvent loading for oil-propane system.

Roper (1989) conducted an experimental phase behavior study of a CO_2-West Sak heavy oil system. This study included conventional PVT tests like constant composition expansion and differential liberation tests and online viscosity measurement with capillary viscometer for West Sak heavy crude oil. The effect on swelling behavior and viscosity of West Sak oil was observed for different loadings of the solvent CO_2. At a CO_2 loading of 60 mol% onward, solid precipitation was observed which increased with increasing pressure. A 75% reduction in live oil viscosity was reported with first contact miscible 60 mol% CO_2-live West Sak oil system. DeRuiter et al. (1994) reported on static equilibrium experiments to measure the solubilities of methane, ethane, propane, butane,

and CO_2 in West Sak heavy oils. Physical properties including viscosity, density, and other volumetric properties were measured for live oil-solvent systems once equilibrium was achieved. They also carried out miscibility measurements with slim tube displacement experiments for selected injection gas/oil system. They concluded that West Sak oil viscosity is strongly controlled by its dead oil properties and the amount of solvent gas but not by the type of gas dissolved. Asphaltene deposition was observed in static and dynamic displacement experiments for West Sak oils at reservoir conditions for propane and butane which were found to be first contact miscible (FCM) and multiple contact miscible (MCM) to immiscible with increased dilution with lean gas. Okuyiga (1992) characterized the EOS and modeled the viscosity data for West Sak heavy oils.

2.1.1 Compositional Characterization

Petroleum crude oils contain thousands of components that determine their physical properties. Compositional description is required in both production and refining of crude oils. Compositional information is the basic information required for modeling phase behavior of the system. ASTM Standard D2892(01) for true boiling point (TBP) distillation is an accepted standard in the petroleum industry for determining the boiling range distribution of crude oils. But TBP distillation is time consuming and requires a large volume of sample. Simulated distillation by gas chromatography (GC) on other hand is a very quick technique for quantification of the composition of crude oil and takes only micro liters of sample. The ASTM Standard D2887(04) is an accepted chromatographic method for oils with final boiling points less than 538°C (1000°F). In this method the boiling range is calibrated by eluting the mixture of n-paraffins in gas chromatograph. But discrepancies occur when the data from these two methods is compared. Chorn (1984) in his experimental study of simulated distillation by GC suggested procedural and methodical modifications to ASTM Standard D2887(78) to improve the match with TPB data. McAllister, et al. (1985) studied the discrepancies between the results of TBP and simulated distillation by GC techniques and proved that the area counts of simulated distillation correspond to mass percent and not volume percent. They suggested the use of an internal standard to calculate the non-eluted fraction of the oil.

Okuyiga (1992) also studied the mismatch between the results of TBP and simulated distillation by GC. An alternative approach was taken to obtain single carbon number

molecular weights and specific gravities by performing a regression using the results from the TBP distillation. In this scheme, initial estimates were made for the pseudo-component molecular weights and specific gravities using the GC-determined weight fractions of the distillation cuts. The calculated values were then compared to the experimental values determined for the cuts in the laboratory with TBP distillation. The difference was used to guide the estimated values toward optimal ones using nonlinear regression. Exponential functions were used to correlate the molecular weights and the specific gravities as functions of carbon number to reduce the regression parameters. The values for the molecular weight and specific gravity of the plus fraction were treated as separate parameters since its equivalent carbon number was unknown. With this methodology the results of TBP distillation and simulated distillation were matched.

2.1.2 Constant Mass Expansion

Constant mass expansion is also known as constant composition expansion (CCE). The reservoir fluid at reservoir pressure and temperature conditions is expanded and the change in volume is measured at isothermal conditions. This enables computation of the bubble point pressure which is taken as a point at which the slope of volume vs. pressure plot changes abruptly. Compressibility of the oil is calculated by the following equation:

$$Co = -\frac{1}{V}\left(\frac{\partial V}{\partial P}\right)_T \tag{2.1}$$

2.1.3 Differential Liberation

This experiment is carried out on heavy oils. This test simulates the reservoir depletion process. The reservoir fluid is kept in a PVT cell at reservoir pressure and temperatures conditions. The pressure in the cell is reduced and liberated gas is collected in stock tank conditions of 14.7 psia pressure and 60°F. The test is conducted until the pressure of 14.7 psia and final residual oil volume measurement allows for the computation of solution gas/oil ratio and formation volume factor at every step of differential liberation. Figure 2.1 shows a schematic of the differential liberation experiment.

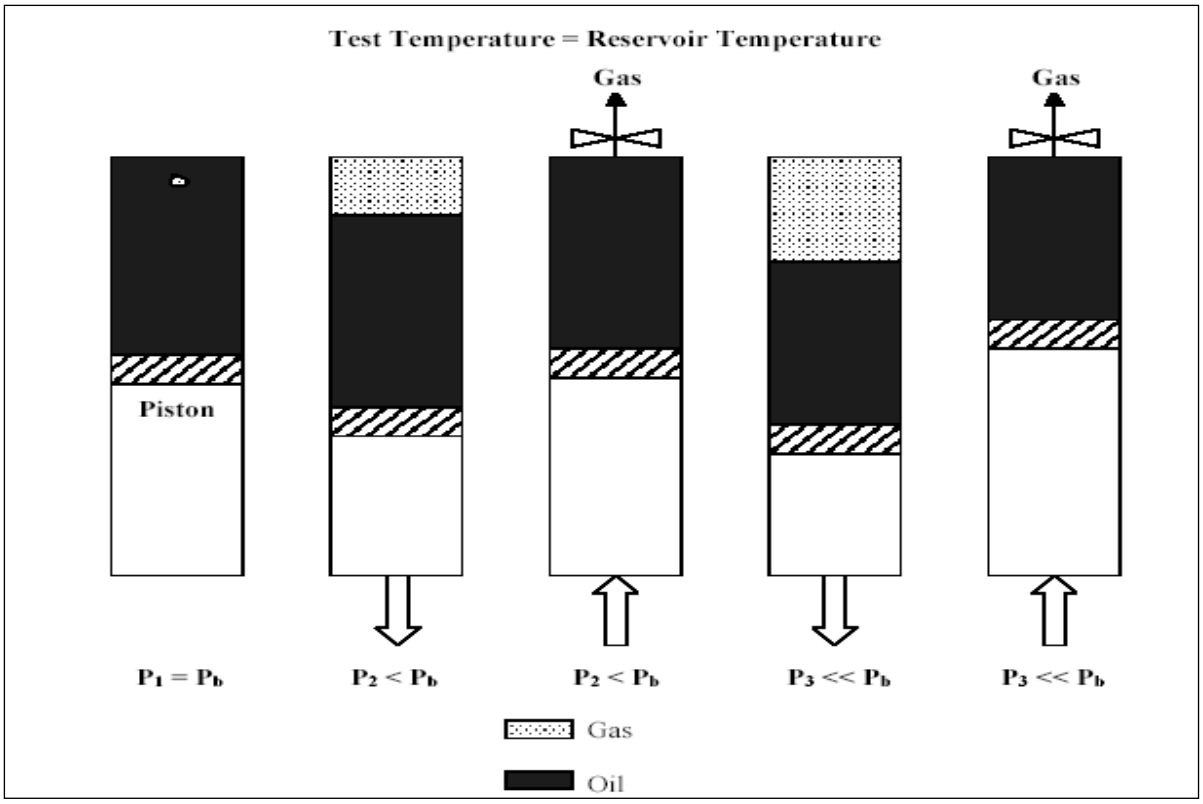

Figure 2.1 Schematic of Differential Liberation Experiment (Dandekar, 2005)

2.1.4 Separator Test

The reservoir fluid at reservoir temperature and pressure conditions is flashed to atmospheric conditions in two or three stages in series. Figure 2.2 provides a schematic of the separator test.

The primary objective of the separator test is to determine the optimum separator conditions that will give:

- A minimum of the total gas/oil ratio,
- A maximum in the API gravity of stock tank oil, and
- A minimum in formation volume factor of oil at bubble point conditions.

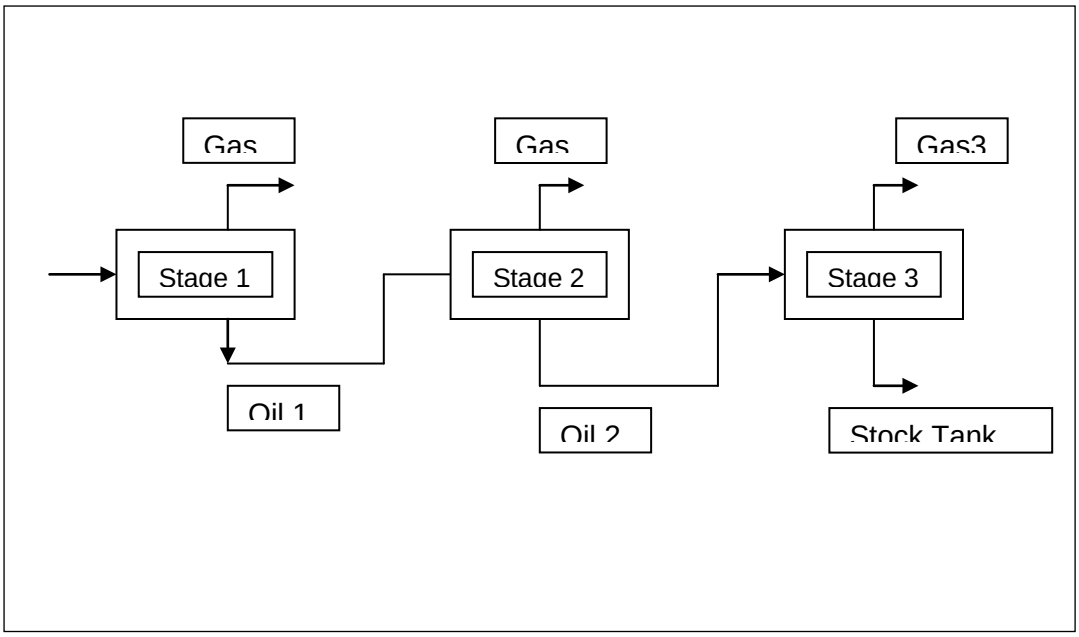

Figure 2.2 Schematic of the Separator Test

2.1.5 Minimum Miscibility Pressure

The miscible displacement process occurs when there is an absence of a phase boundary or interface between the displaced and displacing fluids. This condition is achieved when the interface between the fluids is absent and no interfacial tension exists between the mixed fluid phases. In a miscible displacement process, the injected gas directly mixes and forms a single phase with the reservoir oil when mixed at all proportions at the conditions existing at the interface between the oil and the gas. This results in the elimination of interfacial tension forces between the oil and displacing fluid. The pressure at which the interfacial tension becomes "zero" is termed as the Minimum Miscibility Pressure (MMP) (Rao, 1997).

The MMP is one of the most important parameters in the determination of optimum operating conditions involving miscible gas displacement processes and should be accurately measured. "MMP for a CO_2-reservoir fluid system is defined as the pressure at which 80% of the oil in place is recovered at CO_2 breakthrough and 94% of the oil in place at a production gas/oil ratio (GOR) of 40,000 SCF/BBL is ultimately recovered." (Holm and Josendal, 1974). "MMP is the lowest pressure at which all oil available for recovery can be displaced by 1.2 pore volumes of injected solvent." (Metcalfe, 1979).

In a majority of research, the criteria used for interpreting the displacements have included gas breakthrough, ultimate recoveries at a given volume of the solvent injection,

visual observations of core effluents, compositions of produced gases and liquids, shapes of breakthrough, and ultimate recovery curves versus pressure (Rao, 1997).

2.1.6 Factors Affecting MMP

Holm and Josendal (1980) put forth the following conclusions based on the experiments they carried out:

- Dynamic miscibility occurs when the density of CO_2 is greater than dense gaseous CO_2. At this point CO_2 solubilizes C_5 to C_{30} hydrocarbon components in the reservoir oil.
- The MMP increases as reservoir temperature increases.
- The MMP is inversely related to the total amount of C_5 through C_{30} hydrocarbon components present in the reservoir oil. The more the amounts of these hydrocarbon components present in the oil, the lower the MMP.
- Lower molecular weight hydrocarbon components promote miscibility and result in a lower MMP.
- Development of miscibility is almost independent of the presence of components C_2 through C_4.
- The presence of a small amount of methane in the oil doesn't change the MMP appreciably. As a deviation from this rule Alston et al. (1985) proposed a new equation accounting for the inclusion of methane and nitrogen concentration in reservoir oil. The correlation proved that a significant amount of these components in the reservoir oil increases the MMP.

Ahmed (2007) described more parameters which affect the MMP:

- Oil characteristics and properties including API gravity.
- Injected gas composition. The presence of methane in injection increases the MMP.
- Oil molecular weight.

2.1.7 Experimental Methods to Determine the MMP

2.1.7.1 Slim Tube Displacement

Displacement of oil by gas through a porous medium simulates the gas injection process more closely than other tests and often is considered a definitive test. The displacement is conducted either in a core, extracted from the reservoir, or more often in

a long and narrow sand pack, known as a “slim tube”. A slim tube test is conducted to examine the flushing efficiency and fluid mixing during a miscible displacement process. Slim tube results are interpreted by making a plot of cumulative oil recovery versus pore volume of injected gas. Recovery with 1.2 pore volume of gas injection is plotted versus injection pressure. The point at which the recovery/pressure curve starts to flatten, as the displacement approaches near miscibility, and eventually forms a straight line starting at a certain pressure, is called the MMP (Danesh, 1998).

The disadvantages associated with slim tube tests are:

- The experimental procedure is time consuming.
- There are no precise miscibility criteria, resulting in the indirect interpretation of miscibility, such as the prediction of the MMP, from the oil recovery curves.
- Plugging of slim tubes can be a problem.

2.1.7.2 Rising Bubble Apparatus (RBA)

For quick and reasonable estimates of gas/oil miscibility, the RBA technique can be employed. Miscibility is determined by the change in shape and appearance of bubbles of injected gas as they rise through a visual high-pressure cell filled with crude oil. A series of tests are conducted at different pressures of the injected gas and the bubble shape is continuously monitored to determine miscibility. This test is qualitative in nature, as miscibility is inferred from visual observations. Some subjectivity is associated with the miscibility interpretation of this technique and the results, therefore, are somewhat arbitrary. The method requires a small amount of fluid quantities and is cheaper than slim tube tests. Also, no strong theoretical background appears to be associated with this technique and it provides only reasonable estimates of gas/oil miscibility conditions (Ahmed, 2007).

2.1.7.3 Vanishing Interfacial Tension (VIT) Technique

Rao (1997) put forth a new technique to determine gas/oil miscibility by measuring the interfacial tension (IFT) between the injected gas and reservoir fluid phases at reservoir temperature and at different pressures. The VIT technique is based on the concept that the IFT between the gas and crude oil phases at reservoir temperature must reduce to zero as these two phases approach the point of miscibility. The concept of zero IFT is based on the fact that the interface between the phases must vanish as they become

miscible with each other. Thus, MMP can be determined by measuring the gas/oil IFT as a function of pressure, down to as low as the measurement apparatus allows, and then extrapolating the data to zero IFT. The present work deals with this new VIT technique using a pendant drop apparatus.

2.1.7.4 Pendant Drop Method

The pendant drop method is used to measure the gas/oil IFT at high pressures and temperatures. Figure 2.7 shows a liquid droplet hanging from the tip of a needle in a high pressure optical cell filled with equilibrated vapor (Dandekar, 2006).

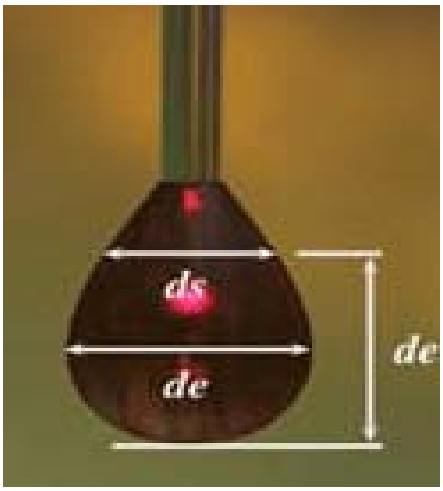

Figure 2.3 Pendant Drop Shape (Source: www.pet.hw.ac.uk)

The shape and size of the liquid droplet at static conditions is dependent upon surface and gravity forces acting at the gas/oil interface. The pendant drop assembly is normally integrated to a high pressure cell that can be maintained at constant temperature and pressure as required for experimental conditions. The equilibrium shape of the hanging pendant drop is a balance between the forces acting on the drop, namely gravity. Gravity pulls the drop down by elongation and surface tension which acts to prevent the growth of surface area and pulls the drop into a spherical shape. The shape of the drop contains both the density and the surface tension of the liquid, and this helps form the gas/oil IFT equation (Dandekar, 2006):

$$\sigma = \frac{g d_e^2}{H}(\rho_l - \rho_v) \tag{2.2}$$

Where,

σ = IFT between the oil and gas phase, dynes/cm.

g = acceleration due to gravity, cm/s^2.

ρ_l = liquid phase density, g/cc.

ρ_v = gas phase density, g/cc.

de = equatorial diameter of the maximum horizontal diameter of the drop, cm.

ds = diameter of the drop measured at a distance de above the tip of the drop, cm.

H = drop shape factor as a function of S = ds/de.

Niederhauser and Bartell (1947) have determined and reported the values of H, by relating the pressure difference across the interface to the interface curvature. First, the value of S is determined and then the drop shape factor, H, can be read from the tables published by Niederhauser and Bartell. In the absence of these tables, the drop shape factor can also be calculated using equations proposed by Misak (1968).

The advantages associated with the pendant drop method are that a small amount of liquid samples is required and the test can be performed at elevated temperatures and pressures. The time required for completion of the experiments is far less than for the slim tube test and the apparatus is easy to set up. The major disadvantage is that this method is not applicable at very low tension values. As miscibility or the critical point between fluid/fluid phases is approached, due to rapid diffusion of drops into the surrounding gas, it is difficult to measure the drop shape factor accurately. As in the case of RBA, this test is qualitative in nature, as miscibility is inferred from visual observations. Hence, some subjectivity is associated with the miscibility interpretation of this technique (Orr Jr. and Jessen, 2007).

2.1.8 MMP Determination Using Equation of State Modeling

Phase behavior calculations of reservoir fluids are routinely made using EOS in the petroleum industry. The phase behavior of oil in miscible injection processes consists mainly of mass transfer as well as composition changes. It is important to tune the EOS, prior to use, for accurate prediction of properties. Cubic EOS like Peng-Robinson (1976) is widely used for convenient and flexible calculation of the complex phase behavior of the reservoir fluids. The Peng-Robinson equation is (Patil, 2006):

$$P = \frac{RT}{V-b} - \frac{a}{V(V+b)+b(V-b)} \tag{2.3}$$

$$a = \Omega_a \frac{R^2 T_c^2}{P_c}\alpha \quad \text{and} \quad b = \Omega_b \frac{RT_c}{P_c} \tag{2.4a \& b}$$

Where,

a and b = mixing coefficients.

Ω_a and Ω_b = constants.

α = correction factor which is dependent on the reduced temperature and quadratic function based on the acentric factor.

P, V, and T = pressure, mole volume and temperature of the components.

Peng-Robinson (1978) recommended a modification to the acentric factor and the resulting equation was described as PR-EOS. Parameters like bubble point, liquid phase densities, and compositions may differ by several percent from experimental values. These inconsistencies in EOS predictions are from insufficient characterization of the plus fractions, inadequate binary interaction coefficients, or incorrect overall composition. Usually, most EOS predictions are not accurate. Therefore, before using these EOS for phase-behavior calculations, it is necessary to calibrate the EOS against the experimental data by adjusting the input values of the EOS parameters to minimize the difference between the predicted and measured values. Critical pressure (P_c), critical temperature (T_c), and acentric factor (ω) of the plus fraction or direct multipliers on EOS constants can be modified for matching experimental data obtained from PVT studies on reservoir fluid (Alurkar, 2007). The adjustment which is done via regression analysis is known as “equation tuning”, and shall be described in the later part of the work.

2.1.9 Previous Work on MMP Measurements Using VIT Technique

Rao (1997) first demonstrated the applicability of VIT to measure the MMP. He experimentally demonstrated the applicability of the VIT technique to show miscibility in a live reservoir crude oil-gas system at reservoir temperature and varying pressures. Rao used different gas enrichment levels to determine the Minimum Miscibility Enrichment (MME). The composition of injectant gas was successfully optimized for the miscibility by performing a VIT experiment with varying gas compositions at an experimental pressure of 30 MPa and 60°C. These experiments were performed on oil samples obtained from Rainbow Keg F Pool reservoir in Canada.

Rao and Lee (2000) performed VIT experiments on Terra Nova Oil Samples. The reservoir temperature and pressure conditions were the same as described above. They compared the results of Minimum Miscibility Composition (MMC) and MMP obtained from VIT experiments with those of slim tube tests and found a good match. In these experiments Rao and Lee used the computerized axi-symmetric drop shape analysis

technique to determine IFT. Rao and Lee showed that an increase in composition of intermediate hydrocarbons in the oil decreases the MMP. The MMPs calculated experimentally were within 5% of those observed visually in the experimental cell. They proved that results obtained from the VIT technique were rapid, reproducible, and quantitative, in addition to providing visual evidence of miscibility between injected gas and live reservoir oil.

Ayirala and Rao (2003) put forth a comparative study of MMP measured using the VIT technique with EOS calculations. For this purpose they used oil samples from Rainbow Keg River (RKR) and Terra Nova reservoirs. PR-EOS within a commercial software package was used and the effects of tuning and non-tuning the EOS on MMP calculations were examined. For these two reservoir cases, tuned PR-EOS yielded significant differences between MMPs from EOS calculations and VIT measurements, while untuned PR-EOS yielded a reasonable match with experiments. In the case of RKR crude oil, the untuned EOS predictions were consistently higher by about 3.0-5.0 MPa than the experimental MMP from the VIT technique. For Terra Nova crude oil, in three out of five cases studied, the visible MMPs from the VIT experiments reasonably matched with untuned EOS calculations. Based on these comparisons of VIT results with EOS predictions, Ayirala and Rao demonstrated that this new technique of VIT is quite promising and reliable.

Rao and Ayirala (2004) applied the VIT technique as a part of IOR using Gas Assisted Gravity Drainage (GAGD) as an alternative for the Water Alternating Gas Injection Process. Process optimization was done by determining miscibility pressures and compositions through the use of the VIT technique.

Yang and Gu (2004) used VIT to study interfacial interaction in the crude oil-CO_2 systems under reservoir conditions. The experimental results were similar as described by Rao in his work. They used the axi-symmetric drop shape analysis (ADSA) to measure the IFT and to visualize the interfacial interactions between crude oil and CO_2 at high pressures and elevated temperatures. A number of important physical phenomena were observed when the crude oil was contacted with CO_2, including the following: oil swelling, light-ends extraction, initial turbulent mixing, skin layer, oil drop movement, wettability alteration, asphaltene precipitation, and bubbling at the crude oil-CO_2 interface. In particular, the light-ends extraction, initial turbulent mixing, and wettability alteration are the major characteristics of CO_2 flooding processes. In addition, Yang and

Gu anticipated that wettability alteration may have significant effects on the ultimate oil recovery and CO_2 sequestration.

Ayirala and Rao (2006) investigated the applicability of the VIT technique to determine miscibility and to measure dynamic gas/oil IFT using the capillary rise technique. Ayirala performed experiments for two standard gas/oil phase systems of known phase behavior characteristics (CO_2-n-decane and 25 mol% methane + 30 mol% n-butane + 45 mol% n-decane with CO_2). Results obtained from the experiments were compared to those obtained from slim tube tests. Their experiments further validated the VIT technique to measure gas/oil miscibility using the capillary rise technique.

Orr Jr. and Jessen (2007) made an analysis of various crude oil systems used in the past to determine MMPs and tried to simulate VIT experiments. They compared estimates obtained from the calculation of MMPs using the VIT technique with those from solutions of the differential equations that describe the interactions of the flow and phase equilibria. They came to the conclusion that results obtained from the VIT technique differed substantially from the MMP observed in displacement experiments. According to Orr Jr. and Jessen, the uncertainty in the VIT estimate of MMP arises from a fundamental limitation of the experiment in that VIT investigates the mixture compositions which are linear combinations of the initial oil and injection gas that are quite different from the critical mixture that forms at the MMP in a gas/oil porous medium like the slim tube test.

Sequeira and Rao (2008) further validated results obtained from Ayirala's experiments and extended the study for CO_2-live oil reservoir systems. In their experiments Sequeira and Rao made detailed compositional analysis and density measurements of vapor and liquid phases to infer information on mass-transfer interactions and to determine the controlling mass transfer mechanism (vaporizing drive, condensing drive, or both) that governs the attainment of miscibility. They further investigated the compositional dependence of MMP and provided results based on varying gas/oil ratios (both molar and volumetric) in the feed mixture. Their results further demonstrated the reproducibility of VIT experiments.

2.1.10 MMP Correlations

Ahmed (1988) briefly described various methods for determination of MMP. These methods were primarily dependant on the molecular weight of C_{5+}, temperature, and the

weighted-composition parameter (based on partition coefficients of C_2 through C_{37} fractions). Some of the correlations studied required only the input of reservoir temperature and the API gravity of the fluid. Orr Jr. and Silva (1987, Part 2) showed that MMP changes as oil composition changes, and hence oil composition should be taken into account while determining MMP. Alston et al. (1985) proved that the presence of methane and nitrogen significantly increases the MMP. The ANS oils contain appreciable amount of methane, hence Alston's correlation was used to compare the results of experimental findings with the correlation findings. The various correlations for the CO_2-crude oil system are described below.

2.1.10.1 Newitt et al. Correlation (1996)

$$EVP = 14.7\exp[10.91 - \frac{2015}{255.372 + .5556(T - 460)}] \quad (2.5)$$

Where,

EVP = Extrapolated vapor pressure, psi.

T = system temperature, °R

The values of EVP can be correlated to MMP for low temperature reservoir (T<120°F), using CO_2 vapor pressure plots.

2.1.10.2 Yellig and Metcalfe Correlation (1980)

$$MMP = 1833.7217 + 2.2518055(T - 460) + 0.01800674(T - 460)^2 - \frac{103949.93}{T - 460} \quad (2.6)$$

Where,

T = system temperature, °R.

Yellig and Metcalfe pointed out that, if the bubble point pressure of the oil is greater than the predicted MMP, then the CO_2 MMP is set equal to the bubble point pressure.

2.1.10.3 Alston et al. Correlation (1985)

Alston proved that presence of significant amount of methane and nitrogen in the crude oil increases the MMP.

$$MMP = .000878(T - 460)^{1.06}(M_{C_{5+}})^{1.78}\left[\frac{X_{vol}}{X_{\text{int}}}\right]^{0.136} \quad (2.7)$$

Where,

T = system temperature, °R.

M_{C5+} = molecular weight of pentane and heavier fractions in the oil phase.

X_{vol} = mole fraction of volatile (C_1 and N_2) oil components.

X_{int} = mole fraction of intermediate oil components (C_2-C_4, CO_2, and H_2S).

2.1.10.4 Firoozabadi and Aziz's Correlation (1986)

For a lean gas/crude oil system use:

$$F = \frac{I}{M_{C_{7+}}(T - 460)} \tag{2.8}$$

$$I = x_{C_2 - C_5} + x_{CO_2} + x_{H_2S} \tag{2.9}$$

where,

I = concentration of intermediates in the oil phase, mol%.

T = system temperature, °R.

M_{C7+} = molecular weight of heptane and heavier fractions in the oil phase.

2.2 Equation of State Modeling of Phase Behavior

Many empirical correlations have been developed by analyzing the PVT reports of oils from different fields to simplify the incorporation of fluid properties into the material balance equation. All these correlations have the absence of composition and are commonly referred to as black oil correlations. These black oil correlations express PVT and fluid properties in terms of solution gas/oil ratio, oil and gas gravities. Many of the black oil correlations have been listed in text of Ahmed (1989). Ostermaan et al. (1983) analyzed the PVT properties of Alaskan oils from the Cook Inlet basin and checked the accuracy of existing black oil correlations in literature. Many of the black oil correlations were developed by analyzing the PVT properties of crude oils of a particular region. The black oil model assumes that the reservoir fluids consist of three components (water, oil, and gas) in a three-phase system (liquid, gas, and gas in solution), with components miscible in all proportions. Due to absence of composition, the effects of fluid phase composition on flow behavior are neglected.

An EOS is a mathematical relationship describing the interconnection between various macroscopically measurable properties of a system. An EOS is completely compositional and is capable of tracing effect of composition on the fluid properties and phase behavior unlike the black oil model. Cubic EOS are commonly used in petroleum industry for simulating phase behavior of hydrocarbon mixtures. Since the development of van der Waals (1873) EOS, more accurate EOS have been developed, and these can describe the thermodynamic properties and phase equilibria of a wide range of substances

with varying degrees of success. Soave (1972), Redlich Kwong (1949) and Peng-Robinson (1976) introduced cubic EOS that are widely used in PVT simulation packages in the petroleum industry. Performance of cubic EOS is, however, questionable on application to petroleum fluids in predictive mode. In order to reproduce the experimental data, the EOS needs its parameters adjusted; this process is known as “tuning” the EOS. There is no standard procedure of tuning for matching the experimental data. But some guidelines and approaches are found in the literature. Merrill et al. (1994) carried out an extensive program of tuning a particular PVT dataset with different approaches. They reported the effect of different C_{7+} characterization schemes on slim tube experiment recoveries and recommended confirming EOS-predicted slim tube recoveries with experimental data prior to incorporating “tuned” EOS into compositional reservoir simulation. Experimental data available for regression typically is comprised of saturation pressures, liquid phase densities, gas oil ratios and formation volume factors from differential liberation experiments. It is quite possible that even after matching some of the parameters, the EOS model predictions may still not be accurate for other properties.

The nature of the oils differs regionally. Some oils are paraffinic while some are napthenic and aromatic. This further complicates the estimation of plus fraction properties like specific gravity and molecular weight, which are used in computation of critical properties. This often affects the predictions of EOS for phase behavior. Most tuning strategies involve characterizing the plus fraction to a suitable carbon number for accurate representation of critical properties. Rafael et al. (2002) presented a tuning strategy that involved characterizing the C_{7+} fraction composition until C_{45+} and matching the saturation pressure by varying the molecular weight of the plus fraction. The components were further regrouped into multiple carbon number groups (MCN) and the volumetric data was tuned. They suggested a methodology to preserve the match of saturation pressure after lumping where the characterized C_{7+} fraction was distributed into two groups. They developed a correlation for distribution of characterized C_{7+} mole fraction into appropriate MCN groups. The volumetric data was matched with final lumped composition by regressing using Peneloux and Rauzy (1982) volume translation parameters which do not affect the vapor liquid equilibrium. Al Meshari et al. (2005) presented a similar EOS tuning strategy except the saturation pressure after grouping was matched by variation of acentric factor of heaviest MCN.

2.3 Review of Viscosity Models

2.3.1 General Purpose Viscosity Models

The gas phase viscosity is primarily a function of the momentum transfer by translation of the molecules with relatively few collisions. On the other hand, the momentum transfer in dense gases and liquids is dominated by collisions and interacting force fields between the densely packed molecules. A theoretical description of liquids is difficult due to intermolecular forces, which consist of the short range (repulsion and hydrogen bonding), wide range (electrostatic), and long range (attraction) effects. Thus, there is no widely accepted simple theoretical method for predicting liquid viscosity (Reid et al., 1987).

Several models for the viscosity of pure components and mixtures are available and summarized in the literature (Monnery et al., 1995). Excellent reviews have also been given by Reid et al. (1987). However, petroleum fluids were not covered in any of these studies. Petroleum liquids are complicated undefined fluids which must be characterized to obtain relevant parameters. Mehrotra et al. (1996) reviewed the most widely known and accepted models for viscosity prediction of hydrocarbons and petroleum liquids. They classified these models in three different categories: (1) theoretical models, (2) semi-theoretical models, and (3) empirical models. The theoretical models, for example a model based on Chapman-Enskog theory, are mainly used to calculate the viscosities of the pure components and their mixtures. Some of these models have been used to model the viscosities of the petroleum mixtures with little success.

Empirical models are mainly described in terms of correlations. The two main types are Andrade (Andrade, 1934) and ASTM (ASTM, 1981) or Walther (Walther, 1931) equations. The Andrade equation has the following form:

$$\ln \mu = a + \frac{b}{T} \tag{2.10}$$

whereas the ASTM equation has the following form:

$$\log \log \left(\mu + 0.7\right) = b_1 + b_2 \log T \tag{2.11}$$

The various modifications of these equations can be found in the literature. Hossain et al. (2005) have listed many of these correlations. The empirical methods also involve another class, viscosity EOS. This approach is based on the phenomenological similarity between the P-V-T and P-μ-T surfaces resulting in a viscosity correlation which is an

explicit function of temperature and pressure. Lawal (1986) and Guo et al. (2001) attempted this approach.

The semi-theoretical methods for viscosity prediction have provided a blend between the theoretical and correlative methods. These methods include models based on the corresponding states theory, reaction rate theory, hard sphere (Enskog) theory, as well as the square well models, Lennard-Jones models, and modified Chapman-Enskog models (Chung et al., 1988). However, of these models, only the ones based on the corresponding states theory have found widespread acceptance in the petroleum industry. The rest of these models are still in the primitive stages, as far as the viscosity modeling of the petroleum mixtures is concerned. Hence, these models are not discussed any further. According to the principle of corresponding states, a dimensionless property of one substance is equal to that of another (reference) substance when both are evaluated at the same reduced conditions. A classical example of the use of the corresponding states model is the Standing-Katz z-factor chart (Standing and Katz, 1942).

2.3.2 Viscosity Models for Petroleum Fluids

The law of corresponding states expresses the generalization that equilibrium properties, which depend on intermolecular forces, are related to the critical properties in a universal way. This provides the single most important basis for the development of correlations and estimation methods. The relation of pressure to volume at constant temperature is different for different substances. Corresponding states theory, however, asserts that if pressure, volume, and temperature are related to the corresponding critical properties, the function relating reduced pressure to reduced volume becomes the same for all substances at the same reduced temperature.

The corresponding states model is also used in terms of the residual viscosity form. Residual viscosity is defined as the difference between the viscosity at a given pressure and temperature and the viscosity of the dilute gas phase, which is usually at one atmosphere pressure and the same temperature. The viscosity correlation most widely used in flow models in petroleum engineering is probably the residual viscosity correlation of Jossi et al. (1962) in the form suggested by Lohrenz et al. (1964). Gas and liquid viscosities are related to a reduced density by a fourth degree polynomial of the form:

$$\left[\left(\mu-\mu^{*}\right)\xi+10^{-4}\right]^{\frac{1}{4}}=a_1+a_2\rho_r+a_3\rho_r^2+a_4\rho_r^3+a_5\rho_r^4 \qquad (2.12)$$

The coefficients a_1 to a_5 are empirical coefficients and are provided by the authors. It is evident from the above equation that the viscosity is sensitive to changes in densities. Especially for highly viscous fluids this may lead to severe errors for the calculated viscosity. Nevertheless, because of its simple form, it is predominantly used in compositional reservoir simulators, where the phase densities are generated from EOS.

A group of substances obey the corresponding states principle with respect to viscosity if the functional dependence of μ_r, on, for example, ρ_r and T_r, is the same for all substances within the group:

$$\mu_r\left(P,T\right)=f\left(\rho_r,T_r\right) \tag{2.13}$$

In that case, comprehensive viscosity data are only needed for one of the components of the group. That component is then used as the reference substance (*o*) and the viscosity of another component (*x*) within the group can easily be calculated. This is the basis of the corresponding states viscosity correlations developed by Ely and Hanley (1981) and Pedersen and coauthors (Pedersen et al., 1984; Pedersen and Fredenslund, 1987).

The Transport Properties Prediction (TRAPP) program of Ely and Hanley (1981) is one of many programs available, which is general and totally predictive for the calculation of the viscosity of gases and liquid mixtures for a wide range of pressure and temperature and different types of fluids. The calculation procedure, however, is iterative and complex. Baltatu et al. (1999) have simplified this procedure to a greater extent.

Pedersen and coauthors (Pedersen et al., 1984; Pedersen and Fredenslund, 1987) presented a method for predicting oil and gas viscosities which is a modified form of the corresponding states method of Ely and Hanley (1981). In this method, the reduced viscosity is expressed in terms of the reduced pressure and reduced temperature. The final expression for the viscosity of the fluid is given as:

$$\frac{\mu_{mix}\left(P,T\right)}{\mu_o\left(P_o,T_o\right)}=\left(\frac{T_{cmix}}{T_{co}}\right)^{-\frac{1}{6}}\left(\frac{P_{cmix}}{P_{co}}\right)^{\frac{2}{3}}\left(\frac{MW_{mix}}{MW_o}\right)^{\frac{1}{2}}\left(\frac{\alpha_{mix}}{\alpha_o}\right) \tag{2.14}$$

By expressing the viscosity in terms of the reduced pressure instead of the reduced density, it is possible to perform a direct calculation of the viscosity. The calculation becomes much simpler, compared to those of Ely and Hanley (1981), where density is calculated using an iterative procedure. The modifications of Pedersen correlation, for heavier oils, are discussed in Section 2.4.2.

Apart from these conventional models, there have been numerous attempts made in recent years to characterize the oil viscosity with completely new concepts. First of all, a compositional model for predicting the viscosity of petroleum fluids as a function of temperature and pressure is presented by Werner et al. (1998). It is based on the original model, termed the Self-Reference Model, developed by Kanti et al. (1989). This model uses a single viscosity value for predicting the fluid viscosity at any pressure and temperature. Werner et al. introduced a suitable mixing rule to take into account the fluid composition. They also classified the original oil mixture into four classes: (1) Gas, (2) C_6–C_{20}, (3) C_{20+} (Saturates + Aromatics + Resins), and (4) C_{20+} (Asphaltenes). The model parameters have been fitted on a large database ranging from 100 MPa (14,500 psia) in pressure and up to 120°C (248°F) in temperature. The range of viscosity covered varies from 2 cP to nearly 23,000 cP. This model is designed to be valid in a large compositional range, especially for liquids containing large amounts of asphaltenes. However, without a reliable analytical characterization scheme for Saturates-Aromatics-Resins-Asphaltenes (SARA), this method cannot be used with confidence.

The recently proposed Friction theory (Quinones-Cisneros, Zeberg-Mikkelsen, and Stenby, 2001; Quinones-Cisneros, Andersen, and Creek, 2005) has become successful as far as oil viscosity modeling is concerned. However, this model is still in the inception stages as far as heavy oil modeling is concerned and at this time is not included in the analysis. In addition to this, Riazi and coauthors (Riazi and Al-Otaibi, 2001; Riazi, Mahdi, and Alqallf, 2005) developed a relation for estimation of viscosity of liquid petroleum fractions by using refractive index at 20°C as one of the input parameters along with the molecular weight and the boiling point. Since this model has not been applied for heavy oils, at present this model is not considered for further analysis.

Recently, Lindeloff et al. (2004) introduced a new viscosity computation method for the heavy oils. The dead oil viscosity is used for the calculation of the viscosity of the corresponding live oil at a desired pressure and temperature. The correlation proposed by Rønningsen (1993) is used to compute the degassed (dead) oil viscosity. The pressure correction is introduced by a simple exponential form. For this method it is necessary to use the characterization method proposed by Pedersen et al. (2004).

2.4 Viscosity Models for Medium-Heavy Oils

The existing semi-theoretical viscosity models can be divided into three main categories: (1) LBC class models, (2) Pedersen class models, and (3) New Generation Models. In this section, an attempt has been made to broadly classify present day semi-theoretical models into the above three categories. It must be noted that only the physical interpretation of each model is described, accompanied by its fundamental governing equation. A complete set of equations can be found in the respective references.

2.4.1 LBC Class Models

The following viscosity models comprise the LBC class models.

1. LBC Model (Lohrenz et al., 1964)
2. Xu Model (Xu and Khurana, 1996)
3. Dandekar Model (Dandekar and Danesh, 1992)
4. Al-Syabi Model (Al-Syabi et al., 2001)

The viscosities calculated by the original LBC model are highly sensitive to the densities, as shown by Equation 2.12. The dependence is as high as to the power of sixteen. A small error in the density prediction, commonly calculated with cubic EOS in compositional simulation models, might cause a high deviation for the viscosity calculation. Additionally, since the above equation was developed for less dense systems, it is certain that it needs to be modified before application to the heavy oils.

Xu and Khurana (1996) extended the LBC correlation for improved prediction of the high viscosity fluids. In their study the original correlation was modified by introducing an exponential term and the density was calculated by a cubic PR-EOS. The modified correlation is expressed as follows:

$$\left[\left(\mu-\mu^{*}\right)\xi+10^{-4}\right]^{\frac{1}{4}}=a_1+a_2\rho_r+a_3\rho_r^2+a_4\rho_r^3+a_5\rho_r^4+\alpha\,\rho_r^3\left(1+\beta\,\rho_r^2\right)\exp\left(\gamma\,\rho_r\right) \quad (2.15)$$

In the above equation, all the terms have the same meaning as in the original LBC correlation, while the α, β, and γ coefficients are determined by regression on pure component viscosity data.

Dandekar and Danesh (1992) re-evaluated the LBC correlation and concluded that it is within ±20% for all normal alkanes with a carbon number less than 8 and a reduced density less than 2.5. For conditions other than those stated above, Dandekar and Danesh proposed the following viscosity correlation:

$$\left(\mu-\mu^{*}\right)\xi=\exp\left(A+B\rho_{r}+C\rho_{r}^{2}\right) \tag{2.16}$$

According to the Dandekar model (Dandekar and Danesh, 1992), for reduced densities less than 2.5, the LBC correlation is used as it is, whereas for reduced densities greater than 2.5 the above correlation is used. In the above correlation, the molecular weight is introduced to capture the structural effects.

Al-Syabi et al. (2001) pointed out the requirement of including the structural and thermal effects for accurate viscosity predictions of dense fluids. The thermal effects were considered in terms of reduced temperatures while the structural effects were accounted by means of the molecular weights. Based on the regression of viscosity data, the LBC correlation is extended as follows:

$$\left[\left(\mu-\mu^{*}\right)\xi+10^{-4}\right]^{\frac{1}{4}}=0.094754+0.062016\rho_{r}-0.0010273T_{r}^{-2.0133}MW^{0.44620}\rho_{r}^{2}+0.00040403T_{r}^{-2.4706}MW^{0.19138}\rho_{r}^{3}+0.000086159T_{r}^{-1.1577}MW^{0.58683}\rho_{r}^{4} \tag{2.17}$$

When the deviations of predicted viscosities from experimental values were plotted using the LBC correlation and above method, it showed that for reduced density values less than 2.5, the deviations of both correlations were comparable. However, for higher reduced densities, the LBC correlation deviates up to ±100%, while the deviation of the modified correlation is within ±20%, demonstrating the significance of including both thermal and structural effects. Nevertheless, a deviation higher than 20% can be observed for methane, using the proposed correlation.

Since real reservoir fluids contain high concentrations of methane, the authors proposed a separate correlation to accurately predict the viscosity of methane. The mixture viscosity is then calculated by splitting the mixture into two components: methane and the rest of the components are lumped together as a pseudo-component. The following mixing rule is applied:

$$\Delta\,\mu_{r}=z_{1}\,\Delta\mu_{r1}+\left(1-z_{1}\right)\Delta\mu_{r2} \tag{2.18}$$

Where,

$\Delta\mu_{r}$ = mixture reduced residual viscosity

$\Delta\mu_{r1}$ = methane reduced residual viscosity

$\Delta\mu_{r2}$ = reduced residual viscosity of the pseudo-component

z_{1} = molar concentration of methane in the mixture

The above mixture reduced residual viscosity is divided by the overall mixture viscosity parameter, ξ, and the resultant is added to the overall mixture dilute gas viscosity, μ^*, to obtain mixture viscosity.

2.4.2 Pedersen Class Models

Another class of semi-theoretical models is the Pedersen class models. It has the following models associated with it:

1. Pedersen Model (Pedersen et al., 1984; Pedersen and Fredenslund, 1987)
2. Aasberg-Petersen Model (Aasberg-Petersen et al., 1991)
3. Moharam Model (Moharam and Fahim, 1995)
4. Dexheimer Model (Dexheimer et al., 2001)

The original Pedersen model is represented by Equation 2.14. However, this model suffers from a serious limitation when applied to heavy oil systems. This is best stated in the authors' own words (Lindeloff et al., 2004), "Pedersen and Fredenslund (1987) found that the viscosities derived from the Hanley model (Hanley et al., 1975) were too low when the methane reference temperature reduced below approximately 90 K. The freezing point of methane is 91 K and accordingly temperatures below 91 K were not covered in Hanley's model. The work of Pedersen and Fredenslund permitted the lower limit of the methane reference temperatures to be lowered from around 90 K to around 60 K. For even lower temperatures, the corresponding states model becomes inapplicable as the methane density, according to the model of McCarty (1974), becomes almost invariant to pressure variations. The viscosity of an oil mixture with a methane reference temperature around 60 K will typically be of the order of 10 cP. As a rule of thumb, oil viscosities higher than that cannot be simulated using the corresponding states principle with methane as a reference component." Hence, over the last two decades, there were several attempts made to improve upon this limitation.

The first of which is the Aasberg-Petersen model (Aasberg-Petersen et al., 1991). This model is also based on the principles of the corresponding states method as interpreted by Lee and Kesler (1975). Teja and Rice (1981) applied the method of Lee and Kesler for the computation of the viscosity in terms of two reference fluids. Aasberg-Petersen et al. (1991) modified the method of Teja and Rice by introducing molecular weight as the interpolation parameter instead of the acentric factor. The idea of this model is to use a heavier second reference component and effectively create an optimum

reference component. Decane is chosen as the second reference component because it is the heaviest alkane for which a significant amount of experimental viscosity data is known. Methane is a natural choice as the first reference component because of its presence in large mole fractions in most reservoir fluid mixtures. The interpolation law is used to calculate the reduced viscosity of the optimum reference component (denoted with subscript *x*) using the reduced viscosities of methane and decane and is obtained using the following expression:

$$\ln(\mu_{rx}) = \ln(\mu_{r1}) + \frac{MW_x - MW_1}{MW_2 - MW_1} \ln\left(\frac{\mu_{r2}}{\mu_{r1}}\right) \tag{2.19}$$

Where, *MW* is the molecular weight and the subscripts 1 and 2 refer to the reference components. The authors used the same definitions as that of Pedersen model (Pedersen et al., 1984; Pedersen and Fredenslund, 1987) for calculating mixture critical temperature and critical pressure.

The Moharam and Fahim model (1995) is essentially similar to that of the Aasberg-Petersen model (Aasberg-Petersen et al., 1991). They use n-decane and n-eicosane as the reference components for predicting viscosity of the petroleum fractions of average molecular weight higher than 142 (molecular weight of n-decane). Viscosity of the reference components is estimated by the method of Orbey and Sandler (1993). The Lucas correlation (Reid et al., 1987) was used to calculate the effect of pressure on the liquid viscosity. This model uses the same mixing rules as that of the Aasberg-Petersen model to compute various mixture properties except the critical temperature, which is calculated by Li's mixing rule (Reid et al., 1987).

Dexheimer model (Dexheimer et al., 2001) proposed a modification of the Pedersen correlation to be applied to black oil systems where there are no compositional data available. In addition to many changes, n-decane was introduced as a reference component to accommodate more viscous oils. The authors have also provided the density and viscosity correlation specifically developed for n-decane. As opposed to directly adapting the proposed method as it is, only the density and viscosity correlations of the n-decane are used. The viscosity and density data for n-decane were taken from various sources covering pressures from 14.7 psia to 7325 psia and temperatures from 492°F-762°F. The density and viscosity data were fitted as a function of P and T using a stepwise regression procedure. The various parameters used in the original Pedersen model are kept as they are and no attempt is made to retune these values.

2.4.3 New Generation Models

These models characterize oil viscosity using new concepts and are summarized as follows:

1. Werner Model (Werner et al., 1998)
2. Friction Theory Model (Quinones-Cisneros et al., 2005)
3. Riazi Model (Riazi et al., 2005)
4. Lindeloff Model (Lindeloff et al., 2004)

The first three of the new generation models are not considered for further analysis. The fourth model (the Lindeloff model) introduced an innovative concept to compute the heavy oil viscosity. As an alternative to using methane as a reference component and using the Pedersen model to determine the corresponding viscosities, the viscosity of the stabilized crude is used as a starting point. Based on viscosity measurements of a wide range of North Sea oils and condensates, a semi-empirical correlation for stabilized crude viscosities was proposed by Rønningsen (1993). It takes the form:

$$\log_{10}\mu = -0.07995 - 0.01101MW - \frac{371.8}{T} + \frac{6.215MW}{T} \qquad (\mu, cP \ \& \ T, K) \quad (2.20)$$

This correlation is valid at temperatures where the fluids behave Newtonian and the effect of precipitated wax is small, i.e., typically higher than about 30°C. The above equation applies to systems at atmospheric pressure. In order to capture the pressure effects on the reference fluid, the following pressure dependence was introduced:

$$\frac{1}{\mu}\frac{\partial\mu}{\partial P} = 0.008\,atm^{-1} \qquad \Rightarrow \qquad \frac{\mu}{\mu_o} = \exp\left[m\left(P - P_o\right)\right] \qquad (2.21)$$

Note that the derivative is evaluated for a constant composition. The parameter *m* in the above equation is used to denote the coefficient of the pressure differential.

Additionally, it is required to correct the stabilized crude oil viscosity correlation for the oil mixtures being live oils, oils that contain gas in solution. Distinction between stabilized oil and live oil in this context can be obtained by evaluating the ratio between the weight-averaged molecular weight and the number-averaged molecular weight. Stabilized oils will typically have:

$$\left(\frac{MW_w}{MW_n}\right) \leq 1.5 \qquad \Rightarrow \qquad MW = MW_n \qquad (2.22)$$

For live oil, the following empirical expression is used:

$$\left(\frac{MW_w}{MW_n}\right) > 1.5 \qquad \Rightarrow \qquad MW = MW_n\left(\frac{MW_w}{1.5\,MW_n}\right)^{0.5} \tag{2.23}$$

The coefficient 1.5 and the exponent 0.5 in above equations are well suited as tuning parameters if the match of the data needs to be improved.

The final scheme works as follows:

1. For equivalent temperature, T_o > 75 K, the original Pedersen model will be used.
2. For equivalent temperature, T_o < 65 K, the Lindeloff model will be applied.
3. For 65 K < equivalent temperature, T_o < 75 K, the weighted average will be taken between the values obtained by the two models to allow a smooth transition between two values.

In the above scheme, the equivalent temperature, T_o, is the pseudo-temperature at which the medium-heavy oil viscosity needs to be evaluated in order to obey the law of the corresponding states (Pedersen et al., 1984).

2.5 West Sak Reservoir

The West Sak reservoir overlies the Kuparuk River formation in the Kuparuk River Unit and is spread over an area of 260 square miles (DeRuiter et al., 1994). Sharma (1993) provides a comprehensive description of the West Sak reservoir.

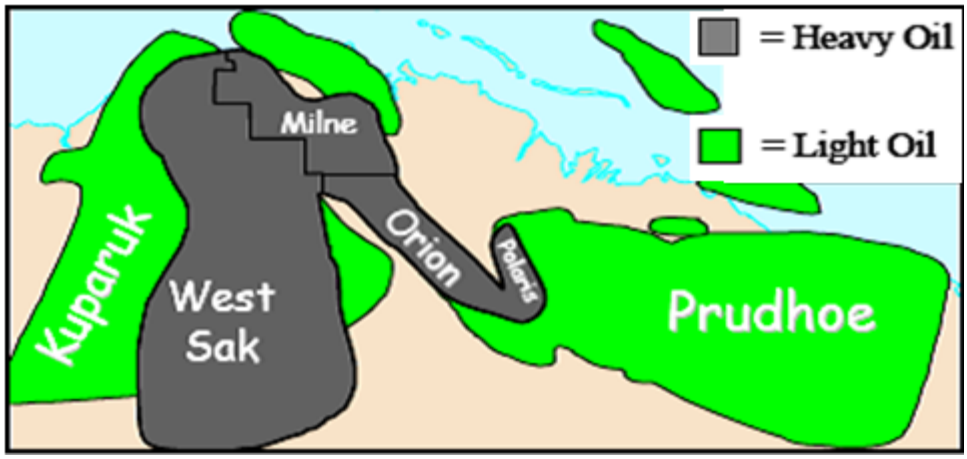

Figure 2.4 West Sak Location (Reconstructed from Targac et al., 2005)

The main challenge that the operators in the West Sak reservoir face has been the economical production of these highly viscous oils. Although water flooding has been moderately successful for the production of these heavy oils, the petroleum industry is on the lookout for alternative means of development like miscible or immiscible gas injection. The viability of any new technique should first be proven on a laboratory scale before its field application. Such a study requires extensive geological and petrophysical data such as, water saturation, porosity, and permeability, to simulate the actual reservoir conditions.

2.5.1 Geological Overview

A detailed geological description of the West Sak reservoir is given by Sharma (1993). Deposited during the late cretaceous and early tertiary, the West Sak sands are shallow marine and deltaic complex sands. Due to their great lateral continuity, they are of great economic importance. The Kuparuk River Unit and Milne Point Unit are both situated between the depths of 2,000 ft and 4,500 ft (1,141m and 1,231 m) below sea level; they are the main oil-bearing horizons within these sands.

The West Sak sands can be broadly divided into two members, the upper and lower. The average thickness is about 300 ft (91 m) in the Kuparuk River Unit and Milne Point Unit areas. The lower member exhibits individual sands beds with thicknesses ranging from 0.2 ft to 5 ft. The individual units characteristically show the presence of ripple bedding and hummocky cross stratifications. These lower member sands are inter-bedded with siltstone and mudstones. Bioturbation is also seen. The upper member exhibits two

distinctly divided and continuous sand units, each about 25 ft to 40 ft thick. The main sedimentary structures seen in this member include massive beds with planar bedding and low-angle cross bedding.

With the help of logs and core samples, a basic cross section of the sands can be visualized. The upper sands are divided into two members, while the lower sands are divided into four members. Thus the 6 individual sands occur as follows:

1. Upper West Sak Sand Member
   - Sand 1
   - Sand 2

2. Lower West Sak Sand Member
   - Sand 1
   - Sand 2
   - Sand 3
   - Sand 4

2.5.2 Petrophysical Properties

Porosity values of the West Sak sands vary a lot, ranging from 15% to 40%. Water saturation of the sands ranges from about 9% to 46%. Net pay thickness ranges from 1 ft to about 37 ft.

From the petrophysical data and its subsequent analysis, it can be seen that the two individual sands of the Upper West Sak Sand Member are the best reservoirs. Their porosity values are high and similar to the first two members (Sand 1 and Sand 2) of the Lower Member. But, the percentage water saturation in the Lower Member sands is noticeably higher. In Lower Sand 3, the water saturation is sometimes as high as 80%. The Lower Sand 4 is discontinuous. Also the net pay thickness is less in the Lower Sands, in many cases less than 10 ft.

This difference in the petrophysical characteristics of the Upper and Lower Sand Members has been attributed to their different depositional histories. The upper sands were deposited in shallow marine and delta front environments, resulting in cleaner and thicker sands, as compared to the Lower Sands, which were deposited in the shelf depositional environment.

2.5.3 Enhanced Oil Recovery

Oil recovery operation primarily utilizes the natural pressure energy of the reservoir in order to produce oil. Low recovery and short life span are problems with such

reservoirs. To enhance the productivity and life span of the reservoir, the industry started practicing secondary and tertiary/enhanced oil recovery methods (Green and Willhite, 1998).

The secondary oil recovery method, the second stage of operation usually follows the primary production decline. Water flooding has been identified as the best example of a secondary recovery process. There have also been instances where water flooding has been used as the primary oil recovery method. Water flooding utilizes the lower mobility in order to increase the overall recovery efficiency and also maintains the required reservoir pressure. Another example of a secondary recovery method is gas injection. Gas injection, as part of secondary recovery, maintains the required reservoir pressure condition.

Tertiary or enhanced oil recovery processes are associated with the injection of a specific type of fluid or fluids into a reservoir. The fluid injection supplements the natural energy left over in the reservoir and displaces the un-recovered oil. The increased interaction between the foreign fluid (injected fluid) and the in-place oil results in alterations in rock and fluid properties. Fluid injection and eventual interaction brings about changes like a lowering in interfacial tension, oil swelling, oil viscosity reduction, wettability modification, and sometimes favorable phase behavior conditions. These changes are mainly attributed to physics and the chemical interaction between the two fluids and also to the fluid injection rate and pressure.

2.5.4 Miscible Displacement Processes

Miscible displacement technique is one of the most popular EOR methods practiced to recover oil from heavy immobile oil reservoirs. The miscible displacement process increases oil recovery by increasing the miscibility at the interface of displacing fluid and the displaced fluid (oil). This is primarily carried out by altering the composition of the immobile heavy oil such that any interaction with an injected fluid of a certain composition will bring about a single miscible phase between the two fluids. Hence, the composition of injected gas is carefully chosen so as to maintain complete miscibility with the in-place oil.

A variety of displacement fluids are used in the miscible recovery process. Some of the most commonly used fluids are CO_2, flue gas, and nitrogen. Fluid selection depends

primarily on availability. Economics also plays a vital role in deciding the level of enrichment.

Displacement fluids have been broadly classified under two categories. The first types are fluids that cause first contact miscibility. Upon injection, these fluids form a single phase upon first contact when mixed in any proportion with the crude oil. The second type causes multi contact miscibility. Miscibility is achieved in situ through the compositional alteration of the crude oil and the injected gas as the displacing gas moves inside the reservoir and comes in contact with the oil several times.

Miscible displacement process substantially increases the microscopic displacement efficiency. Such high efficiency is not possible with water flooding. Water flooding successfully removes oil from big and medium-sized throats but fails to push out trapped oil in the form of isolated drops, stringers, or perpendicular rings etc. This behavior is mainly attributed to the capillary forces. After achieving such conditions oil flow essentially drops to zero and any further injection produces a negligible amount of oil.

Miscible injection technique smartly tackles this problem. The displacing fluid first eliminates the IFT between the in-place oil and itself and becomes a single phase system. The additional pressure produced by the injected fluid then provides additional energy to push the entire single phase out of the reservoir. The reduction in IFT makes the trapped oil mobile and the additional pressure energy is high enough to mobilize trapped oil by overcoming the capillary forces, thereby increasing the overall recovery from the reservoir.

2.5.5 Gas Injection

Oil fields on the Alaska North Slope have always been the target of enhanced oil recovery applications. Enhanced oil recovery is essential for the economic production of these extremely viscous oils. Water flooding has been the most widely used method since the success of water flood pilot project in 1983. Although it was successful, the results suggested a process that would yield a higher oil rate and recovery than water flooding alone would be needed. Naturally, since then efforts have been directed towards gas injection as an EOR technique. The abundance of gas streams on the Alaska North Slope makes this an attractive option (DeRuiter et al., 1994).

DeRuiter et al. (1994) performed phase behavior experiments on West Sak oil. They investigated the solubility of methane, ethane, propane, n-butane, and CO_2 in West Sak

oil. Their detailed work included complete characterization of two oil samples, 1 and 2, from the West Sak Reservoir (Lower and Upper West Sak intervals). The properties of the Lower West Sak interval oil sample (called Oil Sample 1 in this report, Table 2.1) match the type of oil chosen under the present study.

Oil Sample	Molecular Weight	Viscosity at 75°F	Density (g/cm^3) at 60°F
1	330	256	0.9433
2	446	5392	0.9725

Table 2.1 West Sak Oil Properties

Several static experiments were carried out by the team to estimate live viscosity, the live density of an oil sample under different pressure conditions. GOR was measured by flashing the live oil sample to atmospheric conditions. General properties like molecular weight and compositional analysis were also determined. Followed by static experiments they estimated the MMP and MME value by conducting slim tube experiments. The confirmation of miscibility was assumed to happen when oil recovery was higher than 90% and with absence of gas spiking before breakthrough.

DeRuiter et al. (1994) carried out all displacement experiments with Oil Sample 1. Slim tube experiments were performed with pure CO_2 and oil at 2000 psi. With CO_2 in liquid state, despite high displacement pressure, recovery was very low, indicating an immiscible displacement. When several runs were carried with ethane, good recoveries were obtained, indicating the presence of miscible displacement. During these experiments, they also observed some extent of two phase flow, confirming that the miscibility was not First Contact Miscibility. In these experiments, MMP was interpreted to be at the ethane liquefaction pressure.

DeRuiter et al. (1994) concluded that ethane developed miscibility with West Sak oil in its subcritical liquid state. Miscibility was observed to be of the multi contact type and followed a condensing-vaporizing mechanism. When using an enriched gas/lean gas combination they observed a transition from FCM to MCM to immiscible behavior by increasing the lean gas concentration. This transition was observed at enrichments of 42% methane. With further dilution up to 61%, the flow was immiscible but there was an increase in recovery. Recovery behaviors were observed to be unusual at high lean gas concentrations. This was mostly attributed to complex phase behavior of the oil-gas

system. Thus, DeRuiter's work gives an insight into the phase behavior of West Sak Oil and guides in choosing the optimum conditions for performing miscible injection.

Sharma et al. (1989) in their study of the miscible displacement of West Sak crude oil have also concluded that MCM can be developed for enriched gas drives by using a condensing-vaporizing mechanism.

2.5.6 Reservoir Simulation

The predictive capabilities of reservoir simulation software helps engineers design field scale projects. Miscible injection, as an alternative technique to other EOR techniques to enhance production, is dominated by compositional changes taking place due to mass transfer between various phases. To model such a process, a compositional simulator is an ideal choice.

GEM is Computer Modeling Group's advanced general EOS compositional simulator which includes options such as equation of state, dual porosity, CO_2, miscible gases, volatile oil, gas condensate, horizontal wells, well management, complex phase behavior and many more. GEM was developed to simulate the compositional effects of reservoir fluid during primary and enhanced oil recovery processes. GEM is an efficient, multi-dimensional, EOS compositional simulator which can simulate all the important mechanisms of a miscible gas injection process, i.e. vaporization and swelling of oil, condensation of gas, viscosity and interfacial tension reduction, and the formation of a miscible solvent bank through multiple contacts.

Chapter 3 EXPERIMENTAL WORK

3.1 Brief Overview of the Experiments Conducted

For the purpose of simulating the phase behavior and modeling viscosity, it was necessary to measure pressure-volume relationships and viscosities of heavy oils at reservoir conditions. The ANS heavy oils, when flashed to 65°F and atmospheric pressure, release solution gas containing 95% methane (Roper, 1989). Hence, CP grade methane was recombined with the dead crude oils from ANS heavy oil reservoirs to simulate live oils. Experimental tasks performed under this study consisted of the following:

1. Determination of recombined oil composition.
2. Measurement of stock tank oil properties.
3. Viscosity measurements of the dead crude oil at varying conditions of pressure and temperature.
4. Laboratory PVT tests: Constant Composition Expansion and Differential Liberation.
5. Density and viscosity measurements of live reservoir fluids during Differential Liberation.
6. Measurement of MMP using VIT technique

This chapter describes experimental design and procedure for each of the tasks listed above.

3.2 Determination of Composition of Recombined Oil

3.2.1 Simulated Distillation

Simulated distillation (SimDist) is a gas chromatography technique, which separates individual hydrocarbon components in the order of their boiling points, and is used to simulate the time-consuming laboratory-scale physical distillation procedure known as true boiling point distillation. The separation is accomplished with a non-polar stationary phase capillary column. A gas chromatograph is equipped with an oven, injector, and detector that can be temperature programmed. The result of simulated distillation analysis provides a quantitative percent mass yield as a function of the boiling point of the hydrocarbon components of the sample.

Figure 3.1 Thermo Gas Chromatograph (Trace GC Ultra)

Figure 3.1 shows the thermo gas chromatograph (Model: Trace GC Ultra) used for measuring gas and oil compositions. The chromatographer is equipped with Flame Ionization Detector (FID) and Thermal Conductivity Detector (TCD). Simulated distillation by gas chromatography technique was used to analyze the crude oil composition. Crude oil consists of large number of components having varying boiling points and elution times. Simulated distillation technique is based on an assumption that components of crude oil elute in order of their boiling points. Using a mixture of normal paraffins with known composition, a relationship was established between boiling points and retention times. This relationship was used to identify the components of crude oil and hence the composition of crude oil. ASTM D 2887(04), which covers the fractions until a boiling point of 1,000°F was used to determine the compositions of stock tank oils. The parameters of the method used to calibrate the gas chromatograph for simulated distillation of crude oil are listed in Table 3.1.

Column	Thermo TR-Simdist capillary column Length: 10m Diameter: 0.53 mm (ID)
Oven program	Start Temperature: 35°C hold for 1.5 minutes Ramp: 10°C /minute Final Temperature: 350°C hold for 10 minutes
Carrier gas	Ultra pure grade helium Flow rate: 15 ml/min
Injector	Split injection Split ratio: 20:1 Sample injection volume: 1µl Injector temperature: 350°C
Detector	FID Base body temperature: 350°C Hydrogen flow rate: 35 ml/min Air: 350 ml/min Make up gas (Helium): 30 ml/min
Reference standard	ASTM D 2887 Calibration mix

Table 3.1 Parameters for Simulated Distillation Method

3.2.2 Calibration Method

ASTM D 2887 mix (Methylene chloride as solvent) with following composition was used for purpose of calibration.

Elution order	Compound	Concentration % wt/wt	Purity %	Uncertainty %
1	n-Hexane (C6)	6	99	+/- 0.02
2	n-Heptane (C7)	6	99	+/- 0.02
3	n-Octane (C8)	8	99	+/- 0.02
4	n-Nonane (C9)	8	99	+/- 0.02
5	n-Decane (C10)	12	99	+/- 0.02
6	n-Undecane (C11)	12	99	+/- 0.02
7	n-Dodacane (C12)	12	99	+/- 0.02
8	n-Tetradecane (C14)	12	99	+/- 0.02
9	n-Hexadecane (C16)	10	99	+/- 0.02
10	n-Octadecane (C18)	5	99	+/- 0.02
11	n-Eicosane (C20)	2	99	+/- 0.1
12	n-Tetracosane (C24)	2	99	+/- 0.1
13	n-Octacosane (C28)	1	99	+/- 0.1
14	n-Dotriacontane (C32)	1	99	+/- 0.1
15	n-Hexatriacontane (C36)	1	99	+/- 0.1
16	n-Tetracontane (C40)	1	99	+/- 0.1
17	n-Tetratetracontane (C44)	1	99	+/- 0.1
Solvent	Methylene chloride		99.8	

Table 3.2 Composition of Reference Standard

The calibration standard was diluted with methylene chloride solvent (chromatographic grade) and various concentrations of solutions were prepared. This allowed the calibration of FID response to a particular compound over a range of concentrations. Figure 3.2 shows a chromatogram for one calibration run for the simulated distillation method.

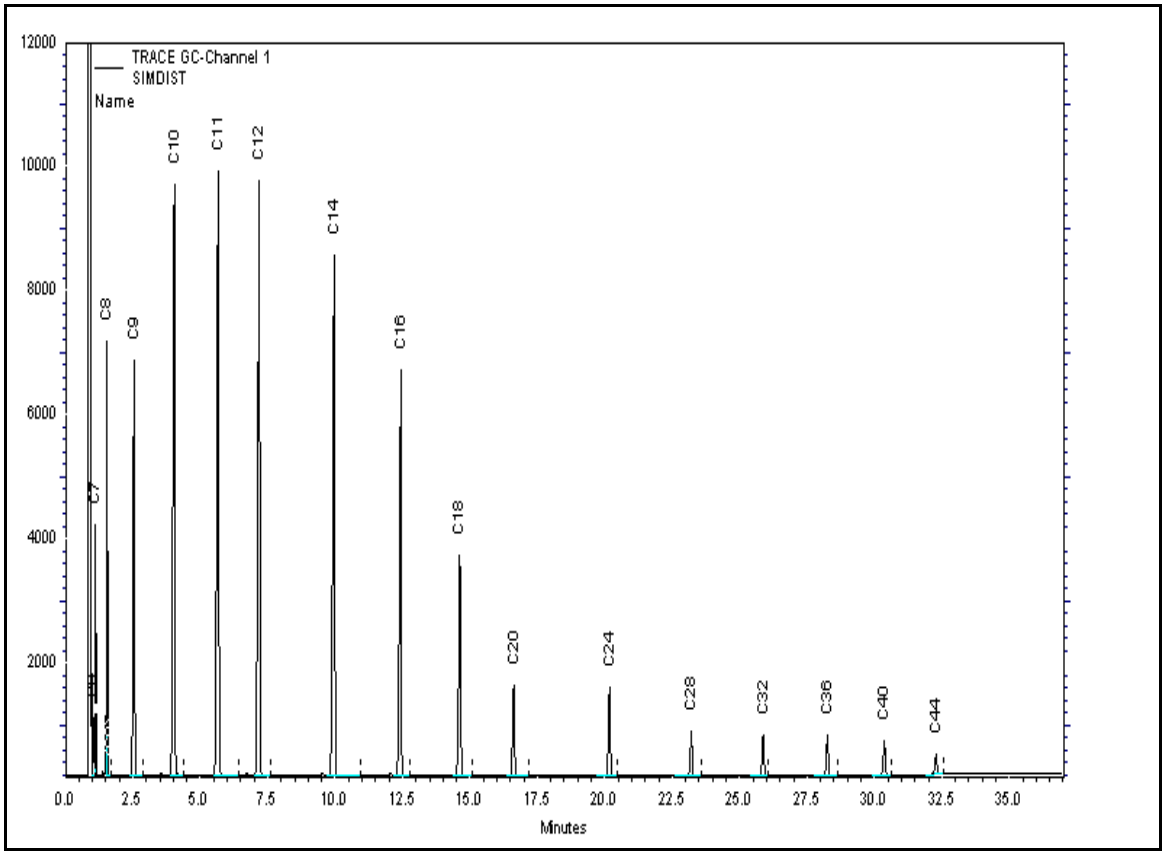

Figure 3.2 Calibration Run for Simulated Distillation

Response factors for the components of a calibration standard of known composition are calculated using Equation 3.1.

$$K = M/P \quad (3.1)$$

Where,

K = response factor

M = weight of component in reference standard, μg

P = peak area of each component

The concentration of each of the components in the unknown sample is then calculated using Equation 3.2

$$M = P \times K \quad (3.2)$$

Where,

M = weight of component in unknown sample

P = peak area of each component in unknown sample

K = response factor.

Response factors of n-paraffins were calculated over a range of concentrations and averaged to get best fit. Response factors of n-paraffin compounds not present in the calibration mix were extrapolated from the plot of Carbon Number vs. Response Factor. Average retention time of every paraffinic compound present in the calibration mix from the calibration runs was correlated with its atmospheric equivalent boiling point (AEBP). The atmospheric equivalent boiling range of single carbon number fractions from a generalized properties table (After Katz and Firoozabadi 1978) was superimposed on the boiling point and elution time correlation obtained from calibration runs. Using this superimposition the boiling range of single carbon number fractions was correlated with elution times.

3.3 Determination of Density of Stock Tank Oil

The density of oil at stock tank conditions is required to calculate the plus fraction specific gravity, an important parameter required to predict the critical properties of plus fraction and to check consistency of compositional data. Most commonly used correlations for estimation of critical properties of plus fraction require molecular weight, specific gravity or normal boiling point of the same.

The experimental set-up is designed to measure density of sample at atmospheric pressure. It consists mainly of an Anton-Paar digital density meter DMA 45 and a circulating constant temperature bath (Brookfield TC-500). This experimental set-up was used in conjunction with the most current revision of ASTM D4052, Density and Relative Density of Liquids by Digital Density Meter, to analyze the density and relative density of petroleum distillates and viscous oils by digital densitometer. The sample temperature is maintained through the circulation of an ethylene glycol water mixture. The density meter DMA 45 determines the density of liquids and gases by measuring the period of oscillation electronically. The oscillator is excited by the electronic part of the meter. The period of oscillation is measured by a built-in quartz clock, every two seconds. The value is transmitted to a built-in processor which calculates density and displays the value in the digital display. Prior to measuring the density of each sample using the density meter DMA 45, the equipment was calibrated. The constants A and B

relate the density of the fluid with measured period of oscillation. After each density measurement, the samples were flushed from the sample tube by giving a proper toluene wash followed by an acetone wash and drying the tube using air.

Figure 3.3 Anton-Paar Densitometer Used for Density Experiments

3.3.1 Calibrating Procedure

To calibrate the densitometer, the desired temperature was set on the constant temperature bath and allowed to equilibrate. Calibration constants A and B are required to calculate the specific gravity of a sample at particular conditions. Constants A and B are functions of temperature and pressure. The calibration constants A and B were determined by injecting water and air into the densitometer and measuring the period of oscillation, T_w and T_a (by setting the display selector beneath the cover plate on top of the DMA 45 density meter to position "T"). After recording the value of T_a and T_w at a particular temperature, the density of air at the set temperature was calculated by using Equation 3.3a (Igbokwe 2006).

$$\rho_a(g/ml) = 0.001293(273.15/T) * \frac{P}{760} \qquad (3.3a)$$

Where,

T = temperature, K

P = barometric pressure, torr

Using a sample calculation for the density of air at 22°C and from Equation 3.3a:

$$\rho_a = \left[\frac{0.0012930}{1+(0.00367*t)}\right]*\frac{P}{760}$$

$$= \left[\frac{0.0012930}{1+(0.00367*22)}\right]*1$$

ρ_a = 0.001196402 g/cc

The density of water at the various test temperatures was obtained from the table illustrating the density of water (refer to the Laboratory Manual for standard ASTM D 4052-96, 1996). Thus, the constants A and B in Equations 3.3b and 3.3c, respectively, were calculated from the observed T-values and reference density values for air and water using the following:

$$A = \frac{\left(T_w{}^2 - T_a{}^2\right)}{\left(\rho_w - \rho_a\right)} \quad (3.3b)$$

$$B = T_a{}^2 - (A*\rho_a) \quad (3.3c)$$

3.3.2 Experimental Procedure

1. The selector switch was set to position "ρ" to measure density. A small quantity of sample (about 0.7 cc) was introduced into the clean, dry sample tube using a suitable syringe. The amount of sample introduced was enough to fill beyond the suspension point on the right-hand side.
2. The sample was allowed to equilibrate to the test temperature before proceeding to evaluate the test sample for the presence of unseen air or gas bubbles. The illumination light was switched "off" immediately after verification, because the heat generated could affect the measurement temperature.
3. The value on the display was recorded once the instrument displayed a steady reading to four significant figures for density and five for T-values, indicating that equilibrium density or temperature respectively had been attained.
4. The sample tube was flushed, dried and the density calibration checked prior to introducing another sample. Steps 1 to 4 were repeated each time a new sample was introduced.

3.4 Determination of Molecular Weight of Stock Tank Oil

Molecular weight of the stock tank oil is required to calculate the molecular weight of the plus fraction component. Cryette A (Figure 3.4) is a precise instrument for measuring the molecular weight of a substance by tracking freezing point depression. The freezing point of a solution is a measure of its concentration or molecular weight. Cryette A consists of specially designed refrigerator with controls to maintain a reproducible environment for the sample, a precision thermometer, and apparatus to hold and seed the sample. Addition of seed could contaminate the sample causing it to freeze unexpectedly hence the seeding is initiated by agitation, thereby preventing the contamination. Cryette A is capable of measuring the freezing point change of 0.001°C.

Figure 3.4 Cryette A for Molecular Weight Measurement of Stock Tank Oil.

3.4.1 Calibration of Instrument

Prior to use calibrate the equipment for the range of interest. The Cryette A is calibrated for the range of interest by running a solute of known molecular weight in benzene solvent. The following procedure was adapted for calibrating Cryette A for organic solutions.

1. The Range switch was placed in left position and bath temperature was allowed to stabilize.
2. Benzene saturated with water to arrest the evaporation losses, was run and allowed to seed. After seeding, the head switch was lifted and lowered again. Adjustment (by moving trimpot to left of the Range switch) on solvent zero was continued until the display read 000.
3. Another sample of water saturated benzene was run and this time calibrator I was adjusted so that the display read 000.
4. Sample of Hexadecane (Mol wt 226.45) diluted with benzene was run and calibrator II was adjusted until the display reading indicated an equivalent freezing point depression resulting in a molecular weight of 226.45. Equation 3.4a relates the freezing point depression with molecular weight and solution concentration. Using Equation 3.4a the freezing point depression (ΔFP) corresponding to molecular weight of Hexadecane was calculated.

$$\Delta FP = \frac{Kf \dfrac{W_{Solute}}{W_{solvent}}}{\dfrac{Mw}{1000 gofsolvent}} \qquad (3.4a)$$

Where,

Kf = freezing point depression of benzene 5.12°C/mol

Mw = molecular weight of solute

W_{Solute} = weight of solute. gms

$W_{solvent}$ = weight of solvent, gms

3.4.2 Operating Procedure

1. Solutions of crude oil with benzene were prepared with a weight ratio of solute to solvent at least 1:25. With lower concentration of solute the variation in Kf is reduced.
2. A 2.5 ml sample was placed into the refrigerator well. The operating head was lowered so that the stirrer and probe entered the sample in the tube.
3. The display reading is -1 when the probe is at ambient temperature and indicates cooling of the sample by becoming positive towards 000 and then running to 1000.

4. On reaching 1000 the seeding takes place by a one-second high amplitude vibration of the rod.
5. The seed light will blink once or twice as sample is successfully seeded. The display was read when the red light turns on. This reading is the actual freezing point depression due to presence of the solute.
6. Equation 3.4b was applied to calculate the molecular weight of the oil.

$$Mw = \frac{Kf \dfrac{W_{Solute}}{W_{solvent}}}{\dfrac{\Delta FP}{1000 gofsolvent}} \qquad (3.4b)$$

3.5 Recombination of Stock Tank Oil

At stock tank conditions oil contains a negligible amount of gas. To simulate live oil, the gas needs to be dissolved into dead oil at the existing gas/oil ratio. ANS live heavy oils when flashed at 65°F yielded separator gas with 96.9% and 98.3% methane for separator pressures of 114.7 psia and 314.7 psia, respectively (Roper 1989). CP grade methane was recombined with stock tank ANS oils at reservoir conditions and at the known gas/oil ratio. Experiments to quantify phase behavior of heavy oils were carried out on these recombined oils. Recombination was carried out in a PVT cell capable of withstanding high pressures (up to 10,000 psig) equipped with a rocking mechanism to speed up the dissolution of gas into the oil. Guidelines provided by McGuire et al. (2005) were followed for the recombination.

3.6 PVT Apparatus Set-up

The schematic of the PVT set-up used in this study is shown in Figure 3.5. The PVT cell capable of handling pressures up to 10,000 psi and temperature up to 350°F is housed in a constant temperature air bath for maintaining the test temperature. An integrated system of valves and tubing is used for purpose of charging and withdrawing the sample. A window is located in one end of the cylinder and is compressed sealed on the periphery. The PVT cell piston has a connecting rod attached to a linear variable – displacement transducer (LVDT) for measuring the position of the piston. The cell is provided with a rocking system and designed so that rocking speed and rocking angle can be easily adjusted as desired. A variable speed motor mounted to the outside oven wall works through a shaft to rock the cell. The liquid contents of the cell may be observed

and measured using software (Smartlevel-3) and a camera located outside the air bath. Operating procedure for PVT cell system is described in the following sections.

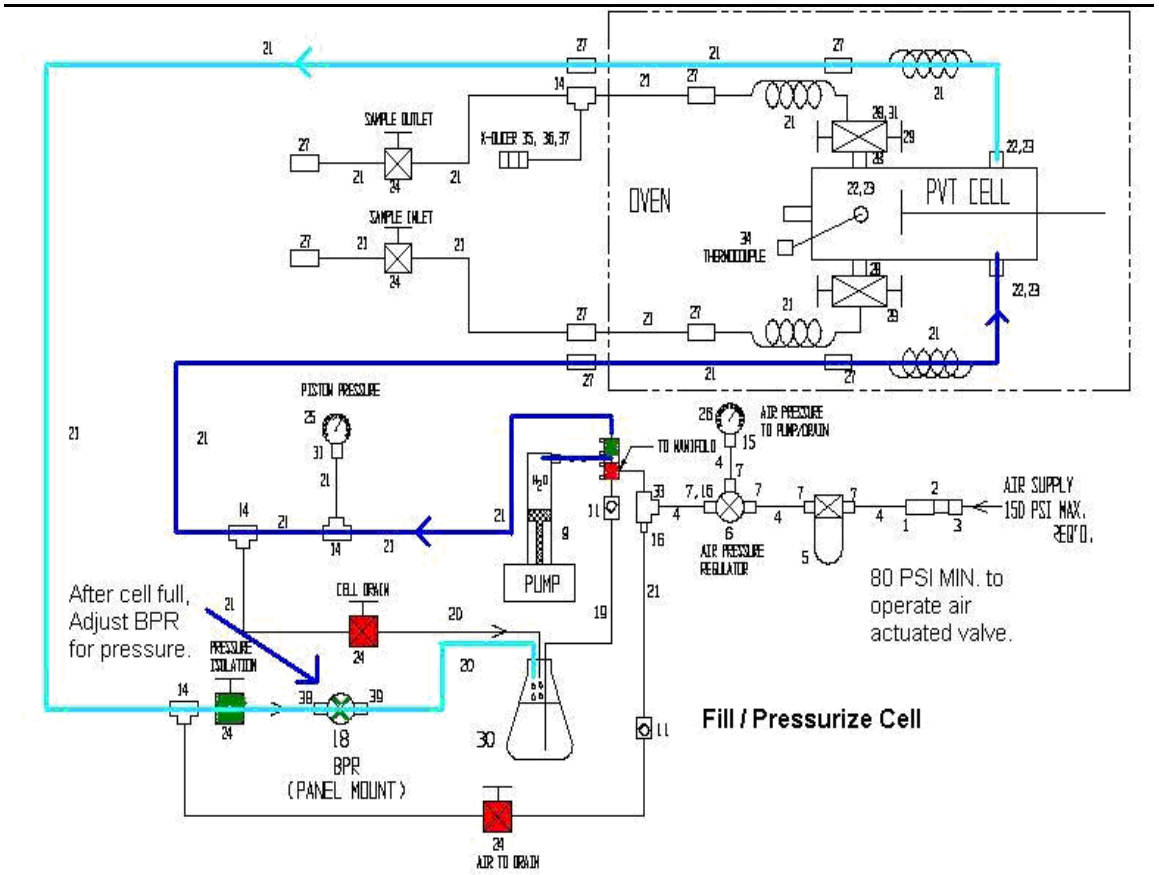

Figure 3.5 Schematic of PVT Cell (Temco Inc.)

3.6.1 Computation of Pressure and Temperature Factors

Under pressure and temperature the PVT cell expands slightly. This increases the volume of the system. This cell expansion was calibrated with the pressure and the temperature through the pressure factor and the temperature factor.

1. A measured amount of fluid of known compressibility (water) was injected on sample side of the cell and the cell was pressurized to 100 psig.
2. Pressure was increased in steps of 1000 psi until maximum operating limit, noting the volume at each step by recording the piston position.
3. The ratio of calculated volume (with compressibility of fluid injected) and measured volume is the expansion factor of the cell.
4. The thermal expansion coefficient for stainless steel was taken as temperature expansion factor.

3.6.2 Recombination Procedure

1. The two piston halves were tightened using the bolts to energize the seal on the piston.
2. The PVT cell was evacuated through the lower valve by connecting the valve to a vacuum pump.
3. A gas cylinder was connected to the sample outlet valve. The bottom valve of the PVT cell was kept closed as the sample outlet line was filled and the system was checked for possible leaks.
4. If no leaks were observed, the recombination gas was injected into the PVT cell by slowly opening the bottom valve of the PVT cell and the pressure on the sample side of the PVT cell was recorded.
5. Gas injection was stopped once the required moles of gas were injected.
6. The back pressure regulator (BPR) was set to a value somewhat higher than equivalent of the cell pressure.
7. The cell should be pointing upwards.
8. Close the valve and, using the BPR, set the pressure to the specified bubble point for the sample.
9. An Isco syringe pump was used to pressurize the PVT cell. The Isco pump was connected to the PVT cell piston end through an air-actuated CV series valve. This valve requires 80 psig of air supply to actuate and allow the pump to pressurize the PVT cell.
10. Using another Isco (syringe pump), the dead oil was charged from the sample cylinder through the sample inlet valve into the PVT cell at a pressure higher than the gas pressure in the PVT cell.
11. Once the required amount of oil sample was charged into the cell, the pump was stopped. LVDT reading will indicate how much sample has been injected into the cell.
12. With the cell drain open initially, the air in the pump was pushed out through cell drain. Once water starts draining into reservoir, the cell drain valve was closed.
13. The drive air pressure was increased beyond 80 psig and the pump was started with the pressure isolation valve closed and the back pressure regulator set to maximum position.

14. Once the sample side pressure reached the bubble point pressure, the pressure isolation valve was opened and the BPR was adjusted to equivalent of hydraulic pressure.
15. Temperature of the constant temperature bath was set to reservoir temperature and the motor was switched on so the cell starts rocking. All the sample inlet and outlet valves were in closed position at this stage.
16. The sample was rocked for 36 hours and then kept standing for 8 hours before any test could be conducted on the sample.
17. It was ensured that the sample was in single phase by recording the images with a camera before testing for phase behavior.

3.6.3 Constant Composition Expansion

1. The pressure on the sample was increased well beyond the anticipated bubble point (600-700 psi) with help of a pump and the BPR was set to an equivalent value.
2. The pump was stopped by reducing the drive air pressure below 80 psig.
3. Pressure on the sample side was decreased in steps of 100-200 psi by turning the BPR counterclockwise. The PVT cell was rocked until pressure equilibrated.
4. LVDT reading was recorded by initiating the logging in the software (Smart level3).
5. The cell was observed through a camera for possible bubble formation. (Cell has to be in upward position to see first bubble). When the sample first reaches two-phase (formation of bubble), the bubble point pressure had been reached.
6. This procedure was continued below bubble point.

3.6.4 Differential Liberation Test

Differential liberation study is performed by reducing the pressure within the cell by a fixed amount at constant temperature. Once equilibrium has been reached, the gas and liquid volumes are measured. Equation of state tuning and viscosity modeling requires density and viscosity data of residual oil at every step of the differential liberation test as gas is removed from cell. Measurement of density and viscosity was carried out by connecting a densitometer and a viscometer online with the PVT cell in series through the

lower sampling valve. Figure 3.8 shows the assembly of the PVT cell with a densitometer and a viscometer. The following sections briefly explain operating procedure for the online densitometer and viscometer.

3.6.4.1 Density Measurement of Live Oil Sample

A DMA 512 P density measuring cell was used to measure the densities of live oil samples. This cell is designed to measure density of liquids and gases under high pressures and high temperatures. Pressure range for continuous operation is 0 to 10000 psia and the temperature range is -10°C to 150°C. When used for high temperature high pressures measurements, the DMA 512 P forms one part of the complete set-up. Evaluation unit mPDS1000 is a powerful processor and display unit connected to the DMA512 P cell as shown in Figure 3.6.

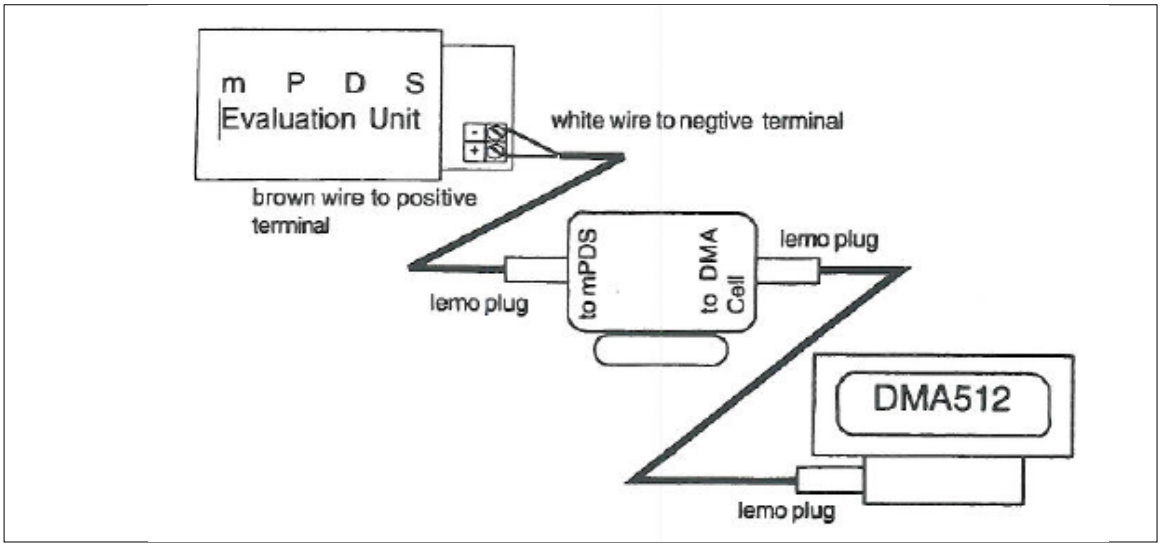

Figure 3.6 Connection of DMA 512 P Cell with mPDS Evaluation Unit

3.6.4.2 Calibration of Densitometer (DMA 512 P)

For calibration of the DMA 512 P two calibration parameters must be fed to the mPDS1000 unit. These calibration parameters, namely A and B, are functions of pressure and temperature for a particular fluid. Two standards of known densities at different temperatures and pressures were used for calibration. An mPDS evaluation unit was kept in mode, in which the period of oscillation is displayed. Standards selected were distilled water and nitrogen. These standards were injected into the DMA 512 P cell kept in constant temperature bath to maintain the required temperature. With the use of different calibration standards there is chance of contamination hence it is important to have clean

and dry tubing, for accurate and relatively stable readings. The densitometer was connected to PVT cell through the lower sampling valve and a digital pressure gauge was connected to the outlet of U tube of densitometer. Periods of oscillation were recorded for a range of pressures and temperatures for both the standards. The range was decided by operating pressures and temperatures of phase behavior experiments. Following equations were used to calculate the calibration parameters A and B.

$$A = \frac{(\rho_1 - \rho_2)}{(t^2_1 - t^2_2)} \tag{3.5}$$

$$B = \frac{(\rho_1 \times t^2_2 - \rho_2 \times t^2_1)}{(t^2_1 - t^2_2)} \tag{3.6}$$

Where,

ρ_1 = density of standard 1, g/cc

ρ_2 = density of standard 2, g/cc

t_1 = period of oscillation of for standard 1, μs

t_2 = period of oscillation of for standard 2, μs

3.6.4.3 Operating Procedure

1. Values of A and B at prevailing condition of pressure and temperature were stored into the memory of the mPDS evaluation unit before measurement.
2. The mPDS evaluation unit was set to indicate density values in units of choice. Sufficient time (about 5 minutes) was allowed for density readings to stabilize and the time average reading was taken as final reading.

3.6.4.4 Viscometer

A Cambridge SPL 440 viscometer (Figure 3.7) was connected to the outlet of the densitometer U tube (Figure 3.8). This viscometer is designed to withstand high pressures up to 10,000 psia and high temperatures up to 150°C. Two electromagnetic coils move the piston back and forth at a constant force. The piston's two-way travel time is used to measure absolute viscosity of the fluid surrounding it. A built-in temperature detector (RTD) senses the actual temperature in the sampling chamber. Fluid flows through ¼ inch OD, (0.086 inch ID) tubing into the measurement chamber. Fluid viscosity is measured under low flow or static conditions. The system measures viscosity, temperature, and temperature compensated viscosity.

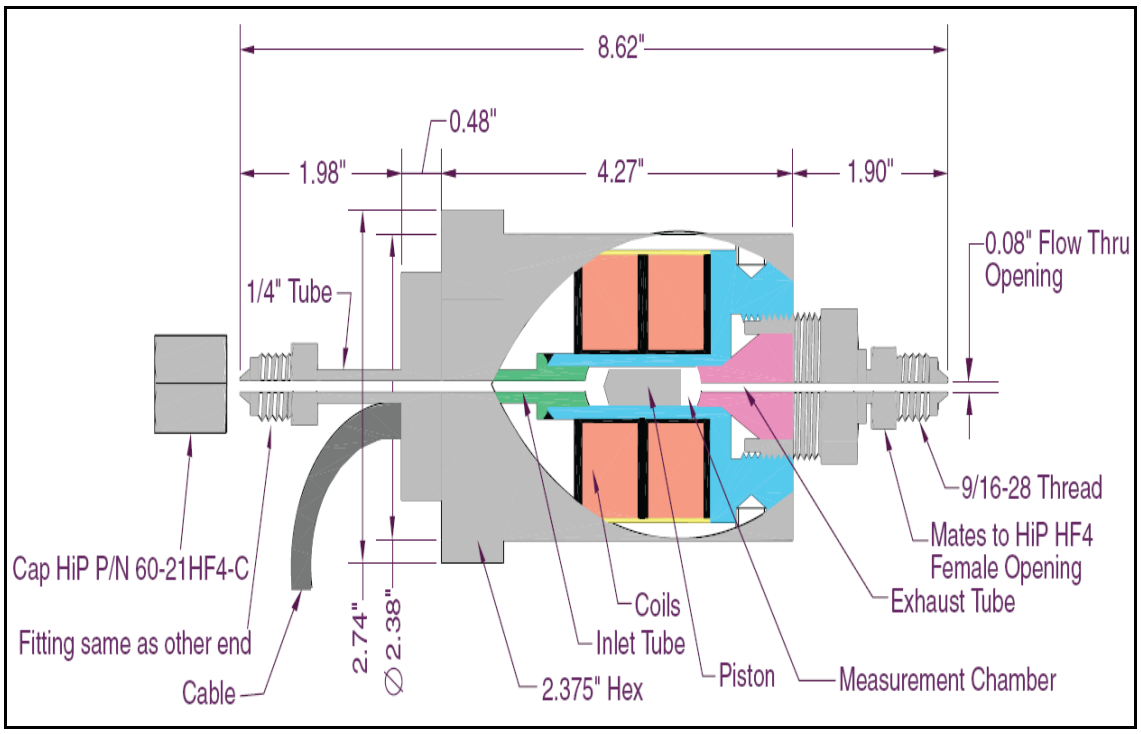

Figure 3.7 Cross-Sectional View of Cambridge VISCOLAB PVT Viscometer (SPL 440).

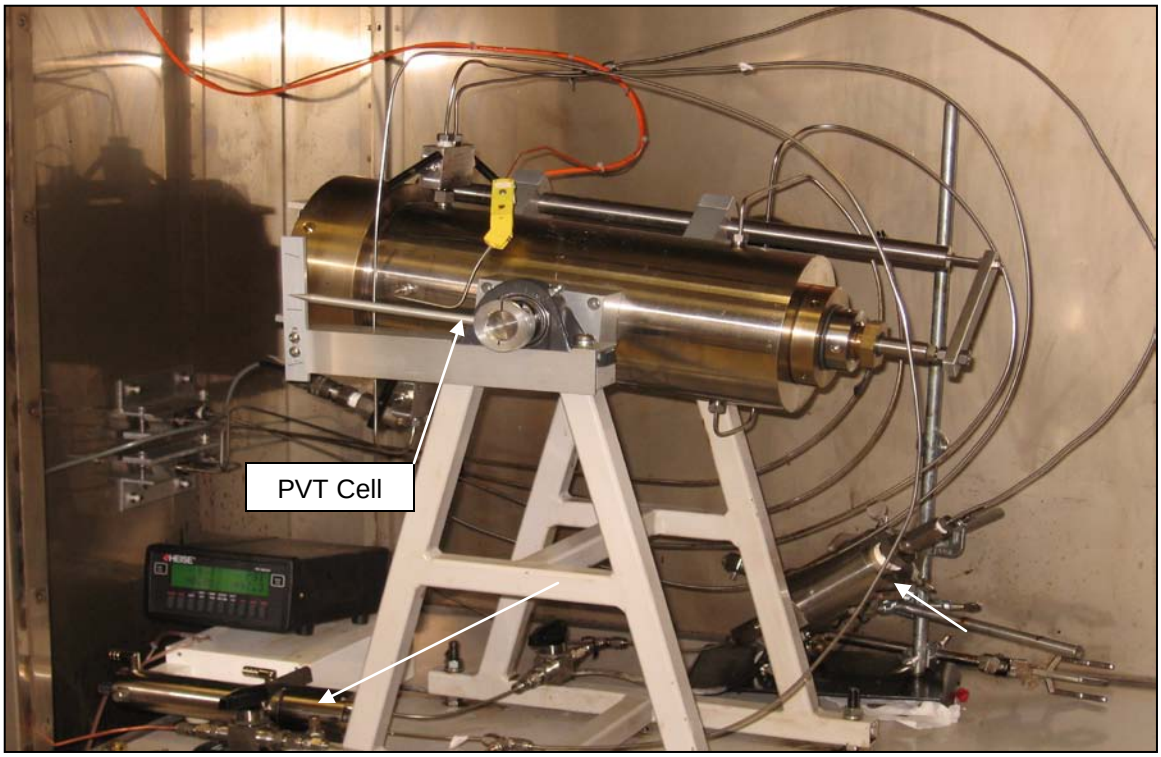

Figure 3.8 Assembly of PVT Cell with Online Densitometer and Viscometer

3.6.4.5 Operating Procedure for Differential Liberation

1. The system was evacuated through the intermediate valve in the PVT set-up and was checked for any leaks.
2. The PVT cell was initially brought to desired operating conditions of pressure and temperature. Pressurized oil was passed through inline densitometer and viscometer by sequentially opening the online valves.
3. The cell was rocked until the pressure indicated on the intermediate pressure gauge stabilized.
4. Density constants A and B were entered into the mPDS evaluation unit, placed outside the constant temperature bath. Rocking of the cell was continued until the single phase condition was reached.
5. The viscosity reading was noted on the viscometer digital display (Visco Pro2000) placed outside the constant temperature bath.
6. The computer connected to PVT cell panel, was initiated to record the pressure, temperature, piston position, and pump pressure readings.
7. The pressure was decreased in steps of 100-200 psi.
8. Once the bubble point pressure was passed ,the image acquisition from the camera mounted outside the constant temperature bath, was initiated for measuring the phase volumes. Phase volume measurement involves locating the gas/oil interface. Once a clear interface was obtained the gas volume was measured. (Refer to Figure 3.9)
9. Gas was removed through the upper sampling valve at constant pressure on the top of PVT cell with the cell in a horizontal position. (Refer to Figure 3.5) Steps 3 to 7 were repeated for every pressure stage.
10. The gas was trapped between the upper sampling valve and the sample outlet valve.
11. The trapped gas was passed into a gasometer (Ruska) where it was expanded to atmospheric pressure and its volume was measured.
12. Toward the test end the sample pressure was reduced to atmospheric pressure by opening the BPR completely. There could be a build-up of pressure as gas is released on decreasing the pressure. The upper sampling valve was kept open to 14.7 psia pressure and the gas was measured in gasometer.

13. Residual liquid volume was measured and then the cell temperature was decreased to 60°F.
14. Finally liquid volume at 60°F was measured.
15. Using a hydraulic pump the remaining oil sample was displaced from the cell through the lower sampling valve (upper sampling valve closed) and the volume measured. This reading should be close to the liquid volume readings of the previous two steps.
16. The cell was cleaned by cycling cleaning solvents (Toluene and Acetone) through the PVT cell and auxiliary lines to ensure a clean system for future runs.

Figure 3.9 Measurement of Phase Volumes through Acquired Image

3.6.5 Viscosity Measurement of Stock Tank Oil Samples

Viscosity modeling requires data on the viscosity of flashed oils as a function of pressure and temperature. A separate set-up (Figure 3.10) was constructed to measure dead oil viscosity data. The set-up consists of a viscometer connected in series with a floating piston sample cylinder. The downstream end of the viscometer was connected to a digital pressure gauge. Temperature control was achieved by placing the viscometer in a constant temperature oven. An Isco syringe pump, mounted outside the constant temperature oven, was used to pressurize the sample in the sample cylinder. Viscosity measurements were carried out for oil (medium-heavy to heavy) samples from ANS between the temperature range of 28°C and 45°C and pressure range of 14.7 psia and 2,500 psia.

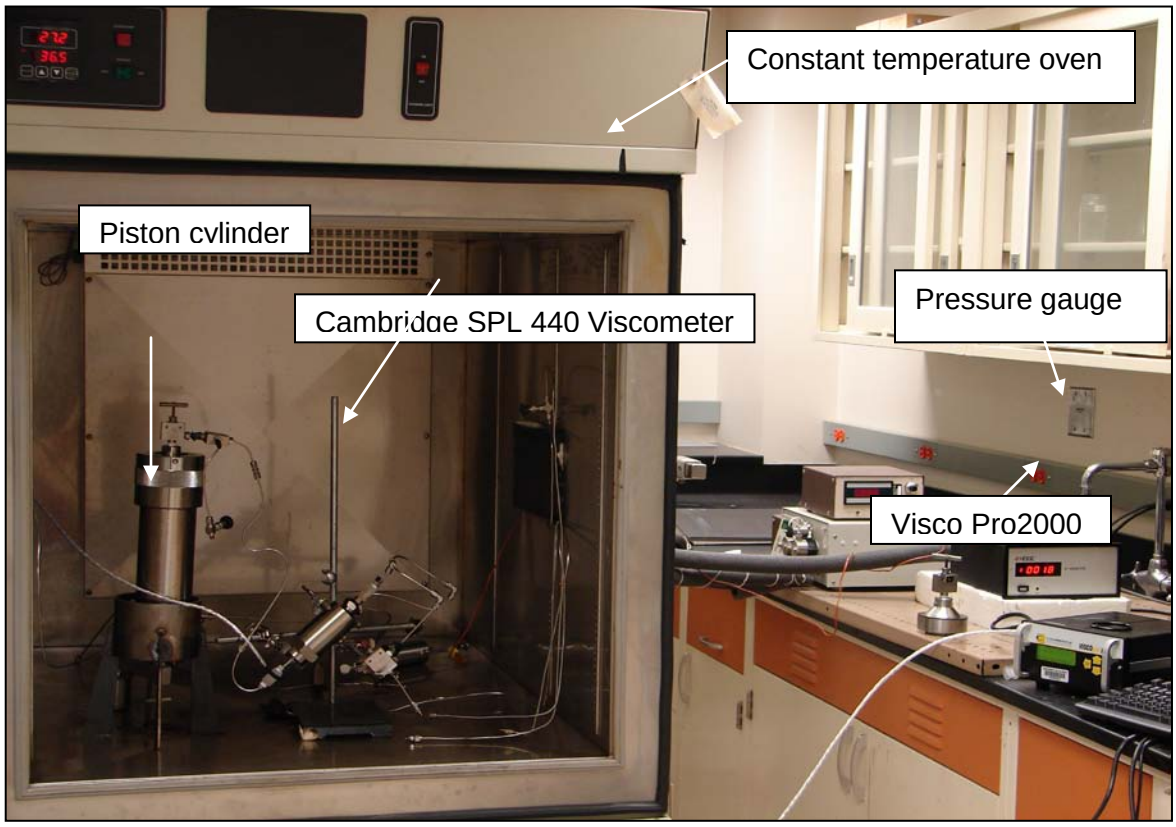

Figure 3.10 Set-up for Viscosity Measurement of Flashed Oils

3.7 Measurement of MMP Using VIT Technique

3.7.1 Experimental Set-up

In this study, the ADSA technique for pendant drop analysis was used to measure the dynamic and equilibrium IFT between the oil/gas systems. Figure 3.4 shows the experimental set-up of the VIT apparatus and Figure 3.5 shows the inside of the optical cell. The IFT set-up consists of a high-pressure optical cell made of stainless steel manufactured by Temco, with glass sapphire windows on the opposite side. The optical cell consists of a capillary tube (needle) at the top, through which oil drops are allowed to hang within the surrounding gas phase. A fluid handling system consisting of a piston pressure vessel and high pressure pumps was used to achieve elevated pressures. The glass windows allowed the capture of drop profile images by using a light source on one side and a camera system on the opposite side. A CF memory flash card stored the pictures recorded by the camera, which were later transferred to a computer for drop-shape analysis.

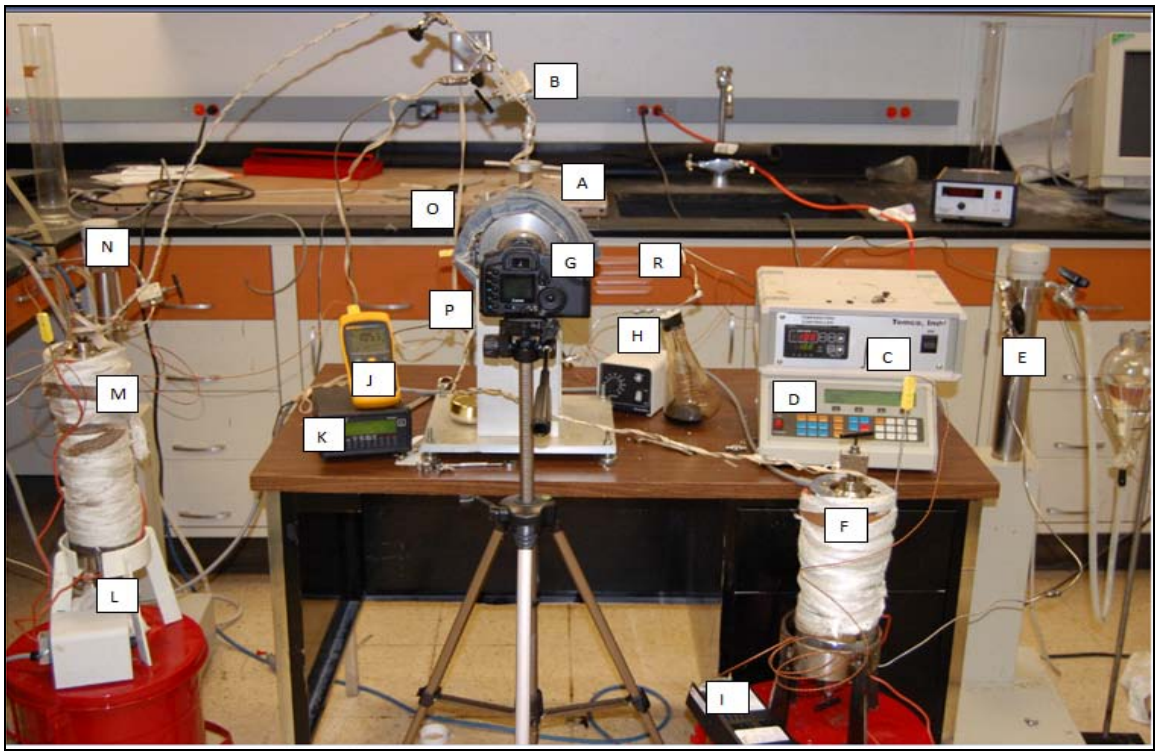

Figure 3.11 Experimental Set-up of MMP Apparatus

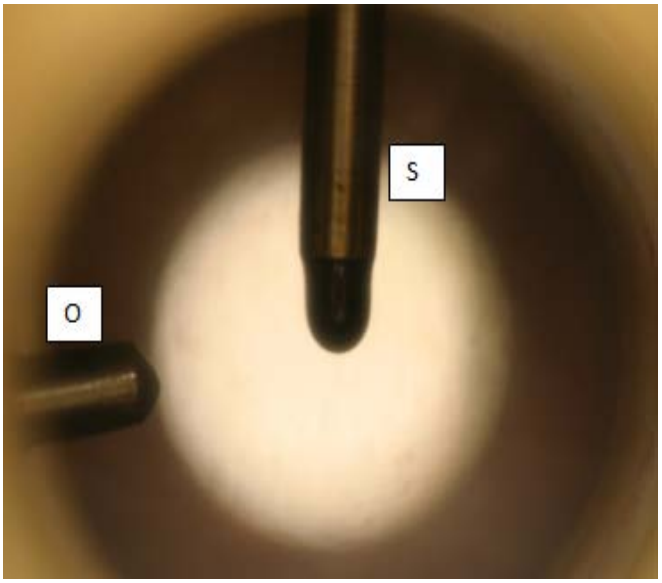

Figure 3.12 Inside Optical Cell

The components (letter codes) shown in Figures 3.11 and 3.12 are described as follows:

A. Optical Cell

The optical cell used in the set-up is rated for use up to 5,000 psi at 300°F. The cell is made of stainless steel and is manufactured by Temco. The cell was heated to the desired

temperature using metallic heating bands clamped to the outer periphery of the cell. The temperature was controlled using a Temco temperature controller “C”, which sensed the temperature from thermocouple “O”. The inside of the cell consists of an adjustable stainless steel needle “S” with an O.D. of 3 mm. The pressure inside the cell was maintained by the injection of pressurized miscible gas and was read from the digital Heise pressure gauge “K”.

B. Non-Return HIP Valve (Oil Inlet Valve)

The non-return HIP valve is made of stainless steel and is capable of handling pressures up to 15,000 psi. The valve was connected to the needle “K”. The valve was instrumental in adjustment of the flow rate of the oil droplets. By precisely adjusting the knob the desired shape of the oil droplets could be formed in the optical cell “A”.

C. Temco Temperature Controller

The temperature controller was used to maintain a desired temperature inside the optical cell. The thermocouple “O” was connected to the temperature controller for adjusting the temperature.

D, E, &N. Controller for ISCO D Series Pump “E”

The ISCO pump is a positive displacement pump used to maintain the pressure inside the oil and gas accumulators. The pump is capable of delivering 3,750 psi and can handle 500 ml of water, used for pressurizing. The controller was used on constant pressure mode to enable the pump to deliver the constant pressure required. The water used was de-ionized water, as per the instruction manual.

F & M. Accumulators for holding oil and gas

The accumulators used were manufactured by Temco and are made of stainless steel. The accumulators are capable of handling 10,000 psi, and contain a PVC piston which helps in pressurizing the fluids contained inside them. The fluid to be pressurized was injected on top of the piston and the bottom part of the piston was pressurized by injecting water using the ISCO pump. The accumulators were heated using silicon heat tapes which were controlled by controllers “I” and “L”. The heating tapes were covered with cotton insulation to avoid heat loss.

G. Camera

A Canon EOS 10D camera was used to record the drop shape images inside the optical cell. The camera was equipped with a high power macro lens for photographing

better pictures of the drop shapes. The camera was operated in sports sequence photography mode so that images of the drop trajectory could be effectively captured.

H, I, & L. Temperature Controllers

Glass-col temperature controllers were used to maintain the temperatures inside the accumulators and the tubing. The temperature in the accumulators and tubing was read off the Fluke thermometer "J". Thermocouples were placed inside the accumulators and on the side of the tubing. These thermocouples were connected to the thermometer "J" to regulate and control the desired temperature.

J. Fluke Thermometer

The Fluke thermometer has multiple inlet ports for plugging in the thermocouples. The thermometer has a digital display and temperatures can be read in °C or K.

K. Heise Pressure Gauge

The Heise pressure gauge has dual input ports for determining pressures of two points. The gauge is capable of handling pressures from the range of 0-5,000 psi. The digital display screen on the gauge makes it easy to read correct pressure inside the optical cell.

P. Gas Inlet Valve

Swagelok high pressure valves were fixed to the optical cell for a gas inlet into the cell. The valves were capable of handling pressures of up to 5,000 psi.

R. Drain/Vacuum Port

The drain/vacuum port was connected to the following:

1. A Welch duo-seal vacuum pump at the start of the experiment to remove traces of air present in the entire set-up.
2. A conical flask to collect the oil/gas mixture after the experiment was over.

3.7.2 Calibration of the Set-up

The cell was calibrated using water and nitrogen. The surface tension of water with nitrogen at atmospheric pressure is known to be 72 dynes/cm. The cell was calibrated in the following manner:

1. The set-up was vacuumed using a Welch duo-seal vacuum pump to remove any impurities.
2. Nitrogen was injected into the optical cell from the gas cylinder at a 15 psi pressure.

3. Water was then injected through the needle at a pressure of 20 psi. A higher pressure was selected so that water droplets could be introduced into the cell by gravity force.
4. The shape of the droplets was recorded using the camera.
5. The density of the nitrogen and water mixture was simulated using CMG's WinProp software.
6. The shapes of drops recorded earlier were analyzed for drop shape factor values.
7. The value obtained was compared to the value of surface tension from literature.
8. Steps 1 through 7 were repeated for different pressures. The values of surface tension and drop shape pictures are shown in Chapter 4 and APPENDIX C**.**
9. After every sample run, the cell was cleaned using toluene and acetone and then purged with nitrogen.

3.7.3 Experimental Procedure

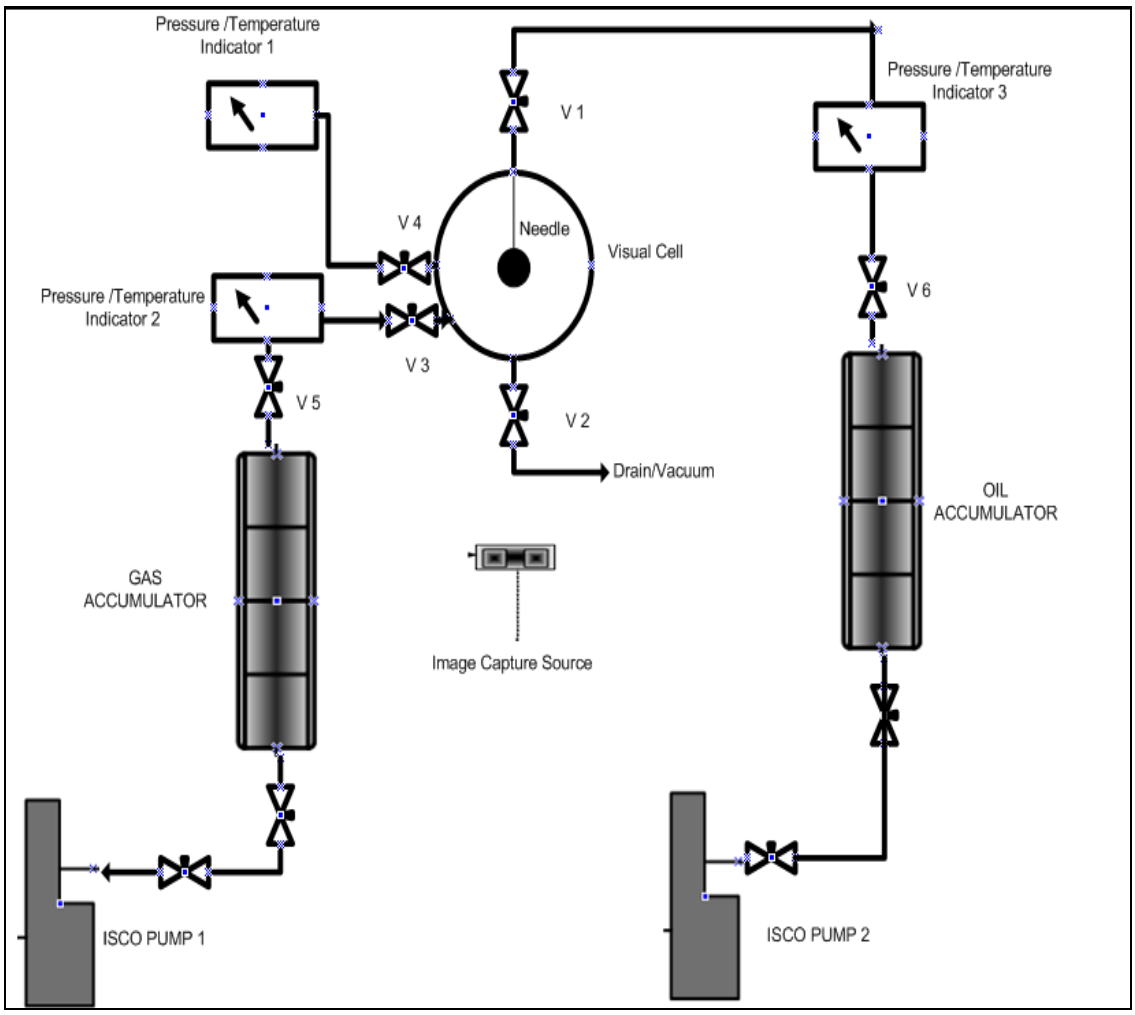

Figure 3.13 Schematic of MMP Set-up

The experimental procedure is described as follows:

1. The optical cell was pressurized by using de-ionized water up to a pressure of 3,750 psi and was checked for leaks.
2. The cell was cleaned using toluene and acetone, and then purged with nitrogen to remove any traces of acetone present. The rubber O-rings were changed and connections were properly fastened to prevent leaks and subsequent pressure drops. The set-up was connected as shown in the schematic diagram (Figure 3.6).
3. All the valves were first kept in closed position.

4. The valves at the bottom of the accumulators connected to the ISCO pumps were opened, and the pumps were kept running at the desired pressure of operation.
5. All the valves, except V5 and V6, were then opened.
6. The drain/vacuum line was then connected to the Welch duo-seal vacuum pump to remove any traces of acetone or air present in the set-up. The pump was kept running until the reading in the Heise pressure gauge showed absolute vacuum.
7. All the valves were then closed and, using the temperature controllers, the temperature in the entire set-up was brought to 95°F. The controllers were left running for about 6 hours to ensure constant temperature throughout the set-up.
8. Valve V5 was then slowly opened and the gas was allowed to come out at constant pressure and temperature. The temperature and pressure of the gas were read from pressure/temperature indicator 2.
9. Similarly, valve V6 was slowly opened and the oil was allowed to come out at constant pressure and temperature. The valves on the oil were opened very slowly so as to avoid flashing of oil. The temperature and pressure of the oil were read from pressure/temperature indicator 3.
10. Valve V1 was carefully opened and a few drops of oil were allowed to enter the optical cell.
11. Valve V1 was closed immediately after a few drops had been collected in the cell.
12. Valve V3 was then opened and a gas at a selected pressure was allowed to enter the optical cell. The gas pressure was maintained slightly lower than the oil pressure so that the gas did not push the oil back.
13. Valve V4 was then opened to measure the temperature and pressure in the optical cell using pressure/temperature indicator 1. Valve V3 was then closed.
14. Valve V1 was slowly opened and pendant drops were allowed to form in the optical cell at a slow flow rate. The image of the first pendant drop of crude oil at the tip of the needle in the optical cell was captured with the digital camera as soon as it contacted the gas phase. Valve V1 was closed once a few

drops entered into the optical cell. The drop shape factors were measured and, using initial densities, the First Contact Miscibility was determined.

15. The fluids were allowed to equilibrate for about 2 hours at the experimental conditions. A pendant drop of the recombined reservoir fluid was allowed to form at the tip of the needle in the optical cell in the gas phase that had already interacted with the oil residing at the bottom of the cell. This image was captured and drop shape analysis was performed. The density was determined by using CMG WinProp software and the IFT was calculated.
16. The same procedure was repeated for about 8-10 pendant oil drops.
17. The pressures of the oil and gas were increased using the ISCO pump and Steps 12 to 17 were repeated.
18. The runs were carried out at different pressures up to 3,750 psi, the maximum pressure for pump operation.
19. After each run the drain/vacuum valve was carefully opened and the sample was allowed to flash in a conical flask.
20. The set-up was cleaned using alternate runs of toluene and acetone and then purged with nitrogen. The O-rings were then replaced in the optical cell and connections were fastened. The entire assembly was vacuumed to remove any traces of air or nitrogen present.
21. All the above steps were repeated for different gas-oil sample runs.

3.8 Viscosity Data Compilation

The heavy oil viscosity data are not readily available in literature. Experimental measured viscosity data are lacking in the literature and are needed for viscosity modeling purposes. In the early stages of this study, many professionals from academia and the industry were contacted successfully. This resulted in the generation of six different data sets. For three of the sets, the viscosity data are available as a function of pressure for three different temperatures. Altogether twelve data sets were used. The data represent major oil producing provinces around the world. The molar composition and the plus fraction properties of all of the data sets are summarized in Table 3.3. Data Set A was obtained from Hernandez (2001) while Data Set B was obtained from Lindeloff et al. (2004). Data Sets C, D, E, and F are confidential.

Component	Set A	Set B	Set C	Set D	Set E	Set F

H_2S	0.00	0.00	0.00	0.00	0.00	0.00
N_2	0.05	0.31	0.17	0.18	0.37	0.14
CO_2	0.00	0.06	0.30	0.33	0.32	0.22
C_1	40.70	14.99	3.19	3.63	12.68	25.17
C_2	3.44	1.13	2.07	2.67	5.80	0.29
C_3	2.15	0.28	4.91	5.02	6.73	0.04
***i*-C_4**	0.89	0.59	1.05	1.10	1.18	0.02
***n*-C_4**	1.13	0.15	3.68	3.52	4.56	0.03
***i*-C_5**	0.74	0.33	1.92	1.52	1.87	0.01
***n*-C_5**	0.54	0.09	3.37	2.37	3.20	0.01
C_6	0.53	0.48	5.66	3.86	4.69	0.02
C_{7+}	49.83	81.59	73.69	75.78	58.60	74.05
MW_{C7+}	433	343	355	363	292	404
γ_{C7+}	0.9759	0.9480	0.9325	0.9336	0.9181	0.9689

Table 3.3 Molar Composition (Mole %) and Plus Fraction Properties

Of the above data, Set A represents Venezuelan oil while Sets B and F represent the oils from the North Sea. Sets C, D, and E are obtained from Middle East. The detailed viscosity data for all of the fluid samples are given by Raut (2007).

In addition to the literature data stated above, two more data sets were generated in-house. These data sets represent the viscosity measurements performed on ANS heavy dead oil samples, recombined with pure methane (99.5% pure) to simulate live oil samples. These two oil samples will be referred to as samples G and H. Phase behavior experiments conducted using samples G and H are discussed in the Chapter 4.

Chapter 4 EXPERIMENTAL RESULTS AND DISCUSSIONS

4.1 Compositional Characterization of Oil Samples

The gas chromatographic simulated distillation method was used to analyze the flashed ANS oil samples G and H. In this method, the boiling range of single carbon number (SCN) fractions, defined in the generalized property table (Katz and Firoozabadi 1978) was calibrated with retention time on gas chromatography. A mixture containing normal paraffin corresponding to each carbon number fraction was run on GC at various concentrations. Their responses at different concentrations were recorded and incorporated into group response factor computations. The SCN fractions from C_6 to C_{24} were calibrated through n-paraffins belonging to the corresponding SCN group for their elution times and response factors. Elution time of SCN fraction was determined by averaging the elution times of n -paraffins at different concentrations of calibration standard mixture, belonging to that particular group. The compositions of flashed oil samples G and H are listed in Tables 4.1 and 4.2, respectively, whereas stock tank oil properties are listed in Table 4.3

Component (SCN)	Area	Area %	Concentration µg	% wt
C6	0	0.000	0.00000	0.0000
C7	0	0.000	0.00000	0.0000
C8	11087487	2.053	0.00004	0.7748
C9	21326948	3.950	0.00016	2.9486
C10	19488486	3.609	0.00014	2.5279
C11	21268152	3.939	0.00015	2.7206
C12	33912916	6.281	0.00024	4.3524
C13	35844196	6.638	0.00026	4.8514
C14	45350536	8.399	0.00032	5.9509
C15	43833652	8.118	0.00031	5.7688
C16	25211838	4.669	0.00018	3.3228
C17	37082060	6.868	0.00028	5.2393
C18	34405712	6.372	0.00025	4.5203
C19	27602118	5.112	0.00020	3.6551
C20	28903392	5.353	0.00022	4.1457
C21	22910256	4.243	0.00018	3.2275
C22	16042830	2.971	0.00013	2.3332
C23	23653088	4.381	0.00019	3.4627
C24	13424586	2.486	0.00011	1.9515
C25+	71574408	13.256	0.00208	38.2466
Total	**532922661**	**100.000**	**0.00543**	**100**

Table 4.1 Compositional Analysis by Simulated Distillation on GC for Sample G

Component	Area	% Area	Concentration	Wt %
C6	23189016	0.648	0.00122	2.6307
C7	18691080	0.522	0.00023	0.4920
C8	18453358	0.516	0.00007	0.1507
C9	41998580	1.174	0.00032	0.6788
C10	70357088	1.966	0.00050	1.0667
C11	113210800	3.163	0.00079	1.6930
C12	135063840	3.774	0.00094	2.0264
C13	244910992	6.843	0.00180	3.8751
C14	227000336	6.343	0.00162	3.4822
C15	304689824	8.514	0.00218	4.6878
C16	172116864	4.809	0.00123	2.6518
C17	233254112	6.518	0.00178	3.8527
C18	196186896	5.482	0.00140	3.0133
C19	284764288	7.957	0.00205	4.4082
C20	175946752	4.916	0.00135	2.9502
C21	149935984	4.19	0.00115	2.4693
C22	138242384	3.863	0.00109	2.3504
C23	159460944	4.456	0.00126	2.7291
C24	82144416	2.295	0.00073	1.5729
C25+	774474240	21.64	0.02471	53.2184
Total			**0.046423215**	**100**

Table 4.2 Compositional Analysis by Simulated Distillation on GC for Sample H

Stock Tank Oil Property	Oil Sample G	Oil Sample H
Molecular Weight lb/lb mole	303	347.5
Density of Stock tank oil (60°F and 14.7 psia) g/cc	0.9466	0.9496

Table 4.3 Stock Tank Oil Properties

The molecular weight of plus faction was calculated by component material balance knowing the molecular weight of the oil sample. The result of simulated distillation is weight % of the SCN. The compositional simulators and viscosity models require composition in mole %. The compositional results, in weight % were transformed into mole %, using molecular weights listed for SCN fractions in the generalized property table. The oil samples were recombined with the CP grade methane of composition shown in Table 4.4 at field GOR to simulate live oils. The final recombined oil composition was calculated by material balance technique. The recombined oil composition was used for compositional reservoir simulations, equation of state tuning

and viscosity modeling. Tables 4.5 and 4.6 list the recombined oil compositions for sample G and sample H, respectively.

Component	Mol%
CO_2	0.01001
N_2	0.4002
CH_4	99.4597
C_2H_6	0.0600
C_3H_8	0.0600
C_4H_{10} +	0.0100
Total	100

Table 4.4 Gas Composition of CP Grade Methane

Component	Mole %
CO2	0.00229
N2	0.09173
C1	22.7938
C2	0.01376
C3	0.01376
C4	0.00229
C8	1.69248
C9	5.69580
C10	4.40944
C11	4.32582
C12	6.31872
C13	6.47970
C14	7.32070
C15	6.54554
C16	3.49845
C17	5.16712
C18+	25.62861
Total	**100.00000**

Table 4.5 Composition Oil Sample G

Plus fraction properties: Oil G
Molecular weight = 561.28
Specific gravity = 1.0511

Component	Mole %
CO2	0.003483
N2	0.13933
C1	34.62326
C2	0.02090
C3	0.02090
C4	0.00348
C6	7.09448
C7	1.16109
C8	0.31915
C9	1.27082
C10	1.80359
C11	2.60887
C12	2.85121
C13	5.01616
C14	4.15167
C15	5.15493
C16+	33.7566
Total	**100.00000**

Table 4.6 Composition Oil Sample H

Plus fraction properties: Oil H
Molecular weight = 531.18
Specific gravity = 1.0014

4.2 Constant Composition Expansion

Constant Composition Expansion tests were conducted on two viscous oil samples at their respective reservoir temperatures of 84°F and 81°F. The results are listed in Tables 4.7 and 4.8 and displayed in Figures 4.1 and 4.2. The data consist of cell contents total

volume as a function of pressure. At the bubble point pressure an abrupt change in slope of the total volume vs. pressure plot was observed. The slope of total volume vs. pressure plot above the bubble point yields compressibility of the oil. Relative oil volume was determined by the ratio of total volume of cell content to total volume at bubble point pressure. The bubble point pressure measured was found to agree with the range of values reported by McGuire et al. (2005). The gas evolution below the bubble point is very slow for heavy oils and a longer time is required to reach equilibrium.

Pressure psia	Total Volume cc	Relative Volume
1919.2	200.23	0.9783
1785.9	200.87	0.9814
1658.4	201.50	0.9845
1548.5	202.13	0.9876
1427.9	202.77	0.9907
1332.7	203.40	0.9938
1182.9	204.67	1.0000
998.8	209.12	1.0217
769.7	215.14	1.0512
484.0	231.65	1.1318

Table 4.7 CCE Data for ANS Viscous Oil Sample G

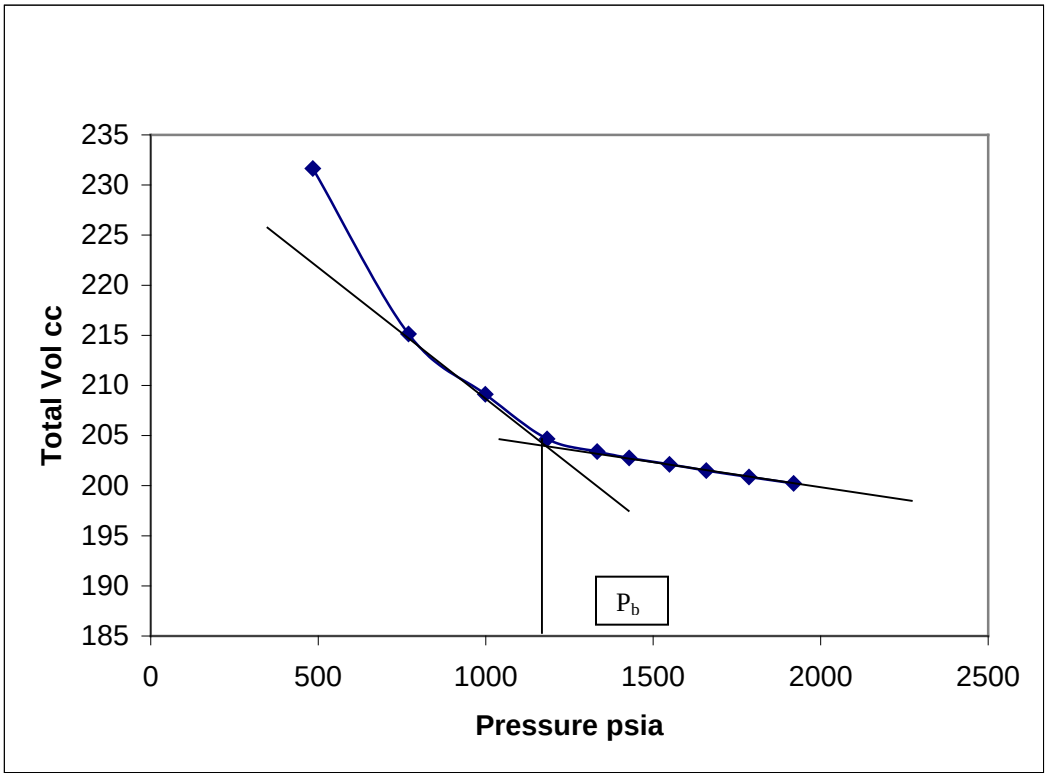

Figure 4.1 Pressure-Volume Relationship of Viscous Oil Sample G

Pressure psia	Total volume cc	Relative Volume
2604.2	111.10	0.97284
2489.3	111.46	0.9759
2342.7	111.99	0.9806
2214.5	112.44	0.9846
2097.7	112.69	0.9868
2001.2	112.99	0.9894
1890.1	113.19	0.9911
1822.2	113.27	0.9918
1740.3	113.31	0.9922
1654.0	114.02	0.9984
1596.2	114.40	1.0017
1572.0	114.22	1.0000
1386.1	118.40	1.0368
1009.7	124.41	1.0894
832.6	129.29	1.1321
635.8	139.05	1.2176

Table 4.8 CCE Data for ANS Viscous Oil Sample H

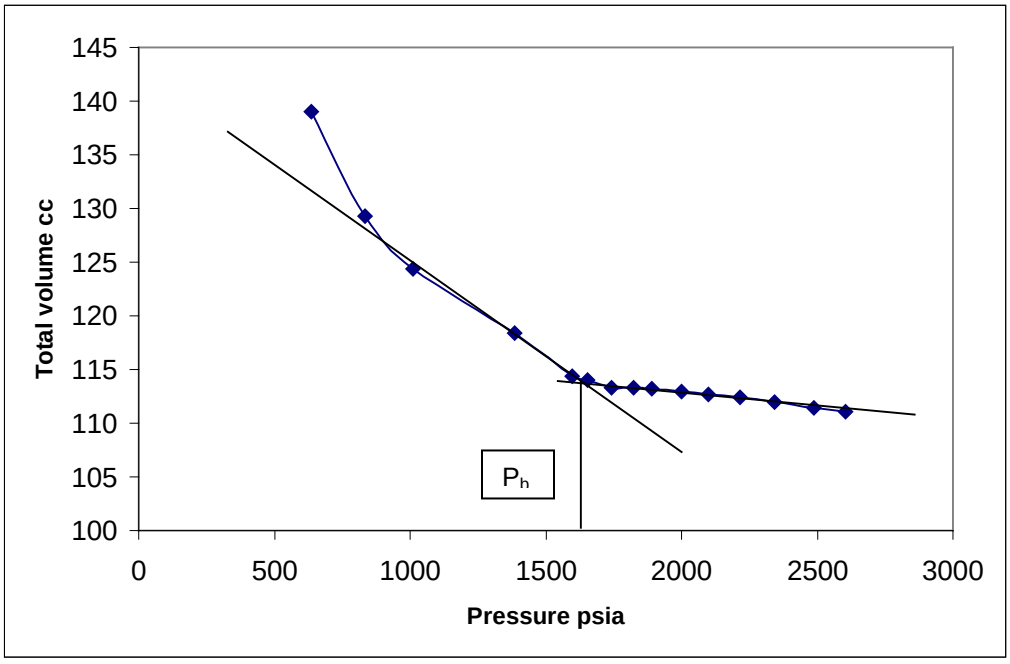

Figure 4.2 Pressure-Volume Relationship of ANS Viscous Oil Sample H

4.3 Differential Liberation

Differential liberation (DL) tests were performed on both viscous oil samples from the ANS. The results of the tests are listed in Tables 4.9 and 4.10 for oil sample G and oil sample H, respectively. The starting point of the differential liberation test is the bubble

point pressure but for the purpose of density and viscosity measurements, the test was started at a pressure above bubble point pressure.

Pressure Psia	R_s Scf/STB	B_o bbl/STB	B_t bbl/STB
1904.0	123	1.0980	1.0980
1762.0	123	1.1053	1.1053
1625.0	123	1.1110	1.1110
1513.0	123	1.1223	1.1223
1406.0	123	1.1337	1.1337
1183.0	123	1.1455	1.1455
959.0	118	1.1210	1.1335
749.0	93	1.1014	1.1972
462.0	72	1.0618	1.3435
225.0	37	1.0320	2.0162
143.0	28	1.0188	2.7616
14.7	0	1.0060	23.9393

Table 4.9 Differential Liberation Test of ANS Viscous Oil Sample G at 84°F

The solution GOR was calculated by the ratio of the volume of gas liberated at a particular pressure below bubble point to the volume of gas when expanded to 14.7 psia pressure and at 60°F. Volumetric properties like oil formation volume factor (B_o) and two-phase formation volume factor (B_t) were obtained by visual measurement of the oil volume. Figures 4.3 and 4.4 illustrate the behavior of Rs, B_o, and B_t as functions of pressure. Since the oil is in single phase above the bubble point, B_o and B_t are identical.

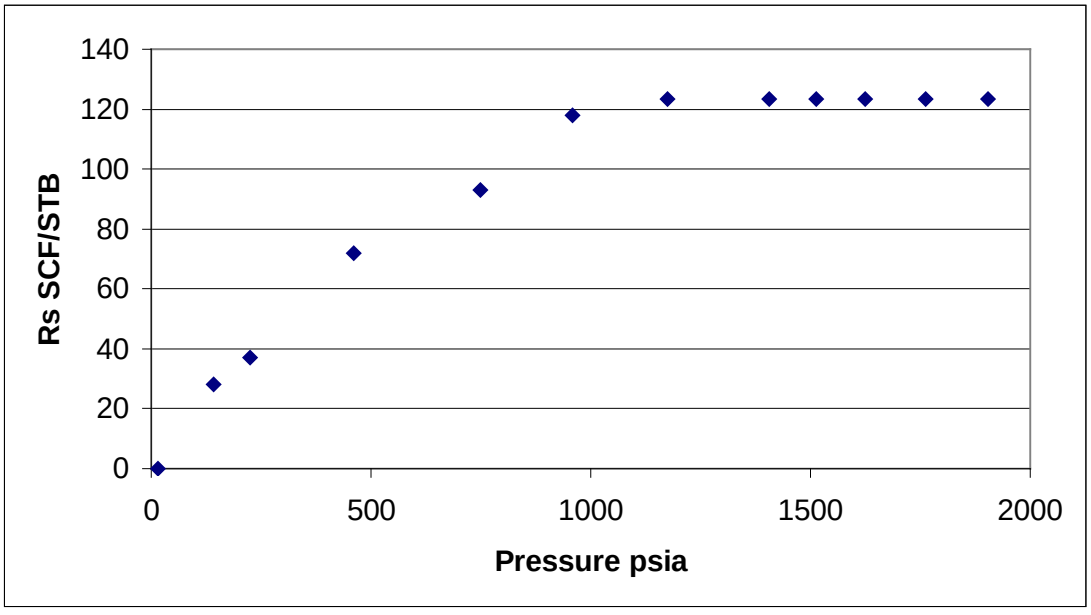

Figure 4.3 Solution GOR vs. Pressure for ANS Viscous Oil G at 84°F

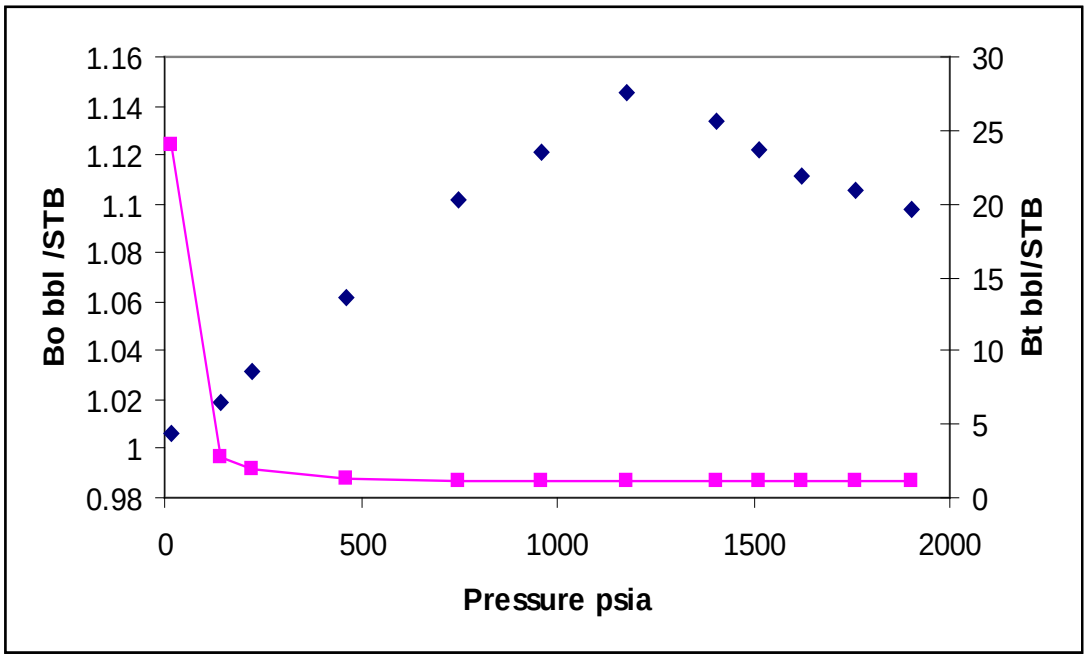

Figure 4.4 Single-Phase and Two-Phase Formation Volume Factors for ANS Viscous Oil G at 84°F

It can be seen that the solution GOR increases with increase in pressure until the bubble point pressure. Beyond the bubble point pressure no more gas is available for dissolution into oil so the GOR remains constant. The sample G exhibits a low GOR of 123 SCF/STB, a typical characteristic of heavy oils.

Pressure psia	**R_s Scf/STB**	**B_o bbl/STB**	**B_t bbl/STB**
2510.7	194	1.0650	1.0650
2396.7	194	1.0750	1.0750
2303.7	194	1.0858	1.0858
2189.7	194	1.0840	1.0840
2050.7	194	1.1030	1.1030
1886.6	194	1.1240	1.1240
1709.7	194	1.1430	1.1430
1586.7	194	1.1600	1.1600
1264.7	189	1.1100	1.1247
1002.7	182	1.0860	1.1218
836.7	159	1.0650	1.1560
646.7	132	1.0570	1.2736
422.7	98	1.0350	1.5184
217.7	47	1.0334	2.7300
14.7	0	1.0000	36.1889

Table 4.10 Differential Liberation of ANS Viscous Oil Sample H at 81°F

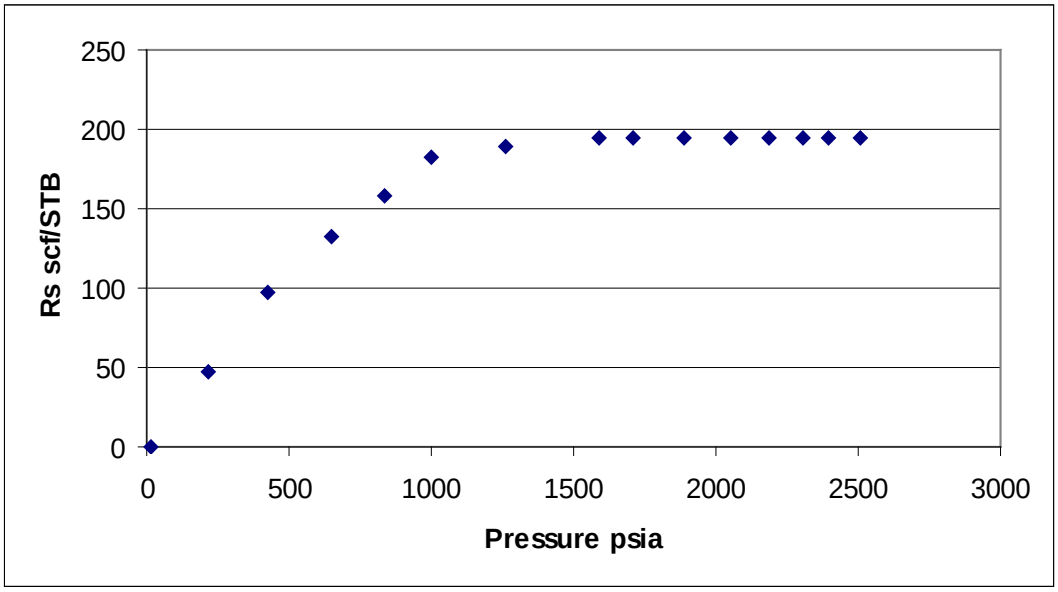

Figure 4.5 Solution GOR vs. Pressure for ANS Viscous Oil H at 81°F

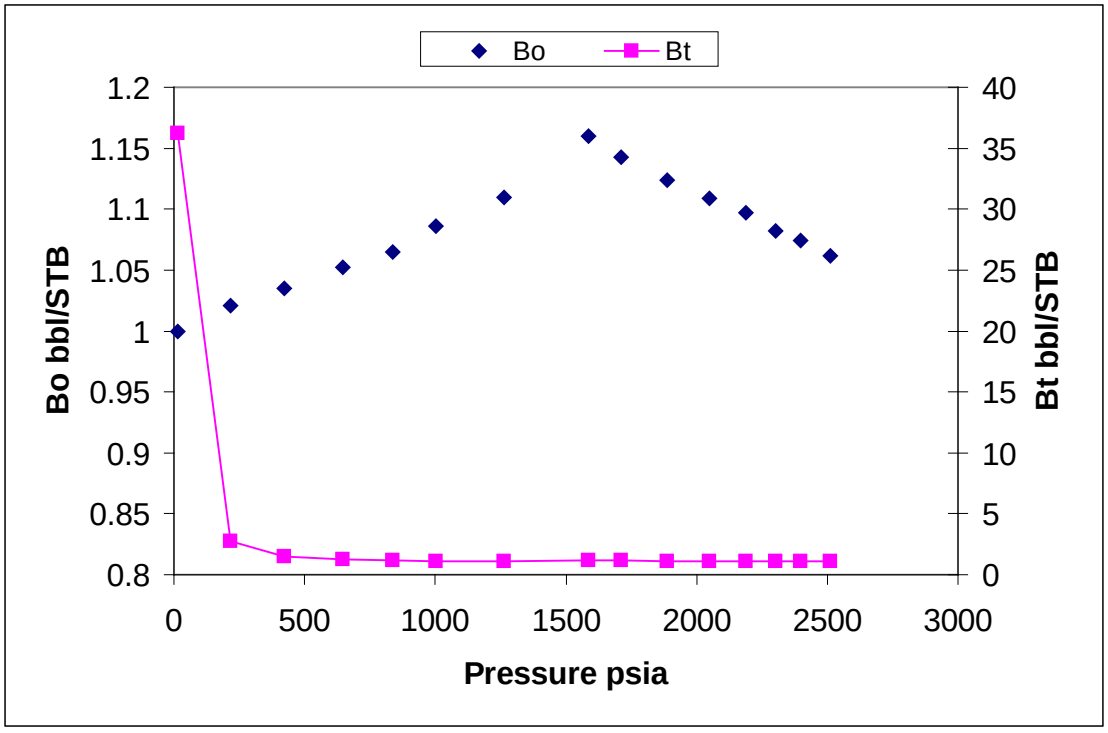

Figure 4.6 Single-Phase and Two-Phase Formation Volume Factors for ANS Viscous Oil H at 81°F

4.4 Density and Viscosity Measurements

The residual oil viscosity and density were measured at every step of differential liberation for both the oils. Tables 4.11 and 4.12 tabulate the acquired data for oil sample G and oil sample H, respectively.

Pressure psia	M cP	Density g/cc
1904.3	232.7	0.9352
1761.7	224.2	0.9345
1624.7	221.7	0.9342
1512.7	214.9	0.9339
1405.5	210.5	0.9335
1183.0	191.5	0.9326
959.0	208.6	0.9329
748.7	221.0	0.9375
461.7	242.0	0.9398
224.7	267.5	0.9407
142.7	299.6	0.9423
14.7	359.8	0.9440

Table 4.11 Density and Viscosity Measurements of Sample G at 84°F

Pressure psia	M cP	Density g/cc
2510.7	322.3	0.9420
2396.7	314.2	0.9405
2303.7	304.9	0.9398
2189.7	297.4	0.9390
2050.7	291.6	0.9379
1886.6	286.3	0.9369
1709.7	281.9	0.9355
1586.7	274.7	0.9348
1264.7	283.9	0.9357
1002.7	292.8	0.9362
836.7	303.2	0.9370
646.7	323.9	0.9377
422.7	341.6	0.9382
217.7	383.2	0.9395
14.7	429.23	0.9429

Table 4.12 Density and Viscosity Measurements of Sample H at 81°F

Figures 4.7 and 4.8 display the residual oil density at every step of the differential liberation test as a function of pressure for oil samples. Density of the oil increases with pressure above the bubble point due to oil compression. The composition of the oil remains unaltered above bubble point and the density increase can be attributed to

pressure. Below the bubble point, pressure effect and compositional effect reciprocate each other. As pressure decreases, gas comes out of solution and the oil becomes heavier, which explains the increase in density. Below the bubble point, the compositional effect dominates the pressure effect and oil density increases with decrease in pressure (see Figures 4.7 and 4.8). A similar trend was observed for oil viscosity as pressure decreases below the bubble point (see Figure 4.9). It should be noted that both the density and viscosity plots are indicative of the bubble point pressures of 1,183 psia and 1,572 psia for oil G and oil H, respectively.

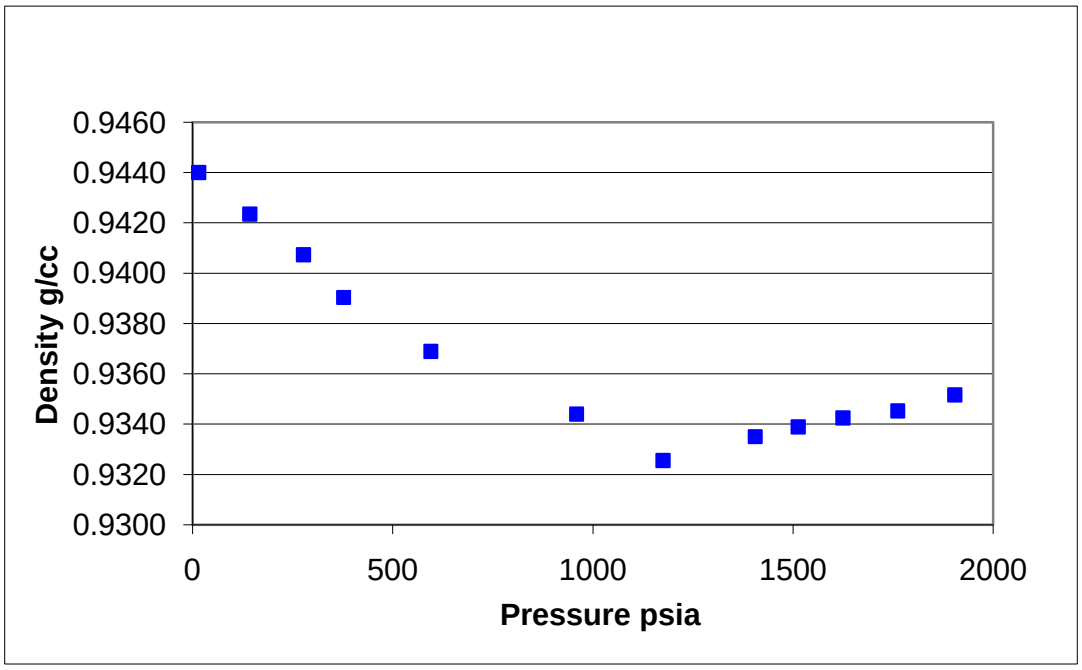

Figure 4.7 Density as a Function of Pressure for Oil Sample G

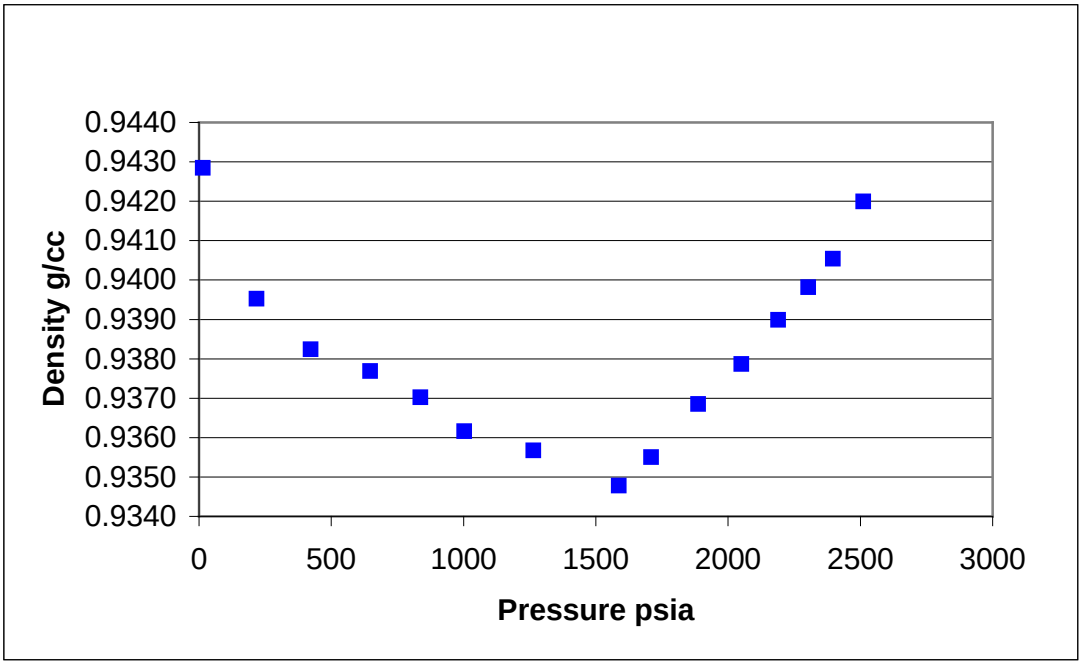

Figure 4.8 Density as a Function of Pressure for Oil Sample H

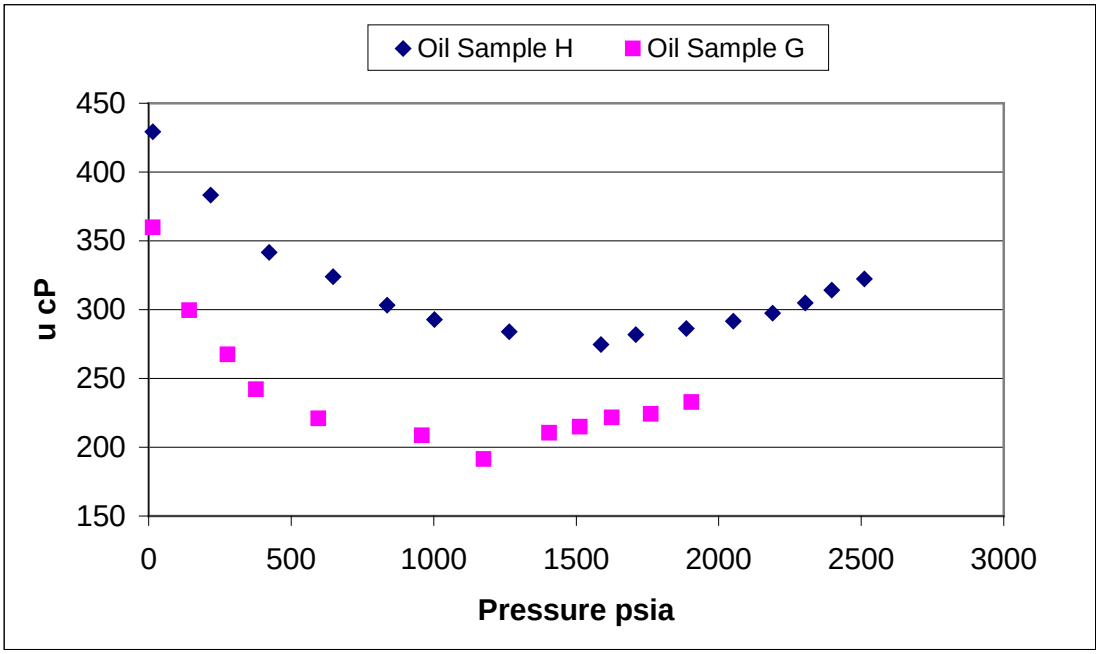

Figure 4.9 Viscosity as a Function of Pressure for Oil G and Oil H

4.5 Viscosity Measurements of Flashed Oils

The viscosities of five flashed oil samples from various heavy oil pools in ANS were measured within the range of the operating pressures and temperatures of field operations. These oil samples are named ANS1 through ANS5. Figures 4.10-4.14 illustrate that the viscosity of the oil samples varies exponentially with pressures at all temperatures. The exponent of the pressure effect on viscosity at every test temperature was obtained by fitting an exponential equation to the experimental data points.

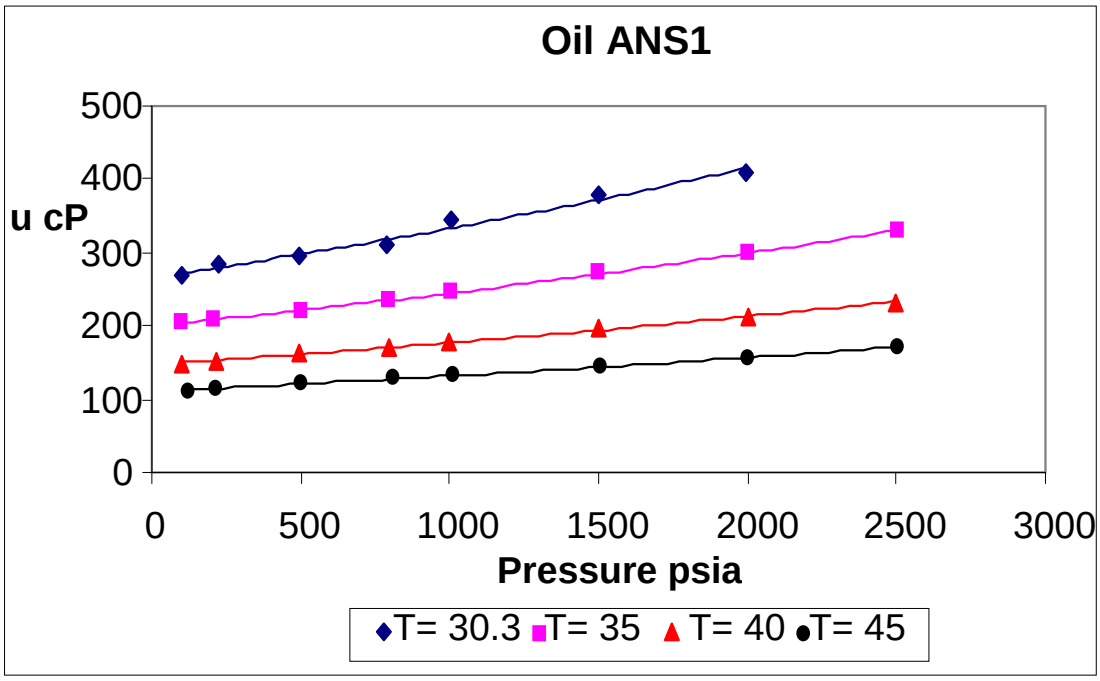

Figure 4.10 Flashed Oil Viscosity as a Function of Pressure at Different Temperatures for Sample ANS1.

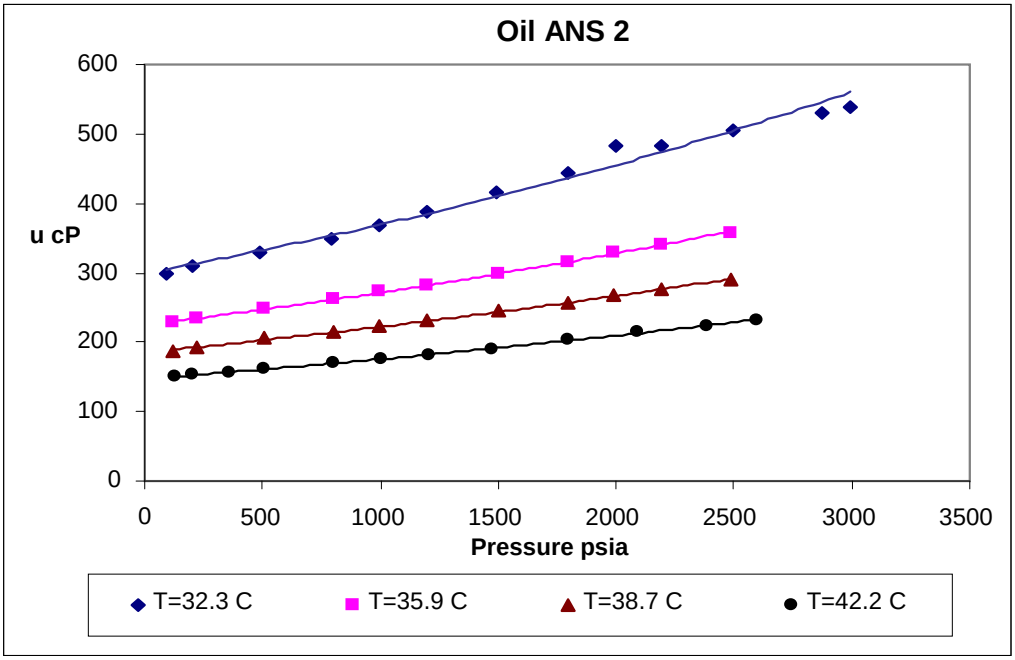

Figure 4.11 Flashed Oil Viscosity as a Function of Pressure at Different Temperatures for Sample ANS2

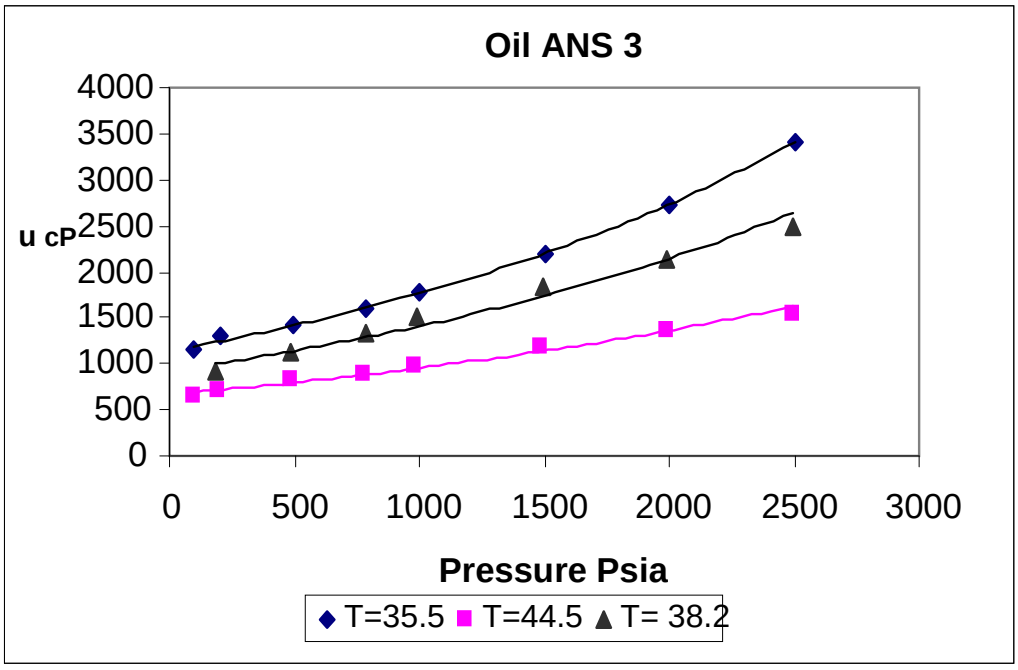

Figure 4.12 Flashed Oil Viscosity as a Function of Pressure at Different Temperatures for Sample ANS3

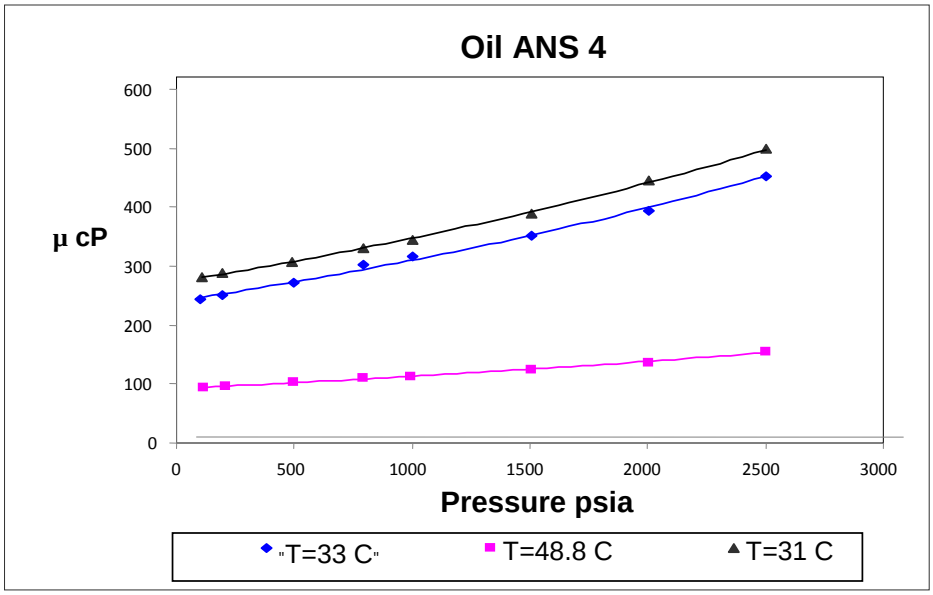

Figure 4.13 Flashed Oil Viscosity as a Function of Pressure at Different Temperatures for Sample ANS4

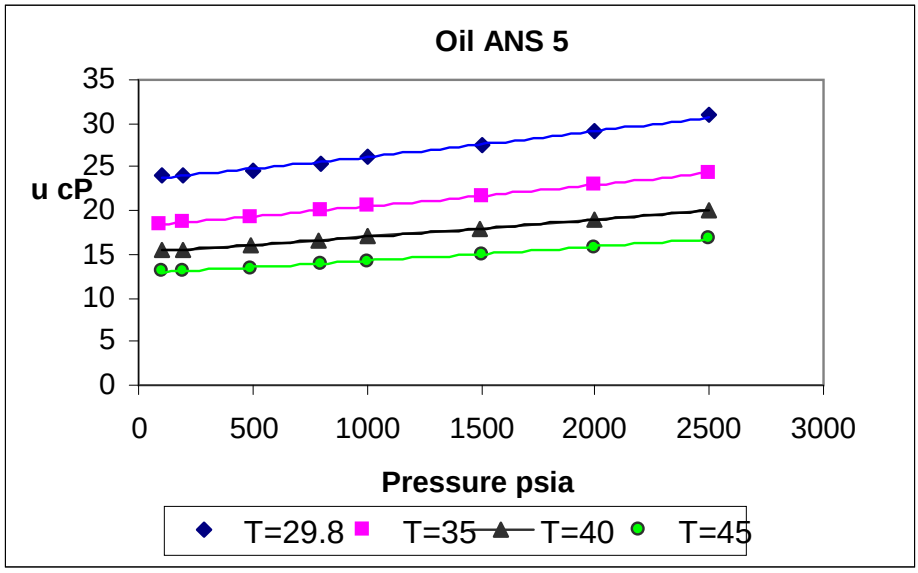

Figure 4.14 Flashed Oil Viscosity as a Function of Pressure at Different Temperatures for Sample ANS5

Viscosity measurements were collected for medium-heavy or viscous oils (<100cP) to highly viscous oils (>300 cp). The exponent of the viscosity behavior is found to vary with respect to temperature for a particular oil. In order to generalize the relationship of the exponent of viscosity behavior as a function of pressure for different oils, it is expressed as a function of molecular weight and temperature. Equation 4.1 defines functional expression of exponent of viscosity in terms of molecular weight and

temperature. The equation then is related to the exponent of viscosity behavior with pressure through a third order polynomial fit.

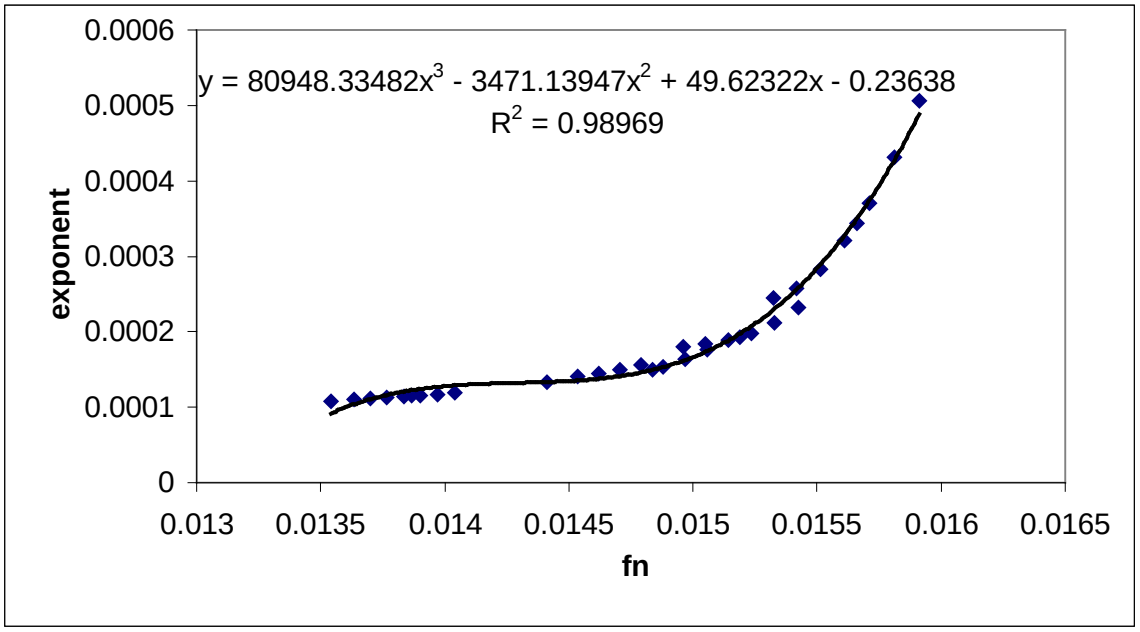

Figure 4.15 Functional Expression of Exponent of Viscosity Behavior with Respect to Pressure

$$\text{fn} = \frac{MW^{0.8318}}{T^{1.6}} + \frac{MW^{-0.155}}{T^{0.5867}} \tag{4.1}$$

Where,

MW = molecular weight of the oil

T = temperature, °R

With this correlation, the pressure effect on the viscosity of dead oil can be obtained with knowledge of molecular weight and temperature. This relation can be used to predict the ANS dead oil viscosity under pressure conditions, which in turn can be incorporated into live oil viscosity models.

4.6 MMP Measurements at 95°F

4.6.1 MMP Calculations by IFT Measurements (Pendant Drop Experiments)

The experimental densities obtained were used to tune the parameters in CMG WinProp's two phase flash simulations. Using the two phase flash calculations, densities were determined at different pressures of oil-gas interactions. The volume of the cell with respect to the volume of drop was determined and the experiments were performed with a

constant gas-oil molar ratio of R_m = 0.7/0.3. The changes in drop shape for CO_2-dead oil Sample A is shown in Figure 4.16.

It was difficult to measure the drop shape factor at higher pressures. The measurement of S values at higher pressures was difficult because the Niederhauser and Bartell (1947) tables report values only up to a drop shape factor ratio of 1. Therefore, in all the cases the values of IFT where the drop shape factor equaled 1 were used to extrapolate to "zero" dyne/cm. The pressure corresponding to extrapolated "zero" IFT was termed Minimum Miscibility Pressure (MMP).

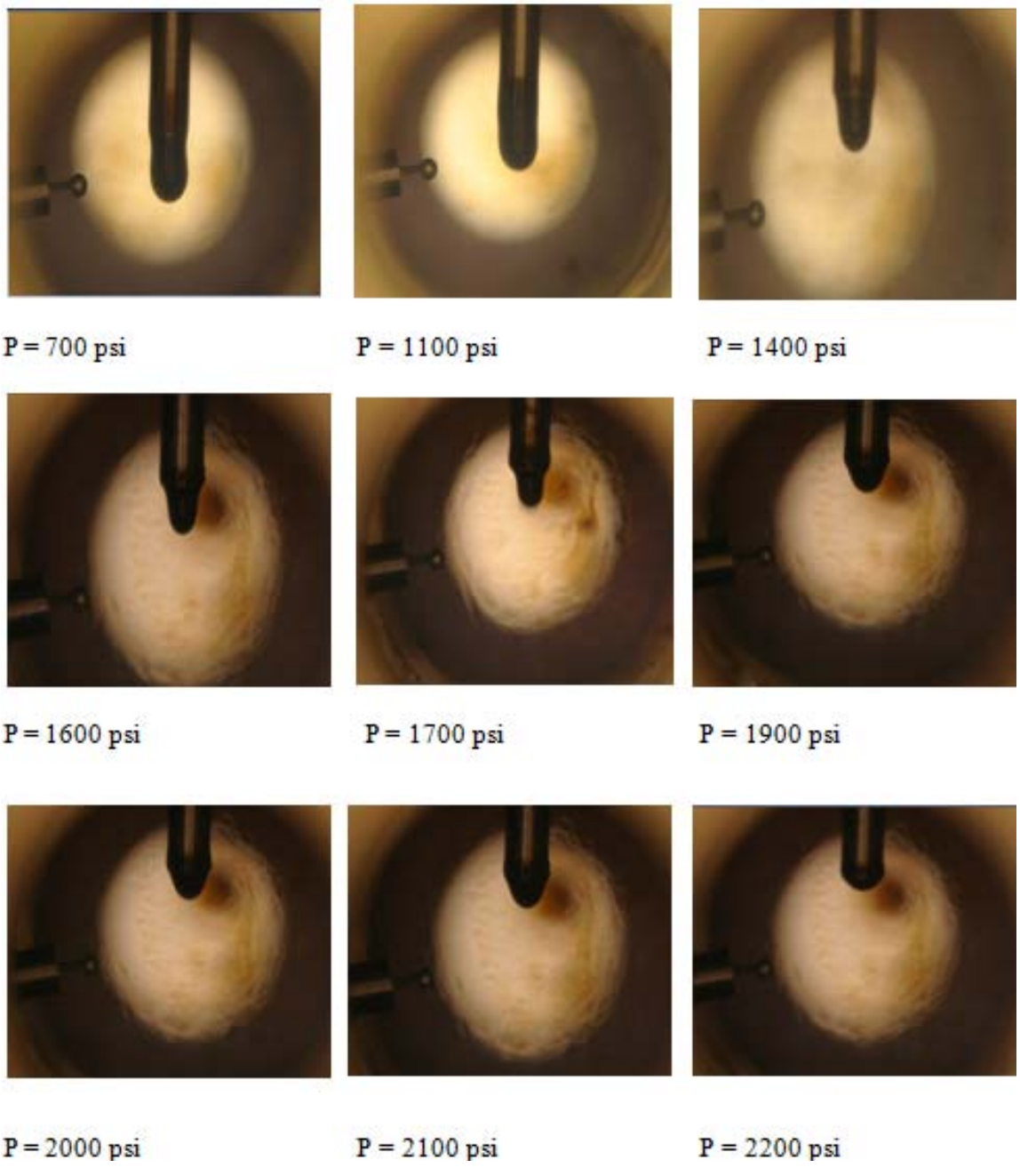

Figure 4.16 CO_2-Dead Oil Sample A Drop Shape Analysis

The composition at each step was determined using two-phase flash calculations. The values of IFT measurements for different gas-oil samples are shown in the following tables, and the extrapolated graph for MMP calculations are shown in the figures following the tables. Also, included in the tables are the equilibrated one-phase compositions of the oil-gas systems at MMP conditions.

P, psi	**σ, dyne/cm**	**Δρ (density difference), g/cc**
700	12.8645	0.7803
800	12.2484	0.7514
900	11.4267	0.7224
1000	10.8845	0.6823
1100	9.7785	0.6174
1200	8.7648	0.5788
1300	6.7309	0.2927
1400	5.9667	0.2438
1500	4.9473	0.1996
1600	4.2216	0.1748

Table 4.13 IFT Measurements for CO_2-Dead Oil Sample A

Components	**% Mole at MMP**
CO2	70.0028
C 8	0.65871
C 9	2.2167
C 10	1.71609
C 11	1.683567
C 12	2.45919
C 13	2.52183
C 14	2.84913
C 15	2.54745
C 16	1.36155
C 17	2.01099
C 18+	9.9744

Table 4.14 Equilibrium Composition of CO_2-Dead Oil Sample A at MMP

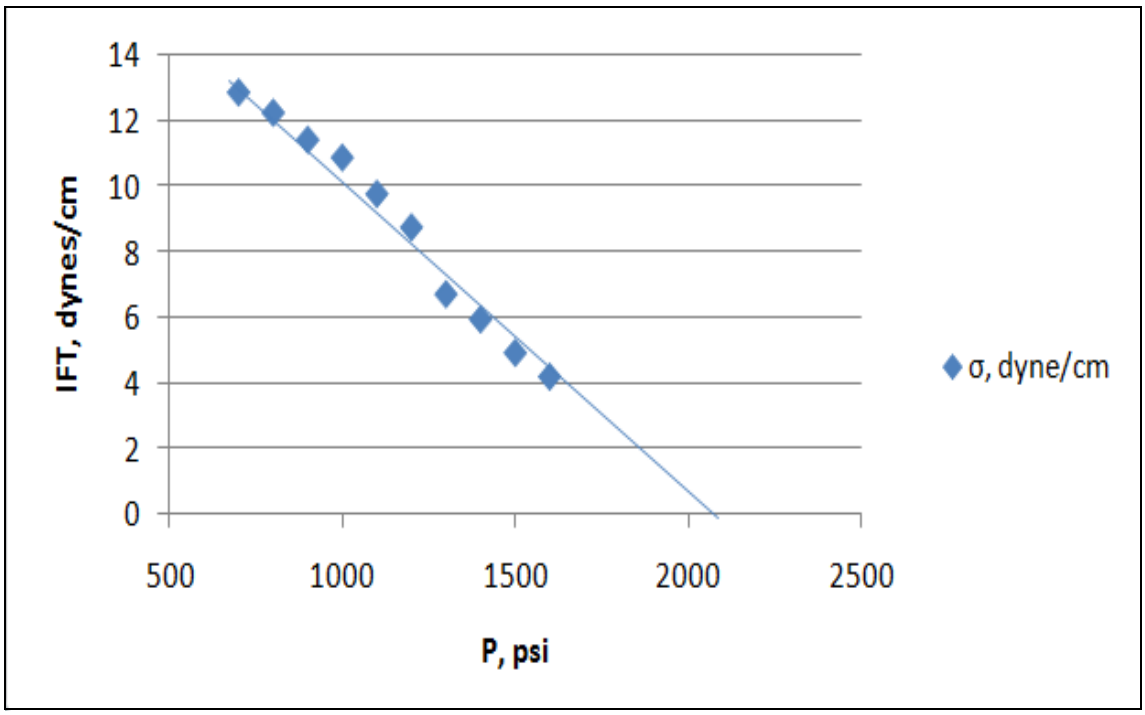

Figure 4.17 MMP Measurement for CO_2-Dead Oil Sample A

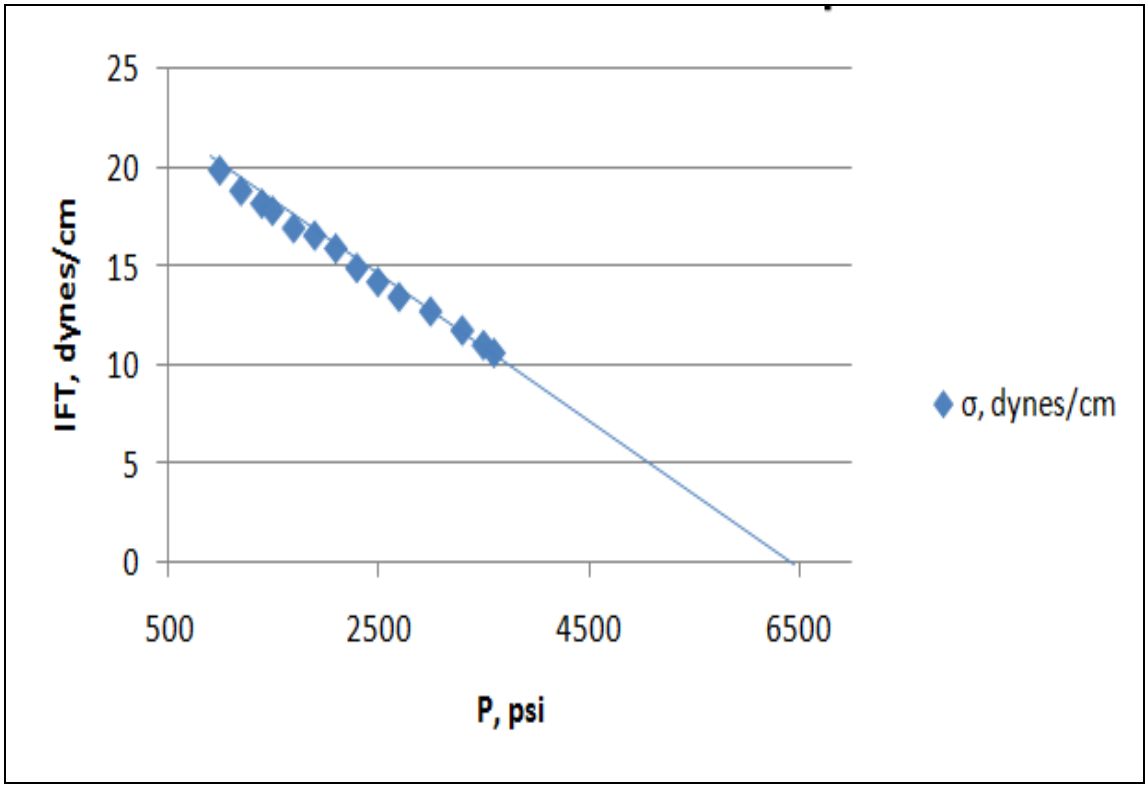

Figure 4.18: MMP Measurement for CH_4-Dead Oil Sample G

P, psi	σ, dynes/cm	Δρ, g/cc
1000	19.9234	0.829
1200	18.8902	0.8117
1400	18.2434	0.8022
1500	17.8845	0.7939
1700	17.001	0.7866
1900	16.6255	0.7672
2100	15.973	0.7542
2300	14.98823	0.7397
2500	14.2724	0.7249
2700	13.5135	0.7101
3000	12.783	0.6931
3300	11.8256	0.6792
3500	11.0823	0.6635
3600	10.6769	0.6541

Table 4.15 IFT Measurements for CH_4-Dead Oil Sample G

Components	% Mole at MMP
C 1	69.9921
C 8	0.65871
C 9	2.2167
C 10	1.71609
C 11	1.683567
C 12	2.45919
C 13	2.52183
C 14	2.84913
C 15	2.54745
C 16	1.36155
C 17	2.01099
C 18+	9.9744

Table 4.16: Equilibrium Composition of CH_4-Dead Oil Sample A at MMP

P, psi	σ, dynes/cm	Δρ, g/cc
1000	15.821	0.802
1200	14.232	0.7821
1300	13.003	0.7747
1400	11.9764	0.7671
1500	10.8023	0.7582
1600	9.9992	0.7466
1700	8.8923	0.7382
2000	6.4111	0.7037
2100	5.3846	0.6924
2200	4.4253	0.689

Table 4.17 IFT Measurements for VRI-Dead Oil Sample G

Components	% Mole at MMP
CO_2	0.8379
C 1	54.88
C 2	6.2328
C 3	4.1433
C 4	2.9393
C 5	0.7903
C 6	0.15099
C 7	0.02877
C 8	0.65871
C 9	2.2167
C 10	1.71609
C 11	1.683567
C 12	2.45919
C 13	2.52183
C 14	2.84913
C 15	2.54745
C 16	1.36155
C 17	2.01099
C 18+	9.9744

Table 4.18 Equilibrium Composition of VRI-Dead Oil Sample H at MMP

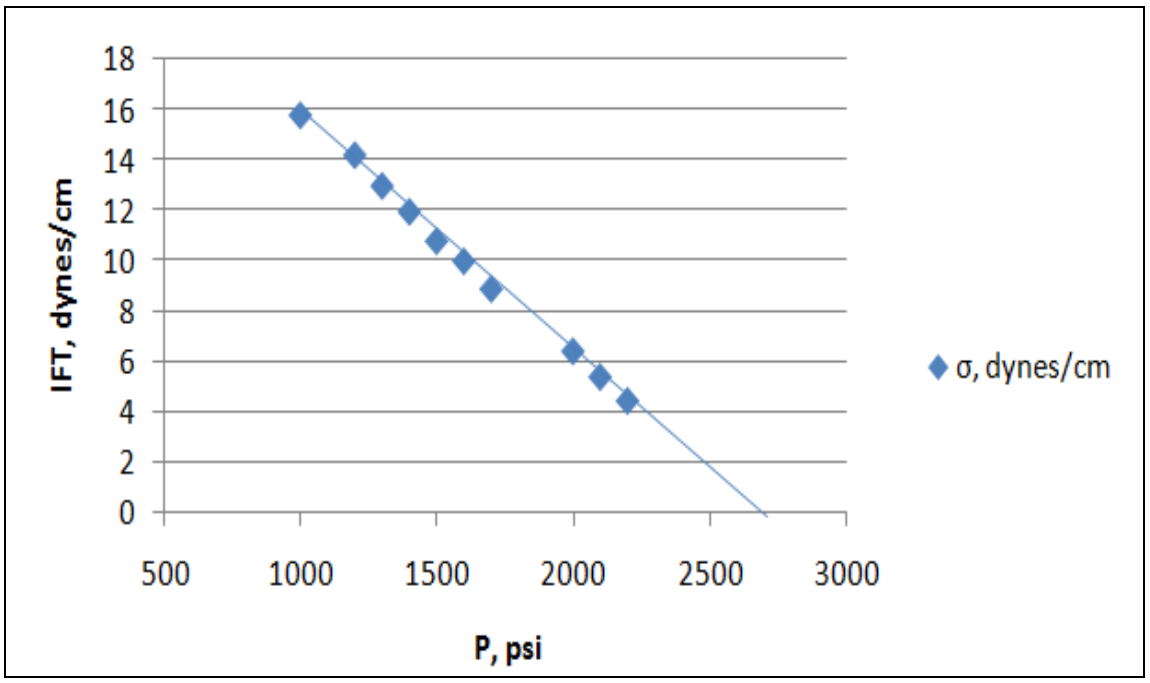

Figure 4.19 MMP Measurement for VRI-Dead Oil Sample A

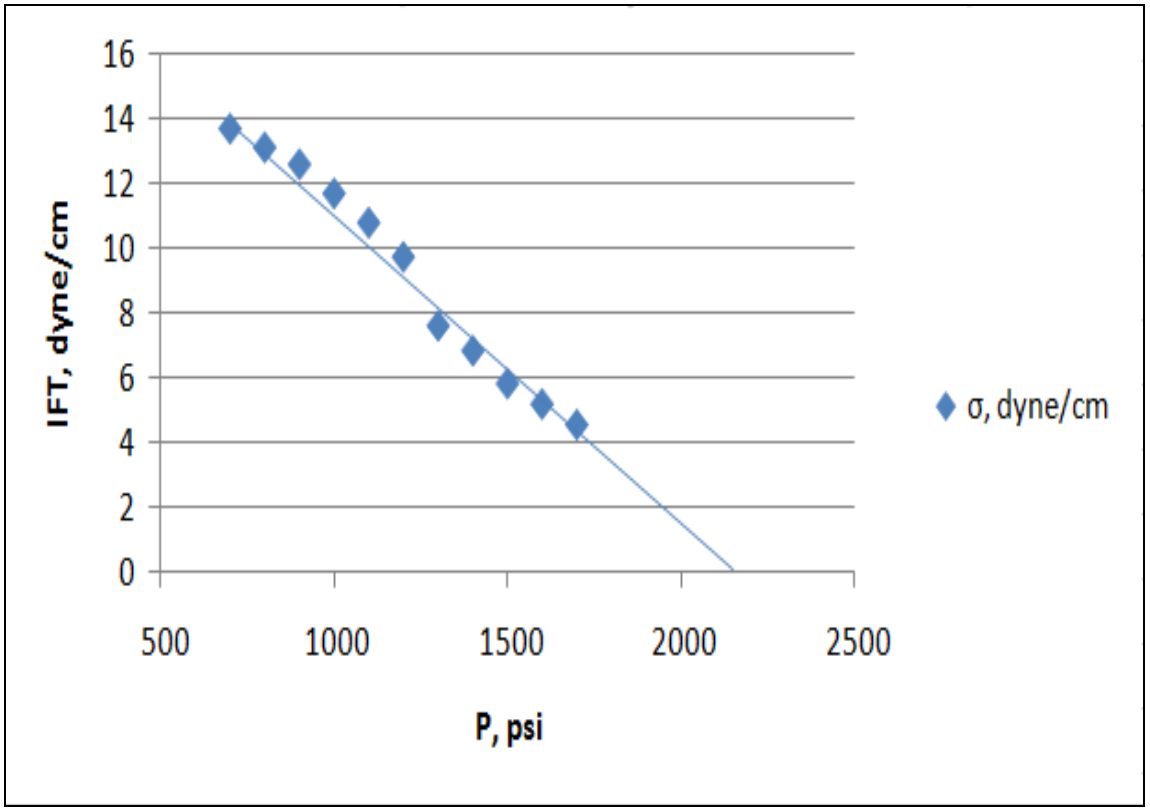

Figure 4.20 MMP Measurement for CO_2-Dead Oil Sample H

P, psi	σ, dyne/cm	Δρ, g/cc
700	13.7235	0.8213
800	13.1486	0.7922
900	12.6237	0.7612
1000	11.7244	0.7241
1100	10.8210	0.6514
1200	9.7623	0.6167
1300	7.6333	0.3381
1400	6.8671	0.2840
1500	5.8481	0.2337
1600	5.2164	0.2161
1700	4.5723	0.1933

Table 4.19 IFT Measurements for CO_2-Dead Oil Sample H

Components	% Mole at MMP
CO2	69.459
C 6	3.2598
C 7	0.53352
C 8	0.1464
C 9	0.583938
C 10	0.82875
C 11	1.19877
C 12	1.3101
C 13	2.3589
C 14	1.90767
C 15	2.36868
C 16+	15.5064

Table 4.20 Equilibrium Composition of CO_2-Dead Oil Sample B at MMP

P, psi	σ, dynes/cm	Δρ, g/cc
1000	20.553	0.865
1200	19.8167	0.8477
1400	18.902	0.8382
1500	18.1134	0.8299
1700	17.6845	0.8226
2000	16.2955	0.8032
2200	15.6255	0.7902
2400	15.0973	0.7757
2500	14.9823	0.7609
2600	14.4724	0.7461
2800	13.7135	0.7291
3000	13.2783	0.7152
3300	12.7256	0.6995
3600	11.6823	0.6901

Table 4.21 IFT Measurements for CH_4-Dead Oil Sample B

Components	% Mole at MMP
C 1	70.0012
C 6	3.2598
C 7	0.53352
C 8	0.1464
C 9	0.583938
C 10	0.82875
C 11	1.19877
C 12	1.3101
C 13	2.3589
C 14	1.90767
C 15	2.36868
C 16+	15.5064

Table 4.22 Equilibrium Composition of CH_4-Dead Oil Sample B at MMP

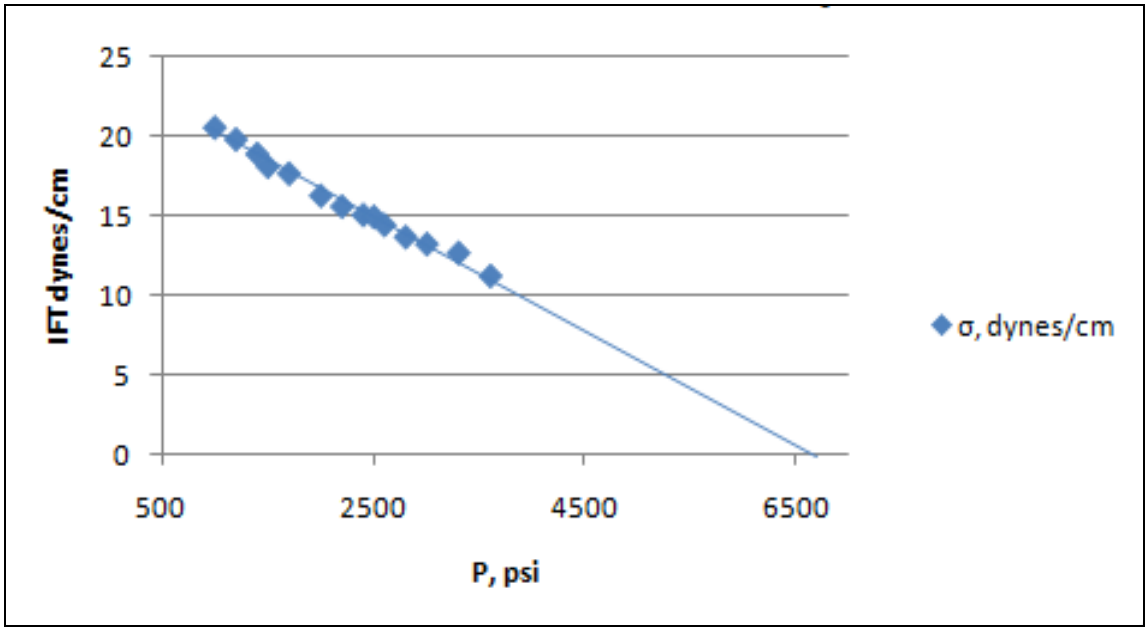

Figure 4.21 MMP Measurement for CH_4-Dead Oil Sample H

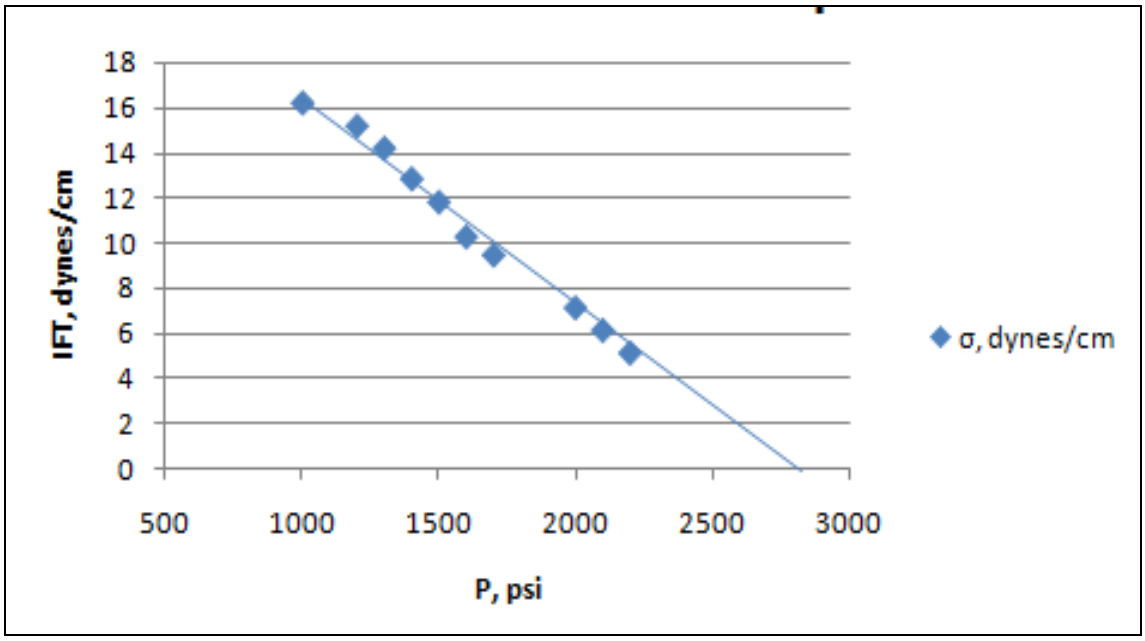

Figure 4.22 MMP Measurement for VRI-Dead Oil Sample H

P, psi	σ, dynes/cm	Δρ, g/cc
1000	16.144	0.838
1200	15.134	0.8181
1300	14.143	0.8107
1400	12.792	0.8031
1500	11.763	0.7942
1600	10.233	0.7826
1700	9.424	0.7742
2000	7.0942	0.7397
2100	6.0985	0.7284
2200	5.0986	0.725

Table 4.23: IFT Measurements for VRI-Dead Oil Sample H

Components	% Mole at MMP
CO_2	0.8379
C 1	54.88
C 2	6.2328
C 3	4.1433
C 4	2.9393
C 5	0.7903
C 6	3.4108
C 7	0.56229
C 8	0.1464
C 9	0.583938
C 10	0.82875
C 11	1.19877
C 12	1.3101
C 13	2.3589
C 14	1.90767
C 15	2.36868
C 16+	15.5064

Table 4.24 Equilibrium Composition of VRI-Dead Oil Sample H at MMP

P, psi	σ, dynes/cm	Δρ, g/cc
1400	9.0112	0.44647
1500	8.5785	0.3634
1600	7.6309	0.3092
1700	7.0018	0.2706
1750	6.724	0.2653
1800	6.022	0.2406
1850	5.755	0.2343
1900	5.152	0.2161
1950	4.627	0.1992

Table 4.25 IFT Measurements for CO_2-Live Oil Sample G

Components	% Mole at MMP
CO2	70.000687
N2	0.027519
C 1	6.83814
C 2	0.004128
C 3	0.004128
C 4	0.000687
C 8	0.507744
C 9	1.70874
C 10	1.322832
C 11	1.297746
C 12	1.895616
C 13	1.94391
C 14	2.19621
C 15	1.963662
C 16	1.049535
C 17	1.550136
C 18+	7.688583

Table 4.26: Equilibrium Composition of CO_2-Live Oil Sample G at MMP

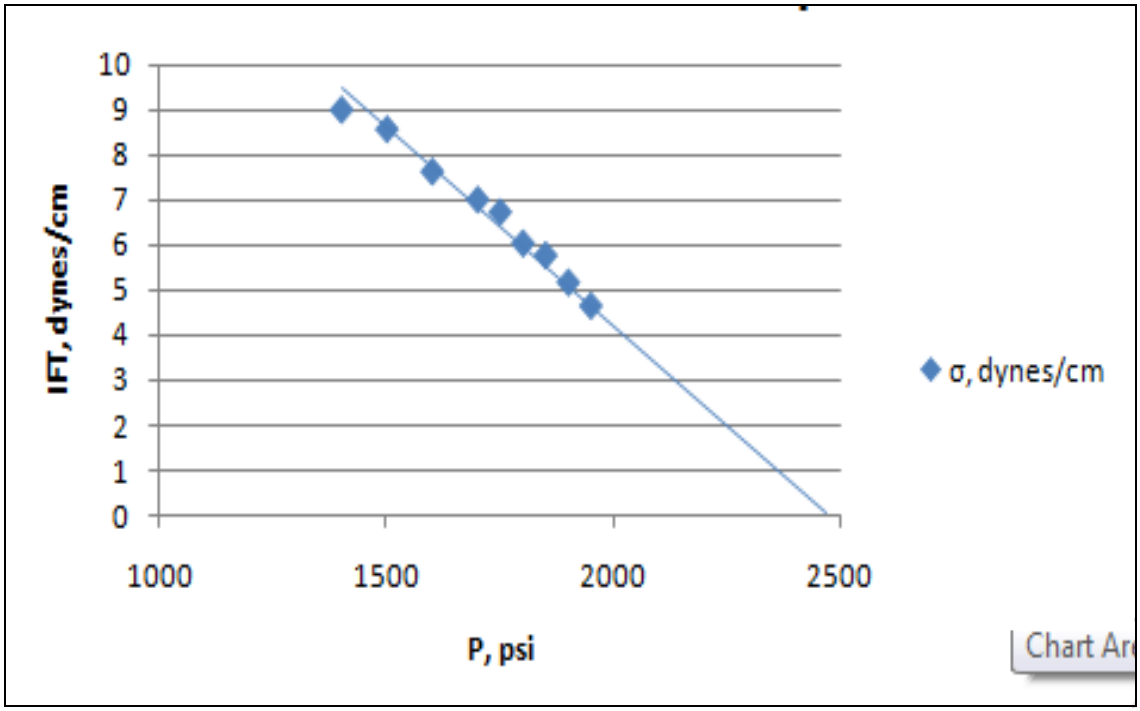

Figure 4.23 MMP Measurement for CO_2-Live Oil Sample G

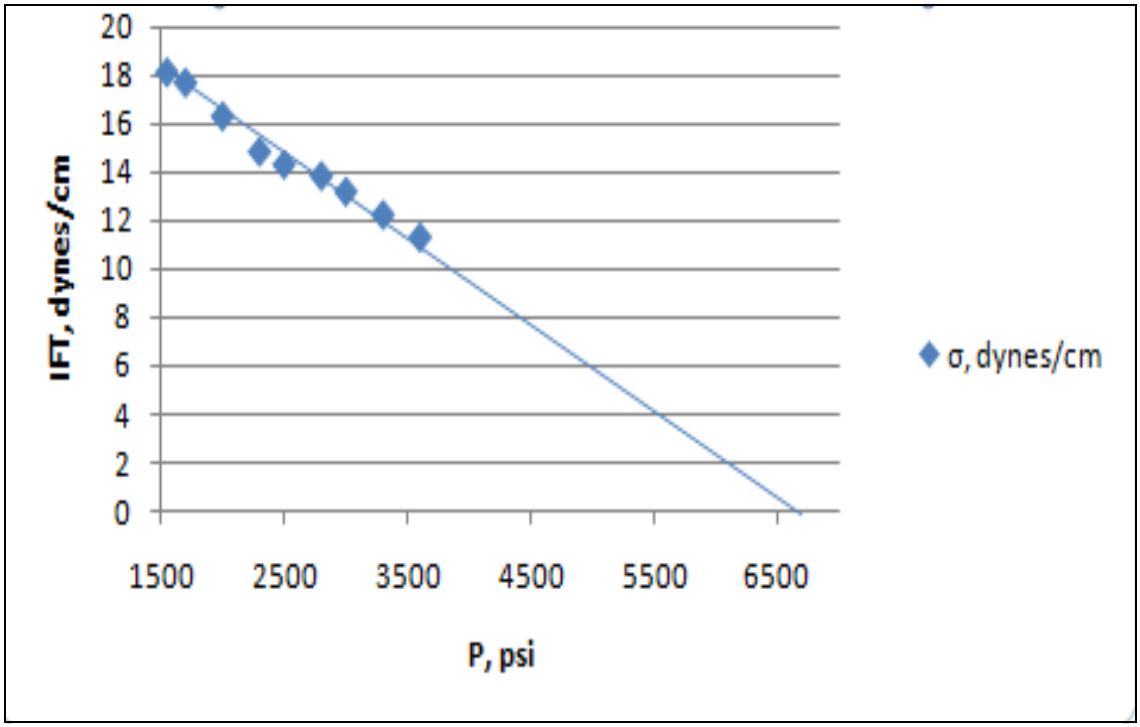

Figure 4.24 MMP Measurement for CH_4-Live Oil Sample G

P, psi	σ, dynes/cm	Δρ, g/cc
1550	18.1134	0.7859
1700	17.6845	0.7672
2000	16.2955	0.7242
2300	14.8255	0.6997
2500	14.2973	0.674
2800	13.823	0.6371
3000	13.1724	0.6138
3300	12.2135	0.5897
3600	11.2783	0.5551

Table 4.27 IFT Measurements for CH_4-Live Oil Sample G

Components	% Mole at MMP
CO2	0.000687
N2	0.027519
C 1	76.83814
C 2	0.004128
C 3	0.004128
C 4	0.000687
C 8	0.507744
C 9	1.70874
C 10	1.322832
C 11	1.297746
C 12	1.895616
C 13	1.94391
C 14	2.19621
C 15	1.963662
C 16	1.049535
C 17	1.550136
C 18+	7.688583

Table 4.28 Equilibrium Composition of CH_4-Live Oil Sample G at MMP

P, psi	σ, dynes/cm	Δρ, g/cc
1550	11.6764	0.746
1700	10.4452	0.7314
1850	9.2692	0.7162
2000	8.4479	0.7022
2150	7.2529	0.6877
2300	6.4923	0.6732
2450	5.3111	0.6593
2600	4.2319	0.6454

Table 4.29 IFT Measurements for VRI-Live Oil Sample G

Components	% Mole at MMP
CO2	0.84477
N2	0.027519
C 1	61.71814
C 2	6.236928
C 3	4.147428
C 4	2.939987
C 5	0.7903
C 6	0.15099
C 7	0.02877
C 8	0.507744
C 9	1.70874
C 10	1.322832
C 11	1.297746
C 12	1.895616
C 13	1.94391
C 14	2.19621
C 15	1.963662
C 16	1.049535
C 17	1.550136
C 18+	7.688583

Table 4.30 Equilibrium Composition of VRI-Live Oil Sample G at MMP

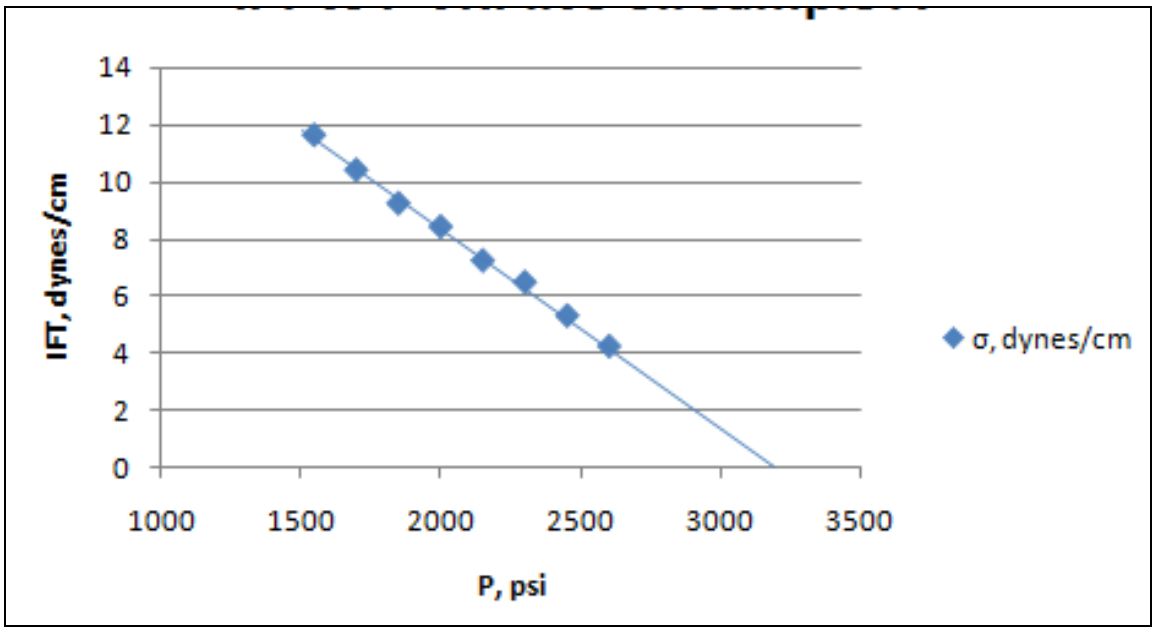

Figure 4.25 MMP Measurement for VRI-Live Oil Sample G

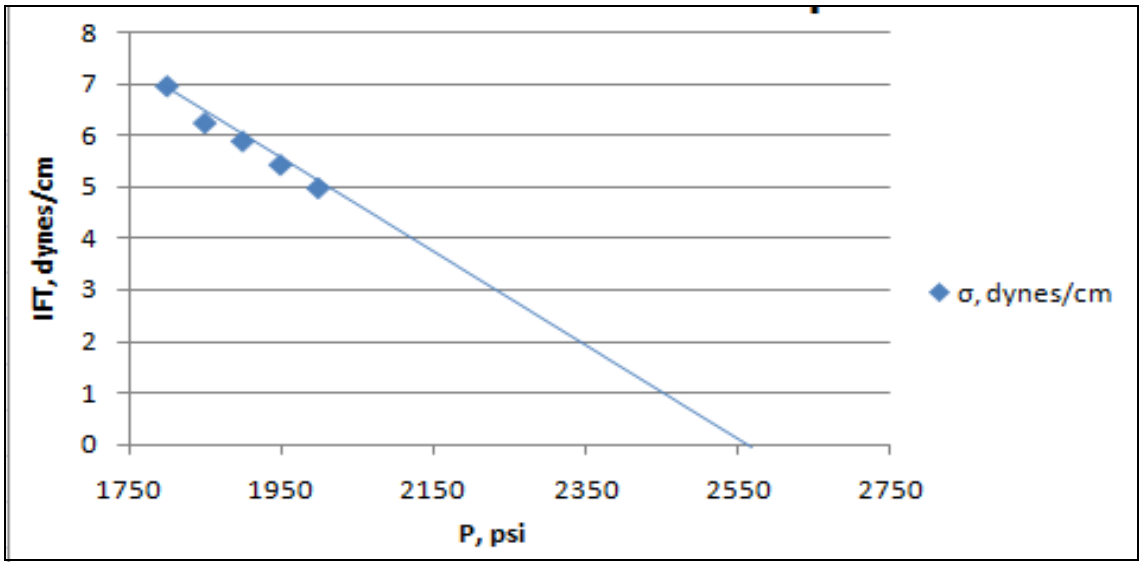

Figure 4.26 MMP Measurement for CO_2-Live Oil Sample H

P, psi	σ, dynes/cm	Δρ, g/cc
1800	6.941	0.253
1850	6.2282	0.239
1900	5.8736	0.2257
1950	5.415	0.2133
2000	4.963	0.202

Table 4.31 IFT Measurements for CO_2-Live Oil Sample H

Components	% Mole at MMP
CO2	70.001045
N2	0.00418
C 1	10.38698
C 2	0.00627
C 3	0.00627
C 4	0.001044
C 6	2.164344
C 7	0.348327
C 8	0.095745
C 9	0.381246
C 10	0.541077
C 11	0.782661
C 12	0.855363
C 13	1.504848
C 14	1.245501
C 15	1.546479
C 16+	10.12698

Table 4.32 Equilibrium Composition of CO_2-Live Oil Sample H at MMP

P, psi	σ, dynes/cm	Δρ, g/cc
1800	17.8845	0.6752
2000	17.001	0.6322
2300	16.6255	0.6077
2500	15.973	0.582
2800	14.98823	0.5451
3000	14.2724	0.5218
3300	13.25135	0.4977
3600	11.783	0.4631

Table 4.33 IFT Measurements for CH_4-Live Oil Sample

Components	% Mole
CO2	0.001045
N2	0.00418
C 1	65.267
C 2	6.23907
C 3	4.14957
C 4	2.340344
C 6	2.31533
C 7	0.377097
C 8	0.095745
C 9	0.381246
C 10	0.541077
C 11	0.782661
C 12	0.855363
C 13	1.504848
C 14	1.245501
C 15	1.546479
C 16+	10.12698

Table 4.34 Equilibrium Composition of CH_4-Live Oil Sample H at MMP

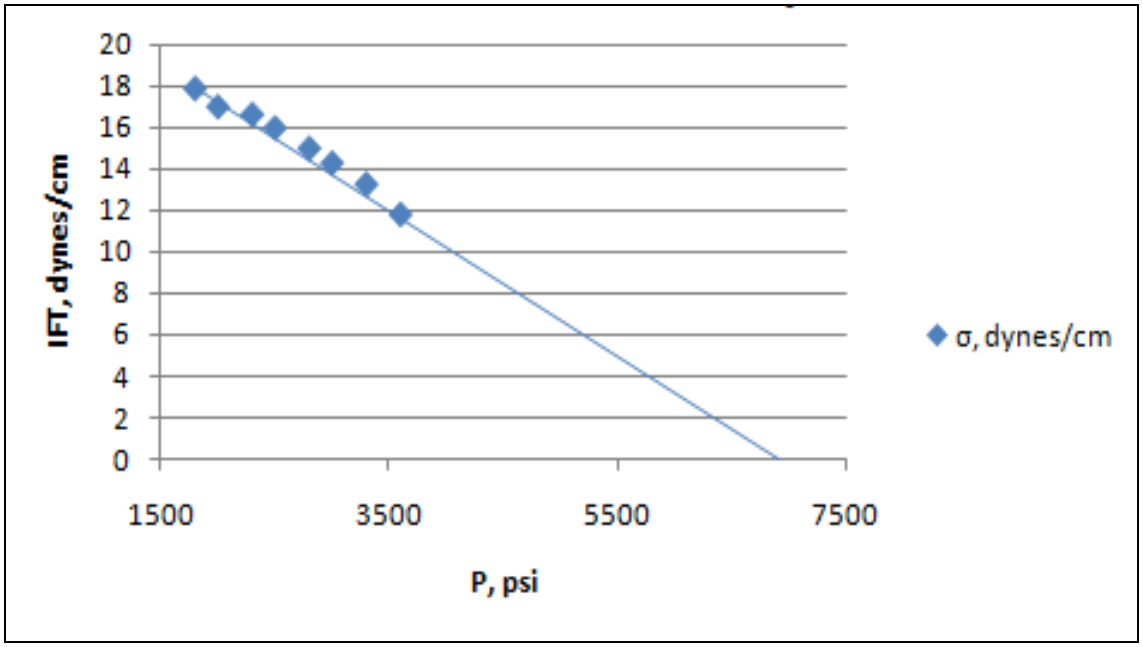

Figure 4.27 MMP Measurement for CH_4-Live Oil Sample H

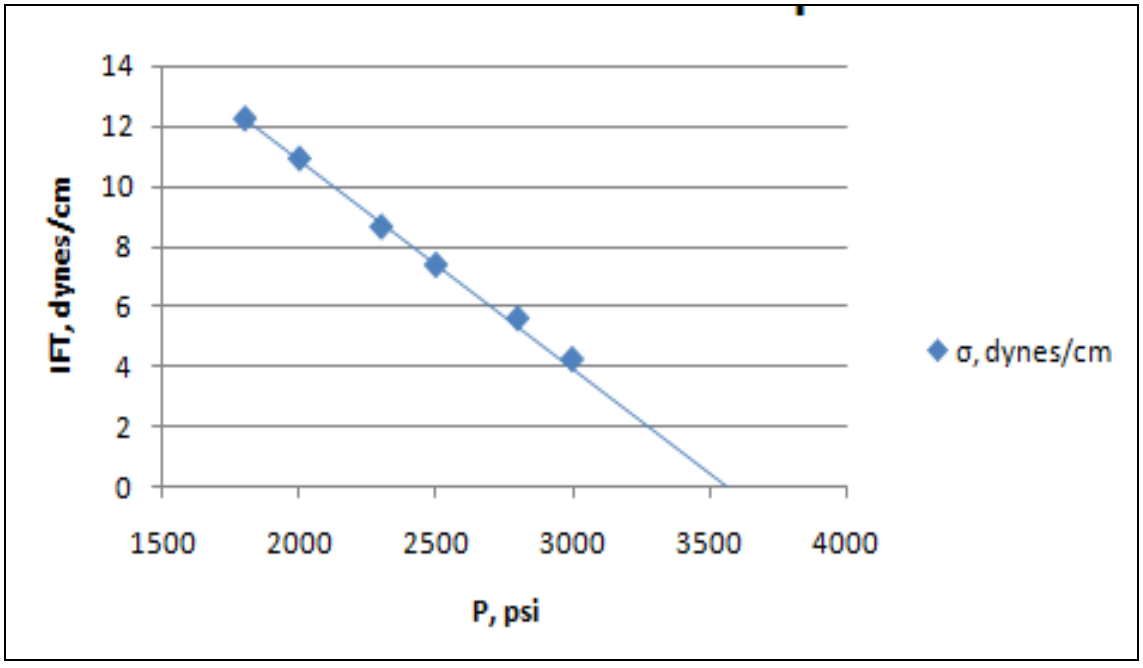

Figure 4.28 MMP Measurement for VRI-Live Oil Sample H

P, psi	σ, dynes/cm	Δρ, g/cc
1800	12.2764	0.7124
2000	10.9452	0.6918
2300	8.6692	0.6687
2500	7.3923	0.6472
2800	5.6111	0.6211
3000	4.2428	0.6018

Table 4.35 IFT Measurements for VRI-Live Oil Sample H

Components	% Mole at MMP
CO2	.841383
N2	0.027519
C 1	61.71814
C 2	6.236928
C 3	4.147428
C 4	2.939987
C 5	0.7903
C 6	0.15099
C 7	0.02877
C 8	0.095745
C 9	0.381246
C 10	0.541077
C 11	0.782661
C 12	0.855363
C 13	1.504848
C 14	1.245501
C 15	1.546479
C 16+	10.12698

Table 4.36 Equilibrium Composition of VRI-Live Oil Sample H at MMP

Chapter 5 FLUID PHASE BEHAVIOR AND VISCOSITY MODELING

System pressure, temperature, fluid composition, and component chemistry dictate the reservoir fluid phase behavior. Accordingly, fluids can exist either in single phase or multiple phases. During the production process petroleum fluids undergo changes in pressure and temperature. Changes in reservoir fluid compositions are introduced when a solvent is injected into the reservoir for enhanced oil recovery. These changes are responsible for controlling the fluid phase equilibrium. Even the viscosities of petroleum fluids are impacted by equilibrium phase properties. Compositional reservoir simulators, surface facility designing, and pipeline flow calculations require prediction of the equilibrium phase properties quantitatively and qualitatively. The most reliable source for obtaining data on equilibrium fluid phases is laboratory experiments. However, measuring fluid properties at all conditions of pressures and temperatures through laboratory studies is time consuming and not practical. Thus, equations of state (EOS) models are employed to carry out the vapor-liquid equilibrium calculations and predict the phase properties. These EOS models can simulate laboratory tests like CCE, DL, and MMP and can also be incorporated into compositional reservoir simulations for predicting the phase properties at each grid block in whole reservoir.

5.1 Equation of State Modeling

An equation of state is an analytical expression that relates the pressure, temperature, and volume of the fluid. One of the simplest EOS is the ideal gas law, which is roughly accurate for gases at low pressures and high temperatures. However, this equation becomes increasingly inaccurate at higher pressures and lower temperatures and fails to predict condensation from a gas to a liquid. In order to improve predictions for the liquid phase, a number of accurate EOS have been developed for gases and liquids. At present, there is no single EOS that accurately predicts the phase properties of all the fluids at all temperatures and pressures. The Peng-Robinson equation, developed in 1976 with modification introduced in 1978, and the Soave–Redlich–Kwong equation are widely used in most PVT simulators and compositional reservoir simulators. The Peng-Robinson EOS performs similar to the Soave equation, although it is generally superior in predicting the liquid phase densities of many fluids, especially nonpolar ones. In this work the Peng-Robinson EOS was used to simulate PVT tests and predict the phase behavior of heavy oils.

Normally most EOS predictions are not accurate. Parameters like bubble point, liquid phase densities, and compositions may be off by several percent from experimental values. These inconsistencies in EOS predictions are due to insufficient characterization of the plus fractions, inadequate binary interaction coefficients, or incorrect overall composition. The predictions of an EOS can be improved by tuning the parameters in the EOS to match experimental fluid phase properties. Most of the time critical pressure (P_c), critical temperature (T_c), and the acentric factor (ω) of the plus fraction or direct multipliers on EOS constants can be modified for matching experimental data obtained from PVT studies on the reservoir fluid. The following sections present EOS modeling and tuning results for experimental PVT data listed in Chapter 4 for ANS viscous oil samples G and H.

5.1.1 Equation of State Tuning

The Peng-Robinson (1978) EOS was used to simulate phase behavior of viscous oil samples. A compositional PVT simulator (WinProp®), developed by Computer Modeling Group (CMG), was used for this task. Figures 5.1 through 5.4 display the results of regressed PR-EOS for sample G. The sample G was characterized compositionally until $C18^+$ and used in a PVT simulator. Figures 5.1 to 5.5 show the match for the solution gas/oil ratio, saturation pressure, and density of oil is satisfactory whereas the liquid formation volume factor, the average deviation between experimental, and regressed EOS prediction increases after 500 psia. The match of density and saturation pressure was given preference over formation volume factor mainly because density measurements are more likely to be accurate compared to formation volume factor, which is a ratio. A small error in measurement of oil volume at standard conditions can give rise to relatively large error in oil formation volume factor.

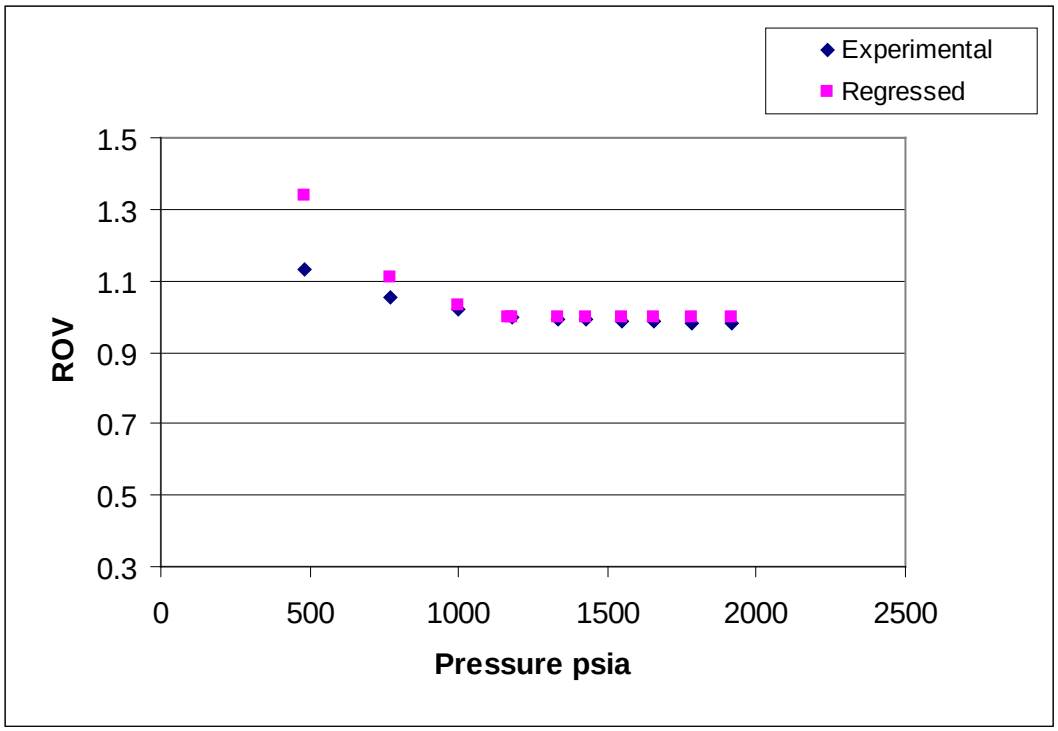

Figure 5.1 Predictions of Tuned Peng-Robinson EOS for Relative Oil Volume of ANS Viscous Oil Sample G

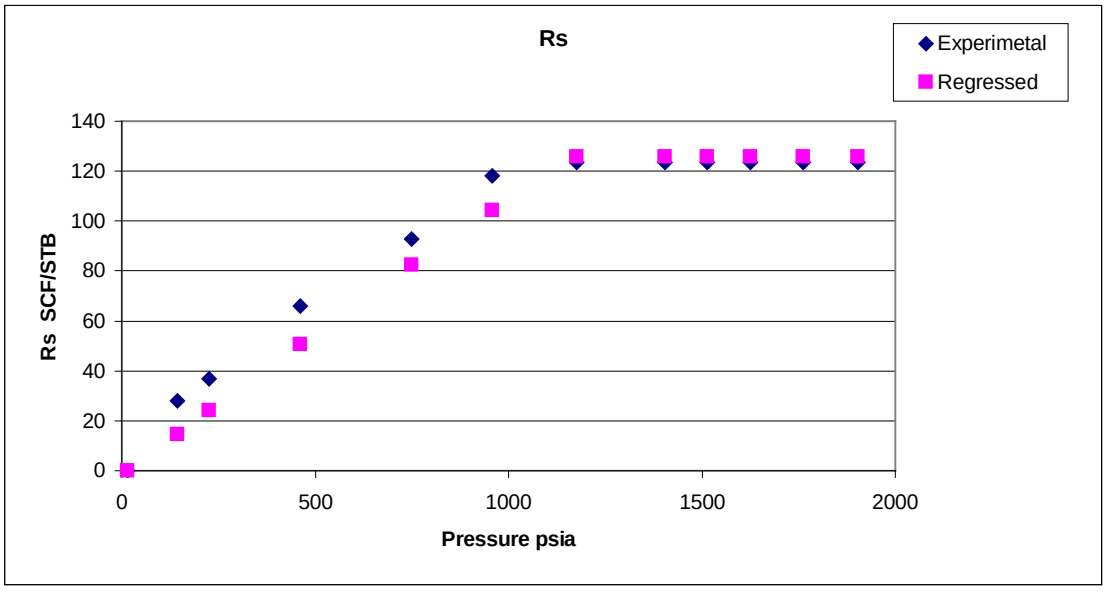

Figure 5.2 Predictions of Tuned Peng-Robinson EOS for Solution Gas/Oil Ratio of ANS Viscous Oil Sample G

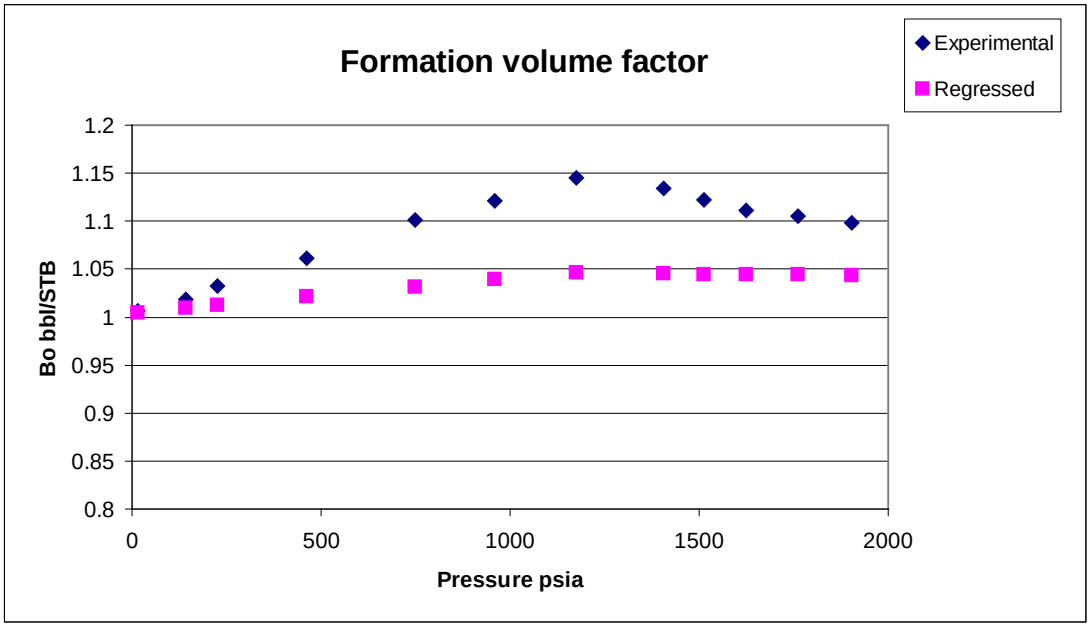

Figure 5.3 Predictions of Tuned Peng-Robinson EOS for Oil Formation Volume Factor of ANS Viscous Oil Sample G

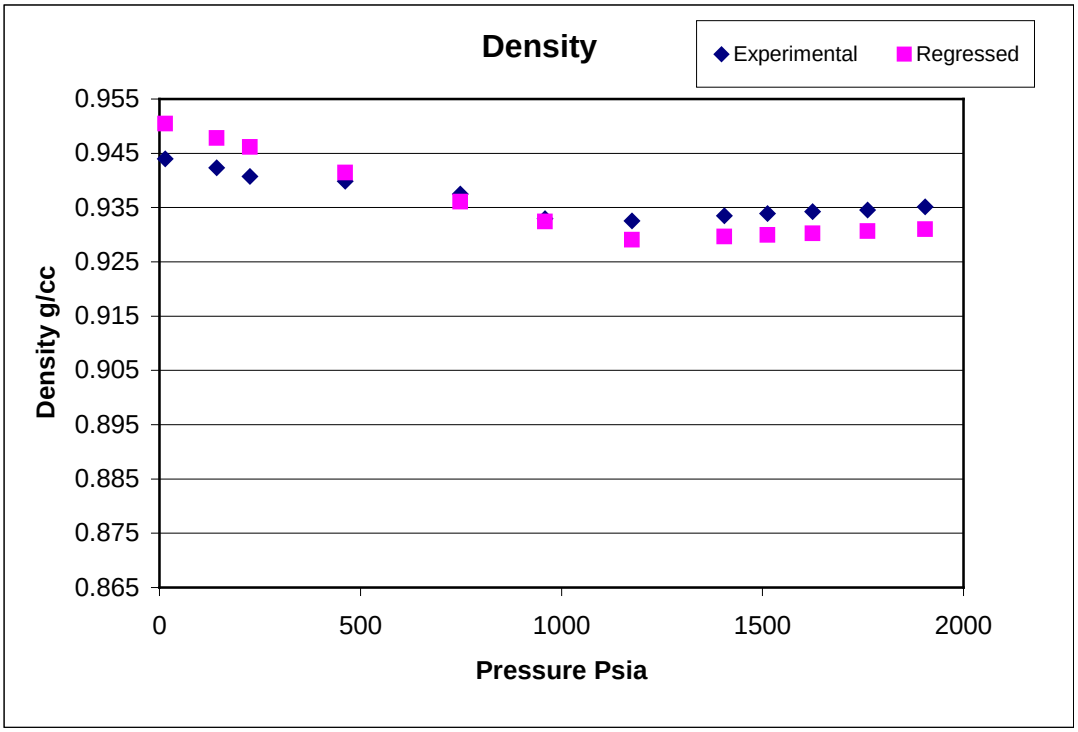

Figure 5.4 Predictions of Tuned Peng-Robinson EOS for Oil Density of ANS Viscous Oil Sample G

Critical properties (P_c, T_c), acentric factor (ω), and molecular weight of the plus fraction along with omega A and omega B parameters for methane, were used as

regression parameters for tuning PR-EOS of Oil sample G. Additionally, volume shift parameters were used to match volumetric data without affecting the equilibrium calculations. Similarly, the PR-EOS was tuned for PVT results of Oil sample H. Figures 5.5 through 5.8 display results of tuning PR- EOS for oil sample H.

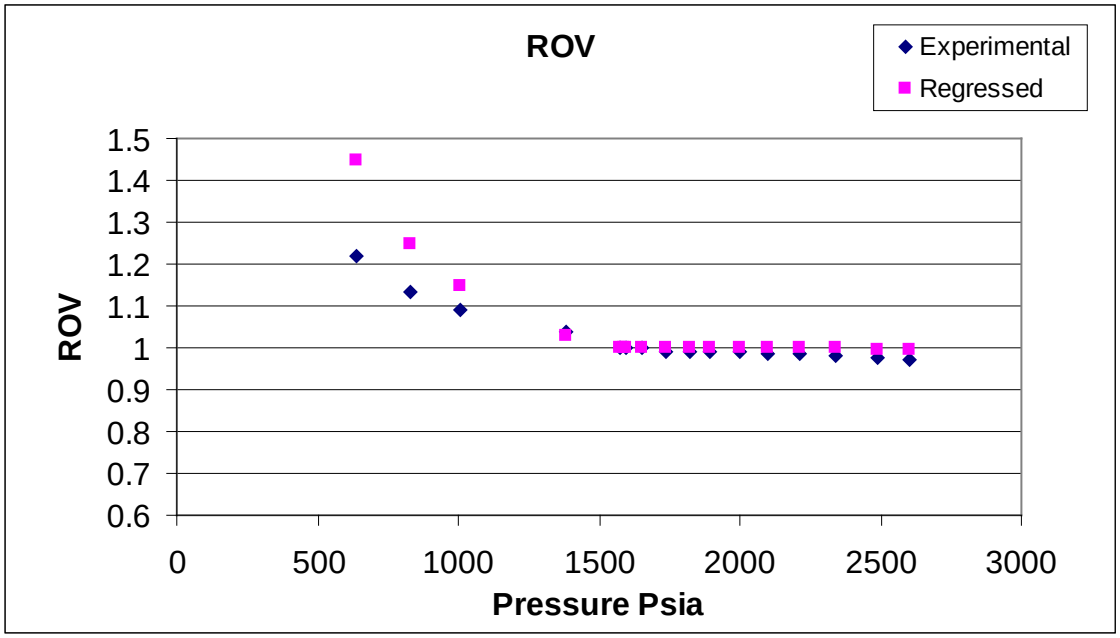

Figure 5.5 Predictions of Tuned Peng-Robinson EOS for Relative Oil Volume of ANS Viscous Oil Sample H

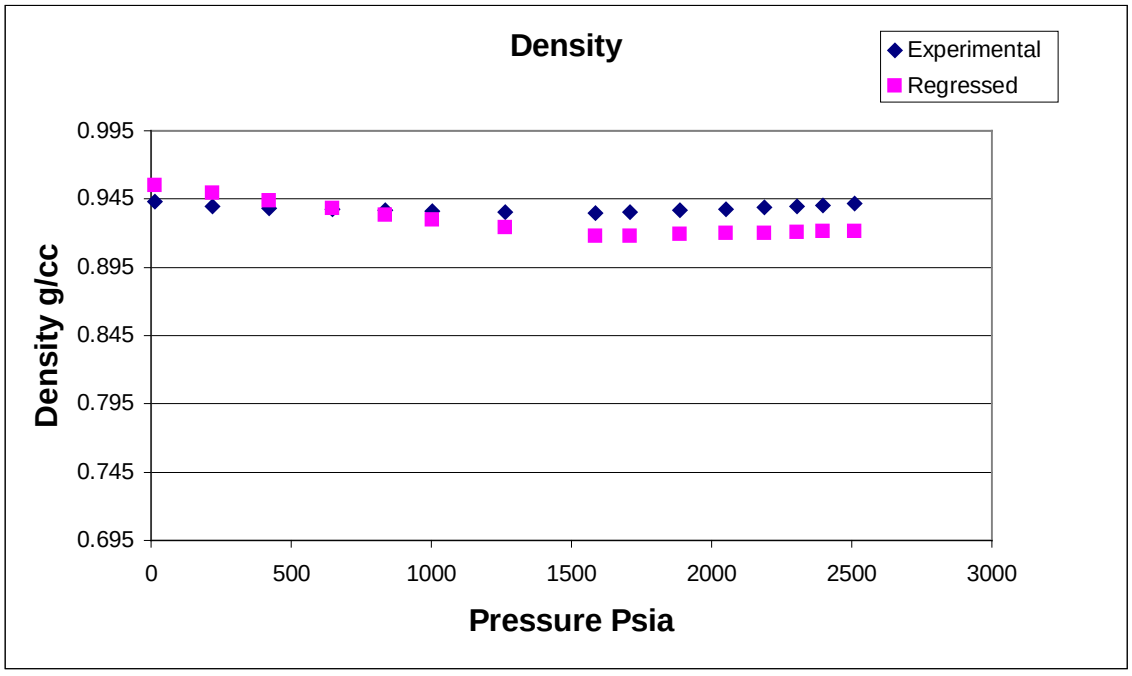

Figure 5.6 Predictions of Tuned Peng-Robinson EOS for Density of ANS Viscous Oil Sample H

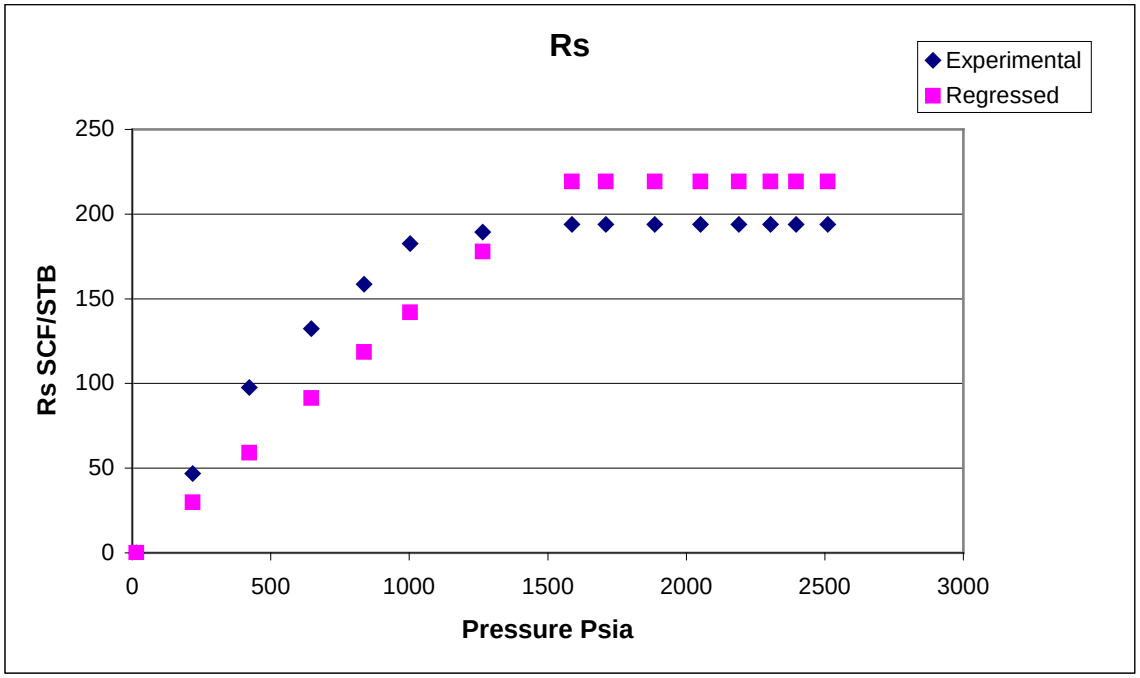

Figure 5.7 Predictions of Tuned Peng-Robinson EOS for Solution Gas Oil Ratio of ANS Viscous Oil Sample H

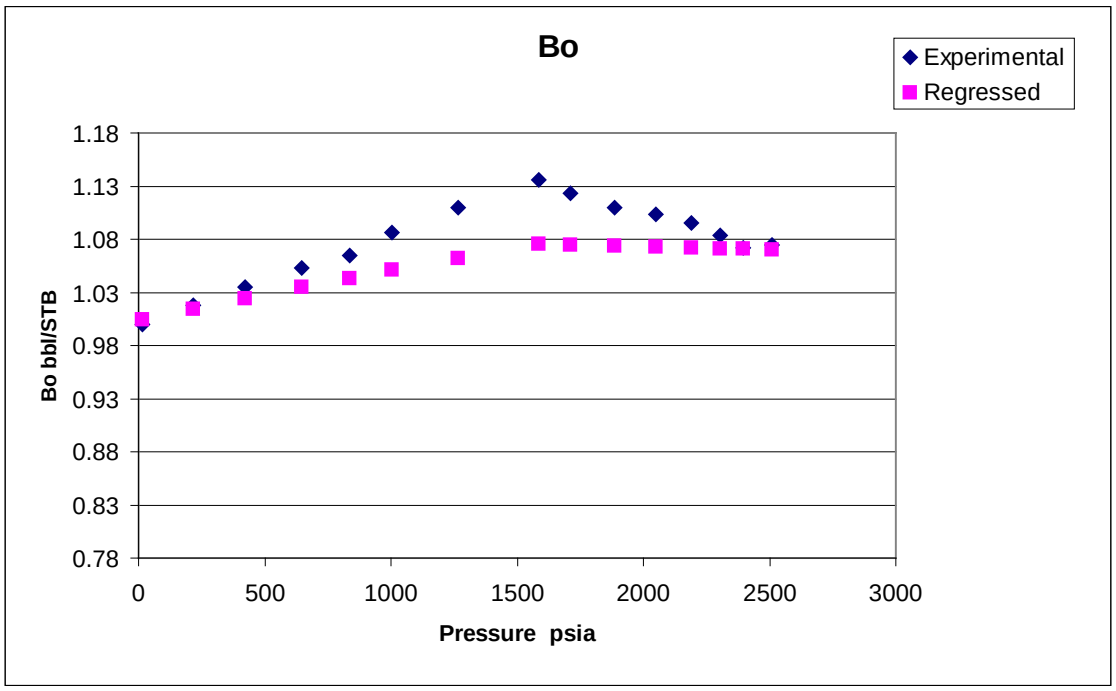

Figure 5.8 Predictions of Tuned Peng-Robinson EOS for Liquid Formation Volume Factor of ANS Viscous Oil Sample H

For tuning EOS for Oil sample H along with critical properties of the plus fraction, omega A, omega B of methane, volume shift parameters and interaction coefficients between each of C_1, N_2 CO_2 with C_{16+} were selected as regression

parameters. As with regression variables the bubble point pressure, densities of oil at various pressures from the differential liberation experiment, and initial solution gas/oil ratio were selected over other experimentally measured properties due to relatively higher accuracy in their measurement.

5.2 Methodology for Viscosity Computation

5.2.1 Characterization of the Plus Fraction

For accurate predictions of phase equilibrium, it is necessary to characterize the plus fraction. Exponential and gamma distributions are the two commonly used distribution schemes for the splitting of the plus fraction. Of these, the exponential distribution scheme is appropriate for the gas condensates and lighter fluids while the gamma distribution is applicable for all types of fluids (WinProp, 2005). For heavy oils, the gamma distribution scheme is commonly employed. However, it requires an experimentally determined parameter, α. This parameter is analogous to the slope parameter used for the exponential distribution types. If extended analysis data are available and α is not specified, it is determined by minimization to best fit the experimental data. Due to the larger number of adjustable parameters in the gamma distribution, the α parameter must be specified if no extended analysis is available. In the absence of this extended analysis, there is no reliable prediction method.

Recently, Pedersen et al. (2004) modified their earlier exponential distribution characterization method for heavy oils. This method allows characterizing the plus fraction to a single carbon number as high as 200. Moreover the authors recommended using this distribution scheme with their new viscosity model for heavy oils (Lindeloff et al., 2004). Due to a large bulk of pseudo-components (C_7 - C_{200}), they are then lumped together by the well known Whitson lumping scheme (Whitson, 1983). For almost all of the oil samples studied, this lumping procedure resulted into a generation of nine pseudo-components. The simplistic Kay's mixing rule is used to find the properties of an individual component.

5.2.2 Estimation of Pseudo-Component/Plus Fraction Properties

For most purposes, the plus fraction specific gravity and the molecular weight are available. Twu (1984) physical properties correlation is used to internally estimate the boiling point of the plus fraction. This boiling point, in addition to known specific

gravity, is then used for the estimation of the critical properties (T_c, P_c) of the plus fraction by Twu (1984) critical properties correlation. For eccentric factor estimation, the Kesler-Lee (1976) correlation is used.

A similar approach is used to compute the pseudo-component properties. The generalized molecular weight and specific gravities (Whitson, 1983) are used whenever necessary. For the Pedersen et al. (2004) characterization scheme, the pseudo-component molecular weight is calculated by the proposed correlation, while the specific gravity is determined by the internally consistent correlation. The critical properties of these pseudo-components are estimated by the EOS specific correlations presented by the authors in the same paper.

5.2.3 Binary Interaction Parameters (BIPs)

The importance of the interaction parameters, δ_{ij}, in the accuracy of the phase behavior calculations, especially saturation pressures, has been demonstrated by Peng and Robinson (1976). Theoretically, BIP is introduced to account for the molecular interaction between dissimilar molecules. Their values are usually obtained by fitting the predicted saturation pressure curves to the experimental data for binary systems.

The hydrocarbon (HC) and non-hydrocarbon (Non-HC) interaction parameters used are from the Computer Modeling Group Ltd. (CMG) database. These values are essentially taken from Oellrich et al. (1981). The HC-HC interaction coefficients are estimated in the following correlation:

$$\delta_{ij} = 1 - \left[\frac{2\sqrt{V_{c_i}^{1/3} \times V_{c_j}^{1/3}}}{V_{c_i}^{1/3} + V_{c_j}^{1/3}} \right]^{\theta} \tag{5.1}$$

In the above equation, θ is used as an adjustable parameter that can be tuned to match the experimental data. Oellrich et al. (1981) have suggested that this value is usually constant and can be set to 1.2 for most calculations. Note that the units of the critical volumes should be consistent with the rest of the calculations. In this work the units of the critical volumes are set to cu ft/lb-mole. If the Pedersen et al. (2004) characterization scheme is used, then the HC-HC BIPs are set to zero as suggested by the authors.

5.2.4 Volume Shift

The Volume Translation technique is used for improving the prediction of phase density with EOS. Since density is an input parameter for some of the viscosity

calculation methods, it is of the utmost importance to correct the liquid-phase volume predicted by the EOS. The Peneloux et al. (1982) method of improving volumetric predictions by introducing a third parameter into a two-parameter EOS is applied to the PR-EOS. This method is particularly attractive because the third parameter does not change the vapor/liquid equilibrium conditions determined by the modified, two-parameter equation, but modifies the phase volumes by effecting certain translations along the volume axis. For simplicity, temperature-independent volume shifts generated by CMG's WinProp module are used in the calculation routines. This shift parameter calculation method is based on the procedure proposed by Jhaveri and Youngren (1988). For the Pedersen et al. (2004) characterization scheme, the temperature dependent volume translation is used. The necessary equations are presented in the aforementioned reference.

5.2.5 Estimation of the Bubble Point Pressure (P_b)

The bubble point pressure is calculated by PR-EOS. The procedure is generic and is readily available in the literature (Dandekar, 2006).

5.2.6 CCE and DL Simulation

The CCE and DL tests are mainly required to obtain the compositional profile and reservoir engineering data for every pressure reduction step below the bubble point pressure. As with bubble point pressure, the simulation procedure is very generic. The simplistic review is provided by Dandekar (2006). The initial guess for the flash calculations is computed from the relationships summarized by Riazi (2005). This guess is very important for the convergence of the flash calculations.

5.2.7 Regression

The EOS parameter tuning is a nonlinear minimization problem. The phase behavior simulated with any EOS often does not match with the experimental data. Hence, it is always necessary to ‘tune’ certain parameters to accurately simulate the experimental data. These parameters are generally the ones with less confidence in their estimated values, e.g., typically the P_c, T_c, and ω of the plus fraction or the pseudo-components.

The objective function can be expressed as:

$$F\left(\vec{x}\right)=\sum_{i=1}^{N}\left\{w_i \bullet \left[\exp_i - \mathrm{mod}el_i\left(\vec{x}\right)\right]\right\}^2 \qquad (5.2)$$

Here x is a vector of tunable parameters. N, w, exp, and $model$ denote the number of data points, the weight factor, and the experimental and model-calculated values, respectively. The typical experimental data points are the bubble point pressure, bubble point density, API gravity, liquid phase densities at different pressures, solution gas/oil ratio, formation volume factors, etc. The weighing factors are generally kept at unity except, in some cases, for the bubble point pressure and density can be set at higher values depending upon the match needed.

This problem is solved with the commonly employed Levenberg-Marquardt algorithm as listed by Agarwal et al. (1990) and Zuo and Zhang (2000). Agarwal et al. have introduced an additional modification to dynamically select the most meaningful regression parameters from a larger set of variables. This selection is extremely useful in EOS fitting because it alleviates the problem of deciding in advance the best regression variables, which is extremely difficult. In order to avoid significant programming efforts to introduce the above modification, a readily available algorithm in MatLab® was used. MatLab® has a built-in *'lsqnonlin'* solver available for nonlinear least squares problems in its Optimization Toolbox. It has two different algorithms available to solve these problems:

1. Large Scale
2. Medium Scale – Levenberg-Marquardt

The comprehensive description of these algorithms can be found in the MatLab's Help section. The large-scale method for *lsqnonlin* does not solve underdetermined systems; it requires that the number of equations (i.e., the number of elements of F) be at least as great as the number of variables. In the underdetermined case, the medium-scale algorithm was used instead. For example, data set A does not have any PVT data available except the bubble point pressure. In this case one has to use the medium-scale algorithm. The prominent tuning parameters are P_c, T_c, and ω of the pseudo-components. It must be stated here that only these commonly employed tuning variables have been used to tune the phase behavior data. No significant efforts were expended to devise the best possible tuning strategy, since the main focus of the project is to model the viscosities. The bounds on these variables were typical in the range of ±20%, ±20%, and ±5%, respectively. In rare circumstances these bounds were exceeded.

5.2.8 Calculation Scheme

1. Basic input parameters: *T*, *P*, composition, and *MW* and specific gravity of the plus fraction
2. Characterization of plus fraction (optional)
3. Modified Exponential Distribution (Pedersen et al., 2004)
4. Estimation of pseudo-component/plus fraction properties
5. Physical and critical properties (Twu, 1984)
6. Acentric factor (Kesler and Lee, 1976)
7. Estimation of bubble point pressure (P_b)
8. PR-EOS
9. Liquid volume correction (volume shift)
10. Binary Interaction Parameters (BIP)
11. Constant Composition Expansion (CCE) simulation
12. Differential Liberation (DL) simulation
13. Evaluation of viscosity with different compositional models
14. Regression of the experimental data and tuning
15. Application of the tuned parameters to various viscosity models

The above calculation scheme is followed to evaluate the data sets. For the given data, an input Microsoft® Excel® file is created. MatLab® is used as a programming platform. The output is written back to the same Excel file in the designated cells.

5.3 MMP Calculations by EOS and by Using Correlations

As described in Section 3.5, the Peng-Robinson (1978) EOS was used to perform numerical calculations to determine MMP. CMG WinProp's MCM simulator was used to perform these calculations. The EOS was tuned by the procedure mentioned in Section 5.5.1. The VIT technique involved contact of fresh reservoir oil with pre-equilibrated CO_2 gas by placing a small amount of oil at the bottom of the optical cell. This process simulated a dynamic (multiple-contact) displacement process occurring in the reservoir, where the injected gas interacts with reservoir oil as it moves ahead in the reservoir, and gradually there is an alteration in composition due to mass transfer between fluid phases so as to become miscible with the original oil. The definition of multiple contact is an approximation which serves well to explain the "continuous interaction" that actually occurs in an reservoir. It is an approximation because an infinite number of such contacts

between phases will be required in order to truly approach the result of their continuous interaction.

Since the IFT measurements were made using the pendant drop technique after complete equilibrium and stabilization of the mass transfer between the fluid phases, it was concluded that the terms “Equilibrium IFT” and “Equilibrium Miscibility” are appropriate to use for this type of an experimental study. Equilibrium IFT typically simulates a real reservoir where the injected CO_2 gas interacts continuously with crude oil as it flows to the producing well. This continuous interaction enables counter-directional mass transfer (vaporizing and condensing) between the fluid phases, thereby allowing the system to attain equilibrium miscibility. The simulations performed using a MCM simulator helped in determining the dominant mass transfer process. In the case of CO_2, the mass transfer occurred by condensing drive, while condensing-vaporizing drive and vaporizing drive were dominant for VRI and CH_4 injections, respectively. The percent deviation between MMP calculated by pendant drop experiments and those obtained from MCM simulations was about 4.86%. The results are shown in Table 5.1.

Oil Sample	**CO_2 MMP**		**CH_4 MMP**		**VRI MMP**	
	Expt.	**Simulated**	**Expt.**	**Simulated**	**Expt.**	**Simulated**
Sample A Dead Oil	2150	2178	6432	6450	2725	2754
Sample B Dead Oil	2215	2243	6618	6645	2884	2900
Sample A Live Oil	2478	2505	6652	6690	3206	3215
Sample B Live Oil	2586	2625	6988	7013	3550	3577

Table 5.1 Comparison of MMP Calculations

MMP was calculated using various correlations described in Section 2.1.10. It should be noted that Equations 2.5 and 2.6 only consider temperature as a parameter for MMP calculations, and hence the results were found to be the same for different CO_2-oil systems at the same temperature. An important assumption while using Equations 2.5 and 2.6 is that, for reservoirs below 120°F, the bubble point pressure should be considered as the MMP. The values obtained by Equation 2.7 were based on temperature and composition of the plus fraction along with composition of methane in oil phase. It should be noted that these correlations were developed for different sets of oil samples which are comparatively different from oil samples used here. Therefore, the values of

MMP using correlations only serve as a base and should not be used for comparisons. The values obtained by MMP correlations are reported in Table 5.2.

Oil Sample	**CO_2 MMP**			**CH_4 MMP**
	equation 2.5	**equation 2.6**	**equation 2.7**	**equation 2.8**
Sample 1 Dead Oil	1163.176	1275.94	2411.23	6623.74
Sample 2 Dead Oil	1163.176	1275.94	2623.16	6815.23
Sample 1 Live Oil	1395	1395	2843.12	7125.44
Sample 2 Live Oil	1786	1786	3012.58	7297.61

Table 5.2 MMP Calculations by Correlations

A comparison between the MMP calculated by simulations and experiments and those by using correlations are shown in Figures 5.9, 5.10, and 5.11, respectively. Note that for calculating values of CO_2-oil systems, only Equation 2.7 was used.

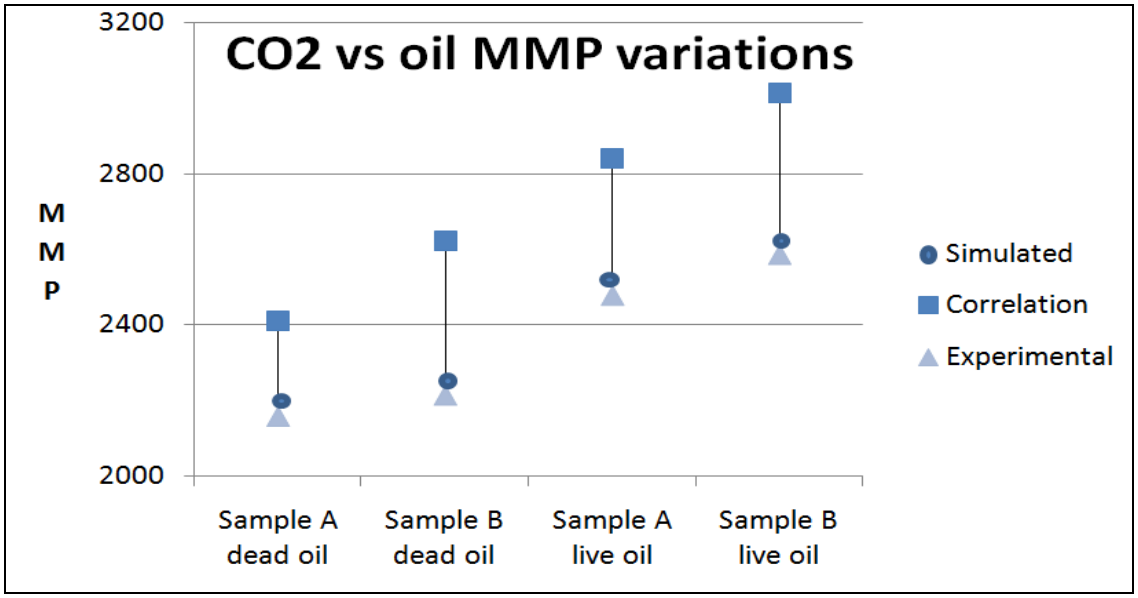

Figure 5.9 CO_2-Oil Samples MMP Variations

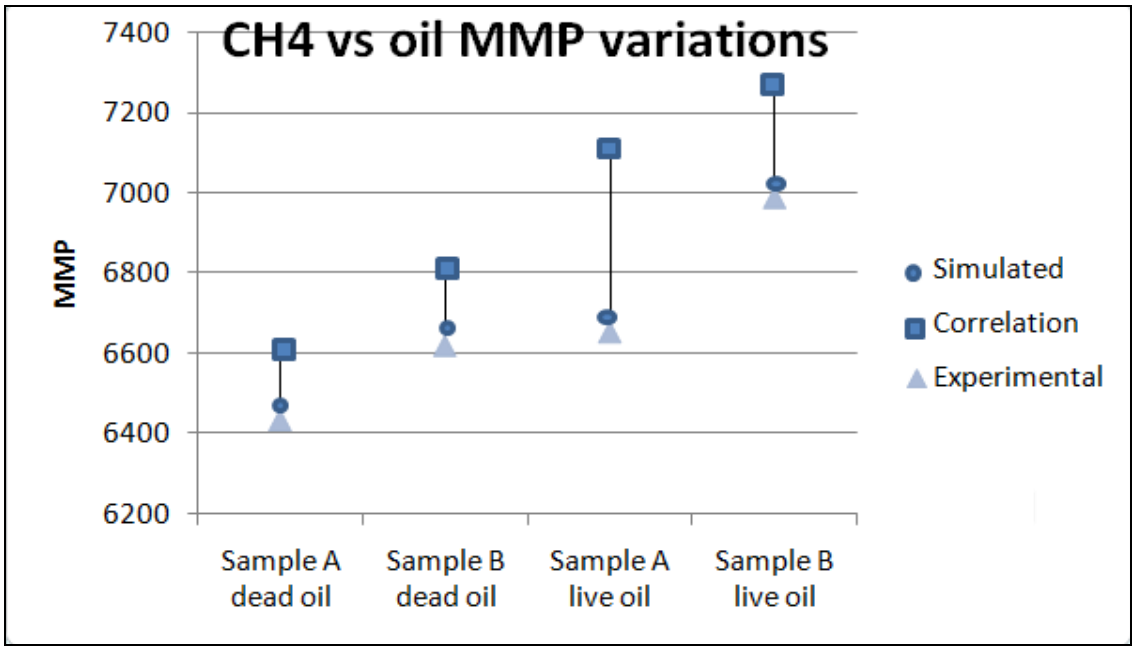

Figure 5.10 CH_4-Oil Samples MMP Variations.

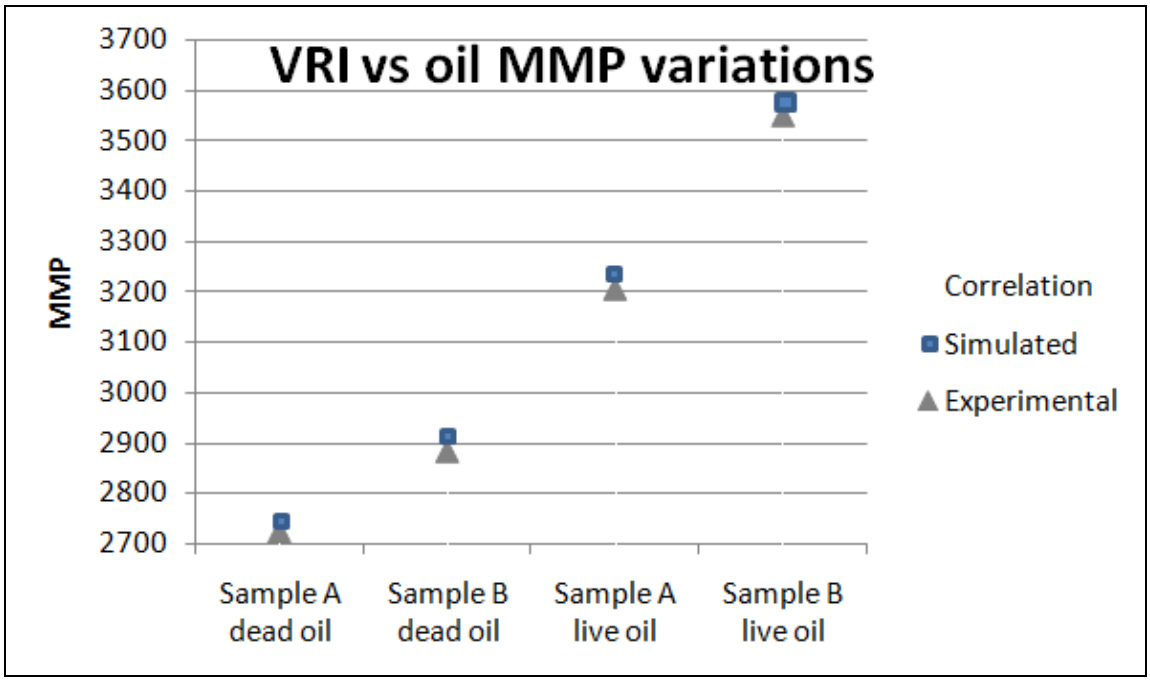

Figure 5.11 VRI-Oil Samples MMP Variations.

Chapter 6 COMPARATIVE STUDY OF VISCOSITY MODELS

6.1 Evaluation Procedure

In this chapter, a comparative study is presented for the LBC and Pedersen class models. The Lindeloff model (Lindeloff et al., 2004) is dealt with separately in the next chapter. The calculation scheme explained in the previous chapter is followed to evaluate each data set. A series of M-files (MatLab® files) is created to calculate the bubble point pressure, CCE and DL simulation, and viscosities by various models. These files are run in the aforementioned order to generate an output. The runs are carried out by two methods: uncharacterized oil sample and after characterizing with the Pedersen et al. (2004) scheme. For most of the oil samples, the molar compositional data was available until C_{7+}. For an uncharacterized oil sample, the plus fraction data (C_{7+}) are used as is. Table 6.1 shows the comparison of the experimental and calculated bubble point pressures.

Data Set	Temp, °F	Experimental P_b, psia	Calculated P_b, psia		% Deviation	
			Uncharacterized	Characterized	Uncharacterized	Characterized
Set A	130	2324	4497.8	3731.9	94%	61%
Set B	171	754	1002.0	1133.7	33%	50%
Set C1	100	178	200.0	232.0	12%	30%
Set C2	140	201	232.7	268.9	16%	34%
Set C3	180	225	267.2	307.6	19%	37%
Set D1	100	165	228.0	261.8	38%	59%
Set D2	140	180	264.8	303.3	47%	69%
Set D3	180	195	302.5	346.1	55%	77%
Set E1	80	510	693.4	877.3	36%	72%
Set E2	120	575	800.0	1005.0	39%	75%
Set E3	160	640	902.0	1127.0	41%	76%
Set F	114	1046	1715.5	1676.0	64%	60%
Set G	84	1183	1376.5	1493.6	16%	26%
Set H	81	1587	2562.2	2674.1	61%	69%
					41%	**57%**

Table 6.1 Experimental vs. Simulated Bubble Point Pressures

Table 6.1 shows the experimental and calculated bubble point pressures do not match. Hence, it is of the utmost importance to match these pressures before any comparison is done. To accomplish this, it is necessary to tune certain variables (e.g. P_c, T_c, of pseudo-components) to match the bubble point pressure. In this study, only the critical pressure

of plus fraction or that of pseudo-components is varied to obtain the match. However, no attempt was made to match bubble point viscosities. Without this, it is difficult to make one-on-one comparison. However, the main purpose of the comparative study is to evaluate the raw prediction capabilities of different viscosity models. So, it is still possible to carry out a qualitative comparison.

Instead of presenting the results for all samples, the representative results are presented only for Data Set C1. This, however, allows discussing the results in great detail for each and every viscosity model considered for this study. Essentially the same trend is observed for all the other data sets with minor variations. The results for the Data Sets A and F are summarized in Raut (2007). The experimental viscosity versus the pressure profile for set C1 is plotted in Figure 6.1.

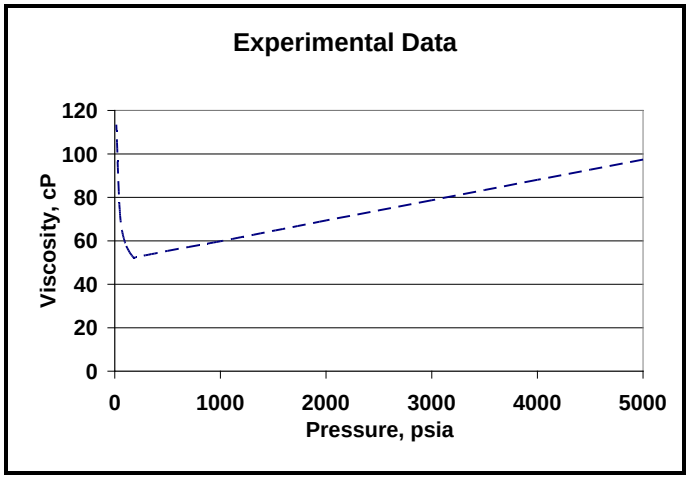

Figure 6.1 Plot of the Experimental Data for Set C1 at 100°F

Figures 6.2 and 6.3 summarize the simulation results for different viscosity models. The results are classified into two main categories: Uncharacterized sample and Characterized sample.

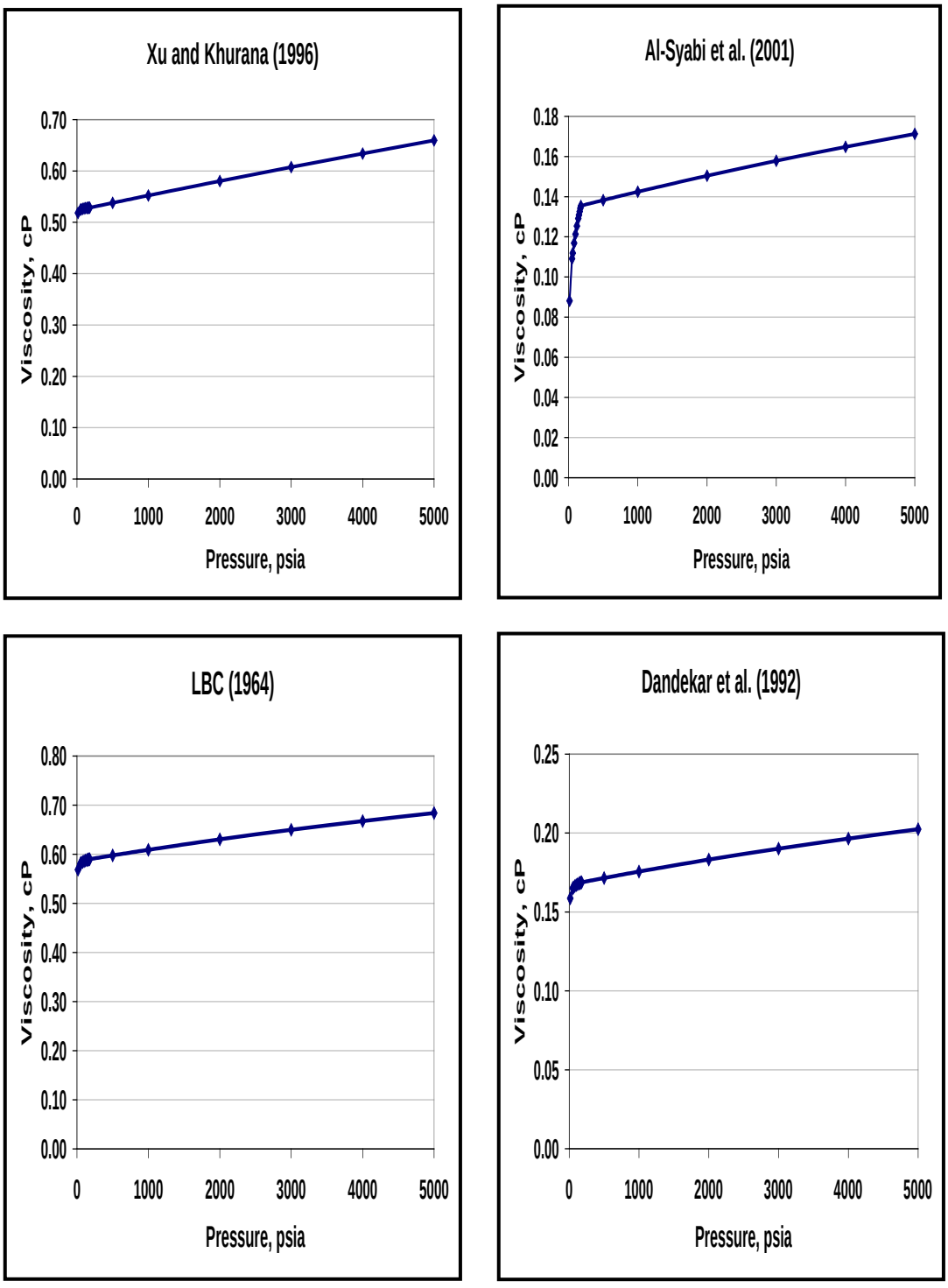

Figure 6.2 Results for Uncharacterized Oil Sample (Data Set C1)

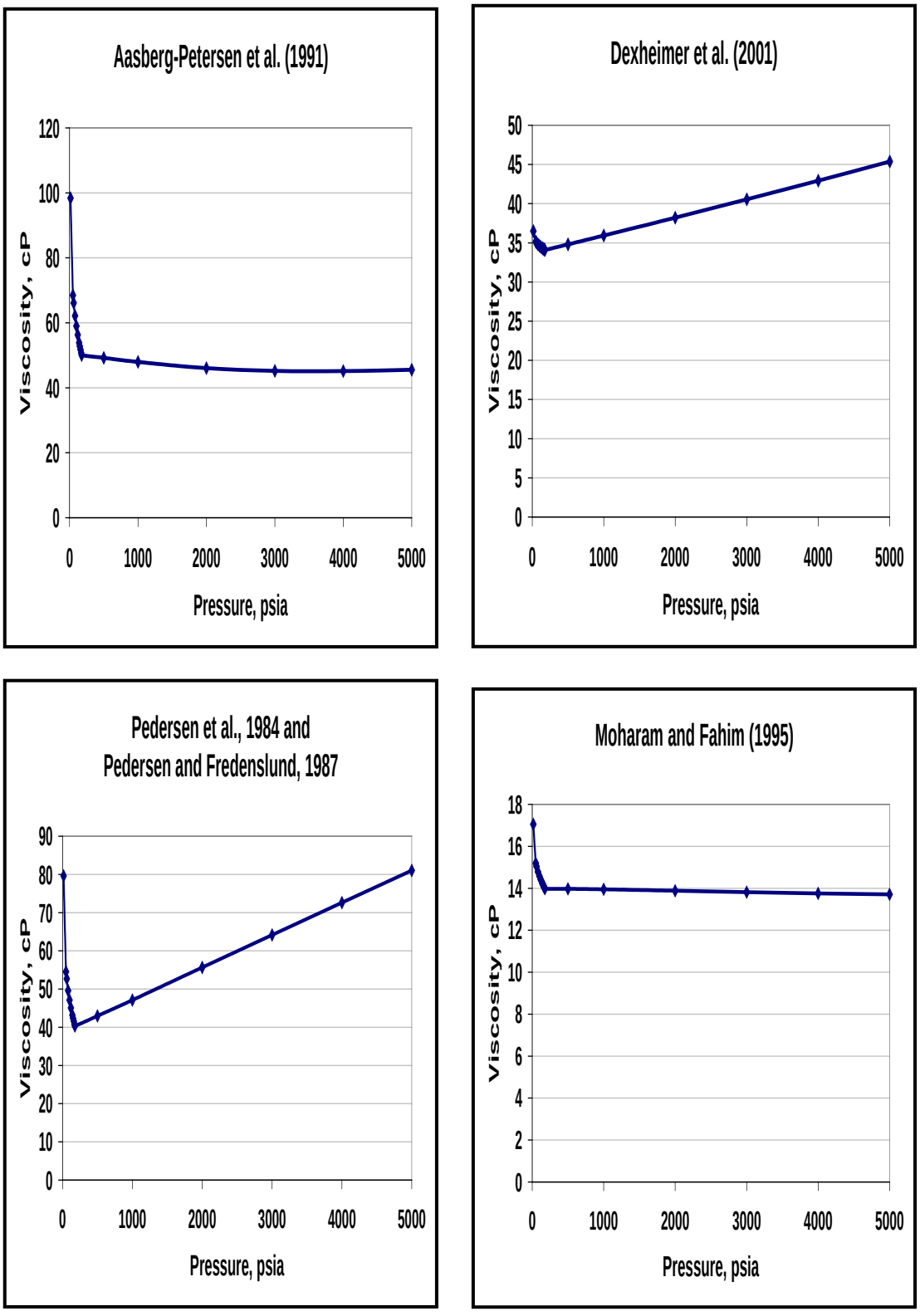

Figure 6.2 (continued) Results for Uncharacterized Oil Sample (Data Set C1)

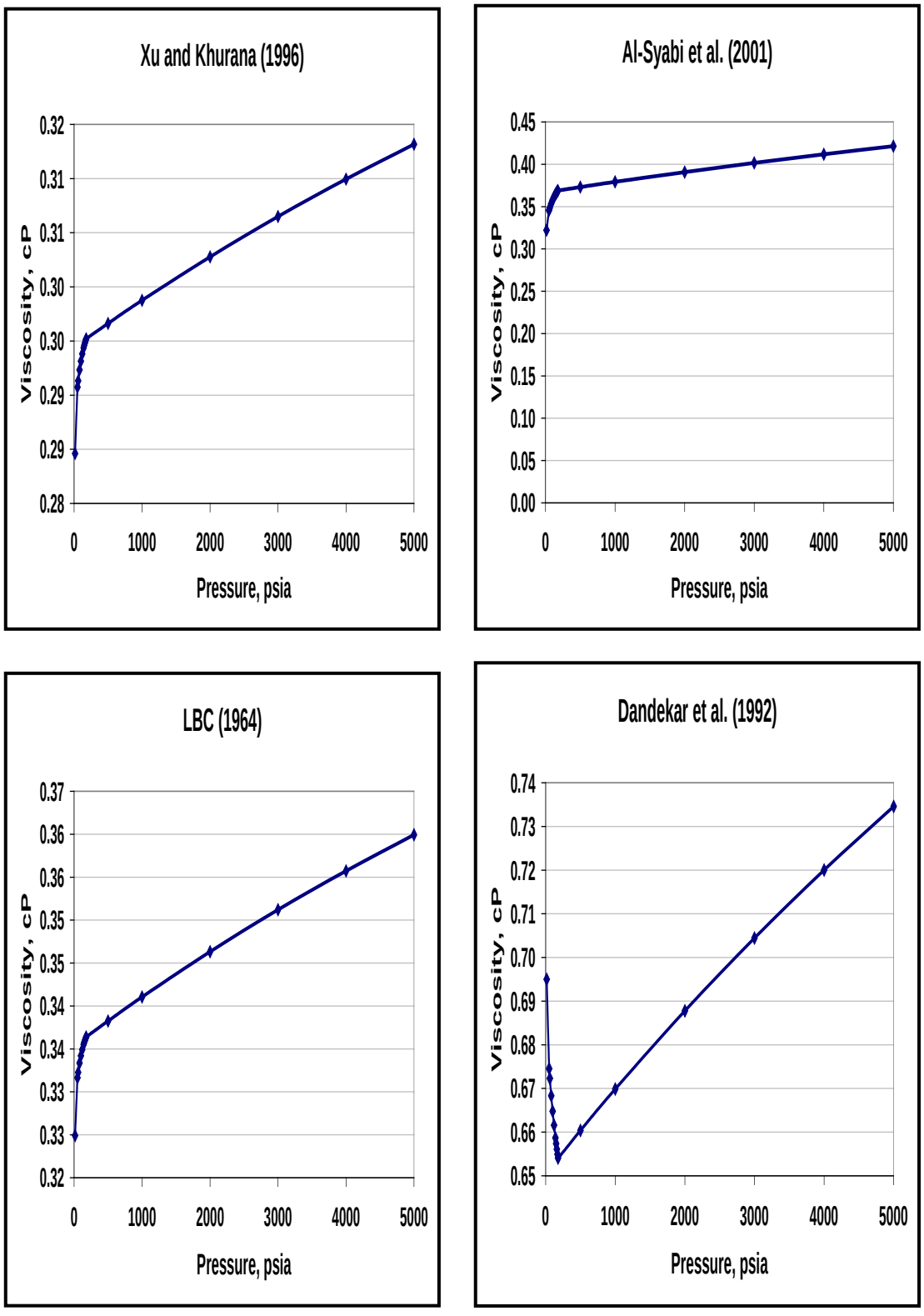

Figure 6.3 Results for Characterized Oil Sample (Data Set C1)

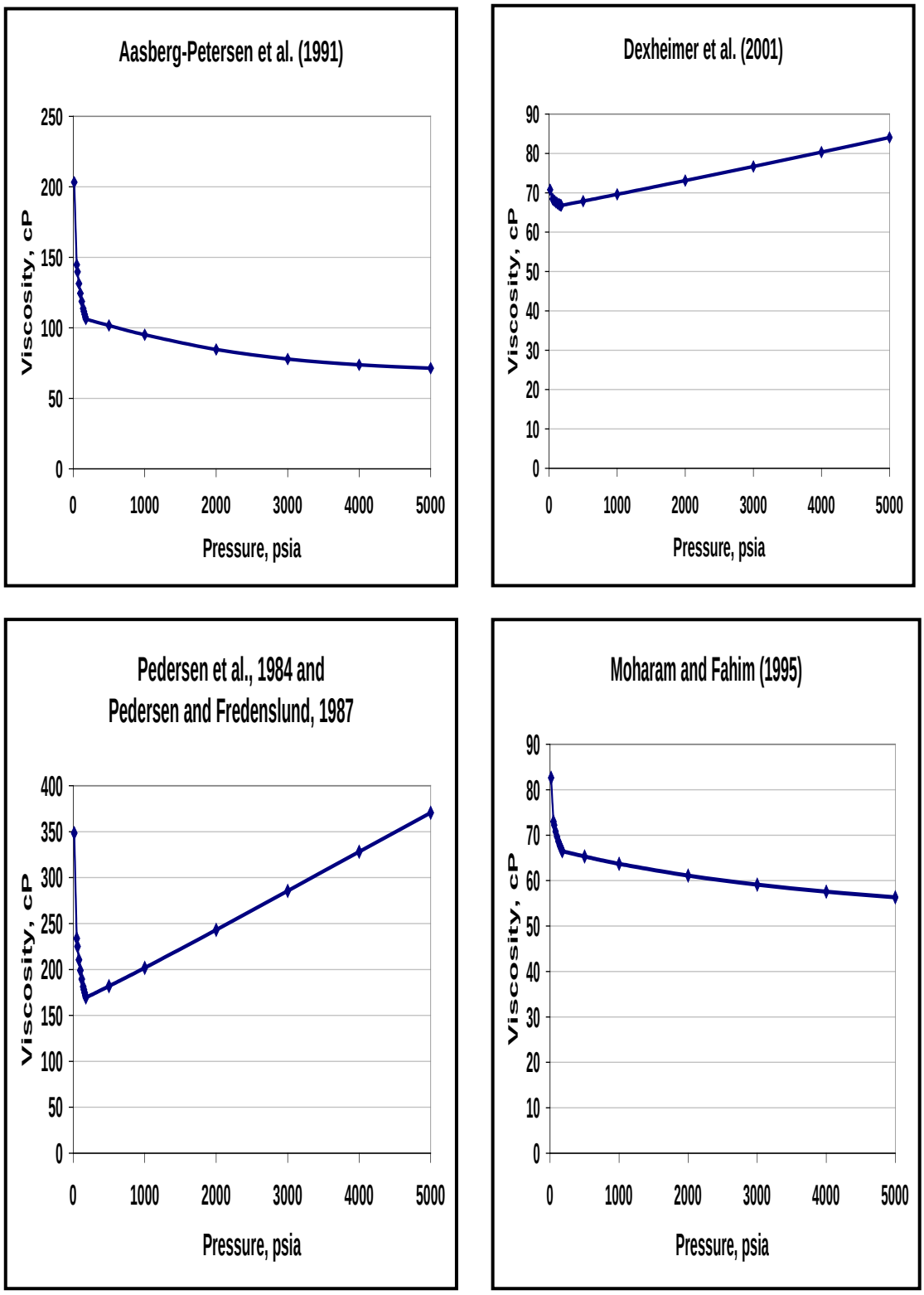

Figure 6.3 (continued) Results for Characterized Oil Sample (Data Set C1)

The above results are further summarized in Figures 6.4 and 6.5.

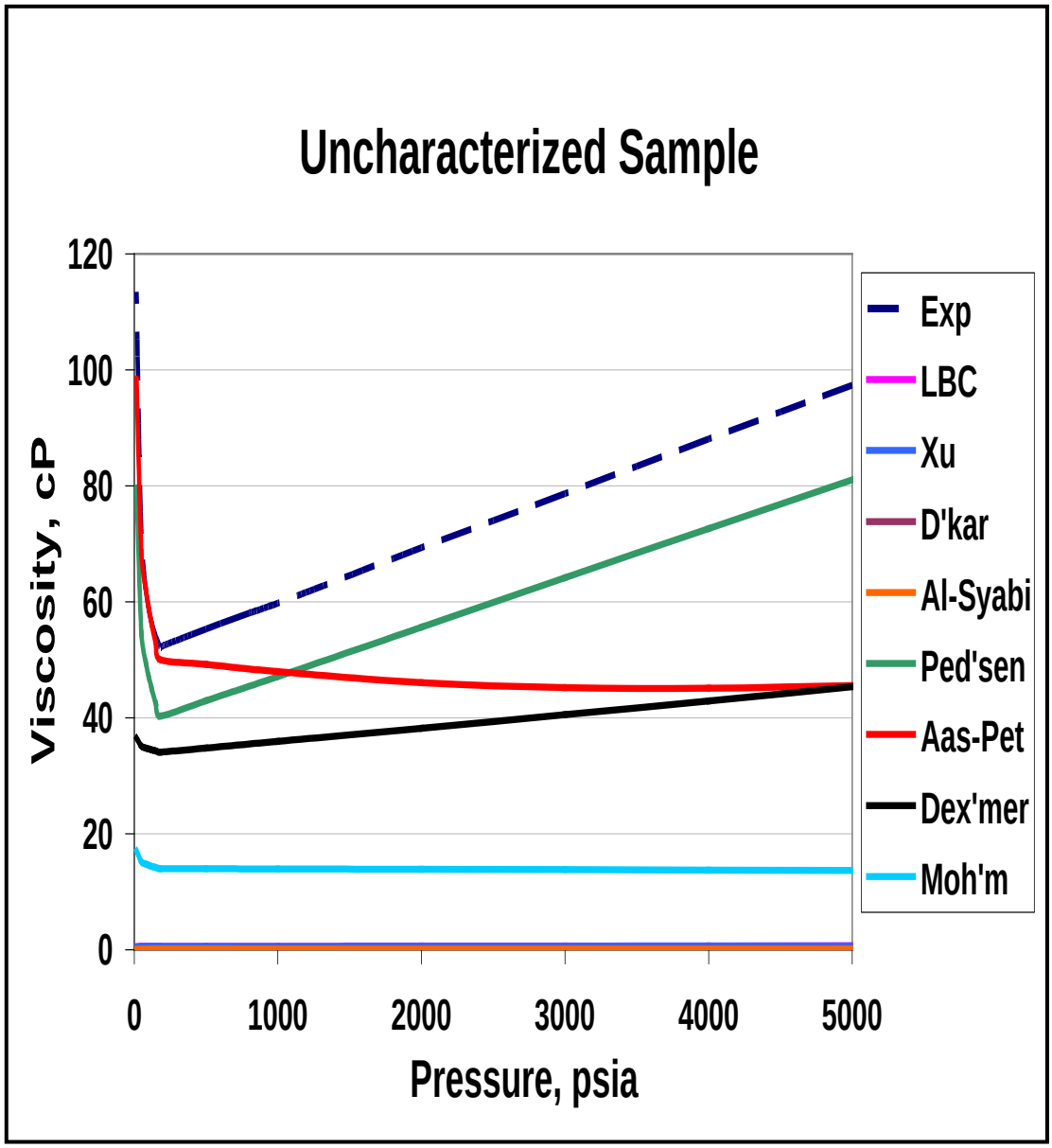

Legend Index: ***Exp*** – Experimental Data; ***LBC*** – LBC Model, ***Xu*** – Xu and Khurana Model, ***D'kar*** – Dandekar Model, ***Al-Syabi*** – Al-Syabi Model, ***Ped 'sen***– Pedersen Model, ***Aas-Pet*** – Aasberg-Petersen Model, ***Dex'mer*** – Dexheimer Model, ***Moh'm*** – Moharam and Fahim Model

Figure 6.4 Summary of Simulation Results for Uncharacterized Oil Sample (Data Set C1)

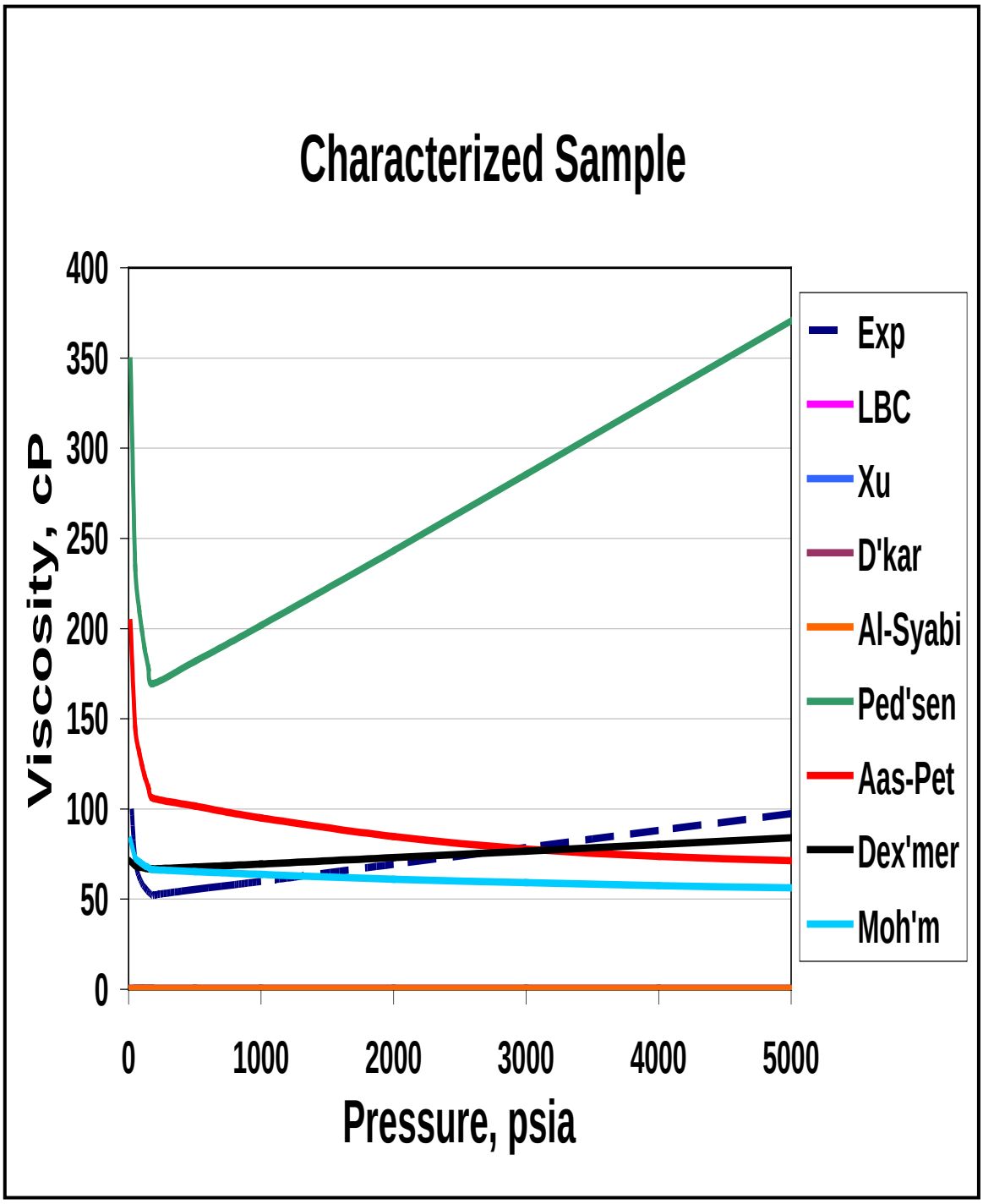

Legend Index: ***Exp*** – Experimental Data; ***LBC*** – LBC Model, ***Xu*** – Xu and Khurana Model, ***D'kar*** – Dandekar Model, ***Al-Syabi*** – Al-Syabi Model, ***Ped 'sen***– Pedersen Model, ***Aas-Pet*** – Aasberg-Petersen Model, ***Dex'mer*** – Dexheimer Model, ***Moh'm*** – Moharam and Fahim Model

Figure 6.5 Summary of Simulation Results for Characterized Oil Sample (Data Set C1)

6.2 Discussion of the Results

6.2.1 LBC Class Models

Figures 6.4 and 6.5 show that all the LBC class models greatly underpredict the medium-heavy oil viscosities irrespective of whether the sample is characterized or not (the thick bottom line in both of the above figures represents all LBC class models). In addition to this, most of the LBC class models show discrepancy for saturated viscosities (Figures 6.2 and 6.3); the viscosities decrease with reduction in pressure. Since this anomaly is generally not observed with light oil samples, it may be specifically related to heavy oils. After careful observation, it is seen that the increase in the critical viscosity parameter, ξ, offsets the increase in the density-powered right hand side of Equation 2.12 for each pressure reduction step in the saturated region. Since it is believed that the critical properties and the densities of these oils are predicted with sufficient accuracy, it is the form of the model that is causing this anomaly. Moreover, the terms in the model like μ^* and 10^{-4} are representative of light oils. Since these terms are kept unaltered in all the modified LBC models, they do not support the modeling of the heavy oil viscosities.

The Xu model (Xu and Khurana, 1996) also seems to underestimate the viscosities after tuning and significantly overpredicts before tuning the bubble point pressures. For the same data set with an untuned bubble point pressure, the model results are shown in Figure 6.6. The legends from Figure 6.4 and 6.5 also applies here. Figure 6.6 shows that the Xu model significantly overpredicts the viscosities. This model has been an upgrade of the original LBC model to account for higher viscosity oils. However, by introducing an exponential term, the model has become highly sensitive to density. Therefore, regressing the model coefficients to match the viscosities is not a good option because of the nature of this model. Additionally, the Dandekar model (Dandekar and Danesh, 1992) and Al-Syabi (Al-Syabi et al., 2001) model are also seen to heavily underpredict the viscosities irrespective of whether the sample is characterized or not.

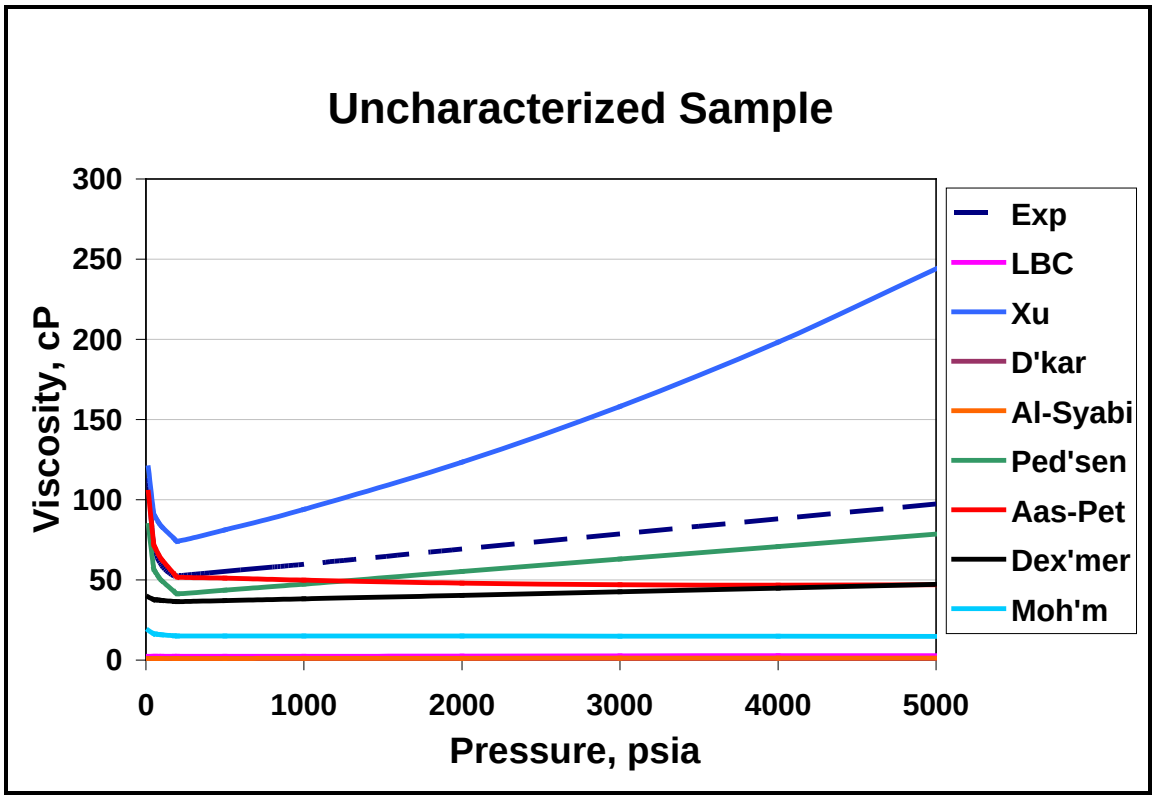

Figure 6.6 Summary of Simulation Results for Uncharacterized Oil Sample (Untuned P_b)

The original LBC model was designed to model the gas and light oil viscosities (< 1 cP) and the model coefficients (and other terms in the model) were introduced accordingly to match the viscosities in this range. It can also be concluded that tuning the model coefficients is not a good idea as the form of the model will not support this procedure. Thus, in overall terms, the nature of these models makes them virtually unsuitable for predicting the medium-heavy oil viscosities.

6.2.2 Pedersen Class Models

For the Pedersen class models, the results are generally in the range of the experimental values. The original Pedersen model seems to be robust in replicating the shape of the viscosity-pressure profile. This model can be used for modeling the medium-heavy oil viscosities, albeit after tuning. However, this model needs to be stretched beyond the range of its applicability as the apparent temperatures are observed to be as low as 35 K, which are significantly below the stipulated temperature of 65 K, as explained by the authors (Lindeloff et al., 2004).

For the other two-reference component viscosity models, the Aasberg-Petersen (Aasberg-Petersen et al., 1991) and the Moharam (Moharam and Fahim, 1995) models,

the undersaturated viscosities seem to be decreasing with an increase in pressure. This trend was observed with most of the samples. After scrutinizing the results for the anomaly, it was observed that the mismatch between the viscosity predictions of the two reference components has resulted in this abnormal behavior. From Equation 2.19, the molecular weight of the oil sample (MW_x) remains the same for the undersaturated viscosities. With an increase in the pressure, the ratio $ln(\mu_{r2}/\mu_{r1})$ should increase. In this study this ratio decreased due to the disproportionate increase between the viscosities of the two reference compounds. In this work, for the Aasberg-Petersen model, the n-decane density was calculated with PR-EOS. This density was used as input to the n-decane viscosity calculation. In the original model, the specifically developed n-decane density correlation is used for this purpose. It seems that the density values obtained from PR-EOS need to be tuned for the subsequent n-decane viscosity model. Since the authors (Aasberg-Petersen et al., 1991) have also stated that as far as petroleum mixtures are concerned the model results are comparable to the original Pedersen model, this model was not investigated further.

In the Moharam model, the saturated viscosities of the reference components are pressure-effected by the Lucas correlation. The Lucas correlation was developed for reduced temperatures until 0.40 only. In most of the cases, the reduced temperatures were in the range of 0.34-0.38, the Lucas correlation seems to underpredict the pressure effect at lower reduced temperatures. The Lucas correlation almost returned flat viscosity profile with increase in pressure. The authors of this paper (Moharam and Fahim, 1995) have also briefly discussed the inadequacy of the Lucas correlation. These viscosity correlations are not exhaustive as those of methane and n-decane correlations used in the earlier models. Additionally, as with Aasberg-Petersen model, the mismatch between the viscosity predictions of the two reference components resulted in this anomaly. The Dexheimer model (Dexheimer et al., 2001) always returns a flat viscosity-pressure profile. While developing this model, methane is replaced with n-decane as a reference component in the original Pedersen model. It seems that the original model empirical parameters need to be recalculated for n-decane before application of this model.

The purpose of selecting various Pedersen class models was to understand the effect of making the reference component heavier in order to model the more viscous fluids. In that case, the dead form of the oil itself can serve as an ideal reference component. However, very accurate density and viscosity correlations need to be developed to make

the models consistent, along with appropriate tuning of the model parameters. It is very difficult to define the behavior of a component not as heavy as n-eicosane. Additionally this qualitative study showed that the results will not be beneficial enough to spend these efforts as compared to the original Pedersen model. Moreover, at present, the industry practice is to tune the Pedersen model coefficients to match the viscosities. However, as stated earlier, this model is already stretched beyond the range of its applicability and as oils become heavier, this is not a good strategy. Hence there is need for a completely new viscosity model. The recently proposed Lindeloff model for medium-heavy and heavy oils shows great promise. This model is discussed in depth in the next chapter.

Chapter 7 LINDELOFF MODEL AND ITS MODIFICATIONS

7.1 Original Lindeloff Model

The existing LBC and Pedersen class models are not capable of accurately predicting medium-heavy (viscous) oil viscosity. The tuning of these models is also not advisable for the reasons explained earlier. Hence, it is seen that there is a need for a completely new viscosity model. The recently proposed Lindeloff et al. (2004) model has shown great promise as claimed by the authors. Theoretically, this model can not only be used to model medium-heavy oil viscosities but also extra heavy oil viscosities.

This model can be applied only after characterizing the sample. The results obtained by this method (for the earlier discussed Data Set C1) are shown in Figure 7.1.

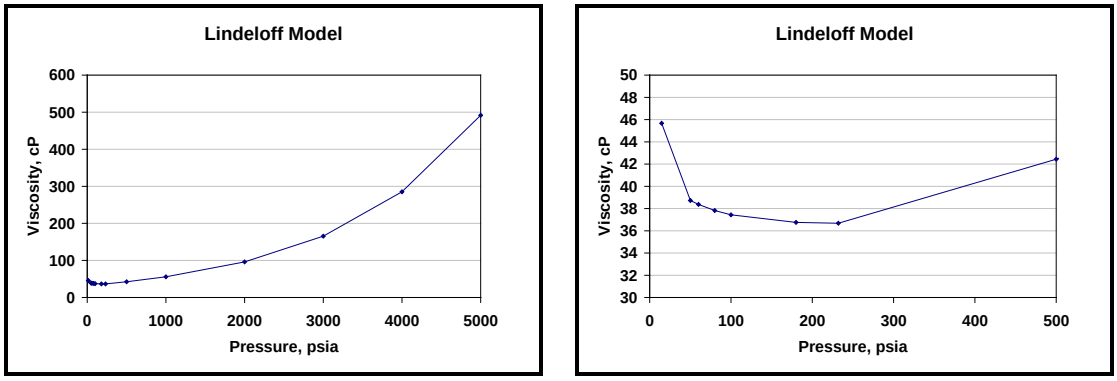

Figure 7.1 Results of Lindeloff Model for Data Set C1 and Corresponding Saturated Viscosities

The model shows very high viscosities for the undersaturated region. Figure 7.1 shows the model has a very low predictive capability. The model relies heavily on tuning the model parameters (coefficient 1.5 and exponent 0.5) to a match with the experimental data. Hence this model has been studied in great detail to investigate if its predictive capability can be improved.

7.1.1 Modifications of the Model

One observation of this model showed that the dead oil viscosity correlation used by the authors applies only until 30 cP. So it might be inappropriate to stretch the relation to hundreds of centipoises. Hence, another dead oil viscosity correlation, recently proposed by Hossain et al. (2005), was appraised.

$$\mu_{od} = 10^{(-0.71523\,API + 22.13766)}\, T^{(0.269024\,API - 8.268047)} \qquad (\mu, cP\ \&\ T, {}^{O}F) \qquad (7.1)$$

This correlation is based on the experimental data consisting of viscosities ranging to thousands of cPs. In above correlation, the API gravity is substituted in terms of the mixture molecular weight. The conversion between the API gravity and the molecular weight is carried out with the following relation by Lasater (1958):

$$MW = \left(\frac{7864.9}{^{o}API} \right)^{\frac{1}{1.0386}} \tag{7.2}$$

In Equation 7.2, *MW* is the C_{5+} fraction molecular weight. In practice, the numerical constants can be readjusted to make it a true mixture molecular weight (to include lighter components). Since the mixture molecular weight is often tuned to match the viscosities, no attempt has been made to modify the constants in Equation 7.2.

Secondly, the authors have maintained the ratio of weight to number averaged molecular weights as a constant, 1.5. The authors further stated that this ratio can be used as a tunable parameter, if desired. This ratio can be obtained easily if a DL simulation is conducted for an individual oil at stock tank conditions. For the oil samples studied, this ratio was observed to remain in the range of 1.3 to 3.0. So this ratio appears to have a physical significance and it need not be a constant or tunable parameter, but should be evaluated for an individual oil sample. In addition to this, the pressure effect for the undersaturated region has been established by the commonly known exponential relationship:

$$\frac{\mu}{\mu_o} = \exp\left[m\left(P - P_o\right)\right] \tag{7.3}$$

In this correlation the coefficient of the pressure differential, *m*, is assumed to be a constant number. This coefficient is not invariable but is a function of many parameters such as temperature, oil gravity, etc. This is illustrated in Figure 7.2.

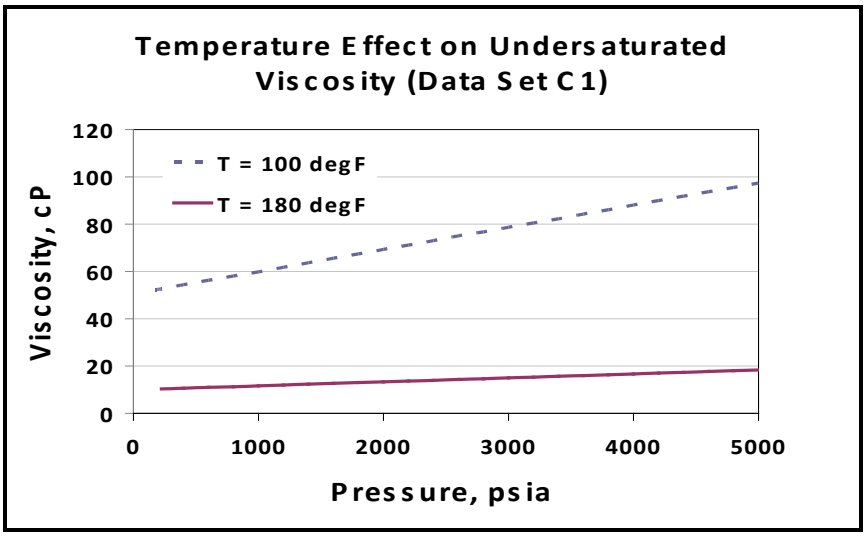

Figure 7.2 Undersaturated Viscosities vs. Pressure Profile for Different Temperatures

Figure 7.2 shows that as the temperature decreases, the pressure effect becomes more pronounced for the same oil studied (higher slope of the line). Many researchers have recognized this effect and have attempted to incorporate it appropriately. For example, Bergman and Sutton (2006) assimilated this effect in terms of bubble point viscosity. But all of these correlations are suited for black-oil simulators. For compositional modeling, it is ideal to have a correlation in terms of abstract variables, e.g. temperature.

In the absence of such a correlation in the literature, one practical approach has been suggested. Ideally, live oil viscosity measurements have to be carried out as a function of pressure for various temperatures. Of the existing data, sets C, D, and E have viscosity data available as a function of pressure for three different temperatures. The undersaturated viscosity-pressure data present for these temperatures have been used to capture the above-mentioned effect. The coefficient *m* has been fitted as a function of temperature. It was also observed that *m* is a weak function of the molecular weight of the oil. As oil becomes heavy, the pressure effect seems to be enhanced. The relation is represented as follows:

$$m = 6.45023 \times 10^{-5} + 1.2489 \times 10^{-7} MW + \frac{1.8086 \times 10^{-2}}{T} \qquad \left(m,\ psia^{-1}\ \&\ T, {}^{O}R\right) \tag{7.4}$$

From this correlation, it is seen that *m* is a strong function of temperature and a very weak function of the oil molecular weight. The molecular weight, *MW*, in Equation 7.4, is the number-averaged molecular weight. After applying all of the suggested changes,

the model is left with only tunable parameter, the exponent 0.5. This can be tuned to get a match with the experimental data.

7.1.2 Results and Discussion

This modified Lindeloff model and the original model were applied to Data Set C1 and the results compared. In the original model, all of the three parameters; coefficient 1.5, exponent 0.5, and the pressure differential coefficient *m*, are tuned to get the match with the experimental data. The original paper (Lindeloff et al., 2004) recommended varying the first two parameters only. It is impossible to get a good match for the undersaturated region with the constant pressure differential coefficient (0.008 atm^{-1}) suggested by the authors. Hence, the proposed *m* correlation was used for this purpose. However, for the modified model, only the exponent 0.5 was tuned to get the fit. The results are shown in the Figures. 7.3 and 7.4.

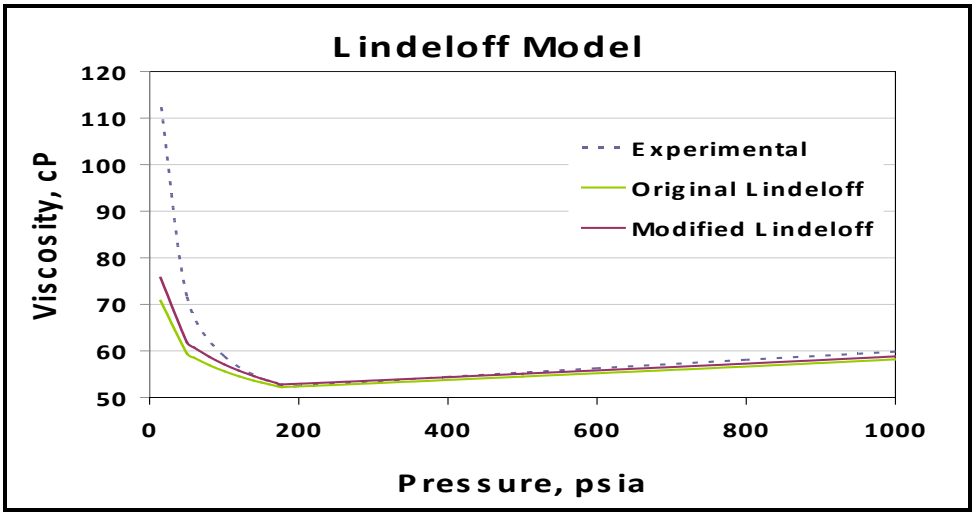

Figure 7.3 Comparison of Original and Modified Lindeloff models (Data Set C1)

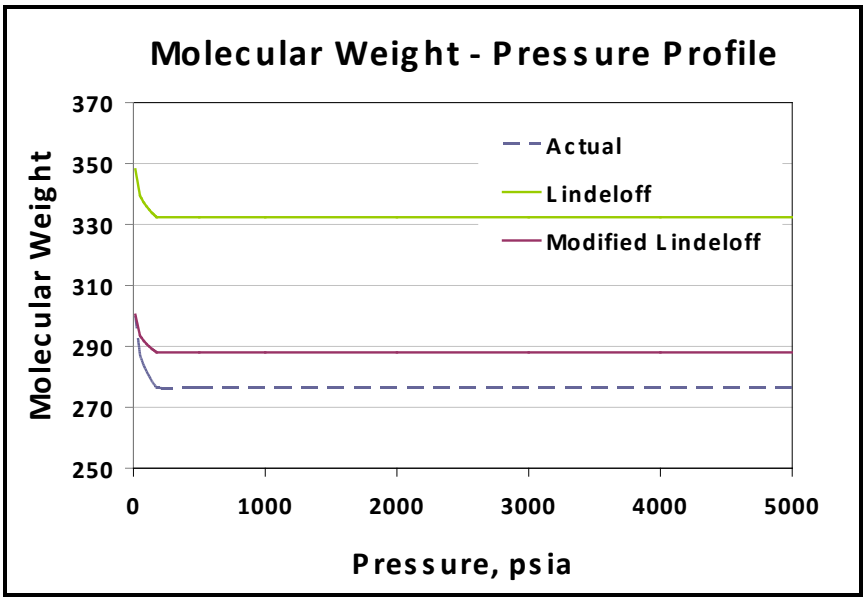

Figure 7.4 Comparison of the Modified Molecular Weights (Data Set C1)

Figure 7.3 shows that both the original and modified Lindeloff models seem to fit the experimental data very well for the undersaturated region. However, a more careful examination of the tuning of the parameters can be judged with the help of Figure 7.4. In all Pedersen class models, the mixture molecular weight is increased by a suitable factor before being applied in the viscosity model. The main reason for this is that heavy molecules contribute more toward the viscosity and need to be accounted for accordingly. It may be also that the gases in liquid phase impart more viscosity than in the gas phase itself. Hence, their molecular weights also need to be increased before substitution in the Pedersen class viscosity models. Carefully studying Figure 7.4, it is evident that the molecular weights have to be increased by a considerable amount in the original Lindeloff model, as compared to the modified model. The new upgrade seems to be fundamentally more accurate and has a higher predictive capability. The only tunable parameter remaining is the exponent 0.5, which can be effortlessly tuned to get a match with the experimental viscosity data.

However, Figure 7.3 shows that the saturated viscosities match is just fine for the original and modified models. So it may be that the phase behavior of heavy oils needs to be restudied for this low pressure region. The phase behavior is utilized, as far as this model is concerned, only in terms of the mixture molecular weight at each pressure reduction step. Because of the high flexibility of this model, it was decided to try to tune the simulated ratio of the weight to number-averaged molecular weights (coefficient 1.5)

to see its effect on the viscosity prediction for the saturated region. Thus the tuning strategy can be summarized as follows.

1. Tune the exponent 0.5 to match the viscosities; mainly the bubble point and the saturated region viscosities.
2. Tune the *m* correlation to match the undersaturated viscosities. This can simply be done by multiplying the suitable factor to the *m* correlation to adjust the slope.
3. Finally, fine tune the ratio of the weight to number-averaged molecular weight (coefficient '1.5') to improve a overall match. This may also warrant the final readjustment of the *m* correlation and the exponent 0.5.

With this tuning strategy, the new result is shown in Figure 7.5.

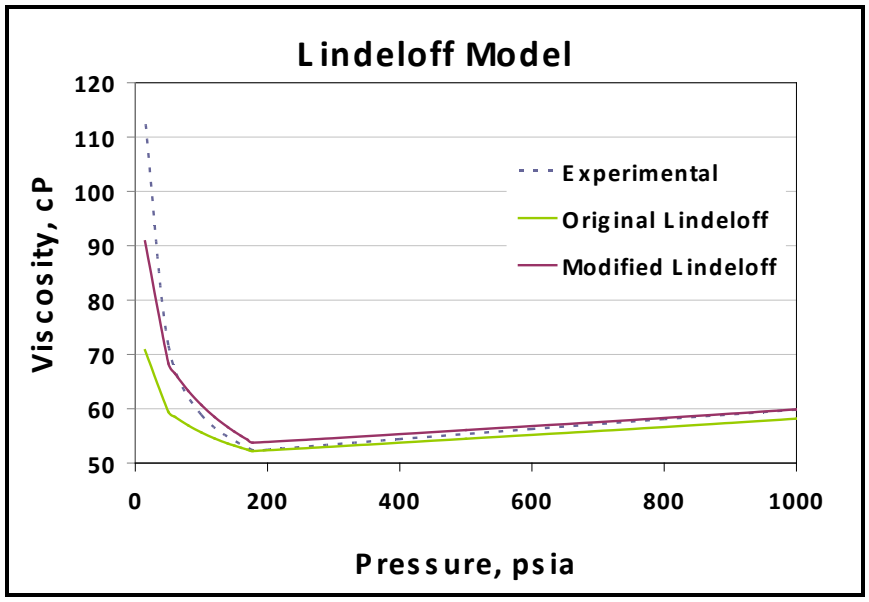

Figure 7.5 Comparison of Original and Modified Lindeloff models with Additional Tuning of Coefficient 1.5 (Data Set C1)

The Percent Average Absolute Deviation (%AAD) for this data set is found to be 4.22%. As compared to Figure 7.3, a better match is achieved (In the earlier case, %AAD was 6.88%). In an earlier fit, the ratio of the weight to number-averaged molecular weight was found to be 1.76, which was tuned to 1.64 to get the above fit. The exponent 0.5 was also readjusted. The molecular weight-pressure profile, shown in Figure 7.4, remained virtually invariant by the above combined change. In this data set, for the last pressure reduction step of 50 psia to 14.7 psia, the viscosity jumped from 72 cP to 114 cP. If this atmospheric viscosity point is excluded, the %AAD improves to 2.25%. In

Figures 7.3 and 7.5, the results are presented to a pressure of 1000 psia to better illustrate the results for the saturated region. For both models, the undersaturated region viscosity match was always good.

A similar strategy was applied to the other data sets. The Sets C, D, and E showed significant improvement over the original Lindeloff model. Since the *m* correlation was developed based on the Sets C, D, and E, these are presumed to give good results for the undersaturated viscosities. Instead, the results for Set A and Set F are presented below. These sets are presented to show the result of the pressure differential coefficient correlation, which was developed independent of these data.

Figures 7.6 (A) and (B) show the results for Data Set A. Figure. 7.6 (A) shows that the *m* correlation, when used as is, under predicted the undersaturated region viscosities. To get a good match, the overall *m* value was tuned (multiplied by factor 1.7) to get a good match for the undersaturated region viscosities. Figure 7.6 (B) shows that the viscosities are accurately predicted. Again, for saturated region viscosities it is seen that for the last pressure reduction step from 300 psia to atmospheric pressure, the viscosity value jumped from 197 cP to 475 cP. If this atmospheric viscosity point is not considered, the %AAD for this data set becomes 3.35%.

Figures 7.7 (A) and (B) show the results for Data Set F. After tuning the *m* correlation, the %AAD for this data set is found to be 5.5%. The model, however, failed to produce a good match for the saturated region viscosities. Since this phenomenon is observed with Data Set C1 and A as well, it seems that this viscosity model is incapable of predicting the viscosity behavior at very low pressures, especially close to atmospheric pressures. Thus this three-parameter model should be further improved to get a simultaneous good prediction for both the saturated as well as the undersaturated region viscosities. It may be also that the compositional changes, which are obviously quite significant, are not adequately captured by the EOS model.

Though the original Lindeloff model also seems to give good results when compared to the modified model, as stated earlier, the mixture molecular weights need to be increased significantly as compared to the new modified model. Moreover, while applying the original model, the original constant pressure correction coefficient (0.008 atm^{-1}) was replaced by the new proposed correlation. Without using the proposed correlation it impossible to get a good match.

(A)

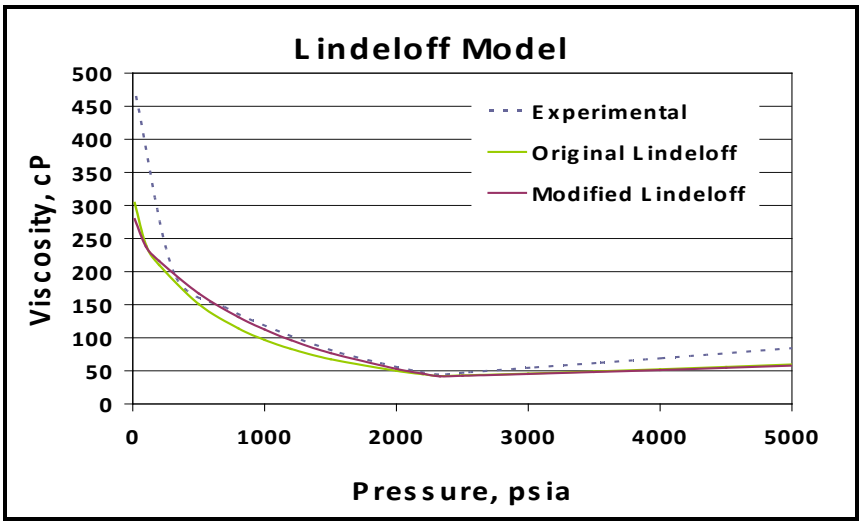

(B)

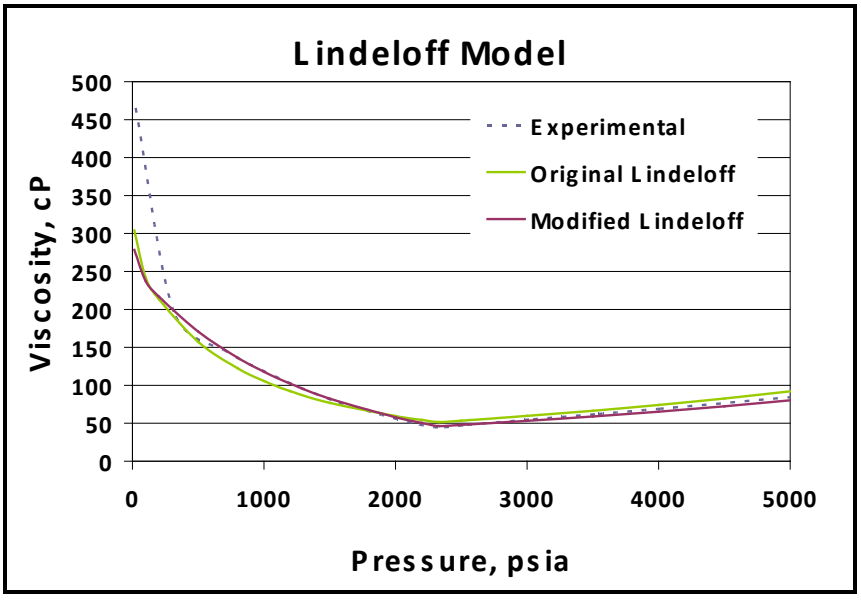

Figure 7.6 (A) and (B) Lindeloff Model: Data Set A with Tuned *m* Correlation

(A)

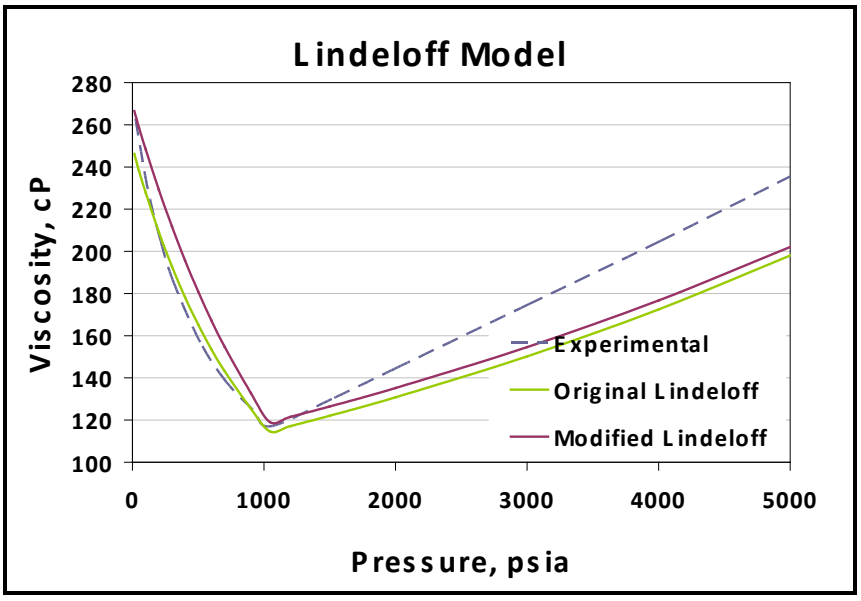

(B)

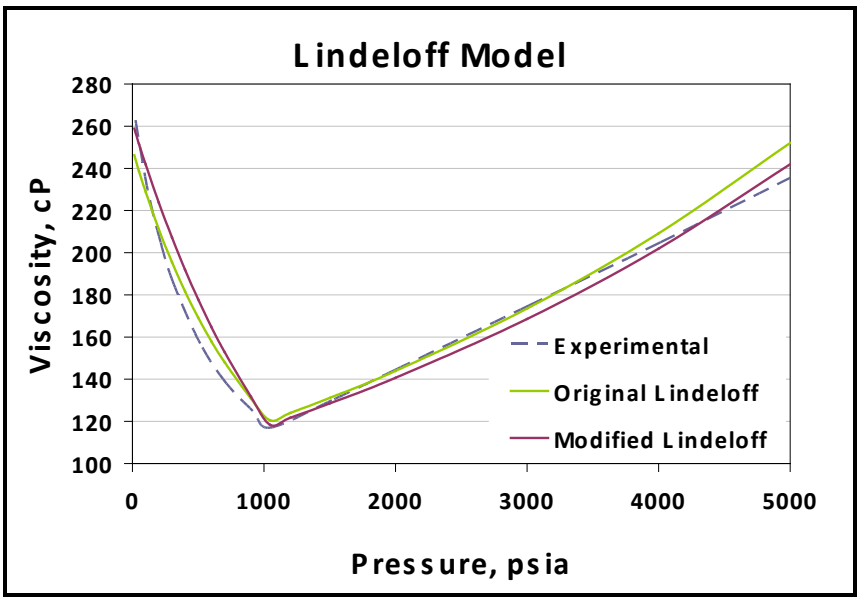

Figure 7.7 (A) and (B) Lindeloff Model: Data Set F with Tuned *m* Correlation

The explicit nature of the Lindeloff model offers the greatest advantage: the various phase behavior properties, such as bubble point pressure, density, solution gas/oil ratio, etc., can be tuned independent of the viscosities. The commonly used tunable parameters, such as P_c, T_c, etc., are not featured in the Lindeloff model. This explicit nature allows carrying out tuning in commonly employed Microsoft® Excel® software. In this case, the above tuning strategy will certainly be practical.

7.2 Further Improvements

As discussed earlier, the proposed modified Lindeloff model was incapable of predicting viscosities at very low pressures. Additionally, it was also concluded that the tuning of the entire viscosity-pressure profile is virtually impossible with the earlier modified three-parameter Lindeloff model. After evaluating various options, the model was split into two regions: undersaturated and saturated viscosities. While moving from the pivotal bubble point viscosity point, for the undersaturated region, the viscosities increase due to increase in pressure itself. On the other hand, for the saturated region, the viscosities increase due to an increase in heaviness of oil (due to compositional changes). The decrease in pressure actually decreases the viscosities. Since, for both the undersaturated and saturated region, the viscosity increase is due to a different physical phenomenon, it is logical to divide model into the two regions. Additionally, this split may better control the tuning procedure.

The same calculations were performed for the two regions except the two Lindeloff parameters would have different values. Despite this, the viscosities close to atmospheric pressure (typically below 60 psia) were not able to produce a good match. This was the case with most of the data sets where the viscosity profile showed a sudden jump for the saturated region. As already known, the Lindeloff model mainly relies in adjusting the mixture molecular weight by a suitable factor to get the viscosity match. This multiplying factor, *MF*, is represented by following equation:

$$MF = \left(\frac{MW_w}{1.5\,MW_n} \right)^{0.5} \tag{7.5}$$

For any saturated viscosity-pressure profile, the ratio of the weight to number-averaged molecular weight continuously decreases as the pressure is decreased. For Data Set C1, this is illustrated in Table 7.1.

Pressure, psia	MW_n	MW_w	MW_w / MW_n
5000	276.3	523.7	1.90
4000	276.3	523.7	1.90
3000	276.3	523.7	1.90
2000	276.3	523.7	1.90
1000	276.3	523.7	1.90
500	276.3	523.7	1.90
178	276.3	523.7	1.90
170	276.8	523.7	1.89
160	277.4	523.8	1.89
150	278.0	523.9	1.88
140	278.7	524.0	1.88
120	280.1	524.3	1.87
100	281.8	524.6	1.86
80	283.7	524.9	1.85
60	286.0	525.3	1.84
50	287.2	525.5	1.83
14.7	300.0	529.1	1.76

Table 7.1 Sample Calculation Showing Variation of Multiplying Factor with Pressure (Data Set C1)

Table 7.1 shows that as the pressure is reduced below the bubble point, the ratio of the weight to number-averaged molecular weight decreases. The authors (Lindeloff et al., 2004) claimed that for dead oil this ratio generally becomes 1.5 or less. For oil samples studied in this work, the lowest value for this ratio was found to be 1.44. For this particular data set in question, the ratio is found to be 1.76. Hence, *MF* also decreases accordingly for constant model parameters, coefficient 1.5 and exponent 0.5. Though the mixture molecular weight increases with decreases in pressure for the saturated region, this ever decreasing nature of *MF* makes it difficult to follow with the much higher low pressure region viscosities. This nature of *MF* is represented in Figure 7.8.

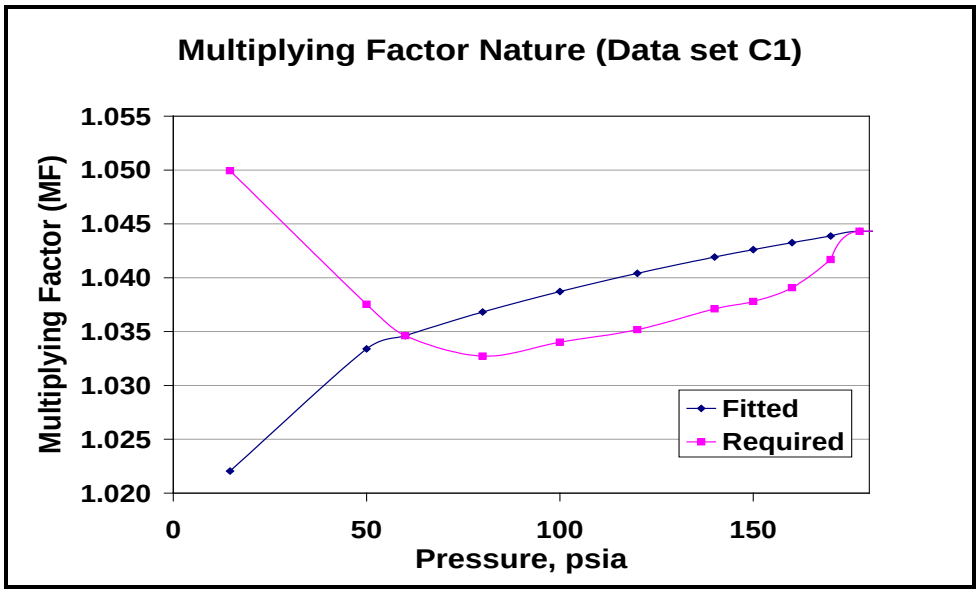

Figure 7.8 Multiplying Factor (*MF*) Nature for Data Set C1

Figure 7.8 also shows the values of *MF* required to get a nearly exact fit with the experimental data. It is clearly seen that to match the low pressure region viscosities, it is necessary to increase *MF*. One option is to divide the saturated region at this particular point (about 60 psia for Data Set C1). It was decided to further split the saturated region at this point. The sum of the mole fractions of either light or heavy components, obtained during differential liberation test simulation, if plotted against corresponding pressure, usually shows a noticeable change in the slope at this split point. This criterion can be used to get the transition point analytically. Different expressions were evaluated to obtain the desired trend for the multiplying factor. But it was decided to use the same earlier expression (Equation 7.5) to maintain continuity in the analysis.

In the Lindeloff model, only the molecular weights are tuned to get a match with the experimental data. This could very well mean that for the same molecular weights at the same temperature, the model will predict equal viscosities. But this is not the case. Compared to light oils, heavy oils are dominated by undefined components, and despite similar molecular weights, viscosities can differ significantly. Therefore, oil chemistry also needs to be taken into account. In absence of this, the model at least requires one more degree of confidence. Otherwise, it will be difficult to differentiate between the two oils with similar molecular weights. For this, the viscosity of the flashed oil (atmospheric pressure and reservoir temperature) is assumed to be known. This data point can easily be obtained and is as good as measuring the dead oil viscosity at a given reservoir temperature. This data point is then used to tune the dead oil viscosity correlation. This

correlation can then correctly represent the dead oil viscosities for varying molecular weights at different pressures below the bubble point pressure.

The undersaturated viscosity versus pressure relation can take various forms, as summarized by Bergman and Sutton (2006). The relation can be mainly of two types: 1. Linear, and 2. Exponential, as shown in the following equations:

Linear relation:

$$\mu = \mu_b + m\left(P - P_b\right) \tag{7.6}$$

Exponential relation:

$$\ln\left(\frac{\mu}{\mu_b}\right) = m\left(P - P_b\right) \tag{7.7}$$

Where,

P_b = bubble point pressure

μ_b = corresponding viscosity

For the calculations performed until this moment, the exponential relation was used. But careful observation showed that the linear relation can properly describe the undersaturated viscosity behavior. This is illustrated in Table 7.2.

Data Set	**Coefficient of Determination (R^2)**	
	Linear Relation	**Exponential Relation**
Set A	0.999	0.987
Set C1	1.000	0.986
Set C2	0.999	0.986
Set C3	0.999	0.986
Set D1	0.999	0.974
Set D2	0.999	0.985
Set D3	1.000	0.985
Set F	0.999	0.988
	0.999	0.985

Table 7.2 Undersaturated Viscosity Behavior: Linear vs. Exponential Relation

Table 7.2 shows that the linear relation better fits the viscosity versus pressure relation for all of the selected data sets. Therefore, in all of the prior calculations, the exponential relation is replaced with that of linear relation.

In an earlier section, a separate correlation was developed for the pressure differential parameter, *m*. A similar correlation can be developed for the linear dependence and can

be equally applied here. But, for a given temperature, it was observed that the variation in the *m* is very small (as appropriately seen in the corresponding correlation, Equation 7.4), where change in the molecular weight has a very weak dependence on the value of *m*). Hence, *m* can be essentially kept the same for all three regions. Additionally, it was decided to keep *m* as a tunable parameter as the introduction of geographically diverse data sets would have voided the reliability of the earlier correlation.

Figure 7.9 summarizes the new changes proposed to the already modified Lindeloff model. The basic steps behind the modeling can be stated here:

1. Calculate the dead oil viscosity for a given molecular weight and temperature.
2. Incorporate the pressure effect by applying the linear viscosity versus pressure relation, as stated earlier in Equation 7.6.

Thus for any given pressure and temperature, irrespective of undersaturated or saturated region, viscosity is computed using the dead oil viscosity and the linear relation between the viscosity and the pressure. For any region, the slope of the line is assumed to remain the same. For tuning purposes, all three regions can be tuned simultaneously but independent of each other.

7.2.1 Tuning Strategy

As noted earlier, the explicit nature of Lindeloff model offers the greatest advantage-phase behavior can be tuned independent of the viscosities. Also, as discussed in Section 5.2, the tuning of EOS is a nonlinear minimization problem. The built-in MatLab® '*lsqnonlin*' solver is used for this purpose.

After setting up EOS with phase behavior data, the Lindeloff model parameters are tuned separately. With further improvements in the modified Lindeloff model, the following seven parameters available for tuning the new viscosity model; the two original Lindeloff model parameters (coefficient 1.5 and exponent 0.5) for three different regions and the slope *m* of the linear relationship. At first, the dead oil viscosity correlation is tuned with the experimental dead oil viscosity data point for the given reservoir temperature. The linear slope, *m*, is fitted exclusively for the undersaturated viscosity data and subsequently employed for the saturated viscosities.

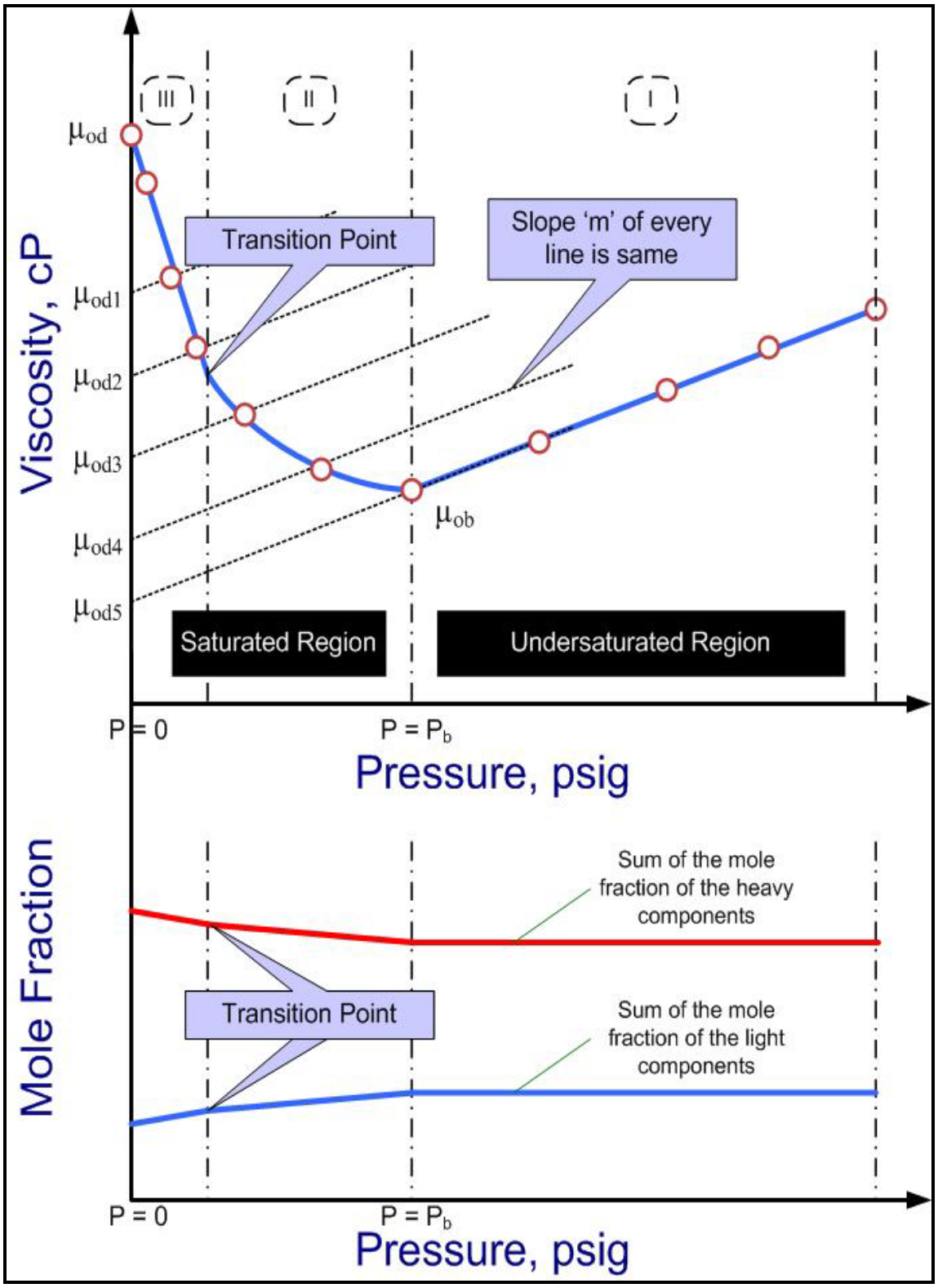

Figure 7.9 Conceptual Representation of Lindeloff Viscosity Model with New Modifications

All three regions are fitted simultaneously but independent of each other. The coefficient 1.5 has a significance of the ratio of the weight-averaged to number-averaged

molecular weight at the stock tank conditions. For the data sets studied, this ratio varied between 1.3 and 3.0. Instead of using the numeral 1.5 in Equations 2.16 and 2.17 as a criterion to determine mixture molecular weight, the ratio of the weight to number-averaged molecular weight for the dead oil itself is used. This forces the atmospheric viscosity data point to match the experimental dead oil viscosity. Additionally for the exponent 0.5, based on the simulation experience, the lower and upper bounds are set to be -1.0 and 2.0 respectively. The negative lower bound suggests that in some cases, the dead oil viscosity correlation predicts higher viscosities for the given number-averaged molecular weights and these molecular weights need to be decreased before proceeding further. For the linear slope *m* these values are 10^{-05} and 0.5 $psia^{-1}$, respectively. The bounds set for the slope *m* are a bit more relaxed. It must be noted that these bounds are based on the data sets studied so far and can have different values as more data becomes available.

7.2.2 Results and Discussion

The new concepts were applied to already existing data sets. At first, only Data Set C is reported in detail. It will be followed by the remaining data sets. For Data Set C, the phase behavior data are available for three different temperatures: bubble point pressure and density, API gravity, undersaturated liquid phase densities, and ROV for constant composition expansion tests. P_c, T_c, and ω of the pseudo-components are tuned so that the tuned values match the data at all three temperatures. The two most important parameters, bubble point pressure and corresponding liquid phase density, are compared in Table 7.3 for the three temperatures. Table 7.3 shows that a good match is achieved.

Data Set	T, °F	Bubble point Pressure, psia		Bubble point Liquid Density, lb_m/ft^3	
		Exp	Tuned	Exp	Tuned
C1	100	178	173.6	55.6	55.38
C2	140	201	202.1	54.6	54.33
C3	180	225	231.9	53.4	53.26

Table 7.3 Comparison of the Experimental and Tuned PVT Data (Data Set C)

After setting up the EOS with the experimental phase behavior data, the viscosity data were fitted with the tuning strategy proposed earlier. The results are shown in Figure

7.10. This figure shows that it is possible to get a very good match with the experimental data by using the new modified Lindeloff model. The percent average absolute deviation (%AAD) values for above three data sets are 0.91, 1.69, and 1.43, respectively. Table 7.4 summarizes the tuned Lindeloff model parameters for the three data sets.

Data Set	T, °F	Region I		Region II		Region III		m, psia^{-1}
		1.5	0.5	1.5	0.5	1.5	0.5	
C1	100	1.9626	0.429	2.6402	0.052	1.4000	0.012	0.0094
C2	140	1.9945	0.478	3.0000	0.030	1.4000	0.031	0.0034
C3	180	1.9462	0.416	2.8314	0.042	1.4000	0.034	0.0017

Table 7.4 Tuned New Lindeloff Model Parameters for Data Set C

Table 7.4 shows that, as expected, the slope *m* decreases as temperature increases. The rest of the tuned parameters also fall within the given bounds, although on few occasions they reach the limits. However, tuned parameters do not show any monotonic trends as temperature increases for the above data sets. It may have to do with the initial tuning of the dead oil viscosity correlation which might have changed the reference point. Nevertheless, the model parameters in individual regions are pretty close to each other and it shows that the model is consistent in nature. The results of this new model for the remaining data sets are shown in Figures 7.11-7.17.

Figures 7.11 through 7.17 summarize the results of the new Lindeloff model for the remaining data sets. Data Sets G and H, represent the samples characterized by Alurkar (2007), representing oils from the ANS. For Data Sets D and E1, the bubble point pressures are very low (<500 psia) compared to the pressures used during the experimental measurements (5000 psia). Hence, a separate analysis is provided for the saturated viscosities. The results can be best judged with the %AADs. Table 7.5 shows the values of model parameters for all data sets and corresponding %AADs. As also depicted by Figs. 7.11 to 7.17, Table 7.5 equally shows that very good match can be achieved with the experimental data. The %AADs are very low and for Data Sets G and H, representing ANS oils, the %AADs are less than one. For Data Set E, only the first subset (E1) was simulated as the remaining subsets viscosity values are in single digits (equivalent temperatures, T_o, are greater than 65 K). Hence these viscosities are not truly representative of medium-heavy oils. For the twelve data sets represented above, the average AAD is 1.37%.

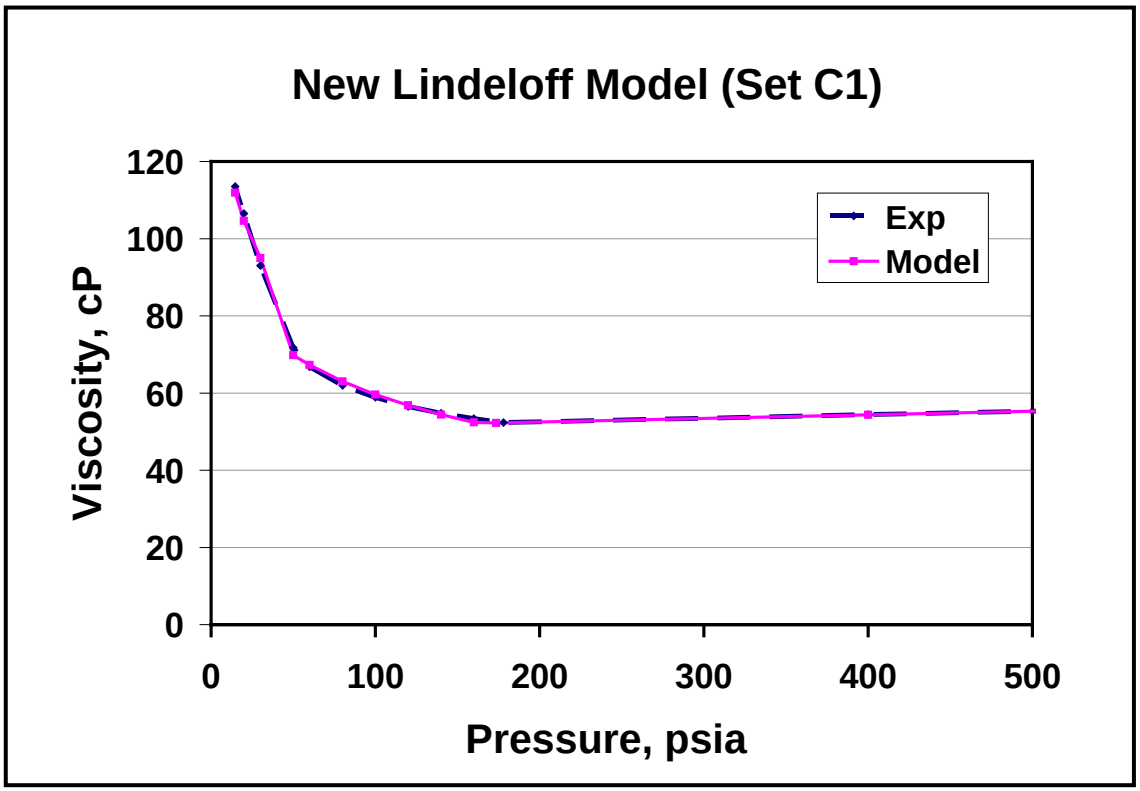

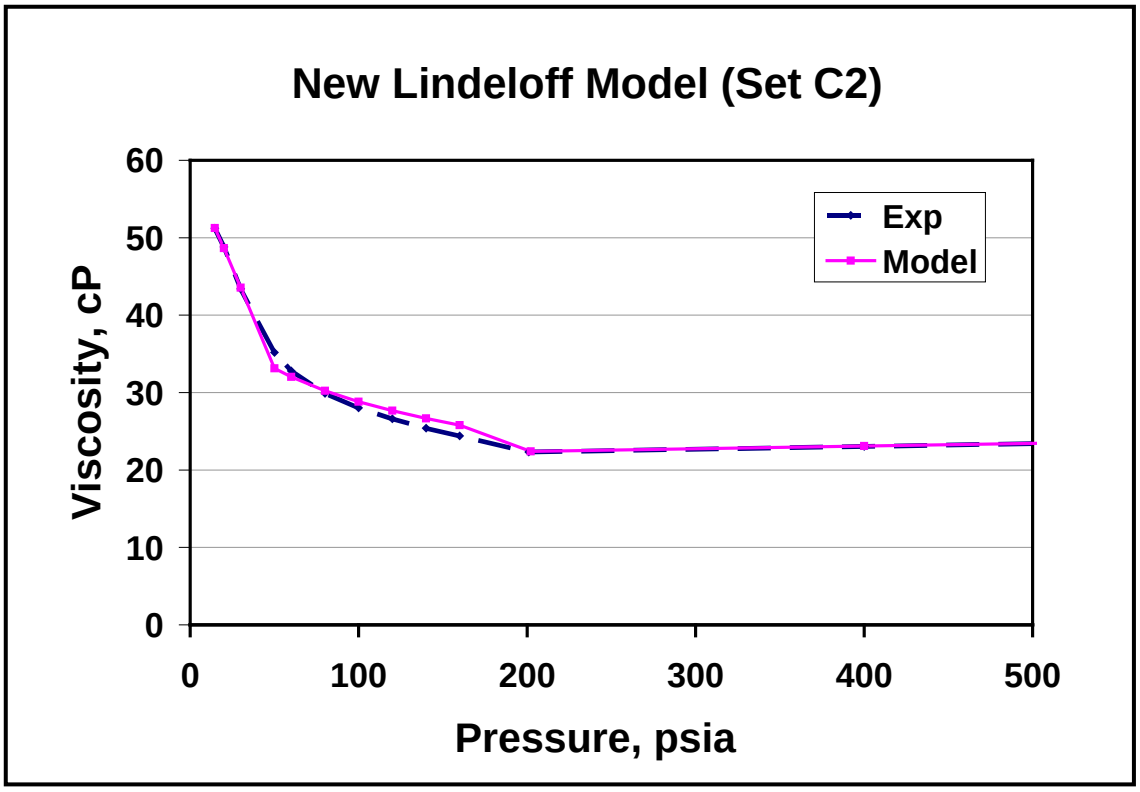

Figure 7.10 Results of New Lindeloff Model for Data Set C (C1, C2, and C3) with Corresponding Saturated Viscosities

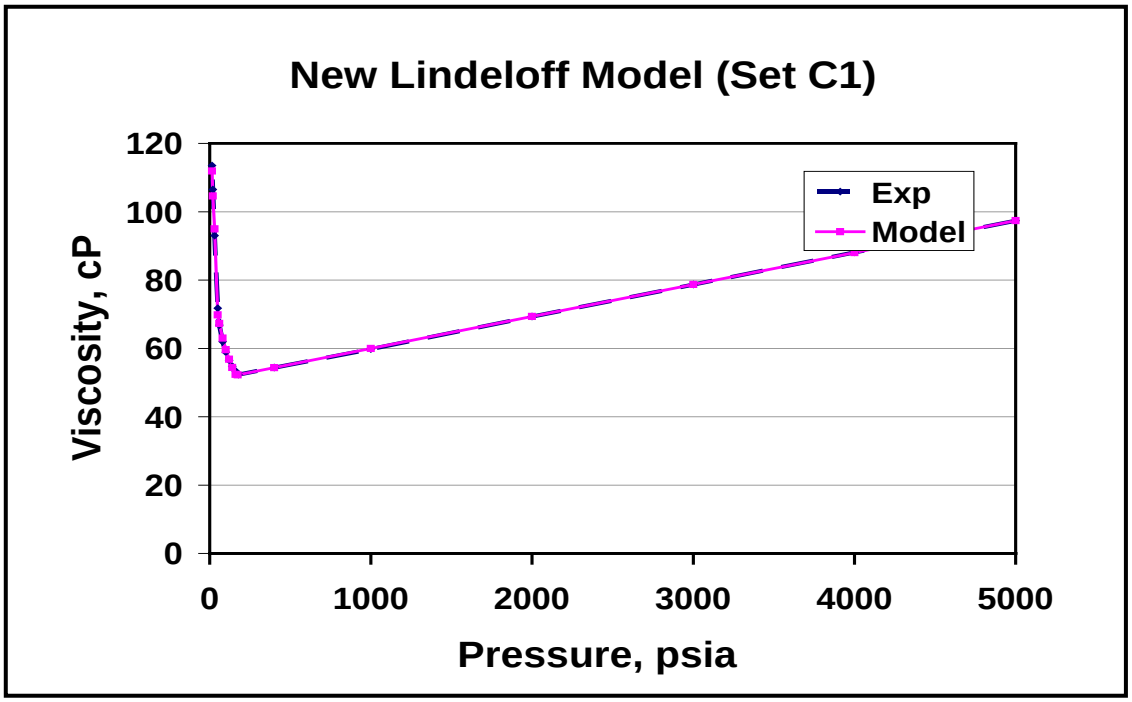

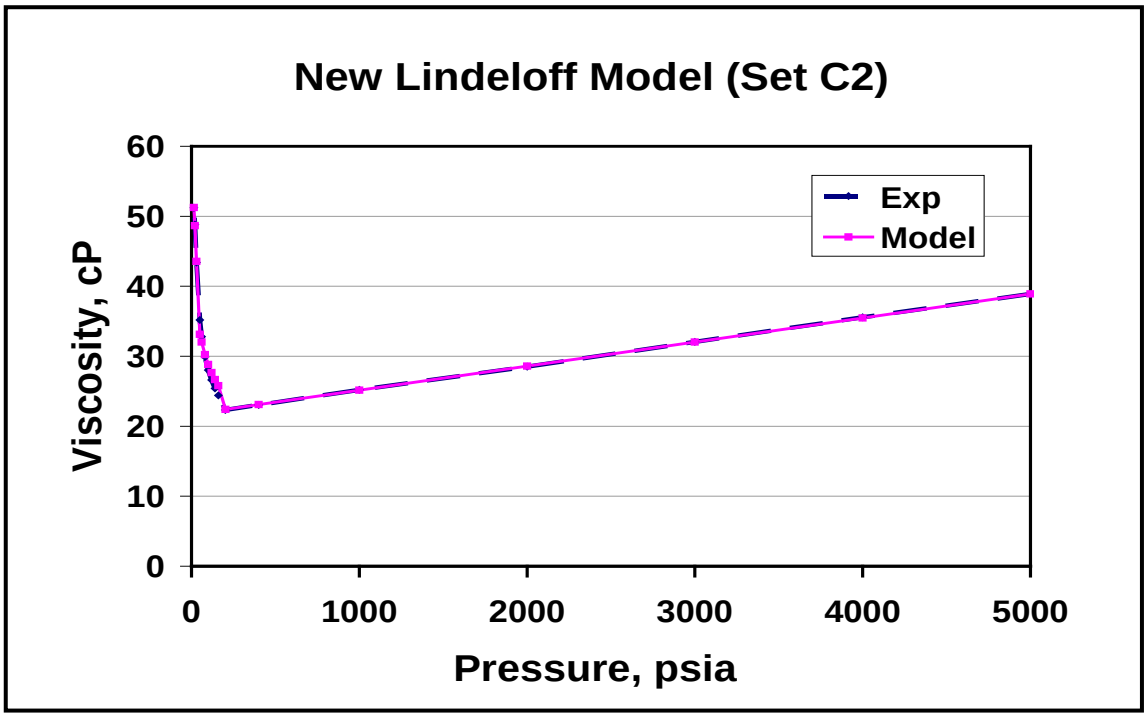

Figure 7.10 (continued) Results of New Lindeloff Model for Data Set C (C1, C2, and C3) with Corresponding Saturated Viscosities

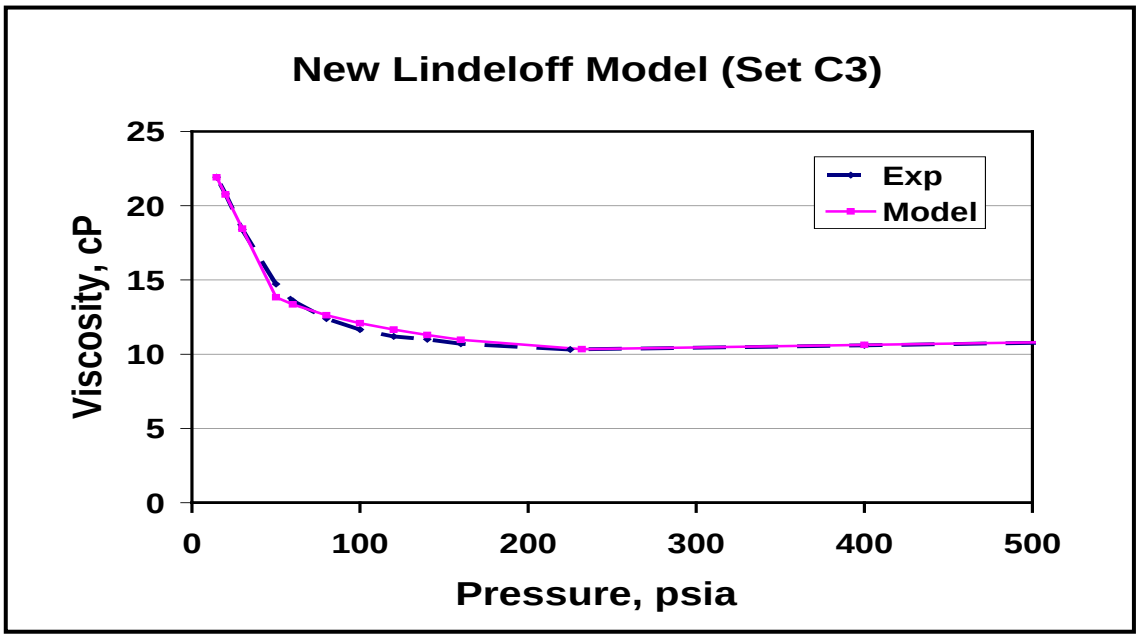

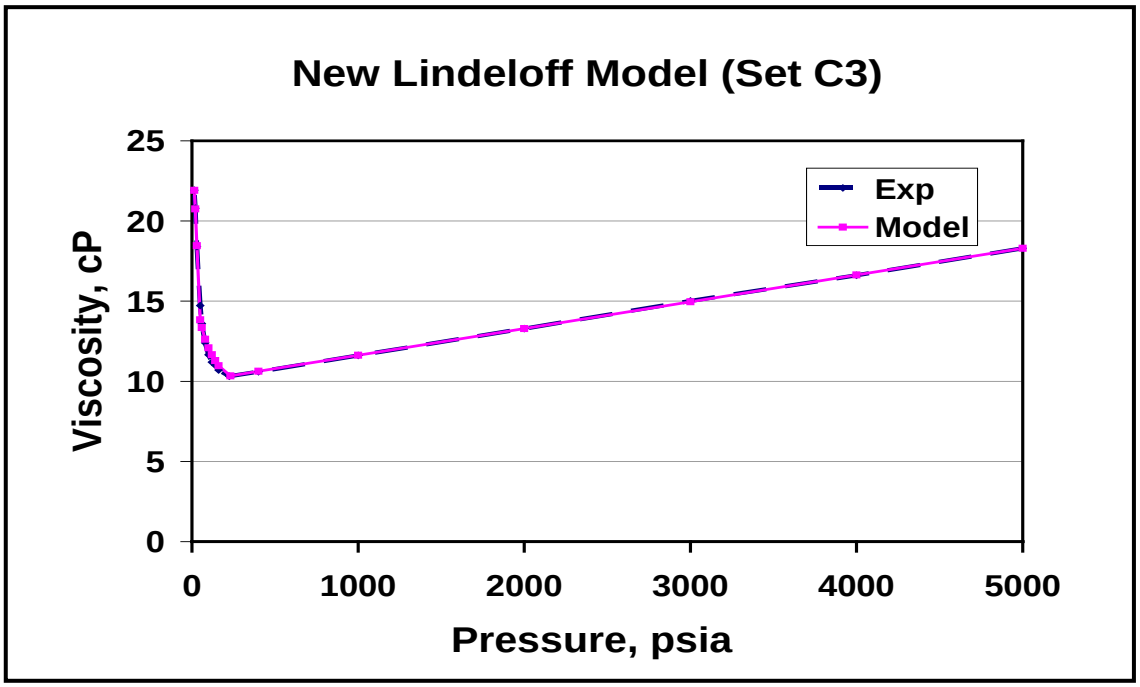

Figure 7.10 (continued) Results of New Lindeloff Model for Data Set C (C1, C2, and C3) with Corresponding Saturated Viscosities

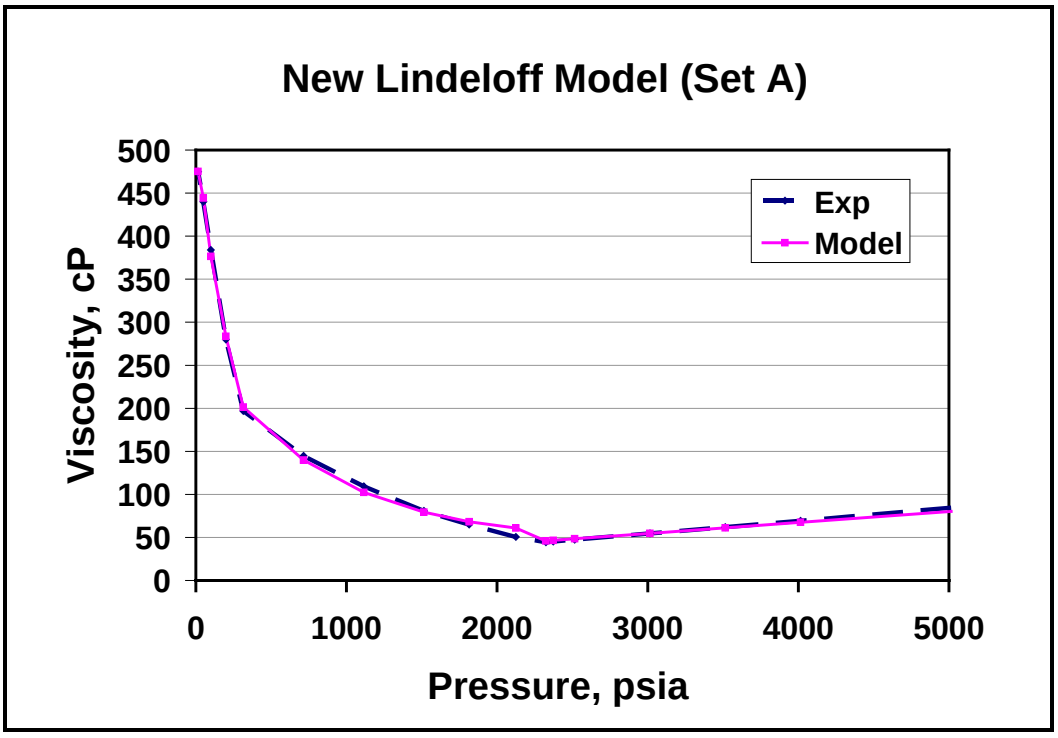

Figure 7.11 Results of New Lindeloff Model for Data Set A

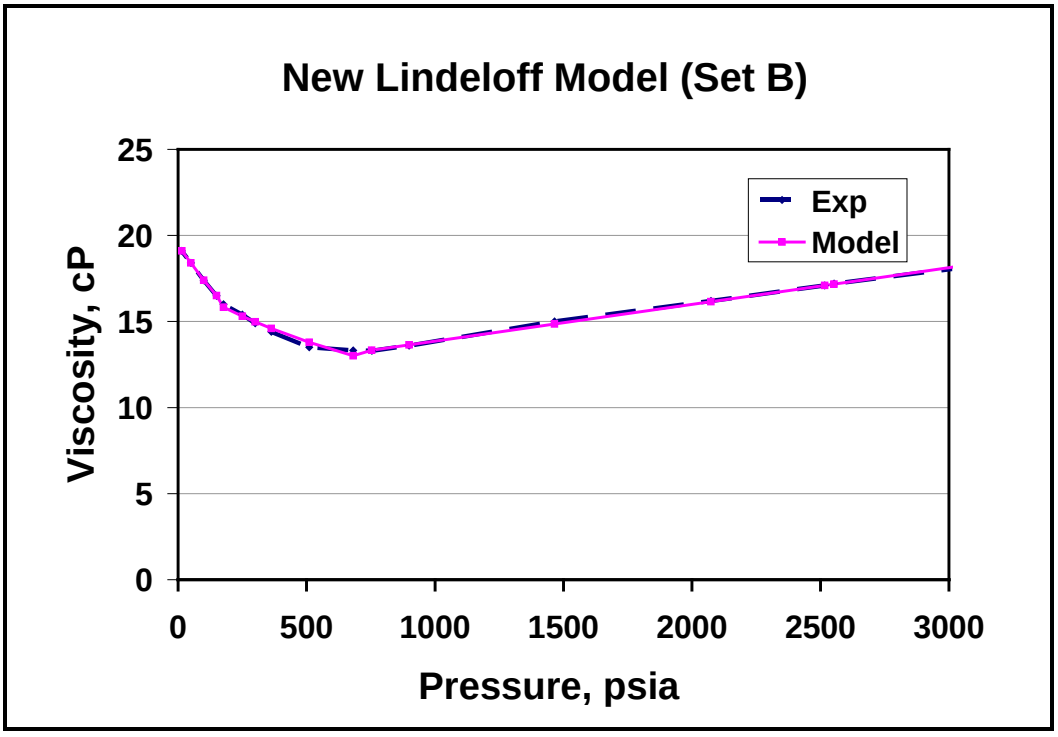

Figure 7.12 Results of New Lindeloff Model for Data Set B

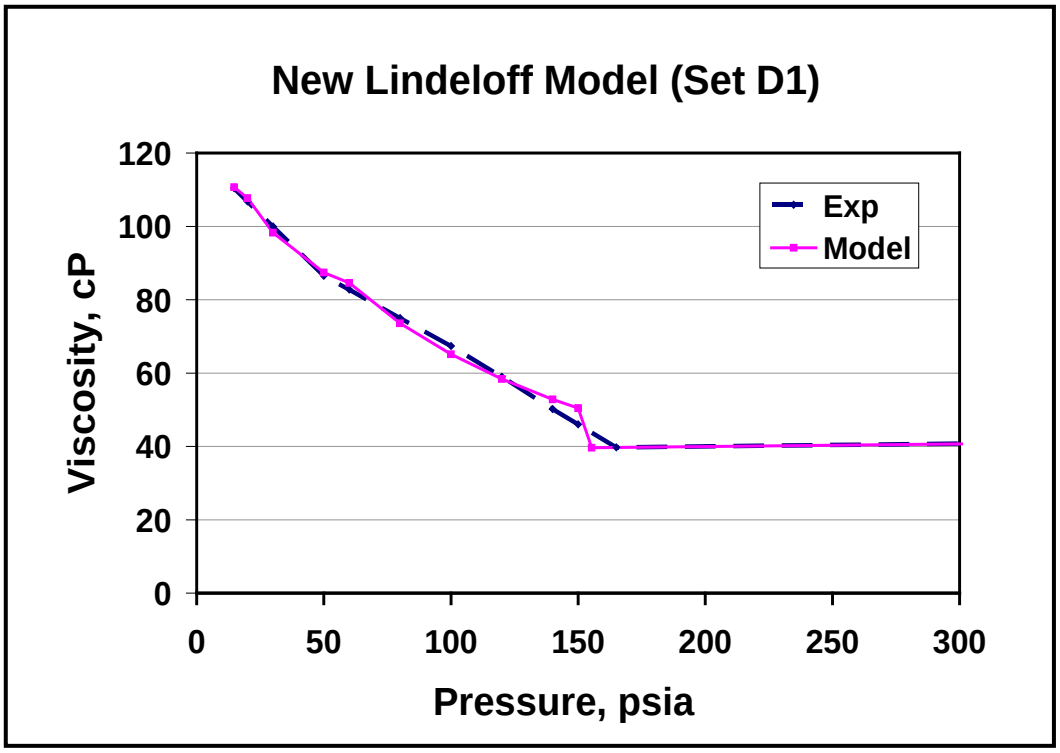

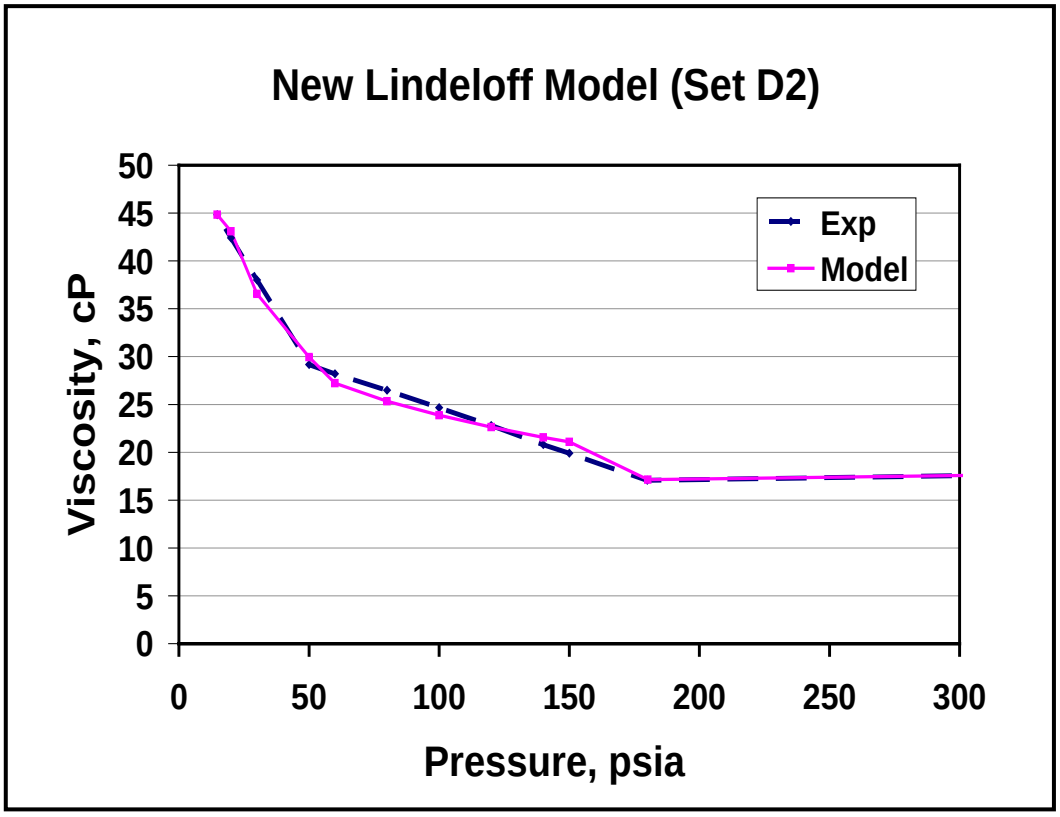

Figure 7.13 Results of New Lindeloff Model for Data Set D (D1, D2, and D3) with Corresponding Saturated Viscosities

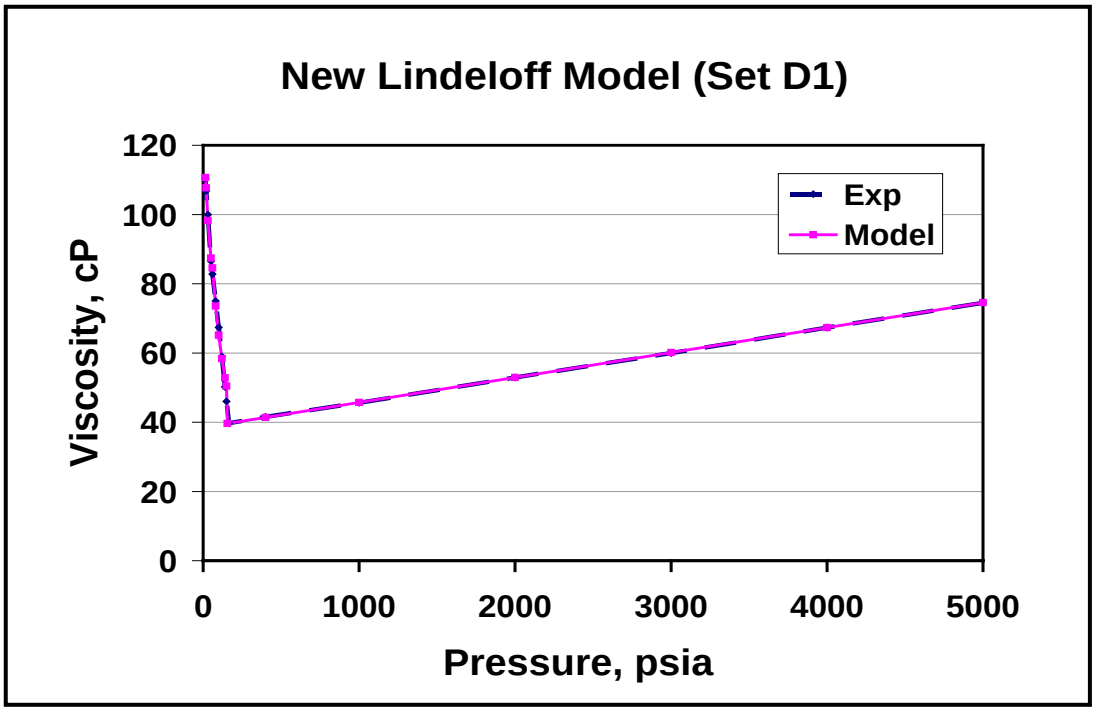

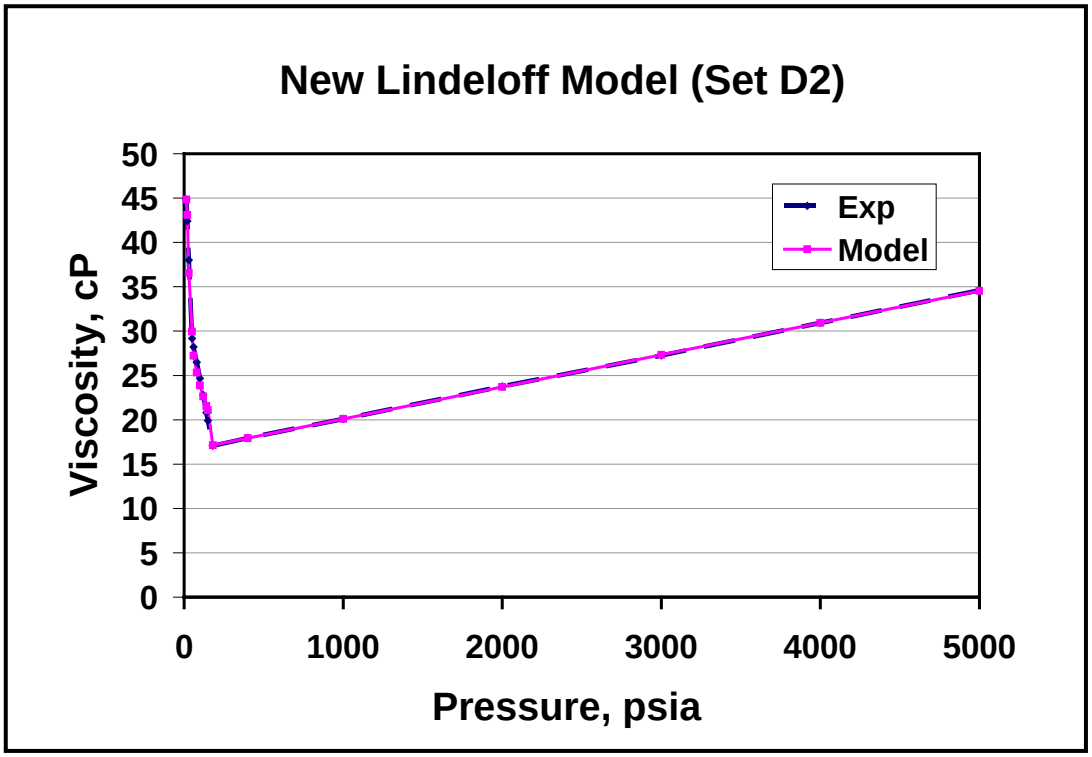

Figure 7.13 (continued) Results of New Lindeloff Model for Data Set D (D1, D2, and D3) with Corresponding Saturated Viscosities

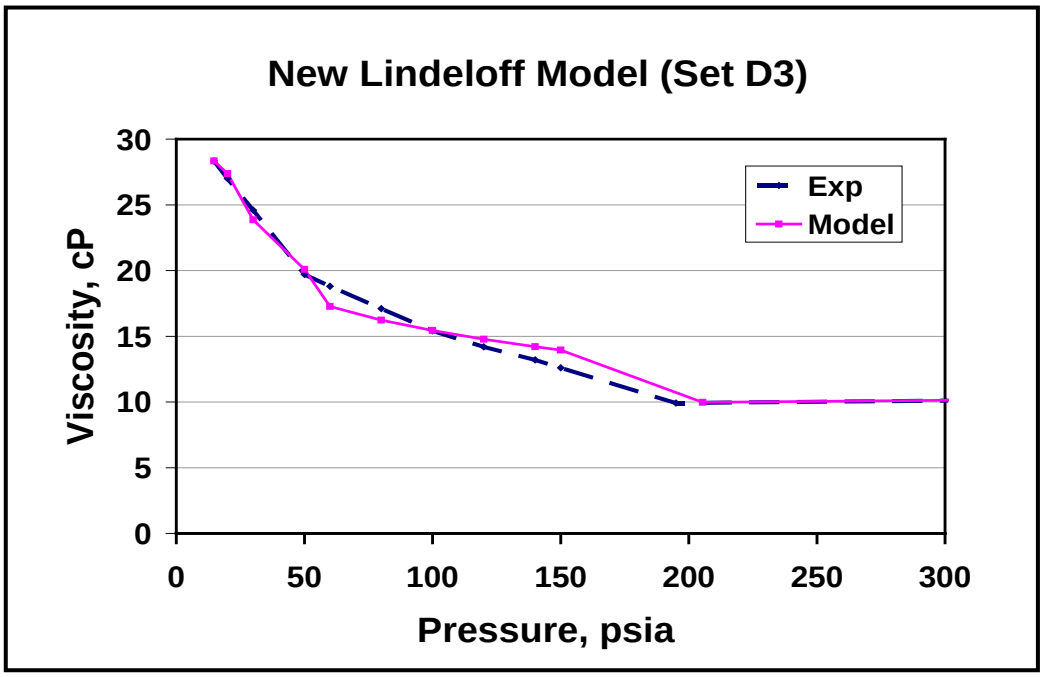

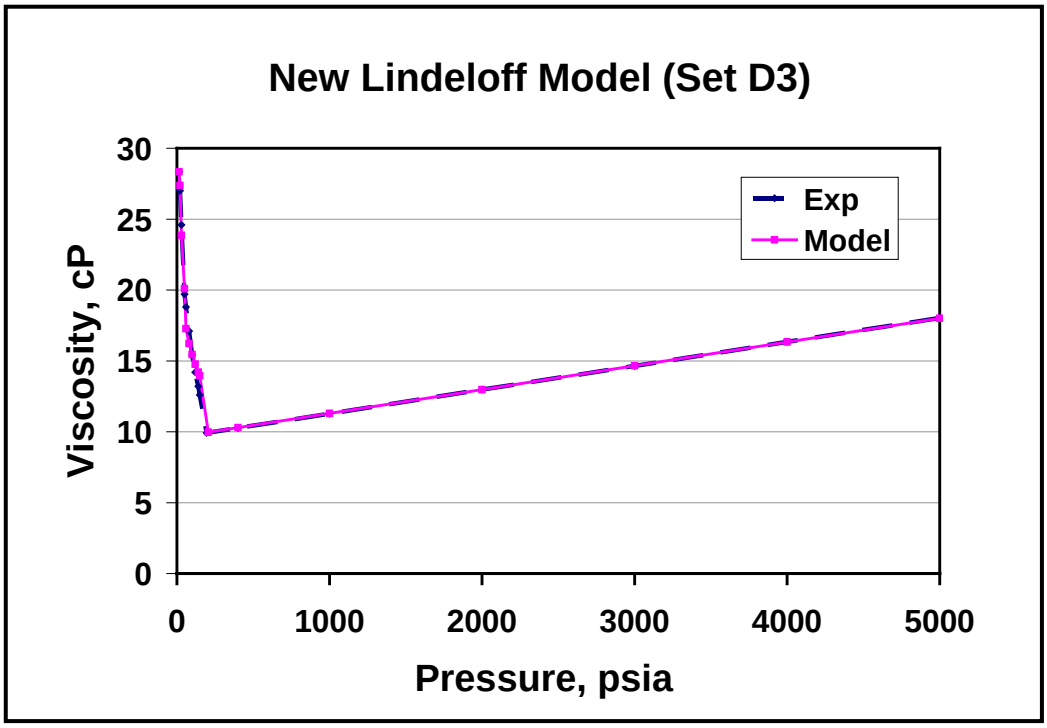

Figure 7.13 (continued) Results of New Lindeloff Model for Data Set D (D1, D2, and D3) with Corresponding Saturated Viscosities

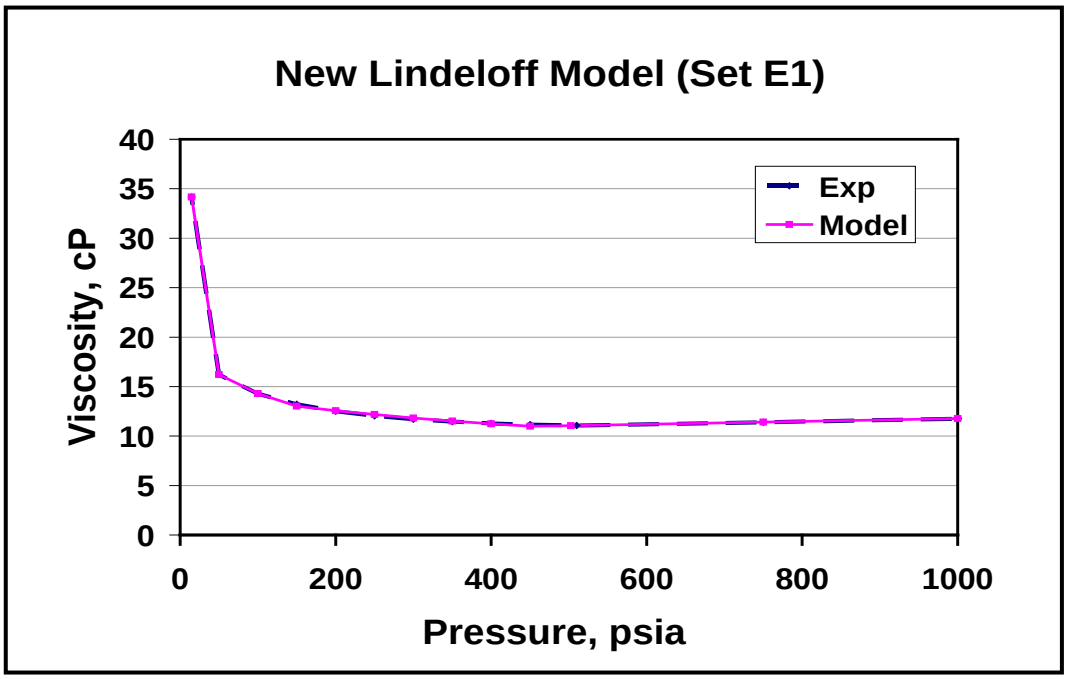

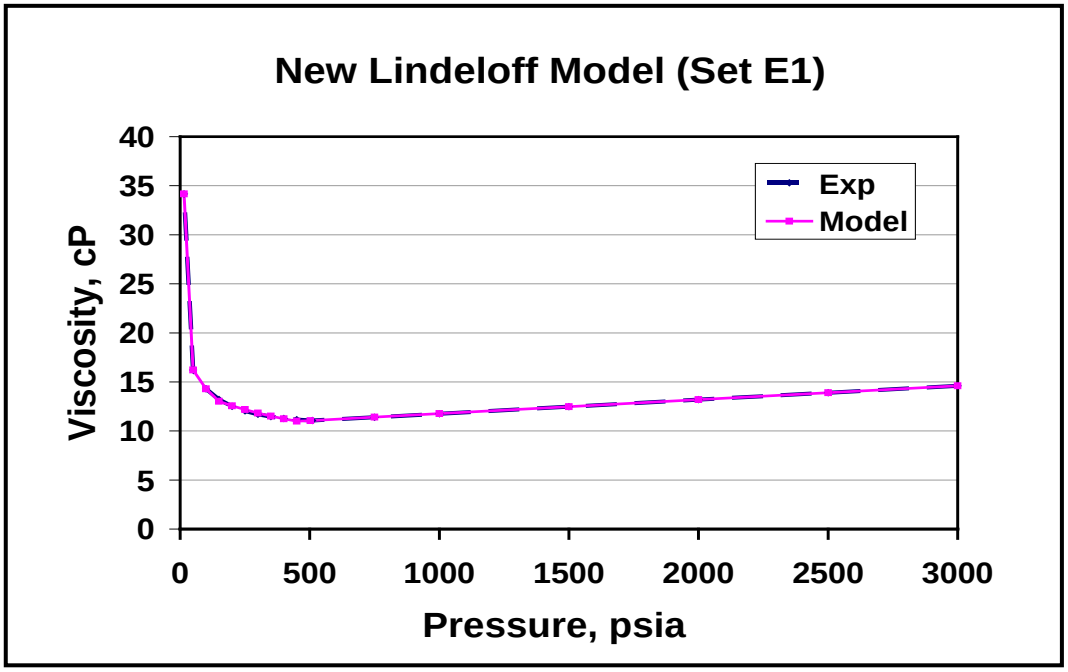

Figure 7.14 Results of New Lindeloff Model for Data Set E (E1 only) with Corresponding Saturated Viscosities

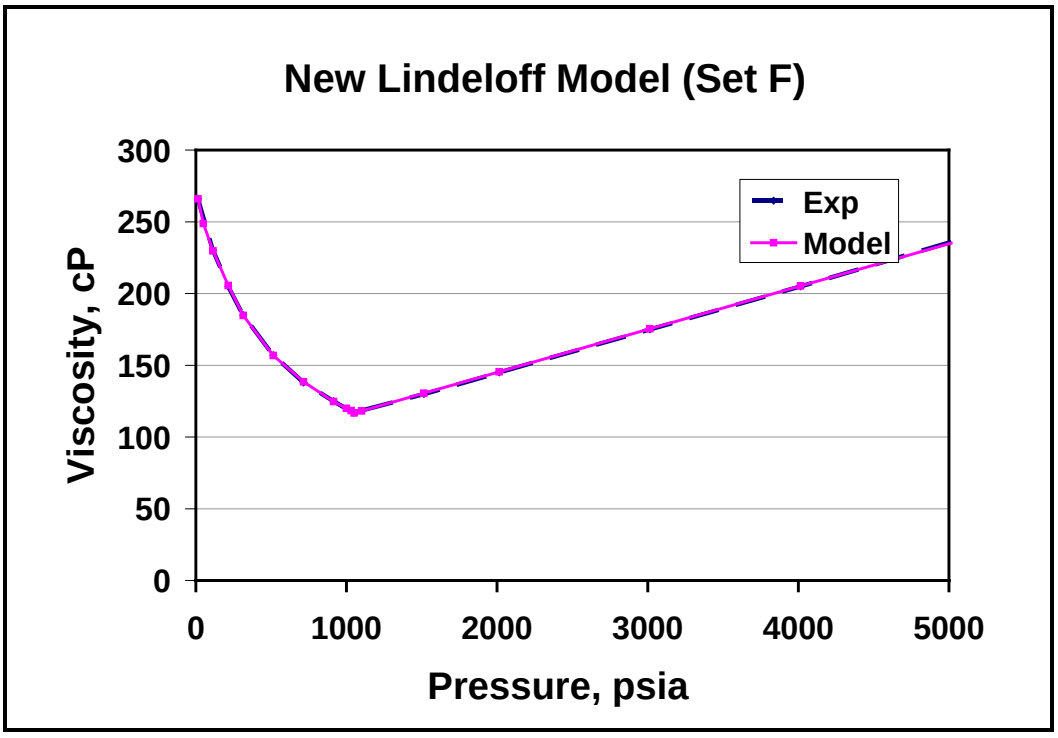

Figure 7.15 Results of New Lindeloff Model for Data Set F

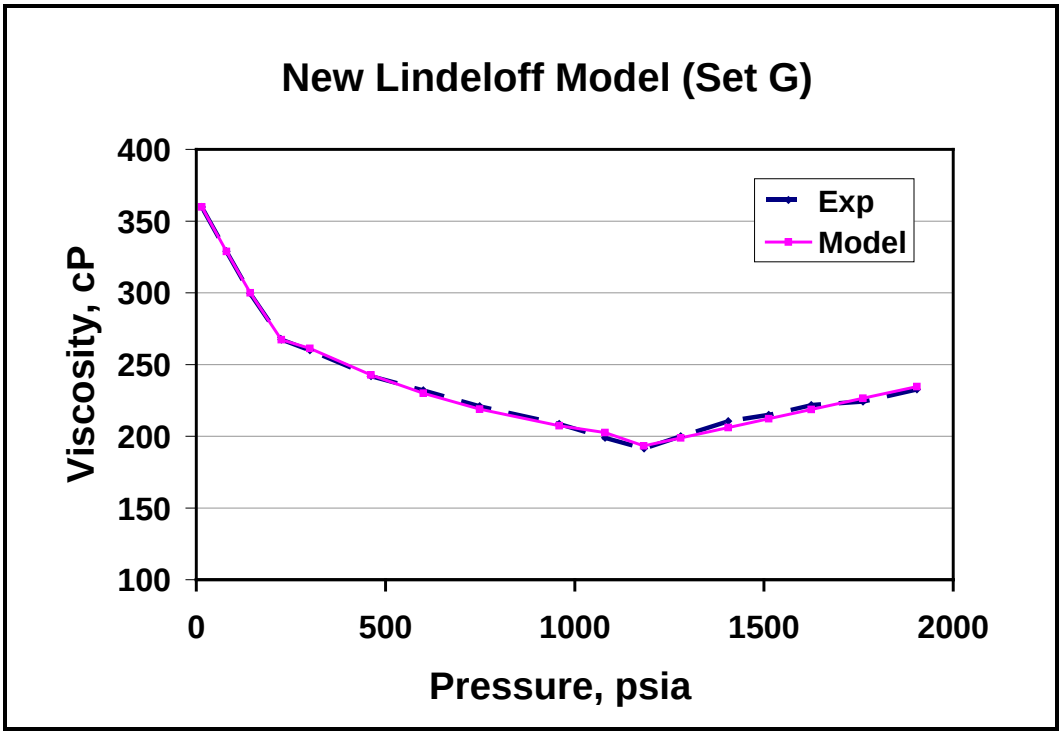

Figure 7.16 Results of New Lindeloff Model for Data Set G

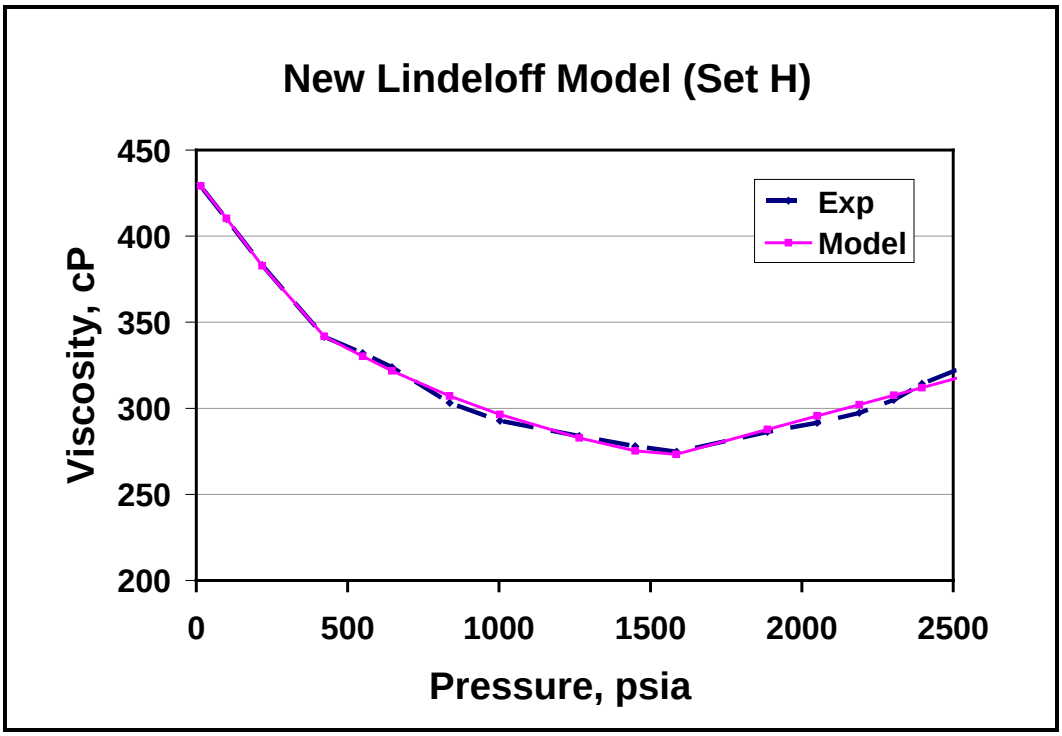

Figure 7.17 Results of New Lindeloff Model for Data Set H

Data Set	T, °F	Region I		Region II		Region III		m, psia^{-1}	% AAD
		1.5	0.5	1.5	0.5	1.5	0.5		
A	130	2.25	0.18	2.17	0.39	1.78	-0.71	0.0128	3.59
B	171	1.59	0.63	1.61	0.61	1.55	0.20	0.0021	0.64
C1	100	1.96	0.43	2.64	0.05	1.40	0.01	0.0094	0.91
C2	140	1.99	0.48	3.00	0.03	1.40	0.03	0.0034	1.69
C3	180	1.95	0.42	2.83	0.04	1.40	0.03	0.0017	1.43
D1	100	2.02	0.52	1.86	-0.68	1.68	0.14	0.0072	1.66
D2	140	2.02	0.52	3.00	0.03	1.77	-0.57	0.0036	1.80
D3	180	2.10	0.63	3.00	0.05	1.74	-0.41	0.0017	2.56
E1	80	1.77	0.85	1.80	0.94	1.78	0.79	0.0014	0.37
F	114	1.80	0.80	1.67	0.54	1.62	0.36	0.0299	0.24
G	84	1.44	0.65	1.44	0.67	1.39	0.22	0.0573	0.79
H	81	1.65	0.97	1.59	0.87	1.57	0.77	0.0477	0.73

Table 7.5 Summary of New Lindeloff Model Results for All Data Sets

7.3 Predictive Nature of the New Modified Lindeloff Model

It was already shown that it is very difficult to make the new modified Lindeloff model predictive. With the data samples from different geographical locations around the world, it is not possible to describe any mathematical relationship between the tuned parameters. However, the Data Sets C, D, and E have viscosity data available for three

different temperatures. Hence, as far as the temperature effect is concerned, the proposed model can be tested in the predictive mode. Data Set E is not considered for present analysis for the reasons stated earlier. To demonstrate this, at first, Data Sets C2 and C3 were simulated with the tuned model parameters for Data Set C1 only. The results are represented in the Figures 7.18 and 7.19 respectively. The results show that a considerably good match can be achieved. The AADs for these two data sets are 3.93% and 2.30%, respectively. As far as Data Set D is concerned, the subsets D1 and D3 are simulated with the model parameters for Data Set D2 only. The results are represented in Figures 7.20 and 7.21, respectively.

The AADs for these two data sets are 7.5% and 10.8% respectively. Considering this wide range (80°F), both the data sets have responded remarkably in the predictive mode. The above results are not completely predictive though. The atmospheric pressure viscosity data point in addition to the pressure differential coefficient, *m*, was also assumed to be known for individual data set. Ideally, the atmospheric viscosity can be predicted if the dead oil correlation can be tuned specifically for similar oils from one particular geographic region. Similarly, a suitable *m* correlation can be developed for these oils if sufficient data are present. Then the model parameters can be tuned to one particular data set only and can be subsequently used for the prediction of the viscosities of the oils of similar nature.

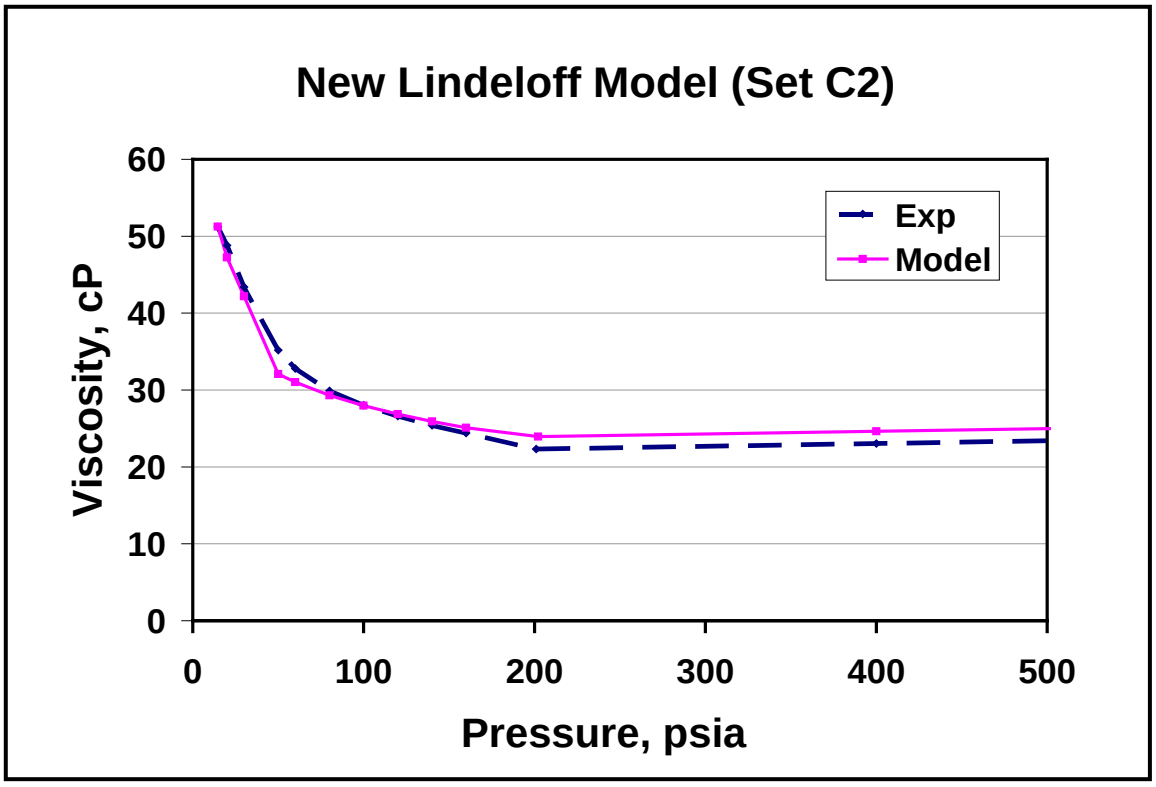

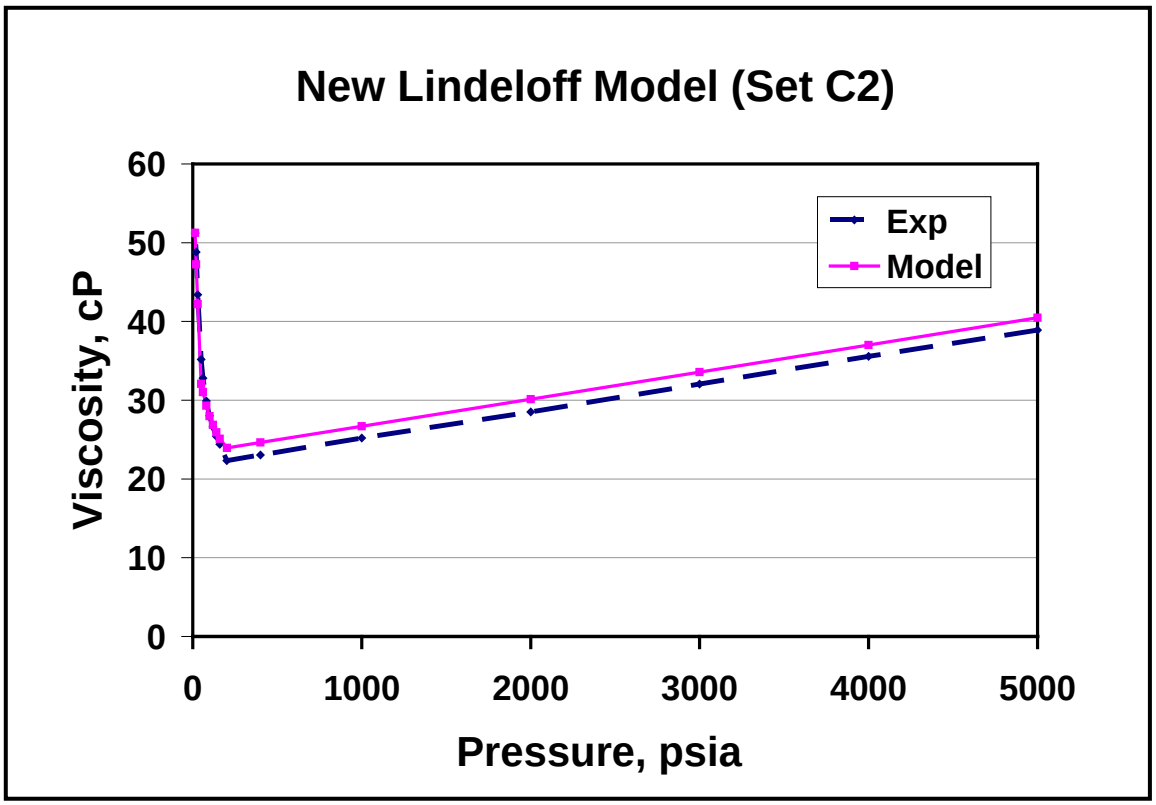

Figure 7.18 Simulation Results for Data Set C2 (and Corresponding Saturated Viscosities) with the Tuned Parameters for Data Set C1

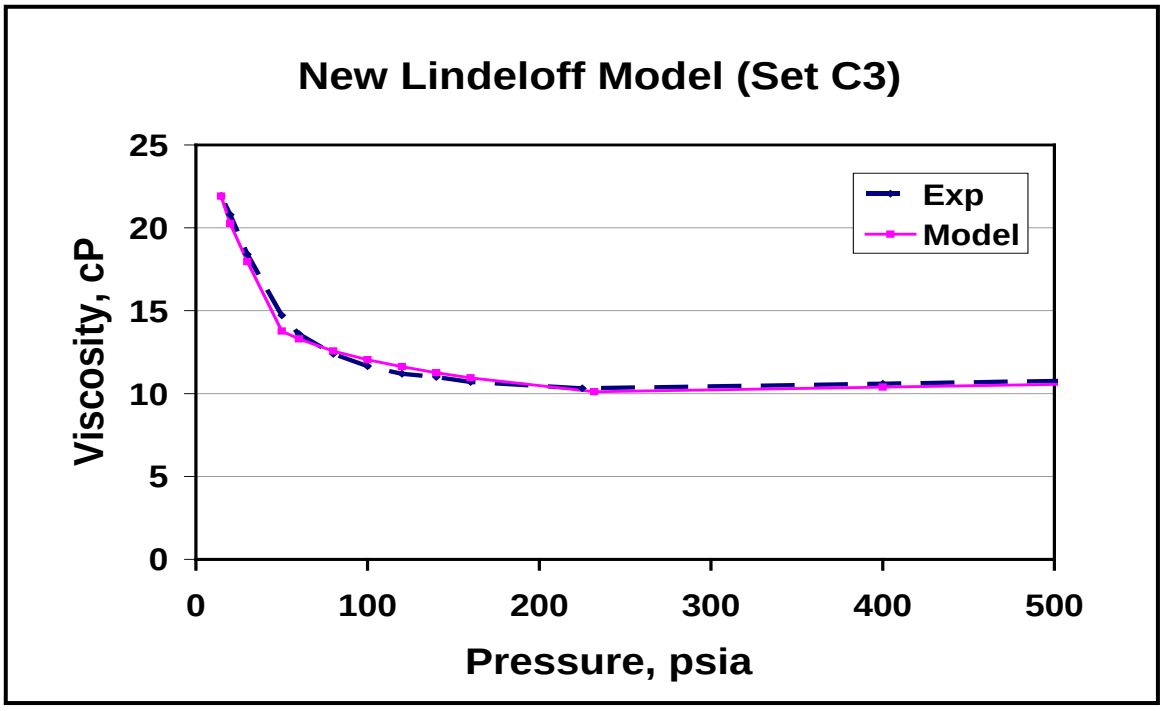

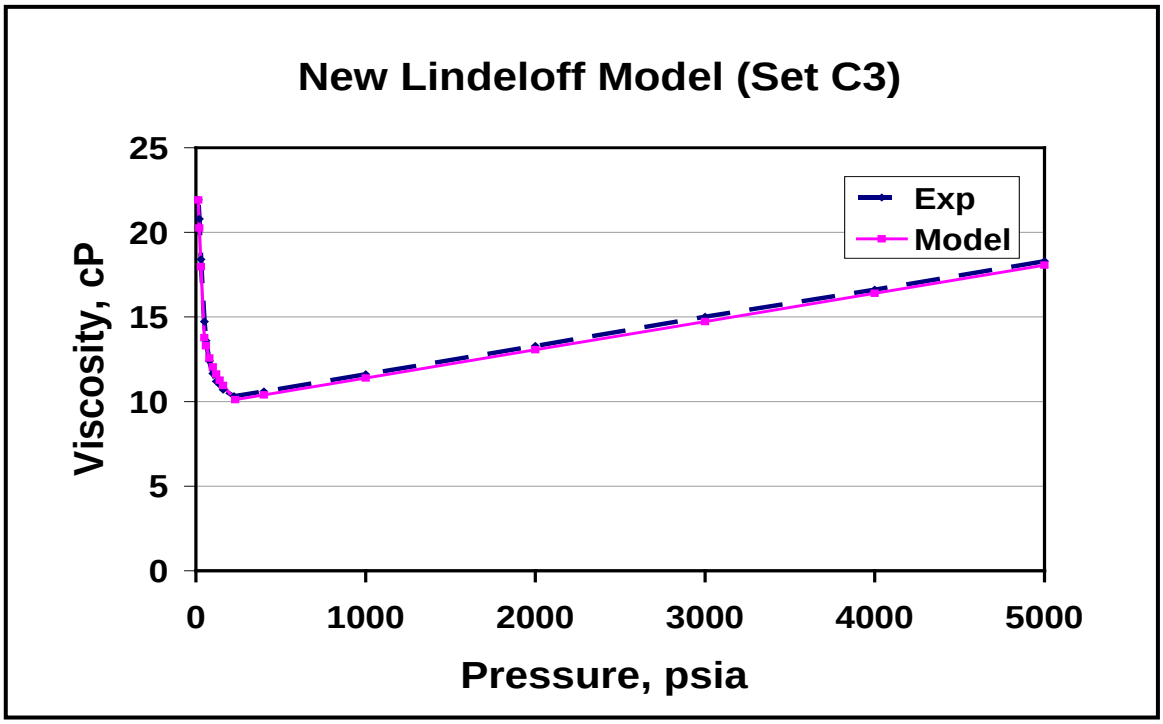

Figure 7.19 Simulation Results for Data Set C3 (and Corresponding Saturated Viscosities) with the Tuned Parameters for Data Set C1

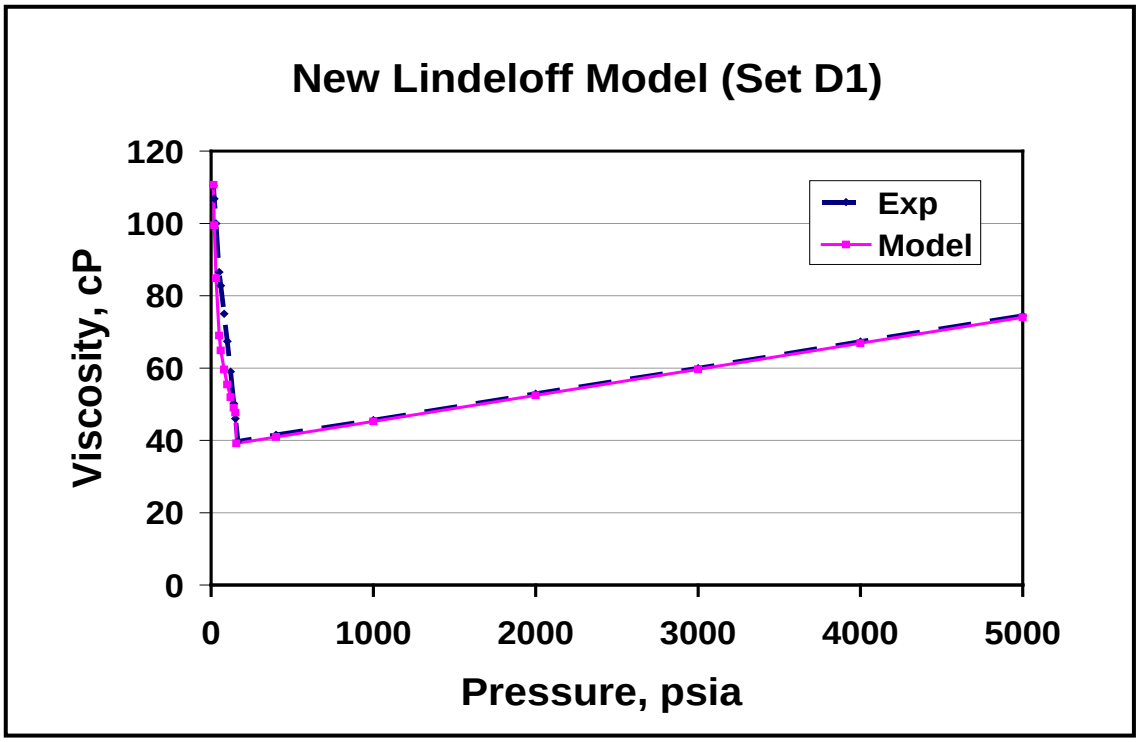

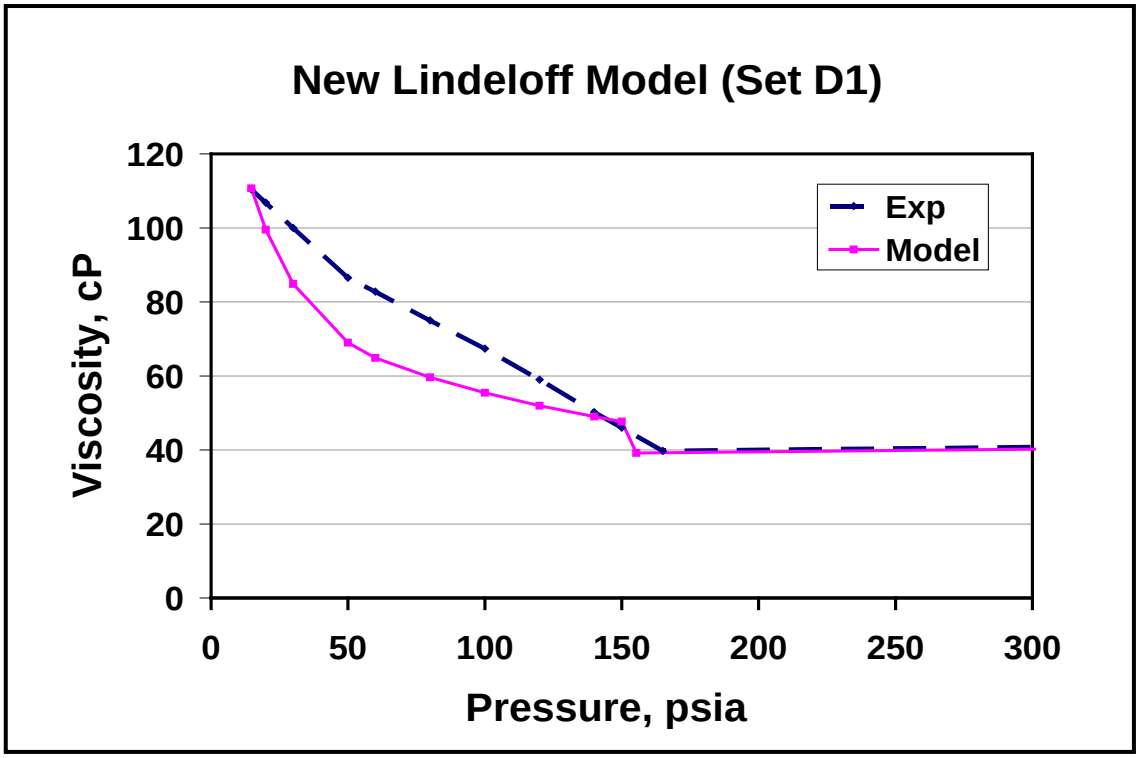

Figure 7.20 Simulation Results for Data Set D1 (and Corresponding Saturated Viscosities) with the Tuned Parameters for Data Set D2

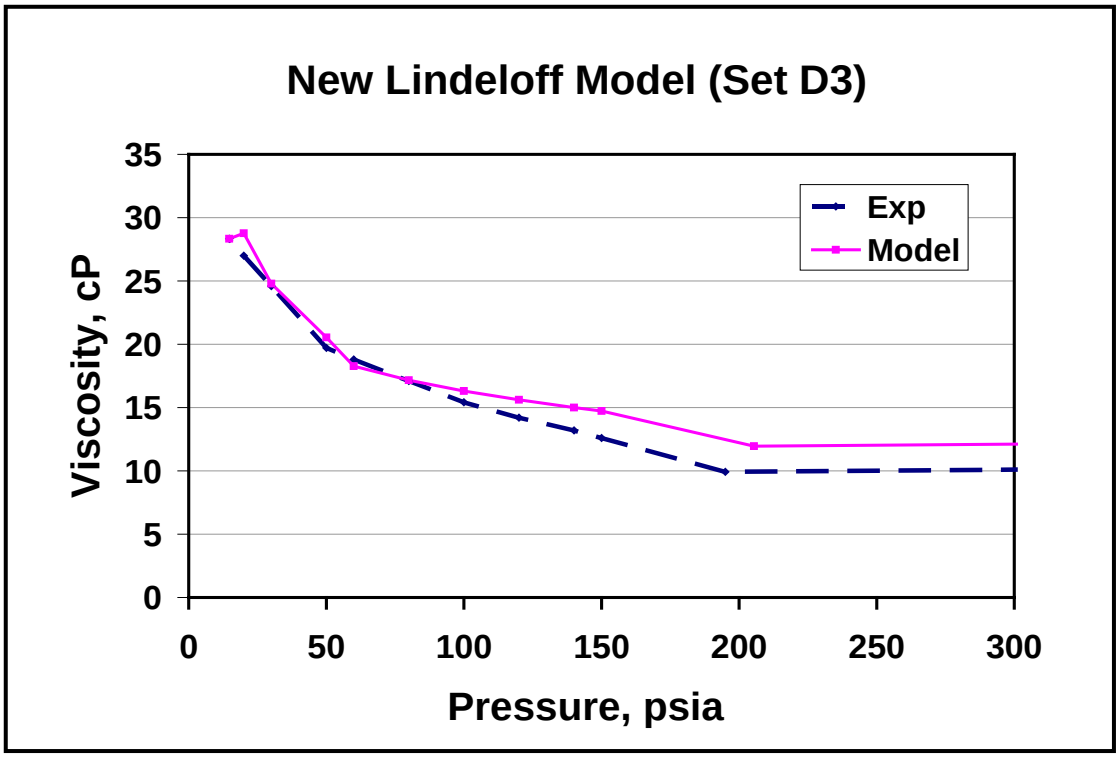

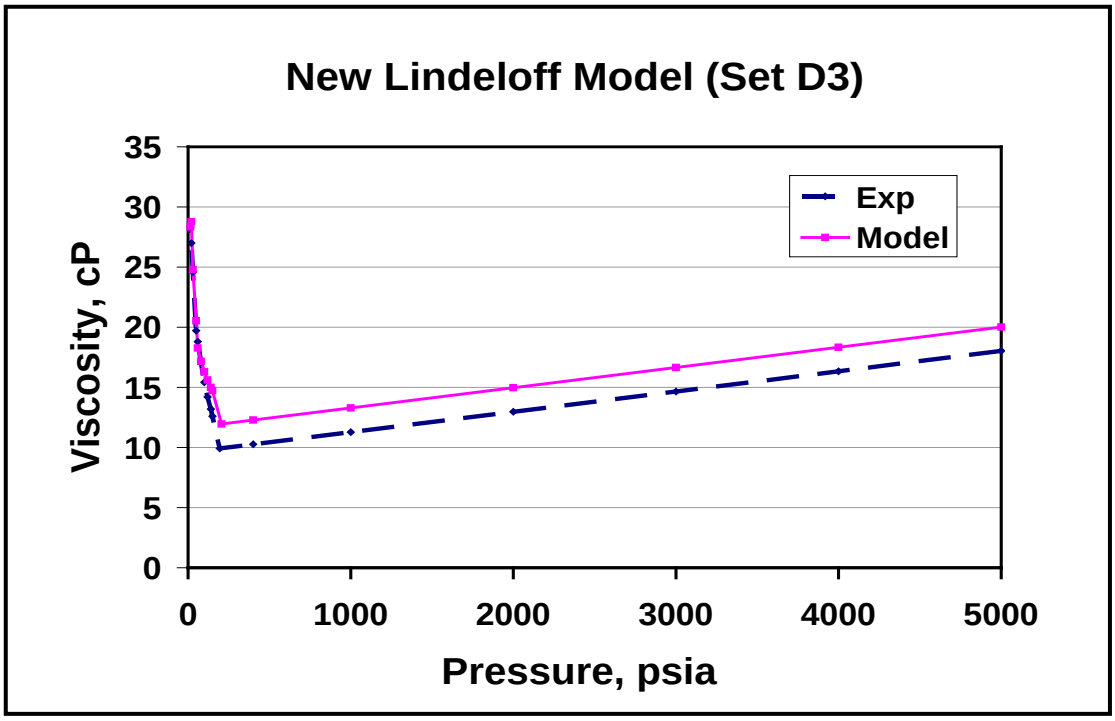

Figure7.21 Simulation Results for Data Set D3 (and Corresponding Saturated Viscosities)

7.4 Strategies for Perfecting the New Modified Lindeloff Model

The new modified Lindeloff model has shown that a very good fit can be achieved. A careful observation of the saturated viscosities, however, shows that there is a characteristic discontinuity in the otherwise continuous curve. This is represented in detail in Figure 7.22 (Data Set D2). The discontinuity is present as a result of the way the data were fitted. In the above figure, the data points between C and C', including point C and C', are used to fit the Region I. While the data points between B and B' (both inclusive) and A and A' (both inclusive) are used to fit the Region II and Region III, respectively. The last data point in the Region III represents the dead oil viscosity at reservoir temperature. This independent tuning of different regions results in a discontinuous curve. However, this is purely a mathematical inadequacy of the present model. The above shortfall of the model can be improved by including both, the bubble point viscosity and transition-point viscosity data points for fitting of Region II. It is not always possible to get the exact match of these data points. Hence, an average is sought between the fitted bubble point viscosity values for the Region II and Region III and the fitted transition-point viscosity values for the Region I and Region II respectively. This allows a smooth curve. This is demonstrated in Figure 7.23 (Data Set C2).

The above strategy can be applied to all of the data sets studied. It must be noted that the resultant fitted values for the model parameters also do change with the this modification. However, the %AAD value improved from 1.69 to 1.03 for the data set concerned.

Another important observation is that the viscosity nature between points B and B' is not a straight line, but concave in shape. For this particular data set, without knowing the actual intermediate data points, a straight line was assumed. Since the viscosity model almost always returns the curved fit, this explains the significant deviation between the experimental results and model predictions for this region. For Data Sets E1 and F, with considerable amount of viscosity data for this saturated region, a very good fit can be achieved as shown in Figures 7.14 and 7.15, respectively.

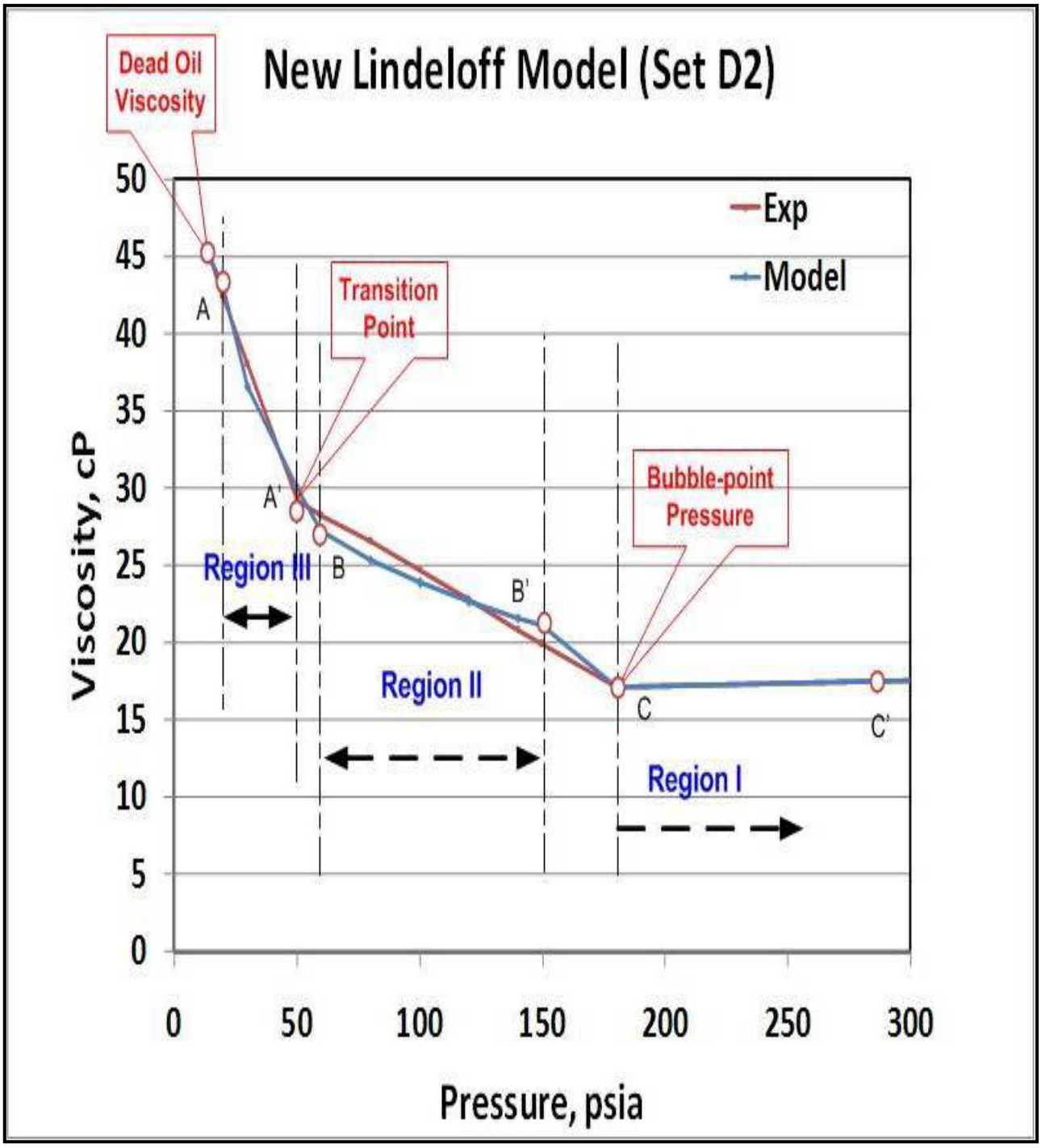

Figure 7.22 Discontinuous Saturated Viscosity-Pressure Curve

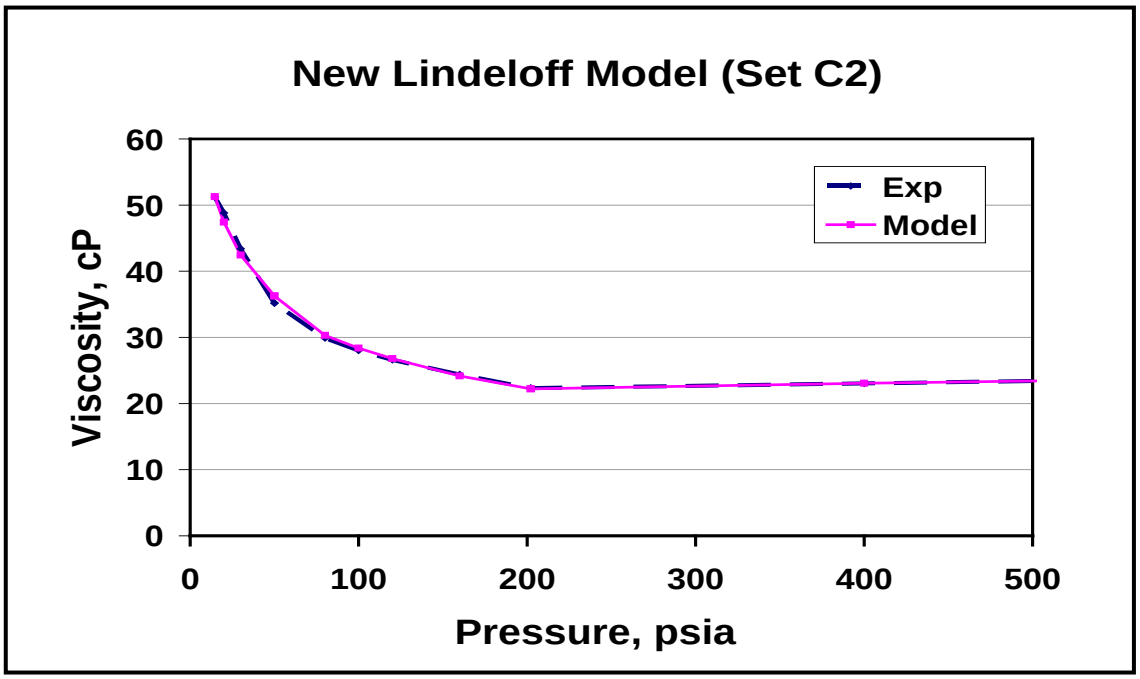

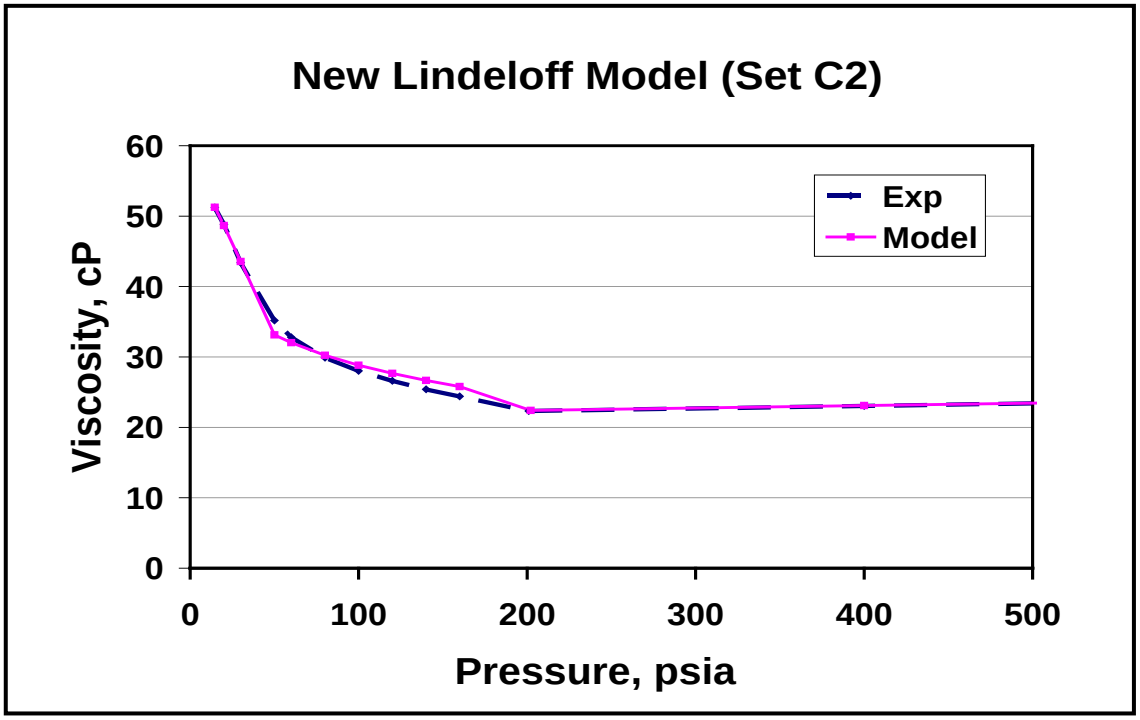

Figure 7.23 Results of New Lindeloff Model for Data Set C2 with and without the Smooth Curve

Additionally, for some data sets, it is quite difficult to determine the transition point between Region II and Region III with the criterion proposed earlier. It may happen that the change in the slope may not be obvious. Nevertheless, it is not necessary to have the

strict determination of the transition point. If above criterion fails, then the behavior of the two-phase formation volume factor, B_t, can be used to determine the transition point. B_t significantly increases due to reduction in pressure below the bubble point pressure. At lower pressures, B_t shows sudden increase due to the evolution of increasing amounts of gas. The pressure at which this sudden change occurs usually coincides with the transition point.

In general, the Region III represents viscosities close to atmospheric pressure. Since these very low pressures are generally not encountered in the reservoirs, this region is not studied in great depth in literature. However, the viscosity prediction in this region is important as far as heavy oil transportation and designing of the surface facilities are concerned. Hence, it is imperative that the heavy oil phase behavior needs to be understood properly for a successful theoretical determination of the transition point.

Chapter 8 RESERVOIR SIMULATION

An equation of state compositional reservoir simulation was conducted to evaluate heavy oil recovery from the West Sak reservoir by applying enhanced oil recovery techniques. The EOS models were tuned using phase behavior data obtained in this study. The following sections describe the reservoir simulation methodology and results.

8.1 Equation of State Model Tuning

The Peng-Robinson equation of state (PR-EOS) was used for the reservoir simulation for the following reasons:

- The PR-EOS uses a universal critical compressibility factor of 0.307, which is closer to the experimental values for heavier hydrocarbons and somewhat lower than the Redlich-Kwong value of 0.333.
- The PR-EOS gives more accurate and satisfactory volumetric predictions for vapor and liquid phases when used with volume translation.

The experimental data used for carrying out the equation of state modeling consisted of the following:

- Compositional analysis of the West Sak oil up to C_{21+}
- Saturation pressure at the reservoir temperature of 80°F
- Pressure-Volume-Temperature experimental data, mainly differential liberation (DL), constant composition expansion (CCE)

To study how well the data fits the PR-EOS, initial runs were carried out using just the compositional data. The shape of the phase envelope was studied along with the predicted saturation pressure. When it was found that the predictions were erroneous in the absence of tuning, experimental data was used to fit the predicted values by regression of EOS parameters. The initial regression runs were carried out using the original West Sak oil composition distribution to narrow down the number of EOS parameters used for regression. Different EOS parameters were selected and regression was carried out until a good match between the experimental data and the values predicted by WinProp was obtained. Careful attention was paid to the number of data points used in the tuning. Too many data points would add to the complexity of regression and the flexibility of the EOS parameters. Too few data points would not give good predictions. Likewise, oil viscosity, liquid volume %, and relative volume were

selected as the experimental data set because it difficult to get a good match of these data points. The main objective during such runs was obtaining a good match of saturation pressure values, oil viscosities, and oil densities. However, the predictions of other PVT properties were maintained within a reasonable range. Apart from changing the combination of EOS parameters selected for regression, different property correlations and the effect of inclusion of binary interaction parameters (BIP) on the EOS predictions were also studied. The percent deviation in the values of the EOS parameters used for tuning was maintained within a permissible range defined by the parameter itself and the regression model.

Once a good match between the experimental values and EOS predictions was obtained, lumping was carried out to reduce the number of components. Lumping reduces the time required for reservoir simulation. Different lumping schemes were used and the results were studied. The main aim was to reduce the number of components without compromising on the accuracy of EOS predictions. A step by step procedure adopted for the EOS model development is given by Moyre (2007).

The same procedure used for a characterized oil sample was adopted to tune the EOS for the lumped sample. Finally, a tuned EOS with the lumped sample was developed and used for West Sak reservoir simulation purposes.

8.2 Reservoir Simulation

After developing the model for the EOS, the next task was to study the potential of the West Sak reservoir for enhanced oil recovery (EOR) using gas injection. As West Sak is a very large reservoir, for simulation purposes a 40-acre area was chosen. Initially a comparative study was performed for different gases to be used as the injectant for enhanced oil recovery. A vertical 5-spot injection pattern was selected with the four injectors at the four corners and a producer well at the center. The project life was 25 years, from Jan 2006 to Dec 2030. After performing a detailed analysis for this vertical injection pattern, the gas with the best performance was selected for study of its effectiveness in a horizontal well pattern case.

CMG’s GEM, a reservoir simulation application, was used for the study. GEM provides features such as the building of grid blocks to define the reservoir and its properties (porosity, permeability, sand layer thickness, depth, water saturation, relative permeability). Operating conditions such as the temperature and pressure can also be

defined. Reservoir performance can be analyzed under various operating parameters such as the well bottom-hole pressure and production rates of oil and gas.

8.2.1 Model Development

To define the reservoir, a three-dimensional Cartesian coordinate system was used for the study. Accordingly, I, J, and K defined the three directional axes; I and J axes perpendicular to each other and in the same plane, and K axis was perpendicular to the IJ plane. The West Sak reservoir was defined to have five producing layers with definite porosity and permeability values, with alternate shale layers embedded in between the sand layers. The shale layer was considered to be impermeable with zero porosity. The entire reservoir was built in the form of grid blocks in all the three directions. Accordingly, for a 40-acre area, there were 25 grid blocks each in the I and J direction and 9 such planes of grid blocks in the K direction making a total of 5625 grid blocks for the entire reservoir. A pictorial view of the reservoir configuration with marked locations of producer and injectors is shown in Figure 8.1. The reservoir properties are listed in Table 8.1. Relative permeability data required for the reservoir model was taken from Bakshi (1991).

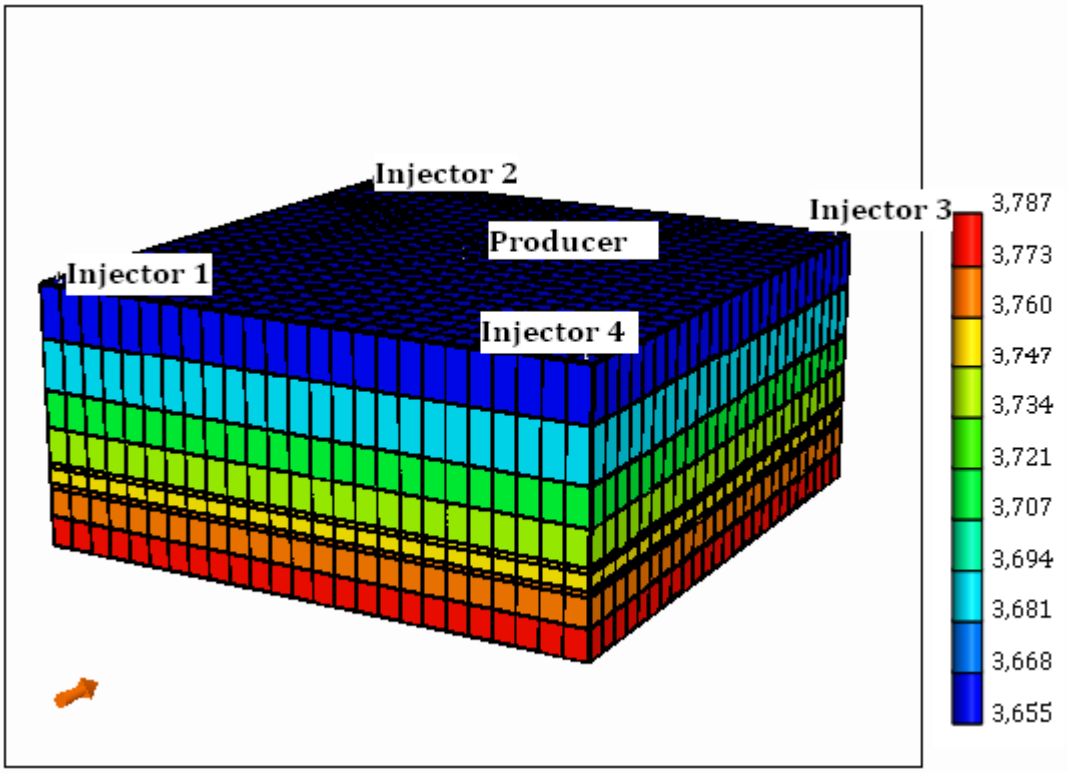

Figure 8.1 West Sak Reservoir Model View

Layer No.	Sand	Interval (ft)	Avg. Porosity (%)	Avg. water saturation, (%)	Net pay (ft)
9-topmost	Upper 1	3544-3584	30	24	30
7	Upper 2	3614-3640	31	31	21
5	Lower 1	3660-3686	23	45	3
3	Lower 2	3695-3760	25	47	3
1-bottommost	Lower3	3776-3814	27	41	17

Table 8.1 West Sak Reservoir Properties (Bakshi, 1991)

8.2.2 Enhanced Oil Recovery

After building the reservoir model, reservoir simulation studies of enhanced oil recovery for the West Sak reservoir using gas injection were performed. The first task was the selection of gases to be used as injectant in the study. Since this was intended to be a comparative study, gases covering a wide spectrum of compositional variations were considered. The basic requirement for such a selection was the availability of the gases on the Alaska North Slope (ANS). Patil (2006) has proposed geologic sequestration of CO_2 as an option to control its emissions on the ANS. This sequestered CO_2 can be utilized as an injectant in EOR. Sharma et al. (1988) estimated the Prudhoe Bay field to contain approximately 29 trillion cubic feet of natural gas, composed mainly of methane. Such a large reservoir of gas can definitely serve as the source gas in any gas injection scheme. Miscible Injectant 1 (MI 1), Miscible Injectant 8 (MI 8), and West Sak Viscosity Reducing Injectant (VRI) are the gases currently used as injectant gases by BP Exploration (Alaska) Inc. (BPXA) on the ANS under various EOR schemes. All these gases were employed for EOR after careful study of the reservoir and the conditions present. West Sak VRI is one such gas designed by BPXA for the West Sak reservoir. VRI simply stands for viscosity reducing injectant and is manufactured by mixing heavy components with the produced gas which is generally lean on the ANS. Some amount of CO_2 stripping is required to achieve miscibility conditions. MI 8 was another such gas used on the ANS. It is an extremely rich gas stripped completely of the heavier fractions (C_{7+}) and CO_2. It has 42% of intermediates mainly rich in C_3 and C_4. MI 1 is a very lean

gas having almost 95% of methane. Figure 8.2 shows a comparison of the compositional variation of the injection gases selected for the present study.

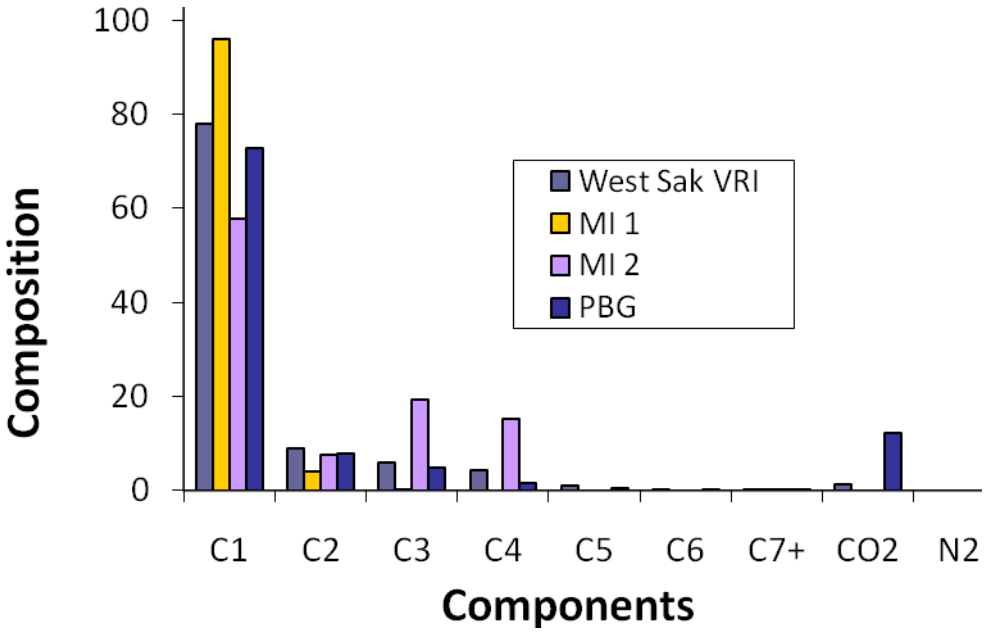

Figure 8.2 Component Distribution Comparison for the Gas Injectants

Having carefully selected the gases for the EOR study, the next step was designing the project. Project life was chosen to be for 25 years. Necessary pore volume (PV) calculations were done and it was decided to use 10%, 20%, 30%, 40%, and 50% as injection PV for different runs. Reservoir operating parameters are of prime importance in any reservoir simulation model. Due consideration to the integrity of these parameters should be given while making this selection. An obvious choice was to select bottom-hole pressure and production rate as the operating parameters. The values of these parameters were fixed after giving due considerations to all the constraints. Some of these considerations were reservoir pressure, reservoir fracture pressure, drawdown, and daily production rates. Accordingly, bottom-hole pressure was set at 1,400 psi and the production rate at 500 bbl/day. These operating parameters were kept fixed for all the gases and all the PV runs to make a uniform comparison. Gas injection pressure for the injector well was determined by the reservoir fracture pressure constraint and was set at a value of 3,000 psi. Gas injection rates are determined depending upon the PV of gas being injected. A vertical 5-spot injection pattern was chosen as shown in Figure 8.3.

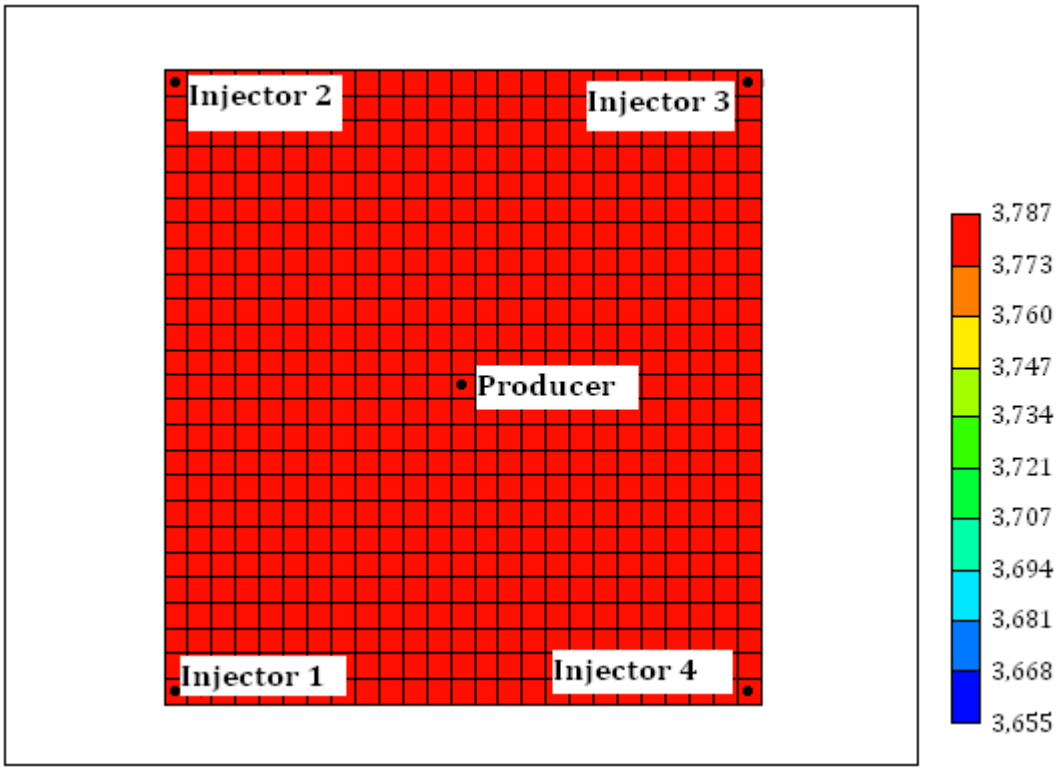

Figure 8.3 Top View of the Reservoir Model Showing the Location of Producer and Injector Wells for a 5-spot Injection Pattern

To compare the potential of different gases as an EOR agents, we compared the production profiles for the entire life of the project for all the gases at different PVs. A simplistic comparison would be to just compare the cumulative recovery calculated in terms of original oil in place for all individual cases.

Plots of percentage pore volume of gas injected versus production rate were drawn to study the results. For the purpose of the comparative analysis of the performance of various gases, percentage pore volume of gas injected versus cumulative recovery was plotted.

After careful evaluation of results for a vertical five-spot injection pattern, simulation runs were conducted to study the performance of the West Sak reservoir for a horizontal producer with a horizontal injector case. Accordingly, two producers and two injectors were placed alternately (Figures 8.4 and 8.5). Only three producing layers out of a total of five were perforated because the remaining two layers were too thin to drill a horizontal well. The gas, MI 8, that performed the best in the case of vertical five-spot injection pattern was chosen as the injectant gas for the horizontal case. The same scheme of injection runs was employed for the horizontal case. Likewise, 10%, 20%, 30%, and 40%

PV injection runs were carried out. Reservoir operating parameters were optimized. It was found that using a bottom-hole pressure of 1,400 psi, which was used for the vertical injection case, the gas breaks through very quickly. It was inferred that in the case of the horizontal injector, since the gas has a much larger space to expand, it expands quickly. Hence the drawdown of 300 psi is too large for this case. After numerous runs, the well bottom-hole pressure was optimized at 1,650 psi. Conditions for the injector wells were maintained at 3,000 psi of injection pressure. Similar plots as those made for the vertical well case were made for horizontal injection to study the behavior. Accordingly, cumulative oil produced was plotted against time.

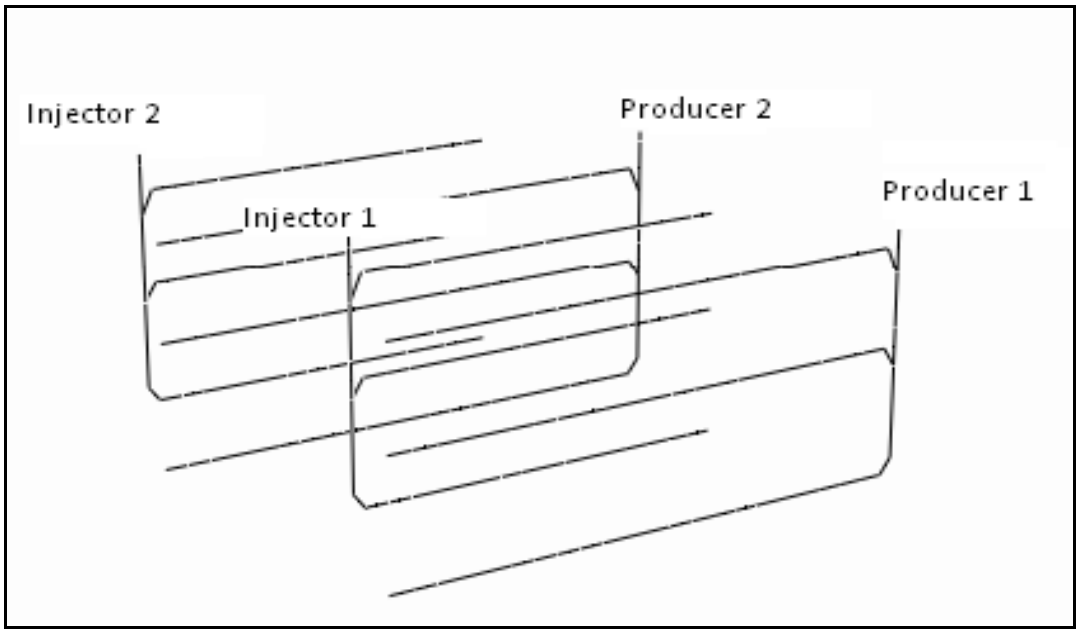

Figure 8.4: Three-dimensional Pictorial Representation of West Sak Reservoir with Alternate Horizontal and Producer Wells

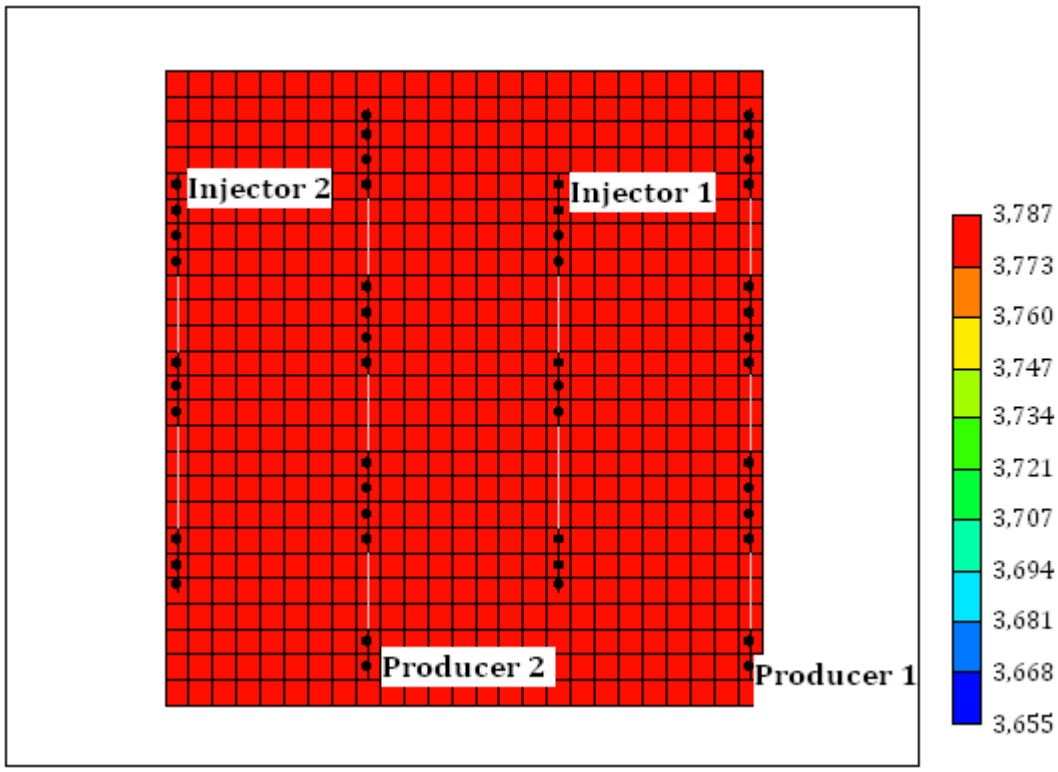

Figure 8.5 Top View of the Reservoir Model with the Producers and Injectors

8.3 Asphaltene Deposition Modeling

Asphaltene deposition is great concern during enhanced oil recovery operations like CO_2 flooding. CO_2 can cause the asphaltene to deposit and reduce the original permeability of the reservoir rock. The main focus of this study is to analyze the change in recovery caused by asphaltene deposition in a reservoir simulation model of the West Sak reservoir from the ANS.

For this study a reservoir model of the West Sak reservoir was made using the Computer Modeling Group (CMG) STARS software. This model is based on a previous CMG GEM model (Morye, 2007) of the West Sak reservoir. This model was checked for accuracy by comparing the oil recovery values obtained by this model with those obtained by the GEM model. After a satisfactory match was obtained with between the two models, the STARS model was modified to account for the effects of asphaltene deposition. A sensitivity analysis was then carried out to understand the effect of asphaltene deposition under different flooding rates.

8.3.1 West Sak Reservoir Model:

A model of the West Sak reservoir was made in CMG builder using the existing CMG GEM model (Morye, 2007) as reference. The following properties were used in designing the reservoir model. The reservoir model is comprised of nine horizontal layers starting from layer 1 (bottom layer) to layer 9 (topmost).Average porosity, permeability, and other values for each of the layer were input in the model. A fluid model for the STARS model was obtained by modifying the GEM fluid model (Table 8.2). This fluid model was then imported into the STARS simulator. The oil recovery obtained from the simulation of the new STARS model was then compared with the GEM model to confirm the new model had all the required data.

Layer No.	Sand	Interval (ft)	Avg. Porosity (%)	Avg. water saturation, (%)	Net pay (ft)
9-topmost	Upper 1	3544-3584	30	24	30
7	Upper 2	3614-3640	31	31	21
5	Lower 1	3660-3686	23	45	3
3	Lower 2	3695-3760	25	47	3
1-bottommost	Lower3	3776-3814	27	41	17

Table 8.2 West Sak Reservoir Properties (Bakshi, 1992)

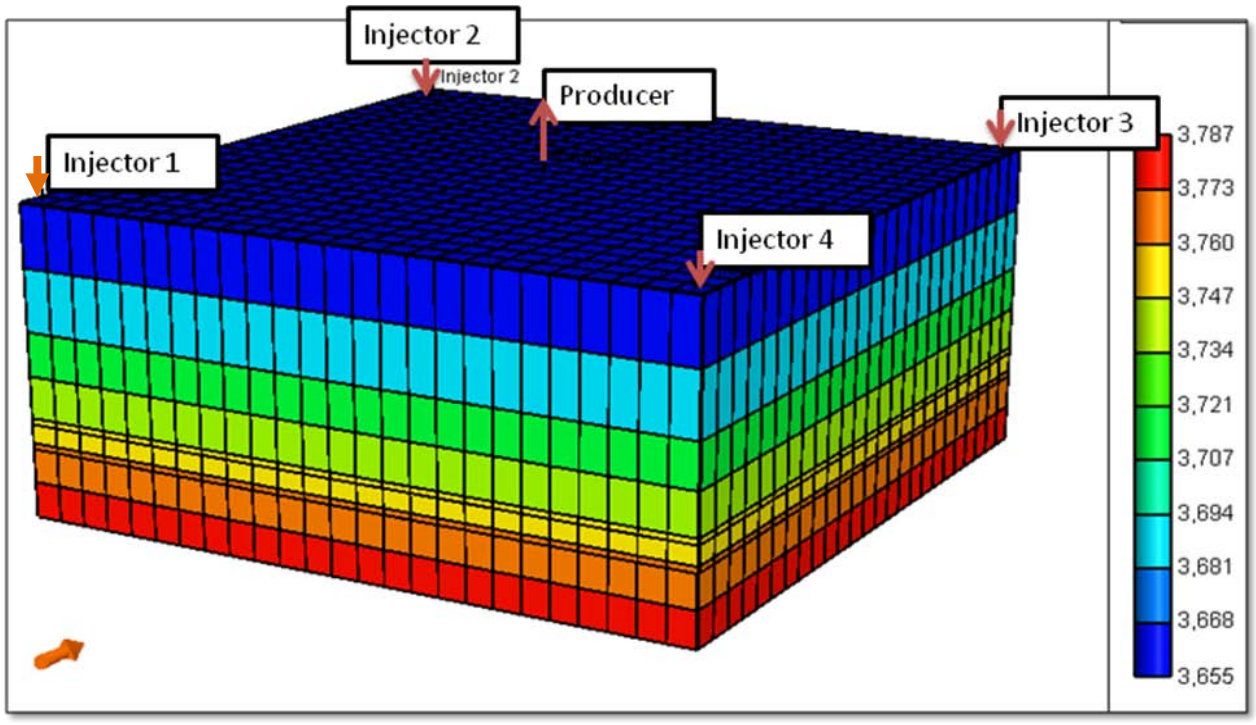

Figure 8.6 West Sak Reservoir Model 3D Views (CMG STARS)

A comparison of the two models shows a very good match in terms of the ultimate recovery obtained as well as the production rate. The graph below shows the production profile during simulation with 10% pore volume CO_2 injection using CMG STARS (red curve) and CMG GEM (blue curve). A good match is indicated since during most of the production period there was less than 10 bbl/day difference between the oil rates calculated by the STARS and the GEM simulators.

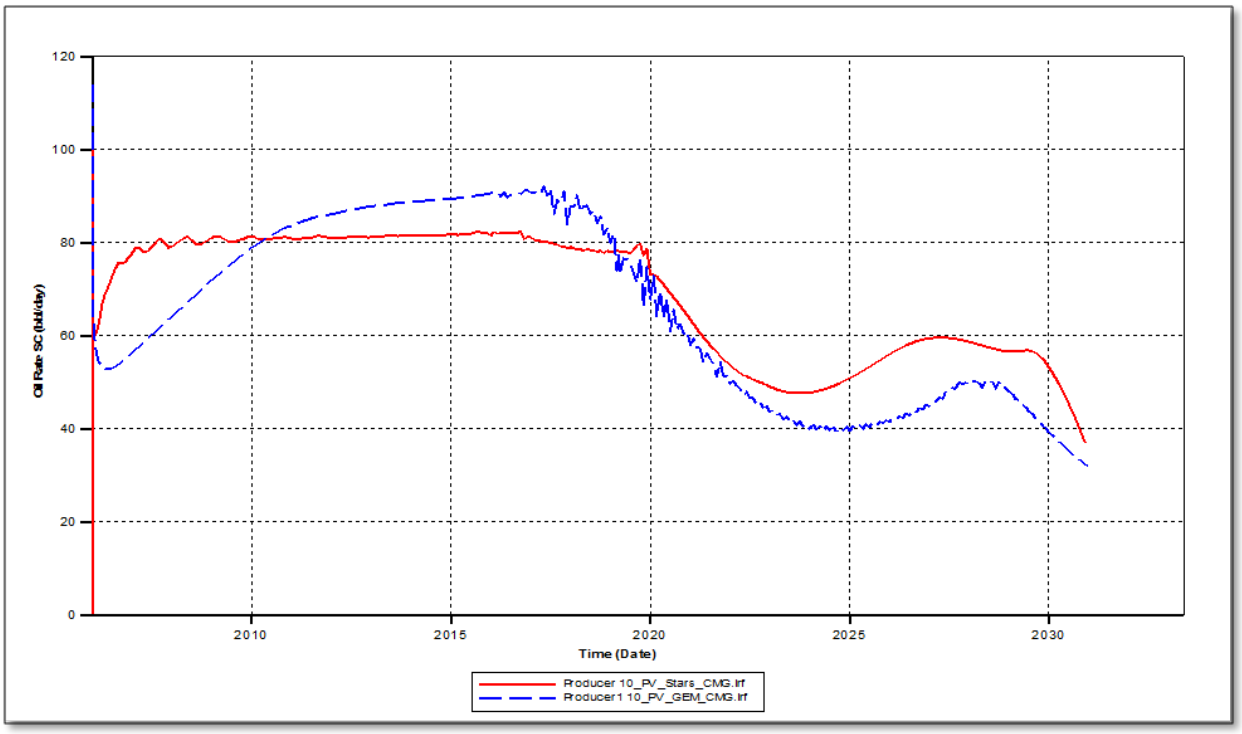

Figure 8.7 Oil Rate Comparison at 10% Pore Volume CO_2 Injection

After a satisfactory match between the STARS and the GEM model results, the STARS model was modified to take into account the effects of asphaltene deposition. This was done by introduction of an asphaltene deposition reaction, introduction of a blockage factor, and splitting the C_{7+} fraction.

- An asphaltene deposition reaction was introduced in the model and tuned to remove any mass balance errors. This reaction helps the simulator in calculating the amount of asphaltene deposited due to CO_2 injection.
- A blockage factor was then introduced to model the reduction in permeability due to asphaltene deposition; this blockage factor was based on the example provided in CMG STARS.
- To correctly model asphaltene deposition the C_{7+} component was split into 2 identical components $C_{7+}A$ and $C_{7+}B$.

8.3.2 Sensitivity Analysis

Once the model was ready, a sensitivity analysis was performed to understand the effects of asphaltene deposition. This was done by running the simulator using different injection rates and different ratios of the $C_{7+}A$ and $C_{7+}B$ fractions. The results were

analyzed by comparing curves of cumulative oil produced versus the time over 9,000 days at different injection rates and C_{7+} fraction split ratios.

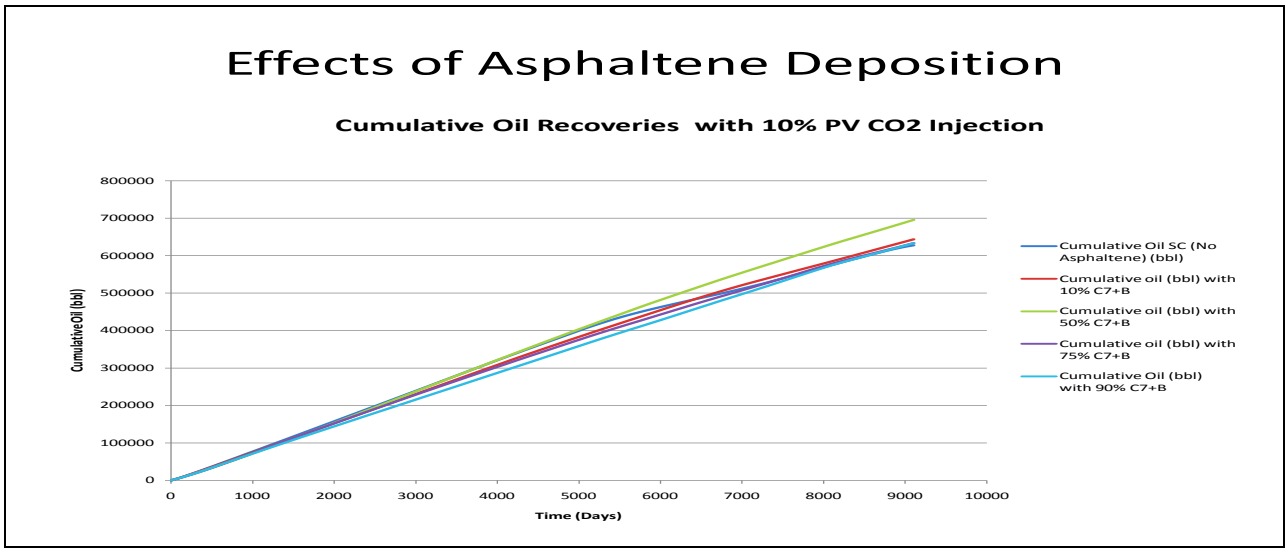

Figure 8.8 Effects of Asphaltene Deposition at 10% PV CO_2 Injection

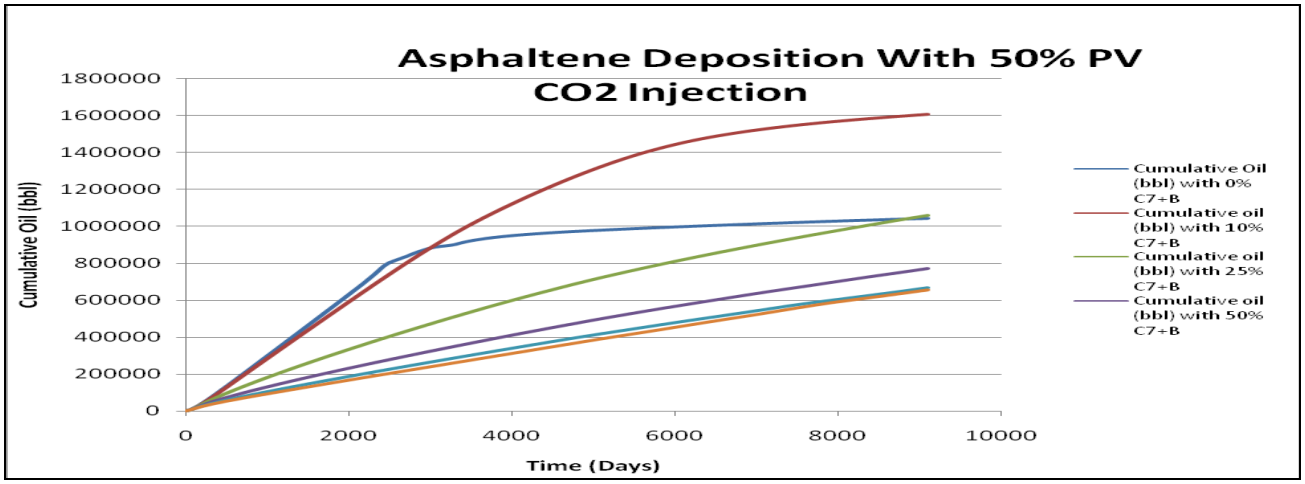

Figure 8.9 Effects of Asphaltene Deposition at 50% PV CO_2 Injection

8.4 EOS Tuning Results

8.4.1 Equation of State Performance

The performance of the untuned equation of state in predicting the phase envelope and the saturation pressure of the West Sak oil is shown in Figure 8.6.

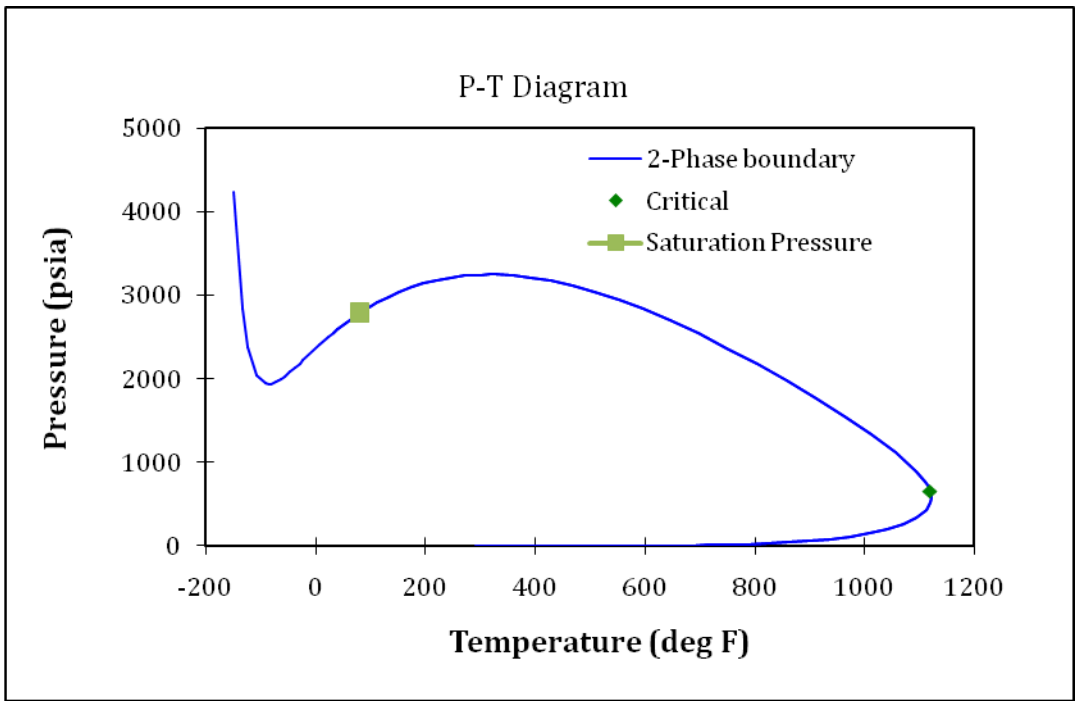

Figure 8.10 Phase Envelope Generated by the Untuned EOS

The saturation pressure value for the West Sak oil predicted by the untuned equation of state was 2,783.869 psia at the reservoir temperature of 80°F. The experimental value was 1,704 psia. The percentage difference in the two values was 63.37%, indicating a significant error in the prediction of saturation pressure. The phase envelope (Figure 8.6) is also indicative of the erroneous predictions of the untuned EOS.

The EOS was then tuned using CMG WinProp. The tuning process improved the prediction of saturation pressure value and the value obtained was 1,702 psia which was much closer to the experimental value of 1704 psia. The improvement in the phase behavior predictions can be seen from the phase envelope generated by the tuned EOS (Figure 8.7).

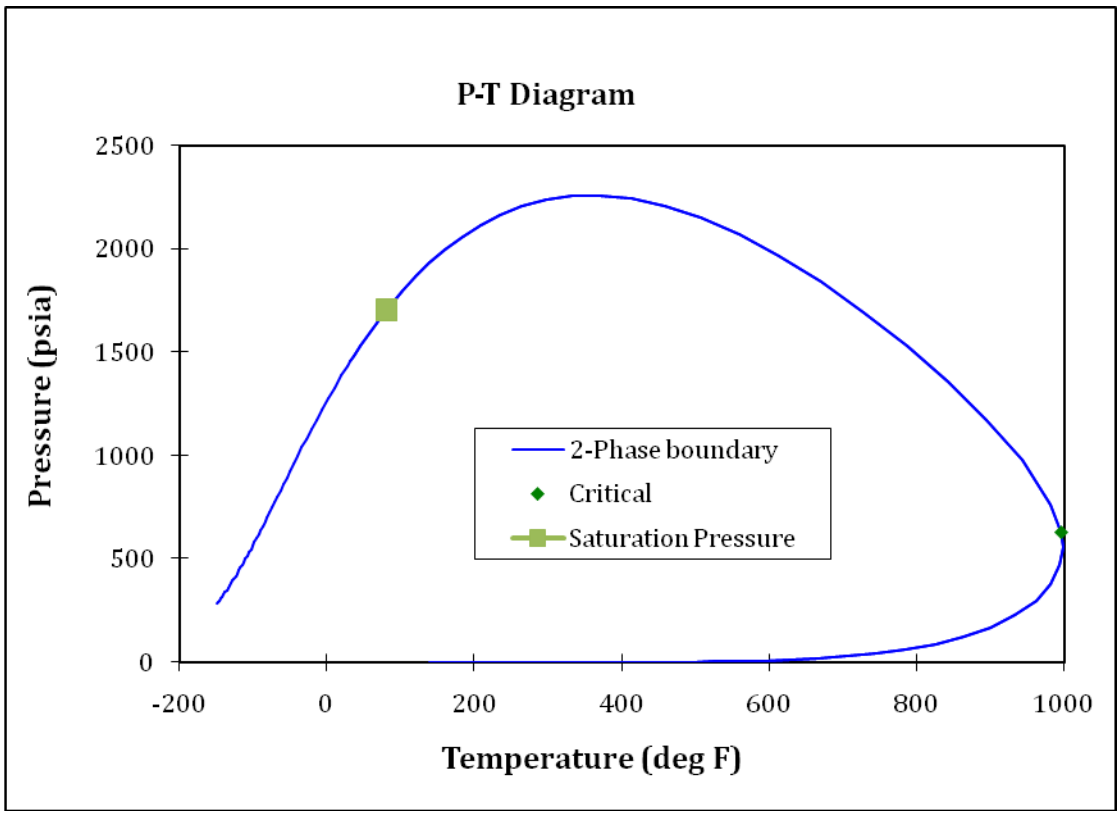

Figure 8.11 Phase Envelope after Tuning the EOS

8.4.2 Regression Scheme

The C_{21+} fraction was split first to C_{45+} using the gamma probability distribution function as the splitting model. The critical properties of the components after splitting were calculated using the Twu correlation. Lumping of components was then performed. Accordingly, components heavier than C_7 were lumped together into a single component fraction as C_{7+}. This plus fraction had components from C_7 to C_{21+}. Lumping was done to reduce the simulation time in the reservoir simulator. The component compositions and properties after lumping are given below in Table 8.2.

Components	Composition	P_c atm	T_c K	Acentric Factor	Mol. Wt.
C02	0.0001597	72.8	304.2	0.225	44.01
N2	0.0003194	33.5	126.2	0.04	28.013
C1	0.3826031	45.4	190.6	0.008	16.043
C2	0.0085537	48.2	305.4	0.098	30.07
C3	0.0035832	41.9	369.8	0.152	44.097
NC4	0.0017866	37.5	425.2	0.193	58.124
NC4	0.0006388	33.3	469.6	0.251	72.151
FC6	0.0019962	32.46	507.5	0.275	86
C7+	0.6003593	12.269	889.54	0.961	368.85

Table 8.3 Composition and Physical Property Data for the Lumped Components

This lumped data series was used for further tuning of the EOS. For the purpose of tuning, several experimental data points were selected and given a weight. This weight scheme acts as the guideline for the regression model signifying the importance of that particular data point. The more a particular data point was weighted, the more forcibly the model tried to fit it. Since the top most priority of any tuning scheme is first achieving a very good match of the saturation pressure, it is always weighted the most. But in this case, the liquid density was found to be very difficult to match and was therefore weighted the most The experimental data points selected and their weights are tabulated in Table 8.4.

Data Point	Weight
Saturation Pressure	30
Liquid Density	50
Oil Specific Gravity SG	50
Relative Oil Volume	1
Liquid Volume %	1

Table 8.4 Weight Distribution for EOS Parameters

The next task was to select the regression parameters. The following parameters were finally selected.

1. Critical Pressure of C_{7+} (P_C)
2. Critical Temperature of C_{7+} (T_C)
3. Acentric Factor of C_{7+} (AF)
4. Volume Shift (SH)
5. Coefficients of Pedersen's corresponding states viscosity model
    a. MW mixing rule coefficient (MU1)
    b. MW mixing rule exponent (MU2)
    c. Coupling factor correlation coefficient (MU3)
    d. Coupling factor correlation density exponent (MU4)
    e. Coupling factor correlation MW exponent (MU5)

The percentile changes in the values of these parameters during regression are given below in Table 8.5.

Variable	**Initial Value**	**Final Value**	**% Change**
P_C	12.269	12.1	-1.37
T_C	889.54	823.04	-7.48
AF	0.961	0.63607	-33.81
SH	0.11515	0.16844	46.29
MU1	0.00013	0.00016	22.7
MU2	2.303	2.4263	5.35
MU3	0.00738	0.00885	20
MU4	1.847	1.4776	-20
MU5	0.5173	0.55698	7.67

Table 8.5 Percentage Changes in Values of EOS Parameters Selected for Regression

The performance of tuned and untuned EOS in matching different PVT properties like the oil viscosity, relative volume, and liquid volume %, is ascertained with the help

of composite plots showing direct comparisons between the values before and after regression. The following plots (Figures 8.8-8.10) show such comparisons, clearly indicating a better match of the experimental values by the EOS after tuning. It is seen that the values obtained after regression (tuned EOS) exactly matches with the experimental values. In the absence of any tuning, it is seen that values before regression (untuned EOS) do not match with the experimental values. EOS predicted values at higher and lower pressures show a good match with the experimental values. The values at moderate pressures (1,000 psia to 2,000 psia) show much deviation from the experimental values. Since these pressures fall within our current operating range, they should be matched accurately.

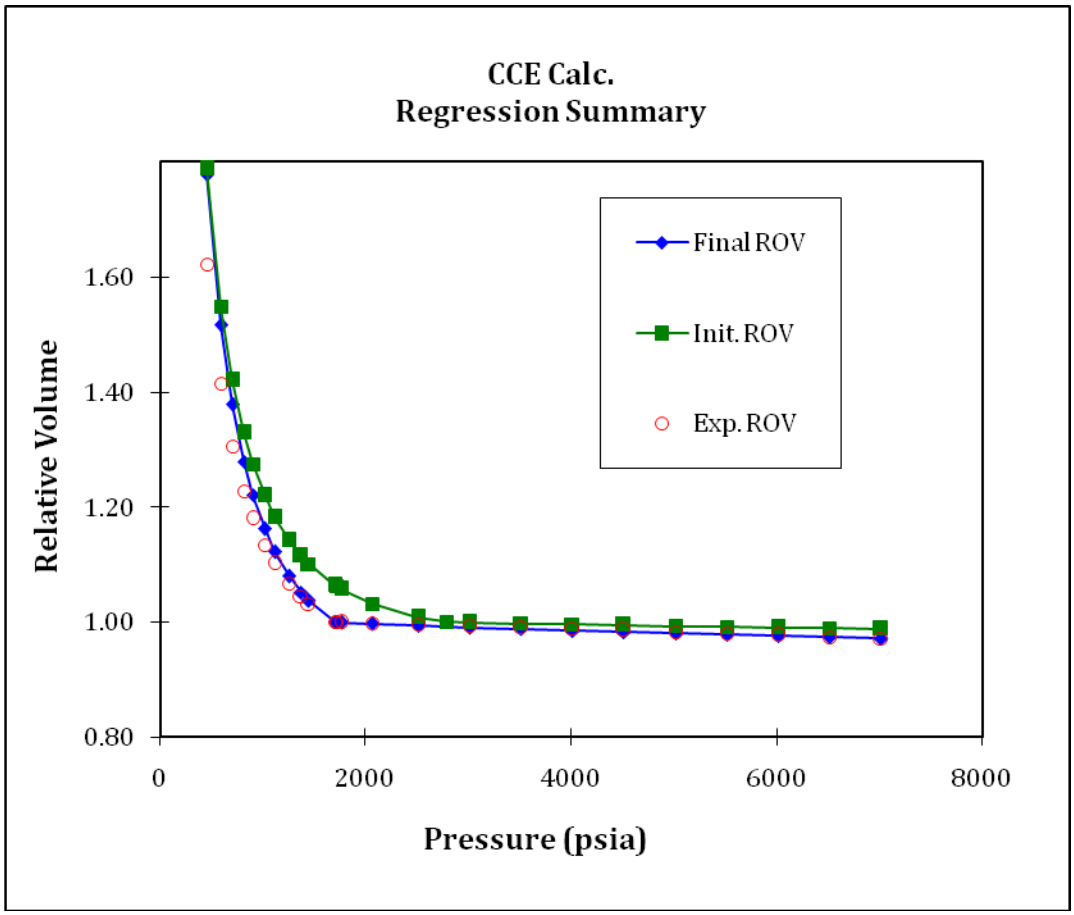

Figure 8.12 Regression Summary for Relative Volume

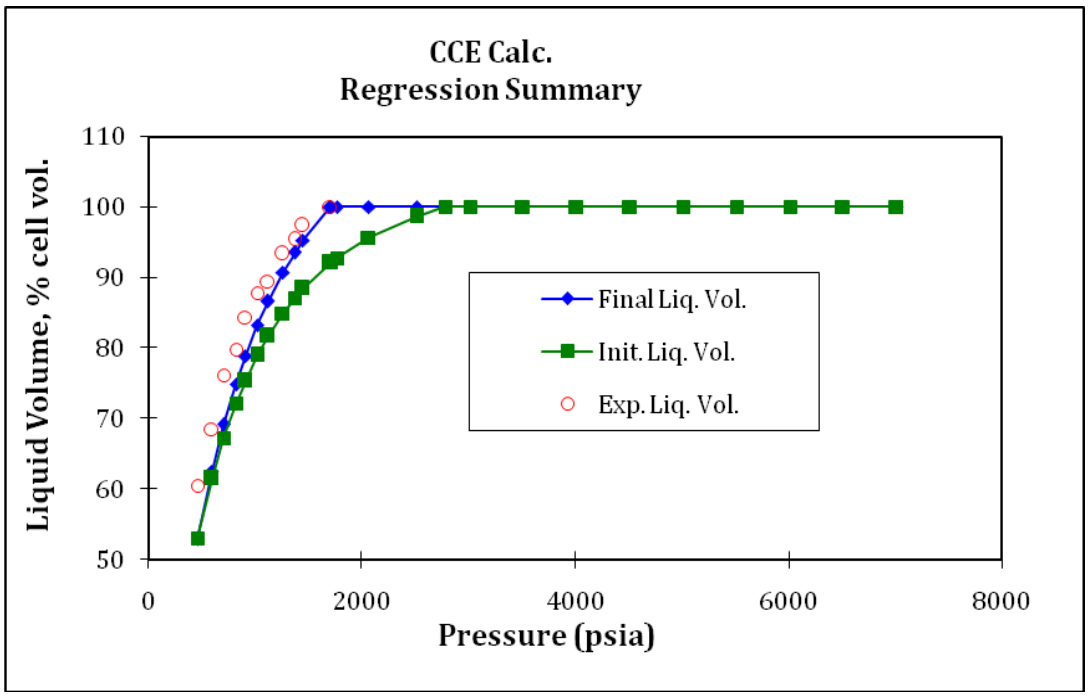

Figure 8.13 Regression Summary for Liquid Volume %

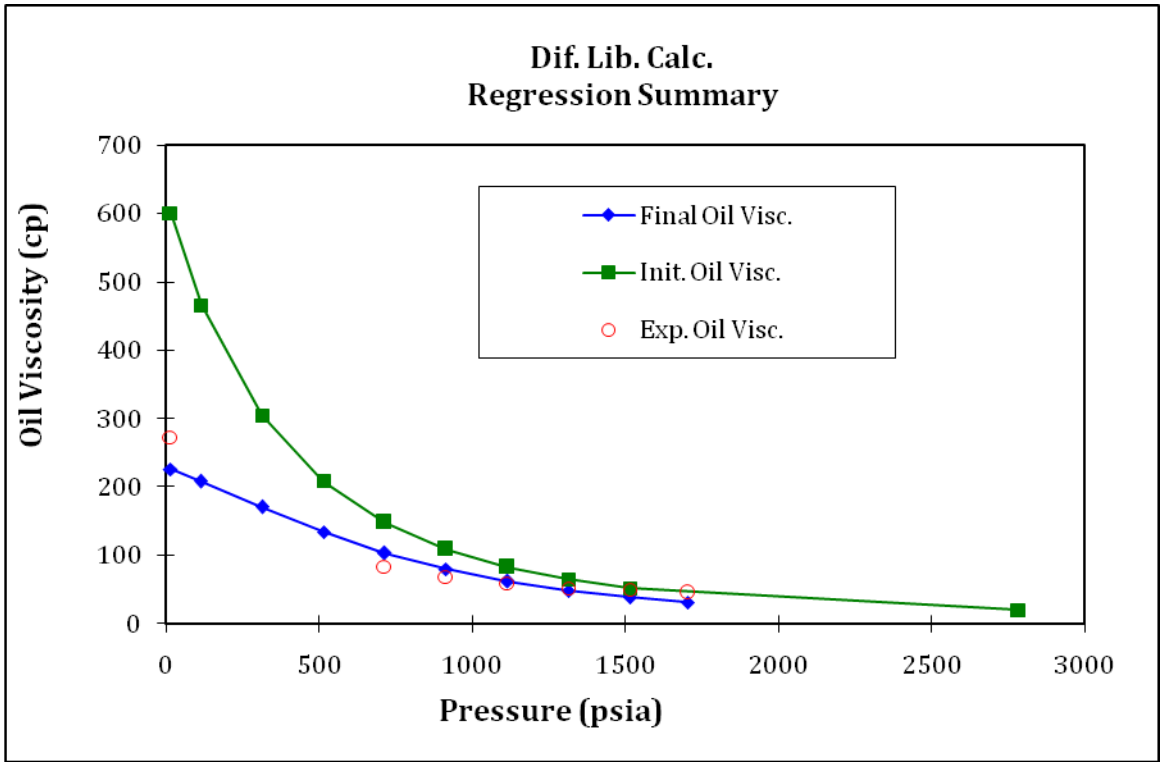

Figure 8.14 Regression Summary for Oil Viscosity

After successfully tuning the EOS, the consistency of the tuned EOS was verified. This was done by comparing the predicted values of the tuned EOS with the experimental

data not used for tuning purposes. Gas formation volume factor (FVF), deviation factor z, and solution gas/oil ratio (GOR) were experimental data sets not used in the tuning operation. The success of the tuned EOS will depend upon how well it predicts the values of these properties. Figures 8.15-8.17 show the comparisons between the experimental data set and tuned EOS. There is a good match between the EOS predicted values and experimental values.

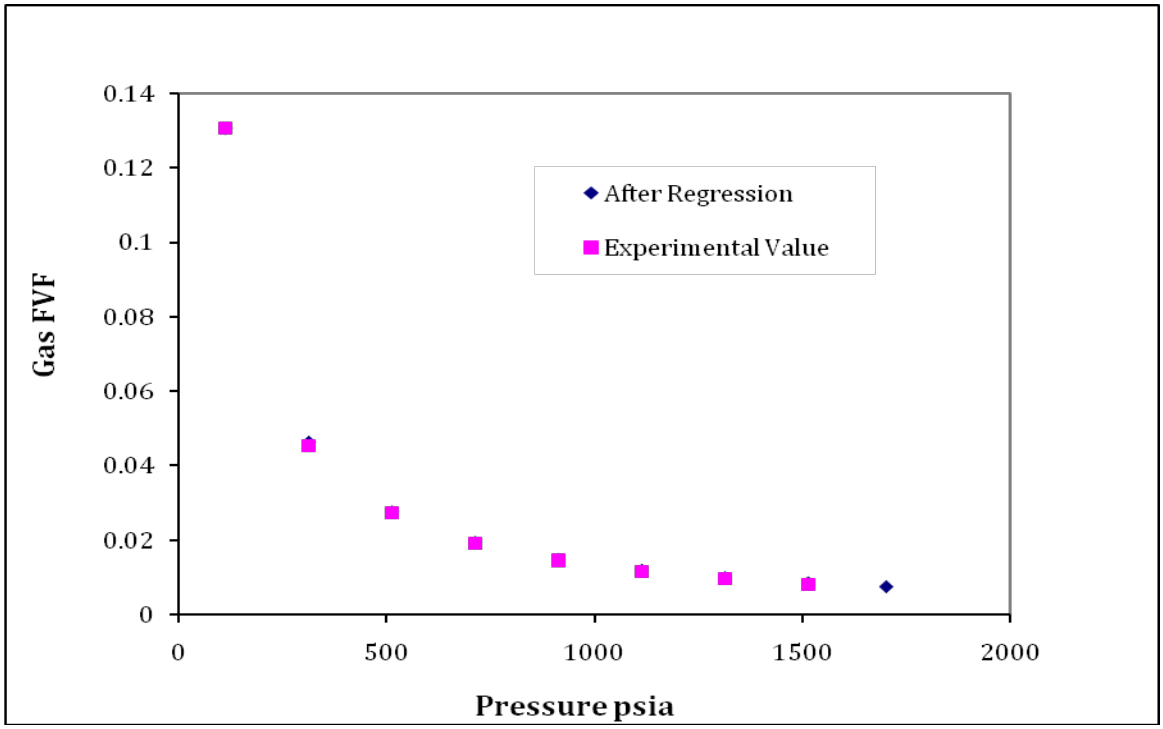

Figure 8.15 Experimental and EOS Predicted Values for Gas FVF

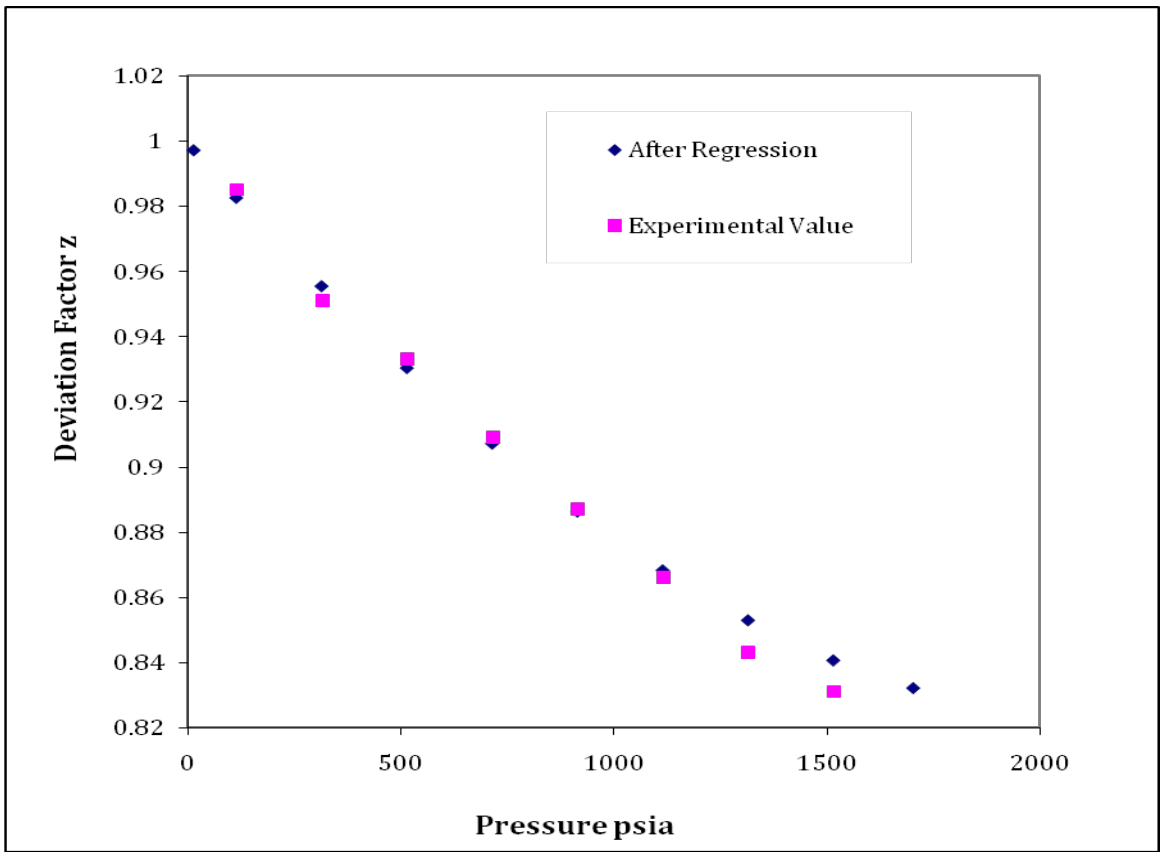

Figure 8.16 Experimental and EOS Predicted Values for Deviation Factor z

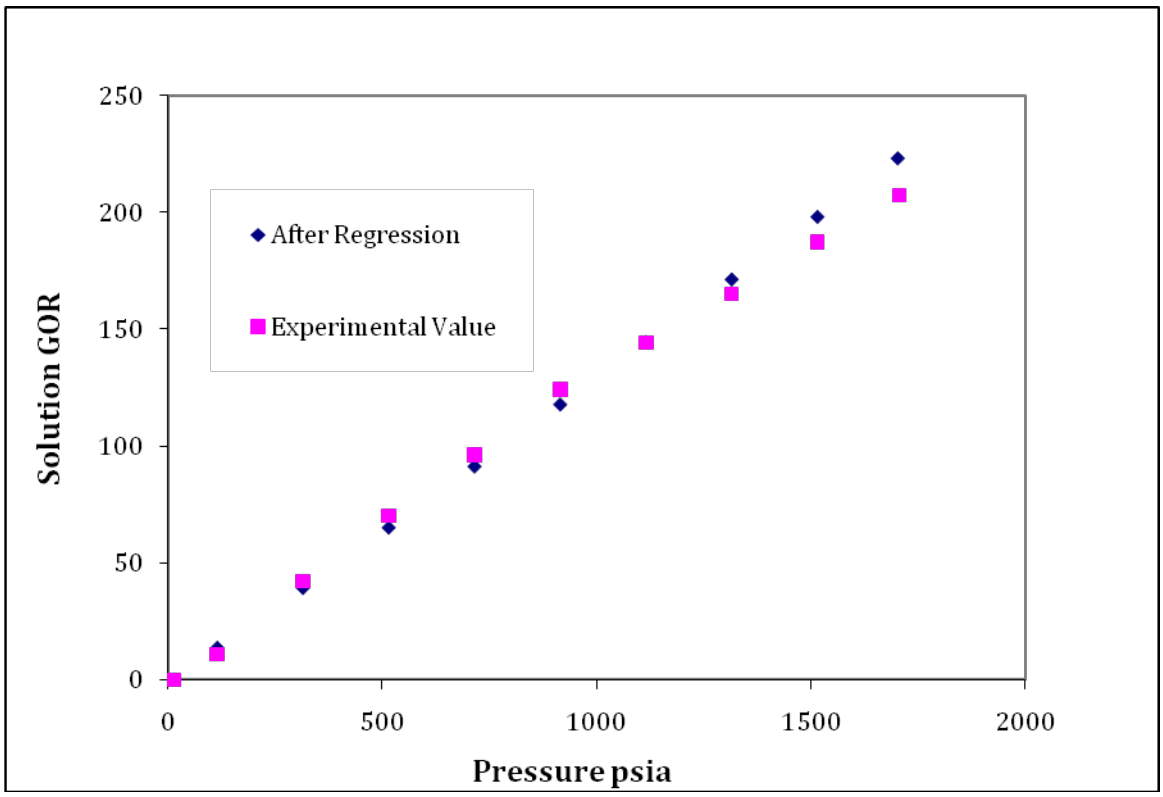

Figure 8.17: Experimental and EOS Predicted Values for Solution GOR

8.5 Reservoir Simulation Results

8.5.1 Vertical Five-spot Injection Pattern

Reservoir simulation to study the potential of EOR using gas injection was carried out next. Accordingly, 10%, 20,%, 30%, 40%, and 50% PV injection runs for all the injection gases were performed. To make a comparative analysis, composite plots of cumulative oil produced and cumulative recovery obtained versus time were plotted for different PV injection runs and for all injection gases used in the study. MI 8, a rich gas, showed the best performance in terms of percentage recovery achieved at breakthrough (Figure 8.18). The onset of breakthrough can be determined by observing the cumulative recovery plot. It is observed that breakthrough is delayed for lower PV injections of the injectant. Hence, for a 50% PV injection the breakthrough occurred after 11.5 years and for a 20% PV injection it occurred after 21.5 years. Thus, a decreasing trend is observed in the occurrence of breakthrough with an increase in PV of gas being injected. But the cumulative oil recoveries shows a positive trend, increasing with the increase in PV of gas being injected. The recoveries achieved with MI 8 are as high as 44% for a 50% PV injection run (Figure 8.18). Daily production plots for rich gas injection are also plotted in Figure 8.19. Using these plots we studied the production profile along the life of project and found the production rate increases until breakthrough and decreases after breakthrough, typical for any injection case. The fluctuations observed in these plots should not be confused with phenomenon of viscous fingering or phase trapping. These fluctuations simply indicate the numerical instability of the model. The model tries to satisfy two operating constraints (bottom-hole pressure and production rate) and when it reaches the limit of one of the operating constraints it switches to the other, resulting in numerical instability.

Figure 8.20 shows that we have a single curve representing all PV injection runs when oil recoveries are plotted versus time in dimensionless form. This is expected because a higher total volume of gas injection would result in higher oil recovery.

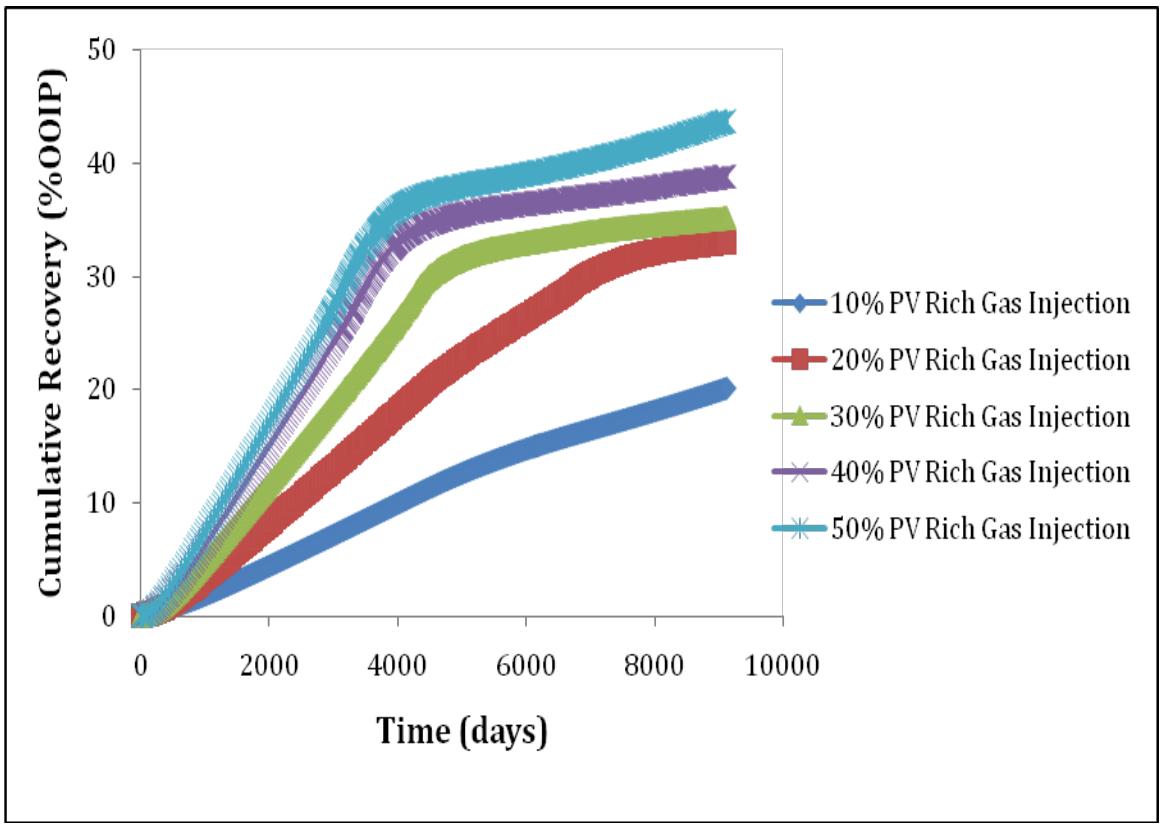

Figure 8.18 Composite Cumulative Oil Recovery Plot for Rich Gas Injection

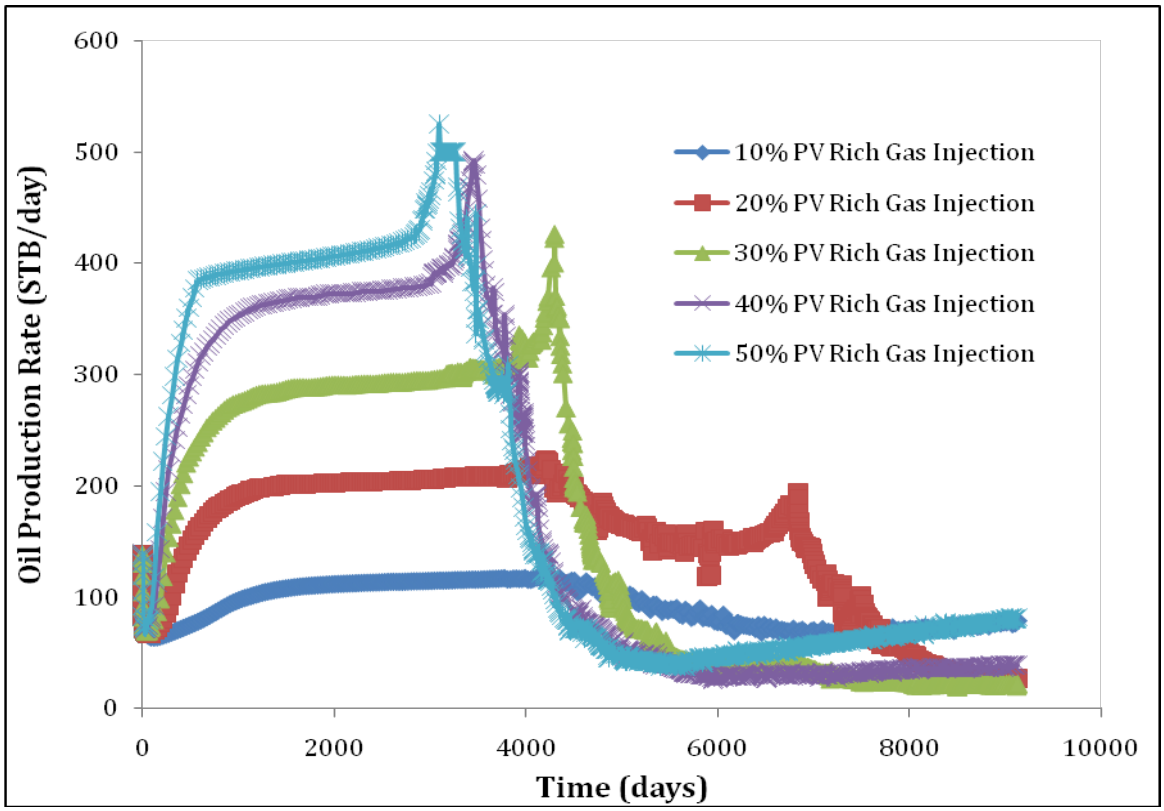

Figure 8.19 Composite Oil Production Plot for Rich Gas Injection

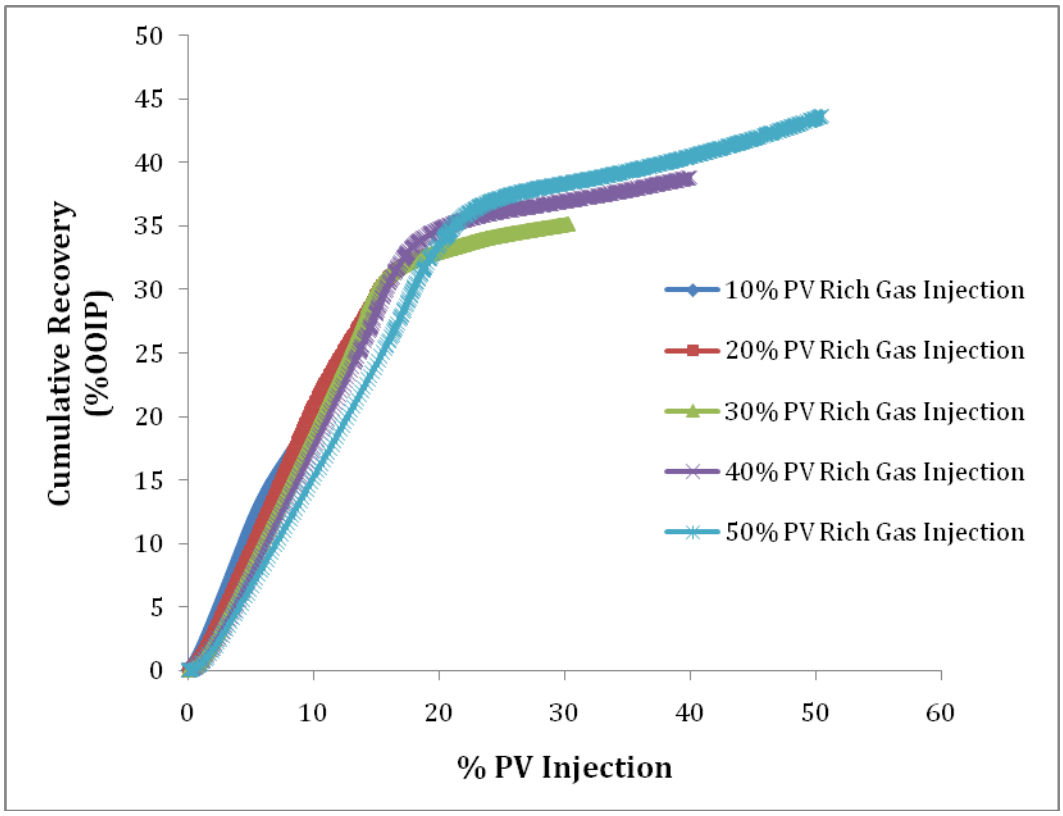

Figure 8.20 Dimensionless Recovery Plot for Rich Gas Injection

The change in the oil saturations in the reservoir over the period of time can also be monitored (Figures 8.21 through 8.23). However, it is not practical to observe the phenomenon of viscous fingering in these profiles. This is because the size of the grid block is much larger than the length or width of the viscous finger. Viscous fingering usually takes place when a lighter phase displaces a much heavier phase. To observe viscous fingering, we would have to select a much finer grid size. (UAF has license for just 10,000 grid blocks and the grid block sizing for the study was selected keeping this limitation in mind)

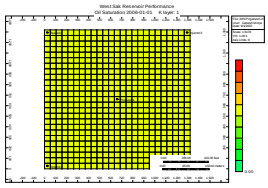

Figure 8.21 Oil Saturation Profile at Time t=0 Years

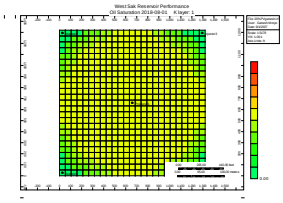

Figure 8.22 Oil Saturation Profile at Time t=12 Years

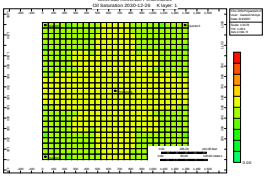

Figure 8.23 Oil Saturation Profile at Time t=25 Years

Figure 8.24 shows that CO_2, as an injection gas, has a much earlier breakthrough than the rich gas injection case. For a 10% PV injection run, we don't see a clear breakthrough point. For a 20% PV injection run, breakthrough occurs around 12 years. For a 50% PV injection run breakthrough is achieved around 7.5 years. The cumulative recovery for a 20% PV injection run at breakthrough is 14.8% while the ultimate recovery for the entire project life is 18.75% (Figure 8.24). Thus we see that there is a slight increase in recovery even after breakthrough is achieved.

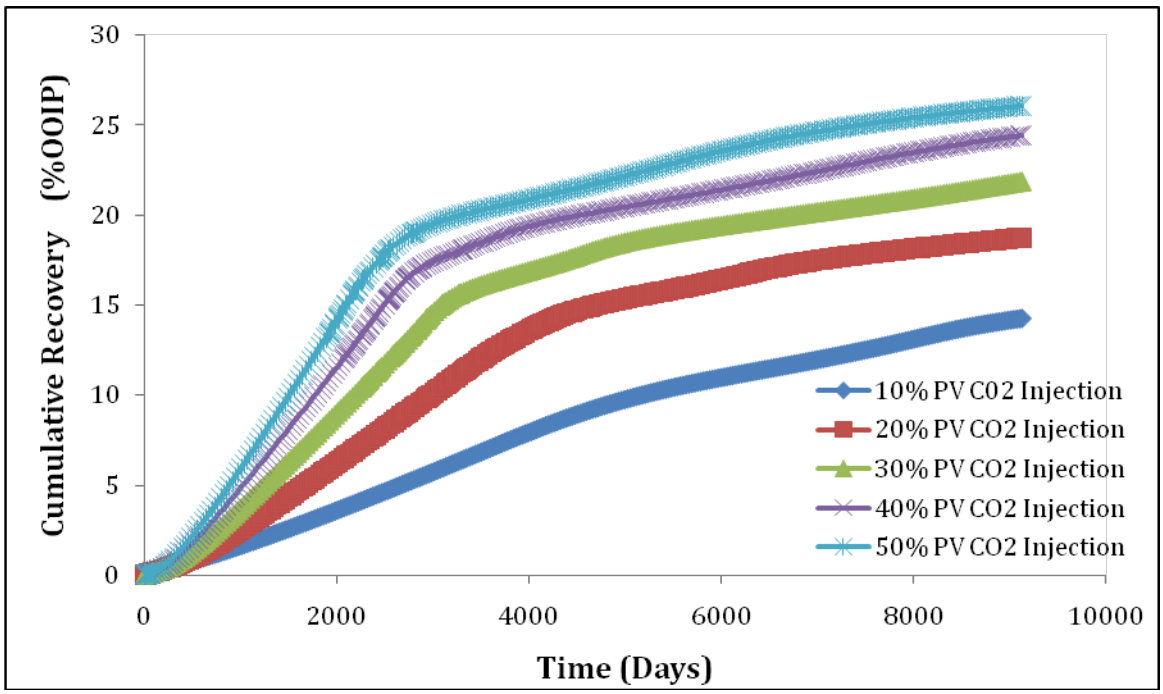

Figure 8.24 Composite Cumulative Oil Recovery Plot for CO_2 Injection

For lean gas injection, we experience very early breakthrough (Figure 8.25). Thus, for a 10% PV injection run breakthrough is achieved in less than 7 years. The cumulative recoveries are far less when compared to the rich gas injection case. For a 50% PV injection run, ultimate recovery is just 14.9%. Also, not much oil is recovered after breakthrough.

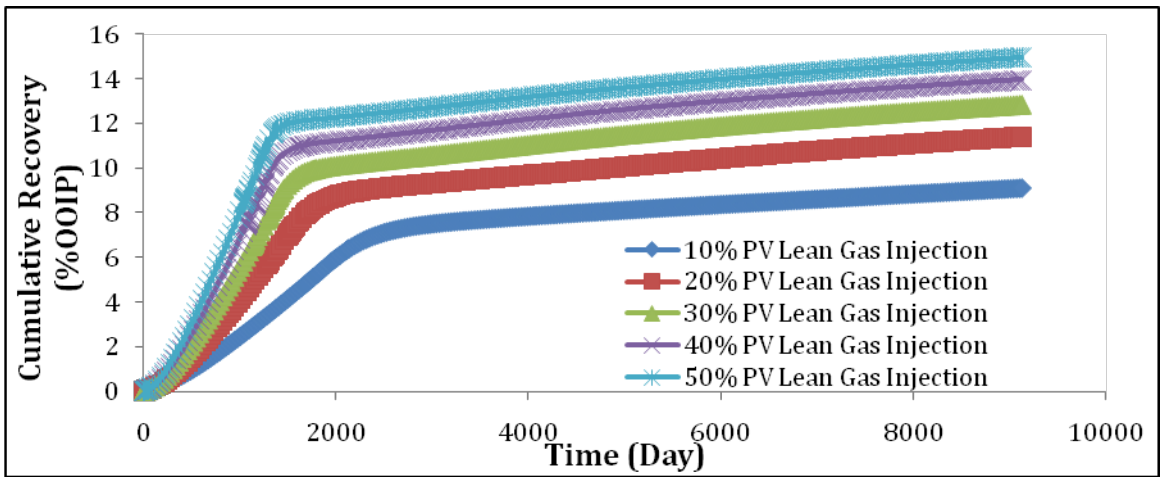

Figure 8.25 Composite Cumulative Oil Recovery Plot for Lean Gas Injection

For the PBG injection case (Figure 8.26), we see a substantial amount of oil is recovered after breakthrough is achieved. Thus for a 50% PV injection run, we see that

the cumulative oil recovery at breakthrough is 17.5% while the ultimate recovery is 25.5%, indicating that a substantial amount of oil is recovered even after breakthrough.

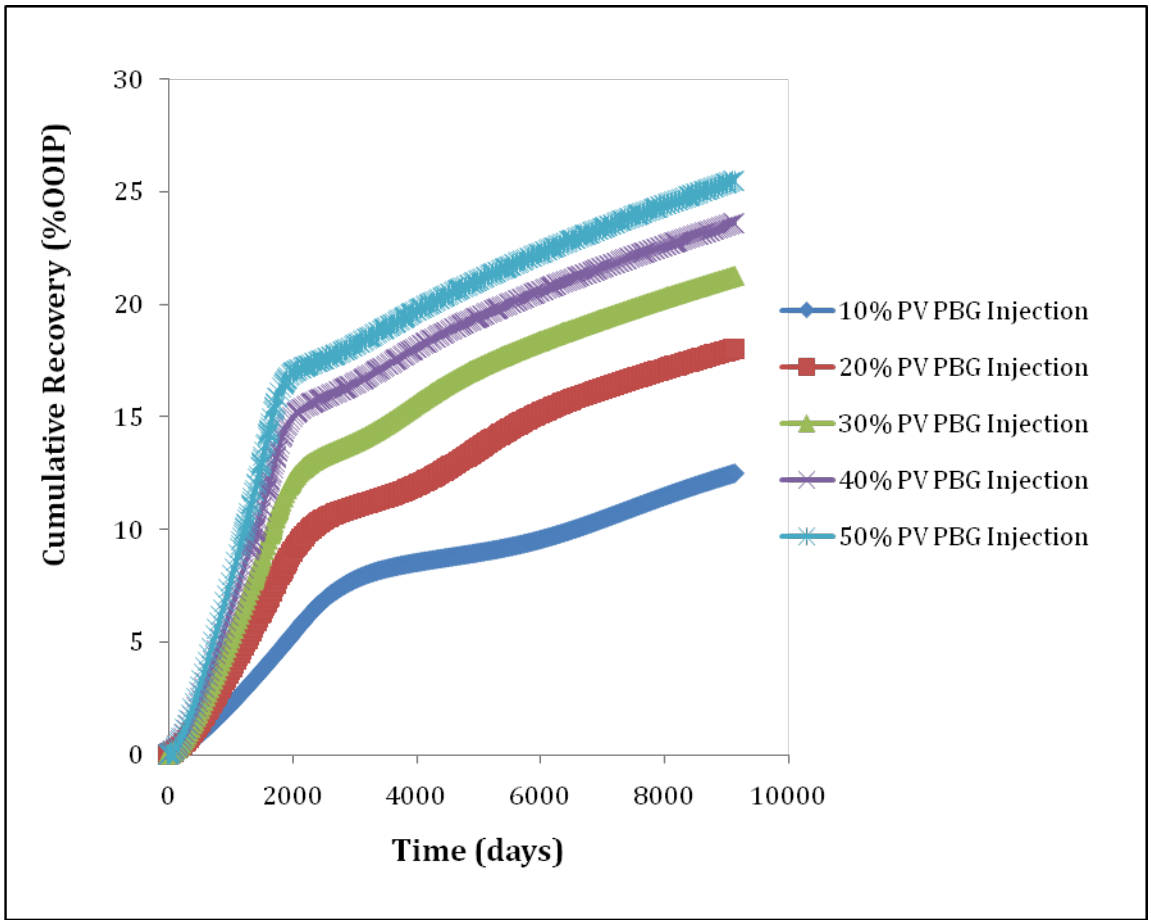

Figure 8.26 Composite Cumulative Oil Recovery Plot for PBG Injection

In the West Sak VRI injection case (Figure 8.27), a substantial amount of oil is recovered after breakthrough is achieved. Thus for a 50% PV injection run, the cumulative oil recovery at breakthrough is 17.5% and the ultimate oil recovery is 28.3%. Even though the recoveries at breakthrough for PBG and West Sak VRI are the same, in the case of the West Sak VRI injection slightly more oil is recovered when compared to the PBG injection case.

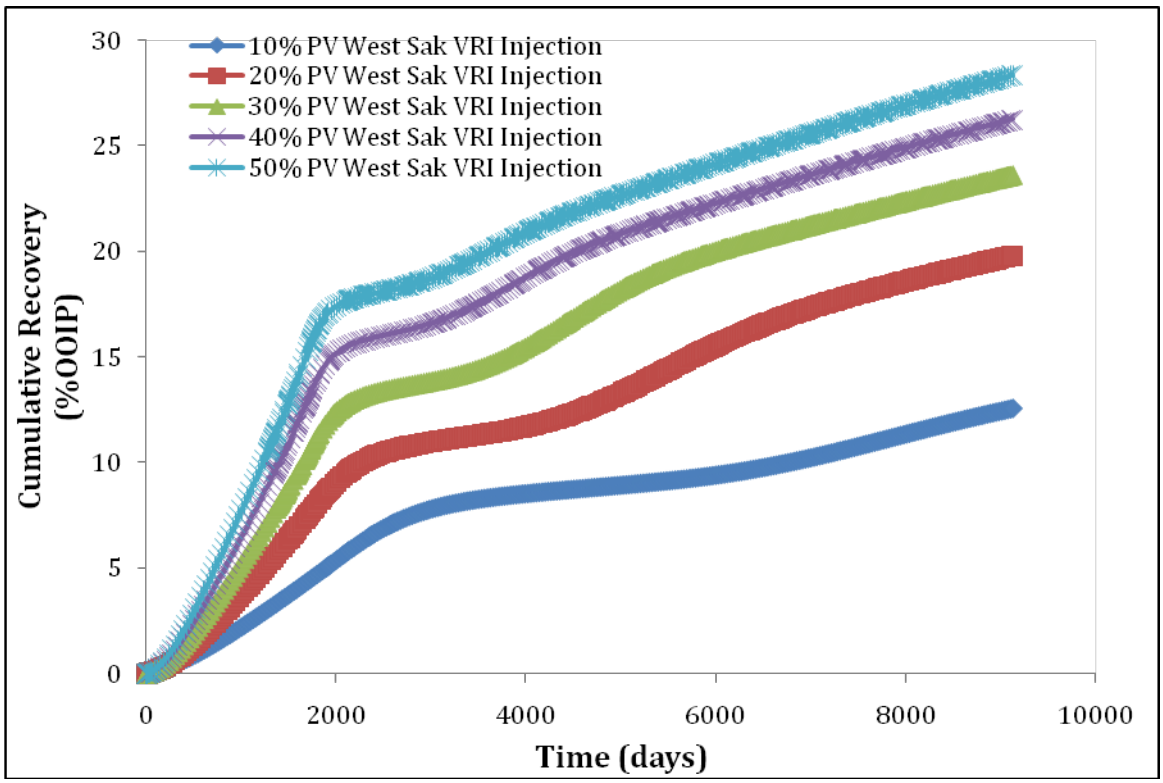

Figure 8.27 Composite Cumulative Oil Recovery Plot for West Sak VRI Injection

Figure 8.28 is a composite oil recovery plot of all the injection gases for a 30% PV injection run. For the rich gas injection case, we experience a much delayed breakthrough when compared to the other injection gases. Also the cumulative oil produced is much greater for the rich gas injection when compared to other gases. It is seen that curves for different gases are represented by a single curve until breakthrough, and it branches out after breakthrough for the respective gas. This kind of behavior is expected for any gas injection scheme and hence it verifies the authenticity of the simulation model.

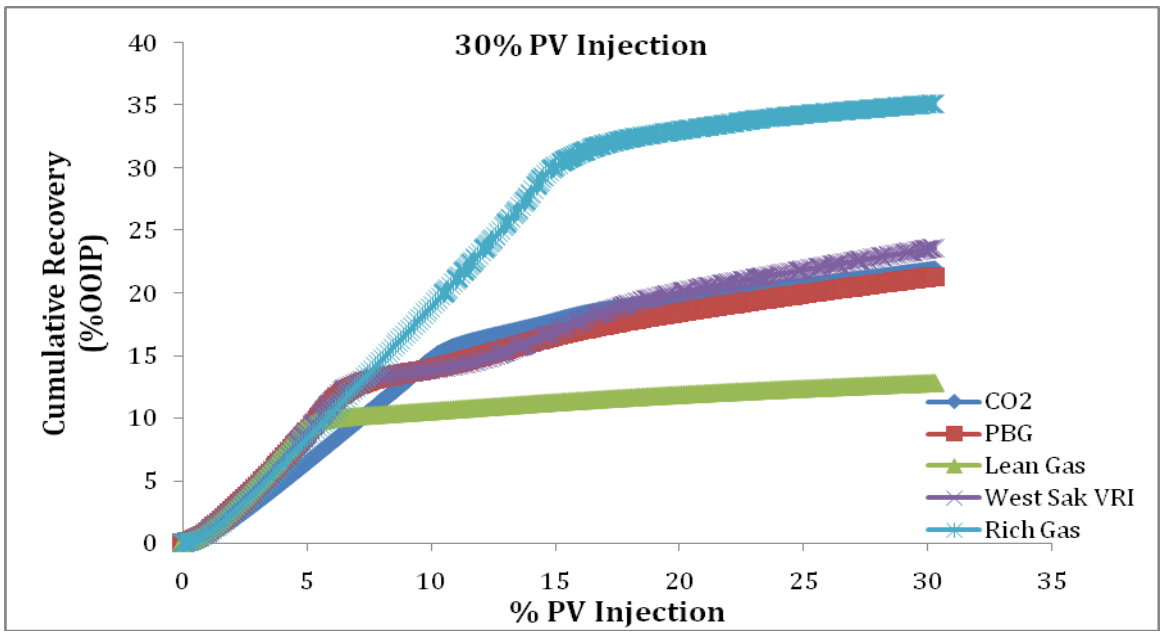

Figure 8.28 Composite Cumulative Recovery Plot for all Injection Gases for 30% PV Injection

Figure 8.29 shows a direct comparison for all the injection gases in terms of ultimate recoveries obtained. The ultimate recoveries of CO_2, West Sak VRI, and PBG fall in the same range. A much superior recovery performance for rich gas injection is seen.

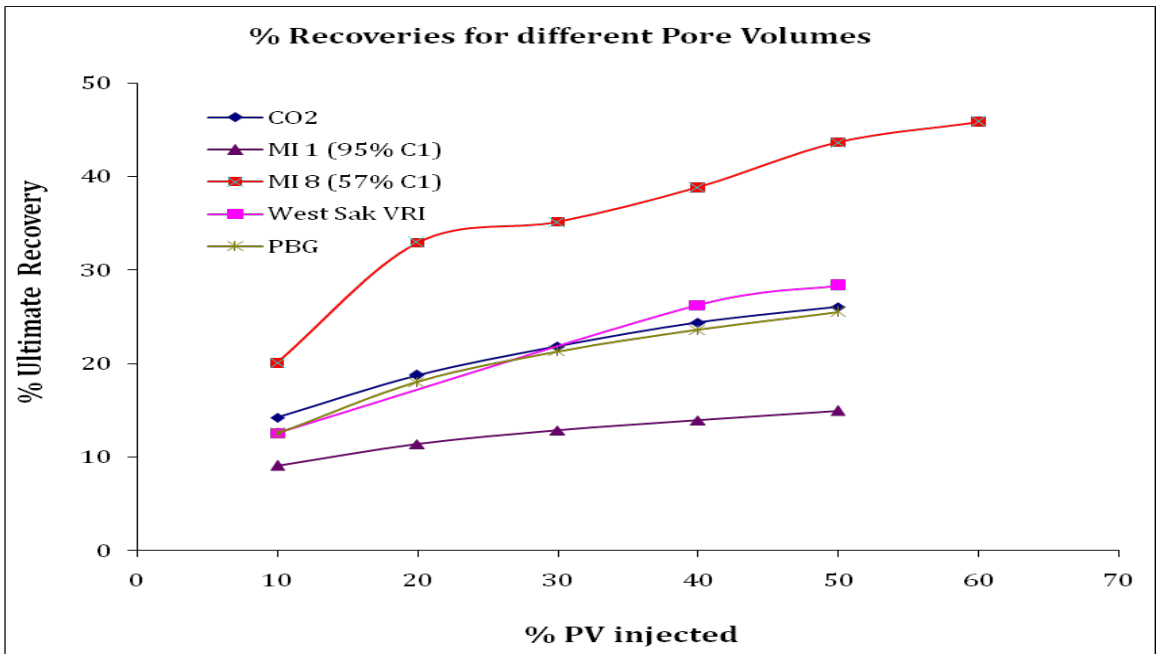

Figure 8.29 Comparison of Ultimate Recoveries Obtained for all Injection Gases

8.5.2 Horizontal Injection Pattern

The performance of the reservoir with horizontal well injection was analyzed the same way as the vertical injector case. Accordingly, cumulative production of oil and cumulative oil recovery versus time for 10%, 20%, 30%, 40%, and 50% PV rich gas injection were studied. A sample recovery plot for 30% PV injection is shown in Figure 8.30. Cumulative recovery increases with the increase in PV of gas being injected. Recoveries obtained for the respective PV are also plotted. A horizontal well is found to have a little less recovery than a vertical well for a particular PV of gas being injected (Figures 8.31 and 8.32). This is mainly because the horizontal well acts as a line drive as the producing layer is represented by only one grid block in the vertical or z-direction.

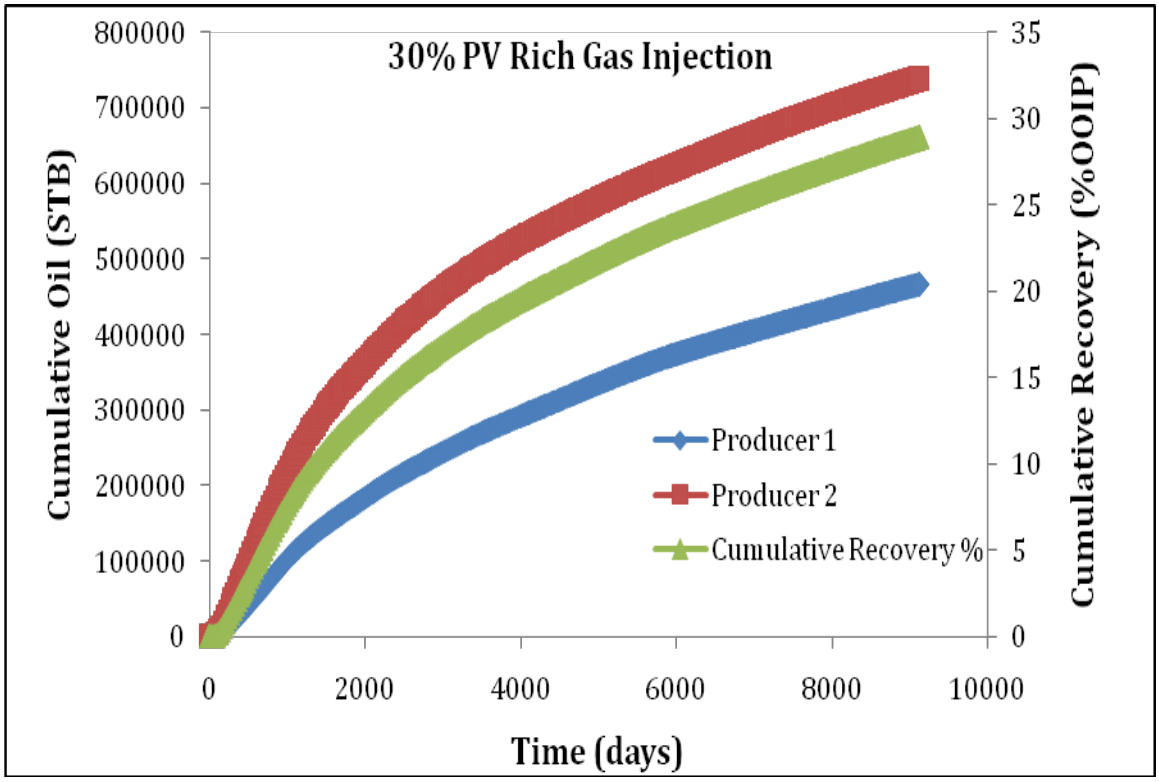

Figure 8.30 Cumulative Oil Produced and Cumulative Recovery Obtained for 30% PV Rich Gas Injection

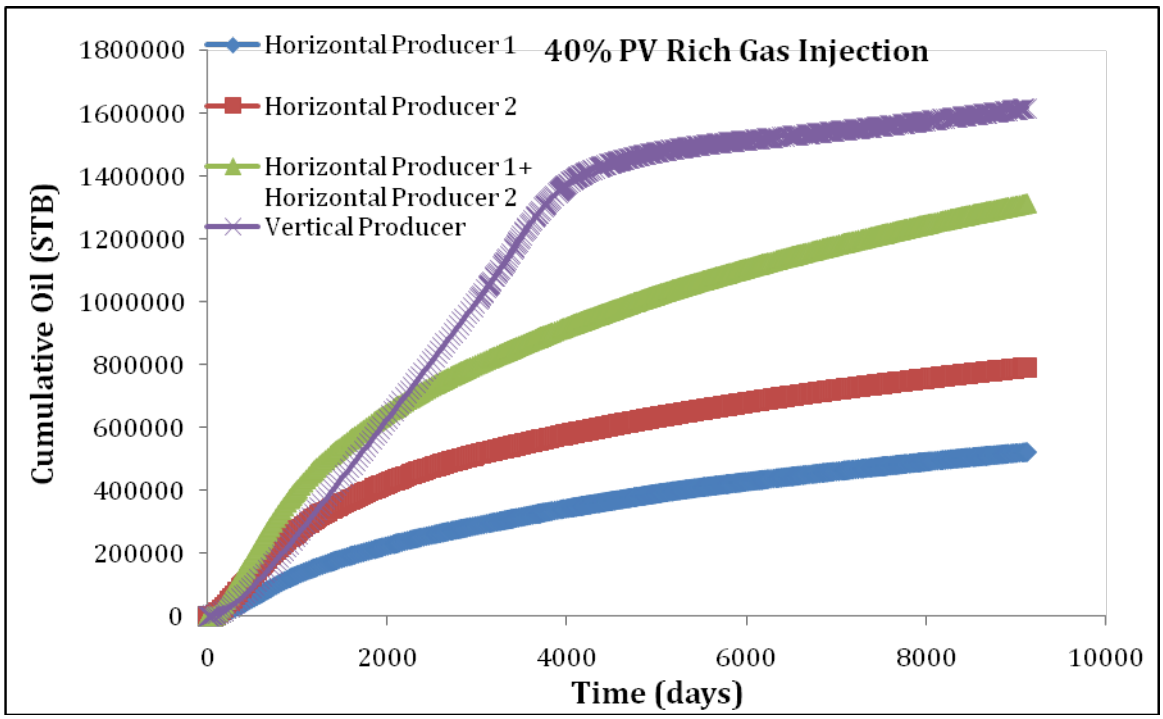

Figure 8.31: Comparison of Performance between Horizontal and Vertical Injection for a 40% PV Rich Gas Injection

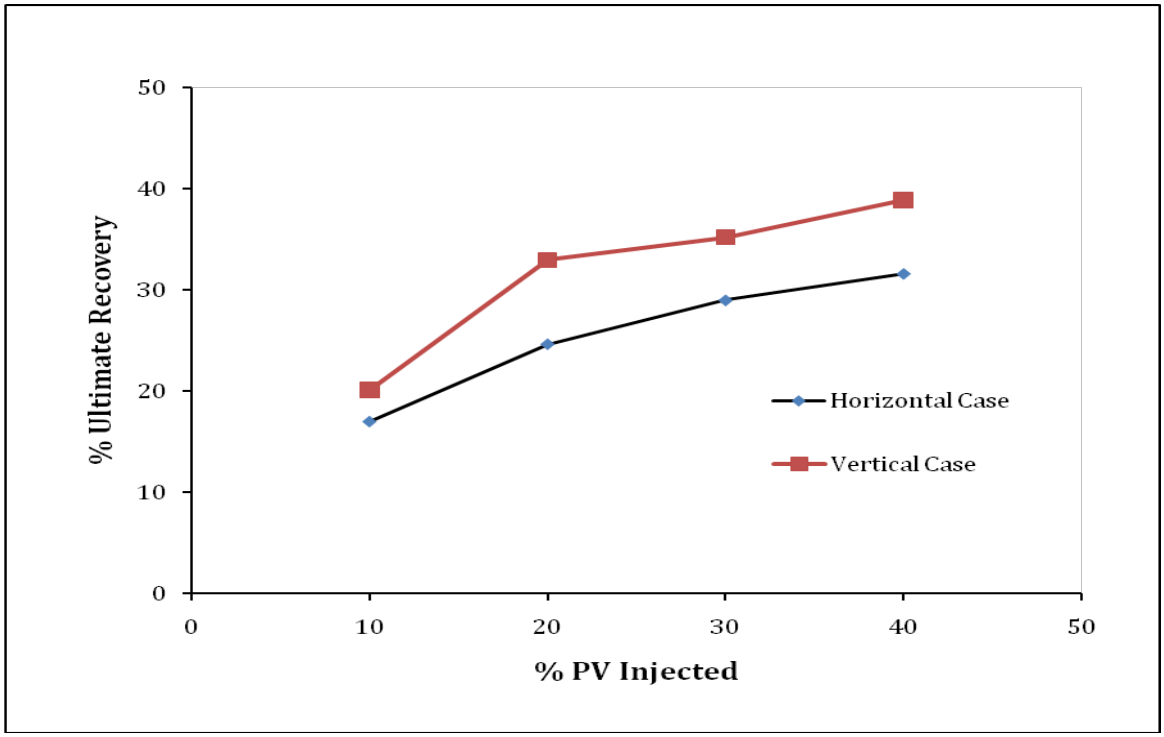

Figure 8.32 Comparison of Ultimate Recoveries for Horizontal and Vertical Injection for Rich Gas Injection

Chapter 9 CONCLUSIONS

A comprehensive research program was undertaken to study the phase behavior and fluid properties of viscous oils from the Alaska North Slope. Phase behavior of heavy oil samples from ANS was studied experimentally and through EOS modeling. Compositional and semi-empirical viscosity models were evaluated for predicting viscosity of medium-heavy (viscous) oils. Modifications were made to the Lindeloff model to improve its predictive capabilities for viscous oils. A compositional reservoir simulation study using tuned EOS was performed to evaluate various EOR scenarios for ANS viscous oil from the West Sak reservoir. A simulation study to analyze the effects of asphaltene deposition was also conducted as a part of this study. The following conclusions were drawn from this study.

1. Validity of simulated distillation by gas chromatography for compositional analysis has been demonstrated by application to heavy oils of ANS.
2. An integrated set up of PVT system, online densitometer and viscometer was successfully designed and used for experimental study on phase behavior and fluid property measurements of ANS viscous oils.
3. Profiles of viscosity and density measurements during differential depletion are in agreement with the proposed ones in theory. Above the bubble point, pressure effect dominates so both viscosity and density of the oil decrease with decrease in pressure. However, below the bubble point, compositional effect dominates and density and viscosity increase as pressure decreases.
4. The experimental procedure developed to measure IFT closely matches the continuous interactions between the injected gas and crude oil occurring in the reservoir. The equilibrium time allowed in the VIT technique simulates the gas and reservoir oil to continuously interact and attain equilibrium.
5. The dominance of the condensing drive mechanism for obtaining miscibility with CO_2 injections can be attributed to the least interactions of CO_2 with reservoir fluid to extract C_2-C_5 components from the reservoir fluid. The multiple contact mechanism leads to the enrichment of reservoir oil with intermediate molecular weight hydrocarbons until it becomes miscible with the injected gas. However, in some cases the vaporization drive was also seen to be dominant.

6. In the case of VRI injections, light intermediate hydrocarbons condense from the fresh injection gas into the oil, thus making it lighter. During the same time, middle intermediate hydrocarbons from the oil are stripped by the injection gas. Since none of these components are present in the injection gas they cannot be replenished back into the oil.
7. CH_4 is sparingly soluble in the reservoir oil at low pressures. Methane gas extracts the intermediate hydrocarbons from the reservoir oil until a sufficient quantity of these hydrocarbons exists at the displacement front to cause the oil to be miscibly displaced (frontal displacement). The miscibility stops at this point due to dispersion mechanism. When the miscibility doesn't exist, the extraction or vaporization mechanism again occurs to re-establish miscibility.
8. The amount of components extracted by the injection gases from the reservoir oils depends on the volumetric ratio between the oil and the gas. Results obtained from MCM simulations showed that MMP was lower for higher injection gas to reservoir oil ratios.
9. The PR-EOS was successfully tuned to experimental data from constant composition expansion and differential liberation. A satisfactory match was obtained with PR-EOS for experimental saturation pressure, gas oil ratio, and liquid density. However predictions of formation volume factor were particularly devious on either sides of the bubble point pressure.
10. The PR-EOS was successfully tuned to experimental data from IFT measurements. A satisfactory match was obtained with PR-EOS for experimental saturation pressure, gas oil ratio, liquid density, and MMP.
11. The correlations used to measure MMP were based on parameters, components which may or may not be present in the gas-oil systems used here. Hence, there was a vast deviation between experimental results and those obtained by correlations.
12. The MMP measurements obtained by MCM simulations prove that the results obtained by the pendant drop technique are accurate and reliable. These results show that the VIT technique is a fast and cost effective method for measuring gas/oil IFT, requiring small gas and oil samples.
13. The VIT method is not applicable for measuring very low IFT values. As miscibility or the critical point between fluid/fluid phases is approached, due

to rapid diffusion of drops into the surrounding gas, it is difficult to measure the drop shape factor accurately.

14. Viscosity of dead ANS crude oils showed an exponential relationship with pressure. An exponent of this behavior was correlated with molecular weight and temperature and a correlation was developed for predicting viscosities of dead ANS crude oil under pressure and temperature conditions.
15. All LBC class viscosity models highly underpredict the medium-heavy oil viscosities. Most of these models show discrepancy for saturated viscosities of medium-heavy oils: the viscosities decrease with reduction in pressure. Tuning of the model coefficients is not a good idea considering the mathematical form of these models.
16. For the Pedersen class models, only the original Pedersen model seems to be robust. This model can be tuned to characterize medium-heavy oil viscosities. However, for most of the medium-heavy oil samples considered in this study, the equivalent temperatures (T_o) are approximately 35-55 K. This is outside the correlation limits of the Pedersen class models (65 K).
17. For the two-reference component viscosity models (Pedersen class), viz. the Aasberg-Petersen model (Aasberg-Petersen at al., 1991) and the Moharam model (Moharam and Fahim, 1995), the undersaturated viscosities decrease with increase in pressure. Accurate density and viscosity correlations need to be developed for the reference components to avoid this anomaly. However, the incremental benefit will not be enough to justify these efforts when compared to the original Pedersen model. Hence there is a need for a completely new viscosity model.
18. Of the new generation viscosity models, the one proposed by Lindeloff et al. (2004) is a simple yet powerful model. This model was upgraded in this study for better prediction of medium-heavy oil viscosities including the low-pressure saturated region viscosities. The new changes have significantly improved the model predictions for medium-heavy oils.
19. Due to the geographic diversity of the data used, it is not possible to make a universal predictive model. However, based on the compiled data, the ranges for different model parameters are stated to reduce the ambiguity. For three data sets, the viscosity data was available for three different temperatures.

Considering a wide temperature range of 80°F, the new model predicted the temperature effect reasonably well.

20. The new modified Lindeloff model can be tuned to the oils from one particular region, albeit after developing necessary correlations for the dead oil viscosity and the pressure differential coefficient *m*. This tuned model can then be used for predicting viscosities of the oils from the same geographical region.
21. The PR-EOS was successfully tuned to predict West Sak viscous oil properties. Validity of the tuned EOS was substantiated by the strong agreement of the tuned EOS predicted values with the experimental values.
22. Enhanced oil recovery using gas injection for production of the viscous West Sak oil was explored using commercial reservoir simulation software. It was found that substantial increase in oil recoveries can be accomplished with the proper selection of an injectant gas and reservoir operating conditions.
23. Oil recoveries for a rich gas injection were as high as 44% for a 50% PV injection, indicating that it might be achieving miscible flow. The recoveries for an immiscible lean gas injection were extremely low.
24. The reservoir model built had limitations in the form of the number of grid blocks that can be selected. Due to this, the vertical 5-spot injection pattern yielded slightly better recoveries as compared to the horizontal injection scheme used in the study. The main reason for this was that the horizontal well was essentially acting as a line drive and a 5-spot pattern always performs better than a line drive.
25. Asphaltene deposition does not show an appreciable effect on the cumulative recovery at 10% PV CO_2 injection (Figure 8.8).
26. At 50% PV CO_2 injection (Figure 8.9) the effects of blockage caused by asphaltene deposition are observed.
27. An initial increase in oil production is seen with an increase in the C_{7+}B fraction. Gas Mass Density distribution data in the reservoir seem to indicate an increase in the sweep efficiency with asphaltene deposition.

Chapter 10 REFERENCES

Aasberg-Petersen, K., Knudsen, K., and Fredenslund, A., "Prediction of Viscosities of Hydrocarbon Mixtures.", *Fluid Phase Equilibria*, vol. 70, pp. 293-308, 1991.

Abedi, S. J., Seyfaie, S., Shaw, J.M., "Unusual Retrograde Condensation and Asphaltene Precipitation in a Model Heavy Oil System", *Petroleum Science and Technology*, 18(9&10), pp 1209-1229 (2000).

Agarwal, R. K., Li, Yau-Kun, and Nghiem, L., "A Regression Technique with Dynamic Parameter Selection for Phase-Behavior Matching", *SPE Reservoir Engineering*, pp. 115-120, 1990.

Ahmed, T., "Compositional Modelling of Tyler and Mission Canyon Formations Oil with CO2 and Lean Gases", Final report submitted to Montana's On a New Track for Science (MONTS), Montana National Science Foundation Grant Program, (1988).

Ahmed, T., "Equations of State and PVT Analysis", Gulf Publishing Company, (2007).

Alaska Oil and Gas Conservation Commission (AOGCC), Conservation Order No.406, (1997), Cited September 07, 2007 < http://www.state.ak.us/local/akpages/ADMIN >

Alaska Oil and Gas Conservation Commission, 2003, Conservation Order No.406a, available online at: http://www.state.ak.us/local/akpages/ADMIN/ogc/orders/co/co400_449/co406a.htm

Ali, S.M. "Heavy OiI Recovery - Principles, Practicality, Potential, and Problems". SPE paper 4935 presented at SPE Rocky Mountain Regional Meeting, Billings, Montana, 15-16 May (1974).

Al-Meshari, A.A., Aramco, S., McCain, W.D.: "New Strategic Method to Tune Equation of State for Compositional Simulation", SPE paper 106332 presented at SPE Technical Symposium of Saudi Arabia Section at Daharan, Saudi Arabia, 14-16 May, 2005.

Alston, R.B., Kokolis, G.P., and James, C.F., "CO2 Minimum Miscibility Pressure: A Correlation for Impure CO2 Streams and Live Oil Systems", SPE, (1985).

Al-Syabi, Z., Danesh, A., Tohidi, B., Todd, A. C., and Tehrani, D. H., "A Residual Viscosity Correlation for Predicting the Viscosity of Petroleum Reservoir Fluids over wide ranges of Pressures and Temperatures.", *Chem. Eng. Sci.*, pp. 6997-7006, 2001.

Alurkar, K D., "Investigation of Phase Behavior and Reservoir Fluid Properties in support of Enhanced Oil Recovery of Alaska North Slope (ANS) Viscous Oils.", M.S. Thesis, University of Alaska Fairbanks, 2007.

Andrade, E. N. da C., "Theory of Viscosity of Liquids.", *Philosophical Magazine*, vol. 17, pp. 497-511, 1934; ibid, vol. 17, pp. 698-732, 1934.

Anna, D. (2005). *DOE-Fossil Energy Techline-Heavy Oil Potential Key to Alaska North Slope Oil Future*. Retrieved August 16, 2007, from Fossil Energy Techline: http://www.fossil.energy.gov/news/techlines/2005/tl_alaska_oil.html

Anton Paar, Instruction manual for DMA 512 P density measuring cell for high pressures and high temperatures.

ASTM D 2887-04: Standard test method for boiling range distribution of petroleum fractions by gas chromatography, Annual book of ASTM standards, ASTM, Philadelphia PA 2004.

ASTM D 2892-01: Standard test method for distillation of crude petroleum, Annual book of ASTM standards, ASTM, Philadelphia PA 2001.

ASTM, Annual Book of ASTM Standards, Part 23, ASTM, Philadelphia, PA, 1981.

Ayirala, S.C., and Rao, D.N., "Comparative Evaluation of a New MMP Determination Technique", SPE paper 99606, presented at SPE/DOE Improved Oil Recovery Symposium at Tulsa, Oklahoma, April 22-26 (2006).

Ayirala, S.C., and Rao, D.N., "Comparison of Minimum Miscibility Pressure Determined from Gas-Oil Interfacial Tension Measurements with Equation of State Calculations", SPE paper 84187, presented at SPE Annual Technical Conference and Exhibition at Denver, Colorado, October 5-8 (2003).

Bakshi, A.K. (1991). Computer Modeling of CO_2 Stimulation in the West Sak Reservoir. M.S. Thesis, University of Alaska Fairbanks . Fairbanks.

Bakshi, A.K., Ogbe, D.O., Kamath, V.A, Hatzignatiou, D.G. (1992). Feasibilty Study of CO_2 Stimulation in the West Sak Field, Alaska. *Presented at the SPE Western Regional Meeting, SPE 24038.* Bakersfield, California.

Baltatu, M. E., Chong, R., A., Huber, M., L., and Laesecke, A., "Transport Properties of Petroleum Fractions.", *Int. J. Thermophysics*, vol. 20(1), pp. 85-95, 1999.

Bergman, D. F., and Sutton, R. P., "Undersaturated Oil Viscosity Correlation for Adverse Conditions.", *SPE 103144*, 2006.

Besson, C., "Resources to Reserves: Oil and Gas Technologies for the Energy Markets of the Future." A Report prepared for the International Energy Agency, 2005.

Bidinger, C. R., Dillon, J. F. "Milne Point Schrader Bluff: Finding the Keys to Two Billion Barrrels" SPE paper 30289 presented at International Heavy Oil Symposium held at Calgary Canada 19-21 June (1995).

BP Exploration, Alaska, "Facts and Figures.", Cited on February 12, 2008, <http://www.bp.com/assets/bp_internet/us/bp_us_english/STAGING/local_assets/downloads/a/alaska_fact11_2007.pdf>.

Bradner, T., "Producers roll up their sleeves to tackle Heavy Oil.", *Alaska Journal of Commerce*, 2007, Cited on December 06, 2007, <http://www.alaskajournal.com/stories/061707/hom_20070617003.shtml>.

Chorn, L.G., "Simulated Distillation of Petroleum Crude Oil by Gas Chromatography Characterizing the Heptane –Plus Fraction", *Journal of Chromatographic Science*, Vol 22, January (1984)

Chung, T. H., Ajlan, M., Lee, L. L., and Starling, K. E., "Generalized Multi-Parameter Correlation for Nonpolar and Polar Fluid Transport Properties", *Ind. Eng. Chem. Res.*, vol. 27(4), pp. 671-679, 1988.

Coats, K.H. & Smart, G.T. (1986). Application of a Regression-Based EOS PVT Program to Laboratory Data. *SPE Reservoir Engineering* , Vol. 1, No. 3, pp. 277-299.

Coats, K.H. (1982). Reservoir Simulation: State of the Art. *Journal of Petroleum Technology* , Vol. 34, No. 8, pp.1633-1642.

Craft, B.C., and Hawkins, M.F., “Applied Petroleum Reservoir Engineering”, Ed.2., Prentice Hall, (1991).

Cupcic, F., "Extra Heavy Oil and Bitumen: Impact of Technologies on the Recovery Factor - The Challenges of Enhanced Recovery.", A Presentation at the *ASPO Annual Meeting 2003*, Rueil, France 26 - 27 May, 2003.

Dandekar, A.Y., Andersen, S.I.A. and Stenby, E.: “Solid Organic Deposition During Gas Injection Studies”, *Petroleum Science and Technology*, 18(9&10), pp. 1209-1229, (2000).

Dandekar, A. Y. “Petroleum Reservoir Rock and Fluid Properties”. Taylor & Francis, (2006).

Dandekar, A. Y., “Interfacial Tension and Viscosities of Reservoir Fluids”, Ph.D. Thesis, Heriot-Watt University, Edinburgh, 1994.

Dandekar, A. Y., and Danesh, A., "A Modified Residual Viscosity Method for Improved Prediction of Dense Phase Viscosities", *7th European Improved Oil Recovery (IOR) Symposium*, Moscow, Russia, 1992.

Dandekar, A. Y., *Lecture Notes*, Advanced Phase Behavior Course (PETE F665), University of Alaska Fairbanks, Spring 2006.

Danesh, A., “PVT and Phase behavior of Petroleum Reservoir Fluids”, Elsevier Science B.V., (1998).

DeRuiter, R.A., Nash, L.J., Singletary, M.S.: “Solubility and Displacement Behavior of a Viscous Crude With $CO_2$and Hydrocarbon Gases” *SPE Reservoir Engineering* , Vol. 9, No. 2, pp. 101-106, May 1994.

Dexheimer, D., Jackson, C. M., and Barrufet, M. A., "A Modification of Pedersen's Model for Saturated Crude Oil Viscosities using Standard Black Oil PVT Data", *Fluid Phase Equilibria*, vol. 183-184, pp. 247-257, 2001.

Ely, J., and Hanley, H., "Prediction of Transport Properties: 1. Viscosity of Fluid and Mixtures", *Ind. Eng. Chem. Fund.*, vol. 20, pp. 323-332, 1981.

Firoozabadi, A., and Aziz, K., “Analysis and Correlation of Nitrogen and Lean Gas Miscibility Pressure”, SPE Reservoir Engineering, February (1986).

Fischer, P. A. "Huge Heavy Oil Recovery Potential being Realized in Arctic Fields" *World Oil Magazine*, vol. 227, no. 8 (2006).

Francois. (2003, May 26). http://www.peakoil.net/iwood2003/ppt/CupcicPresentation.pdf. Retrieved August 15, 2007, from www.peakoil.net: <http://www.peakoil.net/iwood2003/ppt/CupcicPresentation.pdf>

Green, D.W. & Willhite, G.P. (1998). *Enhanced Oil Recovery.* Society of Petroleum Engineers, Richardson, Texas.

Guo, X. Q., Sun, C. Y., Rong, S. X., Chen, G. J., and Guo, T. M., "Equation of State Analogue Correlations for the Viscosity and Thermal Conductivity of Hydrocarbons and Reservoir Fluids.", *J. Pet. Sci. Eng.*, vol. 30(1), pp. 15-27, 2001.

Hanley, H.J, McCarty, R. D., and Haynes, W. M.: "Equations for the Viscosity and Thermal Conductivity Coefficients of Methane", *Cryogenics*, pp. 413-417, (1975).

Hernandez, J.C., “Sensitivity of Reservoir Simulations to Uncertainties in Viscosity.”, M.Phil. Thesis, Imperial College London, 2001.

Herron, E.H., King, S.D. “Heavy Oil as the Key to U.S. Energy Security”, Reports and Presentation, Petroleum Equities Inc, December (2004). <http://www.petroleumequities.com/cgi-bin/site.cgi?t=5&p=energysecurity.html>

Holm, L.W. and Josendal, V.A., “Discussion of a Determination and Prediction of CO2 Minimum Miscibility Pressure”, J. Pet. Tech, May (1980).

Holm, L.W., and Josendal, V.A., “Effect of Oil Composition on Miscible-Type Displacement by CO2”, SPE paper 4736-PA., February (1974).

Holt, T. (2003). *ttp://www.force.org/fresco/seminar2003/Abstracts/simulation_Sintef.htm*. Retrieved from http://www.force.org/: <http://www.force.org/fresco/seminar2003/Abstracts/simulation_Sintef.htm>

Hossain, M. S., Sarica, C., Zhang, H. Q., Rhyne, L., and Greenhill, K. L., "Assessment and Developement of Heavy-Oil Viscosity Correlations.", *SPE 97907*, 2005. <http://www.pet.hw.ac.uk/research/rfs/rfs>

Igbokwe, G.C.: “Experimental Investigation on the Transportation of Commingled Blends of Gas-to-Liquid (GTL) Products and Alaskan Heavy Crude Oil through the Trans-Alaska Pipeline System (TAPS)”. M.S. Thesis, University of Alaska Fairbanks, 2006.

Inganti, M., “Miscible EOR Studies for Schrader Bluff Heavy Oil Reservoir, North Slope of Alaska: Slim Tube Displacement and Fluid Characterization”, M.S. Thesis, University of Alaska Fairbanks, (1994).

Investigation of Efficiency Improvement During CO2 Injection in Hydraulically and Naturally Fractured Reservoirs, Project No. DE-FC26-01BC15361, (2008). <http://www.netl.doe.gov>

Jhaveri, B. S., and Youngren, G. K., "Three-Parameter Modification of Peng-Robinson Equation of State to Improve Volumetric Predictions.", *SPE 13118*, 1988.

Jhaveri, B.S., “Viscous Oil EOR by Viscosity Reducing Immiscible (VRI) WAG Process”, SPE Document Number 112086-DL, presented as a part of SPE Distinguished Lecture Series (2007).

Joergensen, M. & Stenby, E.H. (1995). Optimization of Pseudo-component Selection for Compositional Studies of Reservoir Fluids. *Presented at the 70th Annual Technical COnference and Exhibiton, SPE 30789.* Dallas, Texas.

Jossi, J. A., Stiel, L. I., and Thodos, G., "The Viscosity of Pure Substances in the Dense Gaseous and Liquid Phases", *AIChE*, vol.8 (1), pp. 59-63, 1962.

Kanti, M., Zhou, H., Ye, S., Boned, C., Lagourette, B., Saint-Guirons, H., Xans, P., and Montel, F., "Viscosity of Liquid Hydrocarbons, Mixtures, and Petroleum Cuts, as a function of Pressure and Temperature.", *J. Phys. Chem.*, vol. 93, pp. 3860-3864, 1989.

Katz, D.L, Firoozabadi, A.,” Predicting Phase Behavior of condensate/Crude oil using Methane Interaction Coefficient”, *J Pet Tech*, Vol. 30, pp1649-1655, Nov (1978).

Katz, D.L., (1983). Overview of Phase Behavior of Oil and Gas Production. *Journal of Petroleum Technology* , Vol. 35, No. 6, pp. 1205-1214.

Kesler, M. G., and Lee, B. I., "Improve Predictions of Enthalpy of Fractions.", *Hydrocarbon Processing*, vol. 55, pp. 153-158, 1976.

Kokal, S.L, Sayegh, S.G., "Asphaltenes: The Cholesterol of Petroleum", SPE paper 29787 presented at Middle East Oil Show held in Bahrain, 11-14 March (1995).

Lasater, J. A., "Bubble Point Pressure Correlation.", *Trans AIME*, vol. 213, pp. 379-381, 1958.

Latil, M., "Enhanced Oil Recovery", Gulf Publishing Company, (1980).

Lawal, A. S., "Prediction of Vapor and Liquid Viscosities from the Lawal-Lake-Silberberg Equation of State.", *SPE 14926*, 1986.

Lawrence, J., Teletzke, G., Hutfilz, J., Wilkinson, J. (2003). Reservoir Simulation of Gas Injection Process. *Presented at the 13th Middle East Oil Show & Conference, SPE 81459.* Bahrain.

Lee, B. I., and Kesler, M. G., "A Generalized Thermodynamic Correlation Based on Three-Parameter Corresponding States.", *AIChE*, vol. 21(3), pp. 510-527, 1975.

Lee, S., Moulds, T.P., Narayan, R., Youngren, G., Lin, C., Wang, Y. (2001). Optimizing Miscible Injectant (MI) Compositions for Gas Injection Projects. *Presented at the SPE Annual Technical Conference, SPE 71606.* New Orleans, Louisiana.

Lindeloff, N., Pedersen, K. S., Rønningsen, H. P., and Milter, J., "The Corresponding States Viscosity Model Applied to Heavy Oil Systems", *J. Can. Pet. Tech.*, vol. 43(9), pp. 47-53, 2004.

Liu, K. (1999). Fully Automatic Procedure for Efficient Reservoir Fluid Characterization. *Presented at the SPE Annual Technical Conference and Exhibition, SPE 56744.* Houston, Texas.

Lohrenz, J., Bray, B. G, and Clark, C. R. , "Calculating Viscosities of Reservoir Fluids from their Compositions ", *Journal of Petroleum Technology*, Volume 16, No10, pp1171-1176, October (1964).

McAllister, D.J., DeRuiter, R.A.: "Further Development and Application of Simulated Distillation for Enhanced Oil Recovery", SPE paper 14335 presented at 50 th Annual Technical Conference and Exhibition of the Society of Petroleum Engineers held in Las Vegas, NV September 22-25, (1985).

McCarty, R. D., "A Modified Benedict-Webb-Rubin Equation of State for Methane using Recent Experimental Data.", *Cryogenics*, pp. 276-280, 1974.

Mcguire, P.L., Redman, R.S., Jhaveri, B.S., Yancey, K.E., Ning, S.X., "Viscosity Reduction WAG : An Effective EOR for North Slope Viscous Oils", SPE paper 93914 presented at SPE Western Regional Meeting at Irvine, California, March 29-April 1, 2005.

Mehrotra, A. K., Monnery, W. D., and Svrcek, W. Y., "A Review of Practical Calculation Methods for the Viscosity of Liquid Hydrocarbons and their Mixtures.", *Fluid Phase Equilibria*, vol. 117, pp. 344-355, 1996.

Merrill, R.C, Hartman, K.J, Creek, J.L, “A Comparison of Equation of State tuning Methods”, SPE paper 28589 presented at SPE Annual Technical Conference and Exhibition at New Orleans, LA, 25-28 September (1994).

Metcalfe, R.S., and Yarborough, L., “The Effect of Phase Equilibria of CO2 Displacement Mechanism”, SPE, August (1979).

Misak, M.D., “Equations for Determining 1/H versus S values for Interfacial Tension Calculations by Pendant Drop Method”, SPE paper 2310, (1968).

Moharam, H. M., and Fahim, M. A., "Prediction of Viscosity of Heavy Petroleum Fractions and Crude Oils using a Corresponding States Method.", *Ind. Eng. Chem. Res.*, vol. 34(11), pp. 4140-4144, 1995.

Monnery, W. D., Svrcek, W. Y., and Mehrotra, A. K., "Viscosity: A Critical Review of Practical Predictive and Correlative Methods.", *Can. J. Chem. Eng.*, vol. 73, pp. 3-40, 1995.

Morye, G., “Equation of State Model Development and Compositiong Simulation of Enhanced Oil Recovery using Gas Injection for The West Sak Heavy Oil”, M.S. Thesis, University of Alaska Fairbanks, (2007).

Nagarajan, N.R., Honarpour, M.M., Sampath, K, “Reservoir Fluid Sampling and Characterization—Key to Efficient Reservoir Management” SPE paper 10151 presented at Abu Dhabi International Petroleum Exhibition and Conference, Abu Dhabi, UAE, 5-8 November, (2006).

Newitt, D.M., et al., “Carbon Dioxide”, In Thermodynamic Functions of Gases, vol. 1, Ed. F. Din, London:Butterworths, (1996).

Nghiem, L.X. , Kohse, B.F. , Farouq Ali, S.M., Doan, Q., “Asphaltene Precipitation: Phase Behavior Modeling and Compositional Simulation” SPE paper 59432 presented at SPE Asia Pacific Conference on Integrated Modeling for Asset Management, 25-26 Yokohama, Japan, April (2000).

Niederhauser, D.O., and Bartell, F.E., “A Corrected Table for Calculation of Boundary Tension by Pendant Drop Method”, Research on Occurrence and Recovery of Petroleum, A Contribution from API Research Project 27, 114, (1947).

Oellrich, L., Plocker, U., Prausnitz, J. M., and Knapp, H., "Equation-of-State Methods for Computing Phase Equilibria and Enthalpies.", *Int. Chem. Eng.*, vol. 21(1), pp. 1-15, 1981.

Okuyiga, M. O., “Equation of State Characterization and Miscibility Development in a Multiple-Phase Hydrocarbon System”, SPE Paper 24937 presented at SPE annual technical conference, 4-7 October, (1992).

Orbey, H., and Sandler, S. I., "The Prediction of the Viscosity of Liquid Hydrocarbons and their mixtures as a function of Temperature and Pressure.", *Can. J. Chem. Eng.*, vol. 71, pp. 437-446, 1993.

Orr Jr., F.M., and Jessen, K., “An Analysis of the Vanishing Interfacial Technique for Determination of Minimum Miscibility Pressure”, Elsevier, Fluid Phase Equilibria, July 15 (2007).

Orr Jr., F.M., and Silva, M.K., “Equilibrium Phase Compositions of CO2/Hydrocarbon Mixtures-Part 1: Measurement by a Continuous Multiple Contact Experiment”, SPE paper 14149, (1987).

Ostermann, R.D., Ehlig-Economides, C.A., Owolabi, O.O, “Correlations for the Reservoir Fluid Properties of Alaskan Crudes”, SPE paper 11703 presented at California Regional Meeting, 23-25, Ventura, California, March (1983).

Panda, M.N., “Reservoir Description and a Feasibility Study of Enhanced Oil Recovery Applications to West Sak Field”, M.S. Thesis, University of Alaska Fairbanks, (1988).

Patil, S.B. (2006). Investigation of CO_2 Sequestration Options for Alaska North Slope With Emphasis on Enhanced Oil Recovery. *M.S. Thesis, University of Alaska Fairbanks* . Fairbanks.

Patil, S.L. & Dandekar, A.Y. (2004). *Phase Behavior, Solid Organic Precipitation and Mobility Characterization Studies in Support of Enhanced Heavy Oil Recovery on Alaska North Slope. Research Proposal* Fairbanks, AK: University of Alaska Fairbanks.

Pedersen, K. S., and Fredenslund, A., "An Improved Corresponding States Model for the Prediction of Oil and Gas Viscosities and Thermal Conductivities.", *Chem. Eng. Sci.*, vol. 42(1), pp. 182-186, 1987.

Pedersen, K. S., Fredenslund, A., Christensen, P. L., and Thomassen, P., "Viscosity of Crude Oils.", *Chem. Eng. Sci.*, vol. 39(6), pp. 1011-1016, 1984.

Pedersen, K. S., Milter, J., and Sorensen, H., "Cubic Equations of State Applied to HT/HP and Highly Aromatic Fluids.", *SPE 88364*, 2004.

Peneloux, A., Rauzy, E., and Freze, R., "A Consistent Correction for Redlich-Kwong-Soave Volumes.", *Fluid Phase Equilibria*, vol. 8, pp. 7-23, 1982.

Peng, D. Y., and Robinson, D. B., "A New Two-Constant Equation of State.", *Ind. Eng. Chem. Fund.*, vol. 15, pp. 59-64, 1976.

Peng, D.Y., and Robinson, D.B., “A New Two-Constant Equation of State”, Ind. Eng. Chem. Fundam., Ed. 15, (1976).

Peng, D.Y., and Robinson, D.B., “The Characterization of Heptanes and Heavier Fractions”, Research Report 28, Gas Producers Association, Tulsa, Oklahoma, (1978).

Quinones-Cisneros, S. E., Andersen, S. I., and Creek, J., "Density and Viscosity Modeling and Characterization of Heavy Oils.", *Energy and Fuels*, vol. 19, pp. 1314-1318, 2005.

Quinones-Cisneros, S. E., Zeberg-Mikkelsen, C. K., and Stenby, E. H., "One Parameter Friction Theory Model for Viscosity.", *Fluid Phase Equilibria*, vol. 178, pp. 1-16., 2001.

Rafael, A., Aguilar, Z., William, D., McCain, Jr, “An Efficient Tuning Strategy to Calibrate Cubic EOS for Compositional Simulation”, SPE paper 77382 presented at SPE Annual Technical Conference and Exhibition held in San Antonio, Texas 29 September-2 October, (2002).

Rao, D.N., “A New Vanishing Interfacial Technique for Miscibility Determination”, Elsevier, Fluid Phase Equilibria, June (1997).

Rao, D.N., and Ayirala, S.C., “Development of Gas Assisted Gravity Drainage (GAGD) for Improved Oil Recovery”, SPE paper 89357-MS, presented at SPE/DOE Improved Oil Recovery Symposium at Tulsa, Oklahoma, April 17-21 (2004).

Rao, D.N., and Lee, J.I., “Evaluation of Minimum Miscibility Pressure and Composition for Terra Nova Offshore Project Using the New Vanishing Interfacial Tension Technique”, SPE paper 59338, presented at SPE/DOE Improved Oil Recovery Symposium at Tulsa, Oklahoma, 3-5 April (2000).

Raut, B.D.: “Evaluation of Compositional Viscosity Models for Medium-Heavy Oils”, MS Thesis, University of Alaska Fairbanks, 2007.

Redlich, O. and Kwong, J.N.S., “On Thermodynamics of Solutions V. An Equation of State .Fugacities of Gaseous Solution,” *Chem. Rev*., 44, 233 (1949).

Reid, R. C., Prausnitz, J. M., and Poling, B. E., The Properties of Gases and Liquids., 4th Ed., McGraw-Hill, Inc., 1987.

Riazi, M. R., "*Characterization and Properties of* Petroleum Fractions.", ASTM Manual Series: MNL50, pp. 368, 2005.

Riazi, M. R., and Al-Otaibi, G. N., "Estimation of Viscosity of Petroleum Fractions.", *Fuel*, vol. 80, pp. 27-32, 2001.

Riazi, M. R., Mahdi, K., and Alqallf, M., "A Generalized Correlation for Viscosity of Hydrocarbons based on Corresponding States Principles and Molar Refraction.", *Journal of Chemical and Engineering Data*, vol. 50, pp. 1-5, 2005.

Riazi, M.R. & Daubert, T.E. (1980). Simplify Property Predictions. *Hydrocarbon Processing* , 115-116.

Rønningsen, H. P., "Prediction of Viscosity and Surface Tension of North Sea Petroleum Fluids by using the Average Molecular Weight.", *Energy & Fuels*, vol. 7(5), pp. 565-573, 1993.

Roper, M. ,“An experimental study of CO2 /West-Sak-crude-oil phase behavior”. M.S. Thesis, University of Alaska Fairbanks 1989.

Sahni, A., Gadelle, F., Kumar, M., Tomutsa, and L.,Kovscek, A., "Experiments and Analysis of Heavy Oil Solution Gas Drive", *SPE Reservoir Evaluation & Engineering*, pp 217-229, June (2004).

Satik, C., Robertson, C., Kalpacki, B., Gupta, D. , "A Study of Heavy Oil Solution Gas Drive for Hamaca Field”: Depletion Studies and Interpretations", SPE paper 86967 presented at the SPE International Thermal Operations and Heavy Oil Symposium and Western Regional Meeting, Bakersfield, CA, 16-18, March (2004).

Sequeira, D.S., and Rao, D.N., “Reservoir Condition Measurements of Compositional Effects on Gas-Oil Interfacial Tension and Miscibility”, SPE paper 113333, presented SPE/DOE Improved Oil Recovery Symposium at Tulsa, Oklahoma, April 19-23 (2008).

Sharma, A.K. (1988). A Slim-Tube Study of Solvents For The Miscible Displacement of West Sak Crude. *M.S. Thesis, University of Alaska Fairbanks* . Fairbanks.

Sharma, A.K., Patil, S.L., Kamath, V.A., Sharma, G.D. (1989). Miscible Displacement of Heavy West Sak Crude by SOlvents in Slim Tube. *Presented at the California Regional Meeting, SPE 18761.* Bakersfield, California.

Sharma, G.D. (1990). *Development of Effective Gas Solvents Including Carbon Dioxide For The Improved Recovery of West Sak Oil.* Fairbanks: University of Alaska Fairbanks.

Sharma, G.D. (1993). *Charaterization of Oil and Gas Heterogeneity.* Research Proposal, Fairbanks: University of Alaska Fairbanks.

Sharma, G.D., Kamath, V.A, Godbole, S.P., Patil, S.L. (1988). The Potential of Natural Gas in the Alaskan Arctic. *Presented at the California Regional Meeting, SPE 17456.* Long Beach, California.

Soave, G., "Equilibrium Constants from Modified Redich Kwong Equation of State", *Chem. Eng. Sci*., 27, No 6, 1197(1972).

Speight, J. G. (1991). The Chemistry and Technology of Petroleum. New YorK: Marcel Dekker, Inc.

Stalkup Jr., F.I., "Miscible Displacement", Henry L. Doherty Series, SPE Monograph 1983.

Standing, M.B., and Katz, D.L., "Density of Natural Gases.", *Transactions of the American Institute of Mining and Metallurgical Engineers*, vol. 146, pp. 140-149, 1942.

Targac, G.W, Redman, R.S., Davis, E.R, Rennie, S.B., McKeever, S.O, Chambers, B.C., "Unlocking the Value in West Sak Heavy oil", SPE paper 97856, presented at SPE International Thermal Operations and Heavy Oil Symposium, Calgary, Canada,1-3 November (2005).

Ted, W.J., Kissel, G., (Wendy) Zhou, S., "PVT and Viscosity Measurements for Lloydminster-Aberfeldy and Cold Lake Blended Oil Systems" SPE paper 79018 presented at SPE International Thermal Operations and Heavy Oil Symposium and International Horizontal Well Technology Conference, Calgary, Alberta, Canada, 4-7 November (2002).

Teja, A. S., and Rice, P., "Generalized Corresponding States Method for the Viscosities of Liquid Mixtures.", *Ind. Eng. Chem. Fund.*, vol. 20, pp. 77-81, 1981.

Twu, C. H., "An Internally Consistent Correlation for Predicting the Critical Properties and Molecular Weights of Petroleum and Coal-tar Liquids.", *Fluid Phase Equilibria*, vol. 16(2), pp. 137-150, 1984.

Twu, C., Tilton, B., Bluck, D. (2007.). *The Strengths and Limitations of Equation of State Models and Mixing Rules.* Retrieved August 2007, from SmiSci-Esscor, Simulation Software for Plant Design and Optimization: <http://www.simsci-esscor.com/NR/rdonlyres/3A5E699D-3EEB-4B43-A04C-3F1922585FFA/0/31099.pdf>

Van der Waals, J.D., "Continuity of the Gaseous and Liquid State of Matter" (1873).

Walther, C., "The Evaluation of Viscosity Data.", *Erdöl und Teer*, vol. 7, pp. 382-384, 1931.

Wang, P. and Pope, G. (2001). Proper Use of Equations of State for Compositional Reservoir Simulation. *Journal of Petroleum Technology* , Vol. 53, No. 7, pp. 74-81.

Werner, A., Behar, F., de Hemptinne, J. C., and Behar, E., "Viscosity and Phase Behavior of Petroleum Fluids with High Asphaltene Contents.", *Fluid Phase Equilibria*, vol. 147, pp. 343-356, 1998.

Whitson, C. H. and Torp, S. B., "Evaluating Constant Volume Depletion Data", *Journal of Petroleum Technology*, pp 610-620, March, (1983).

Whitson, C.H. (1983). Characterizing Hydrocarbon Plus Fractions. *SPEJ*, Vol. 23, No. 4, pp. 683-694.

WinProp User's Guide, Computer Modeling Group Ltd., 2005.

Xu, D. H., and Khurana, A. K., "A Simple and Efficient Approach for Improving the Prediction of Reservoir Fluid Viscosity." *SPE 37011*, 1996.

Yang, D., and Gu, Y., "Visualization of Interfacial Tension of Crude Oil-CO2 Systems under Reservoir Conditions", SPE paper 89366, presented at SPE/DOE Improved Oil Recovery Symposium at Tulsa, Oklahoma, April 17-21 (2004).

Yellig, W.F., and Metcalfe, R.S., "Determination and Prediction of CO2 Minimum Miscibility Pressures", J.P. Tech., June (1980).

Zick, A.A., "A Combined Condensing/Vaporizing Mechanism in the Displacement of Oil by Enriched Gases", SPE paper 15493-MS, presented at the 1986 SPE Annual Technical Conference and Exhibition, New Orleans, October 5-8 (1986).

Zuo, J. Y., and Zhang, D., "Plus Fraction Characterization and PVT Data Regression for Reservoir Fluids near Critical Conditions." *SPE 64520*, 2000.

Chapter 11 NOMENCLATURE

Notation	*Description*	*Commonly Employed Units*
Symbols		
a, b	Andrade equation constants	-
A, B, C	Dandekar model parameters	-
a_1 *to* a_5	LBC model parameters	-
b_1, b_2	ASTM equation constants	-
m	Coefficient of the pressure differential for the linear and/or exponential viscosity-pressure relationship	$psia^{-1}$
K	Response factor for thermo gas chromatograph	
MW	Molecular weight	lb_m/lb_{mole}
N	Number of data points	-
P	Pressure	psia, psig
T	Temperature	^oF, ^oR
V	Volume	ft^3
w	Weight factor	-
x	Array of elements	-
z	Mole fraction	-
Greek Symbols		
α	Pedersen model parameter	-
α, β, γ	Xu-Khurana model parameters	-
δ	Binary interaction parameter	-
μ	Viscosity	cP
ξ	Critical viscosity parameter	1/cP
ρ	Density	lb_m/ft^3
Subscripts		
b	Bubble point condition	
c	Critical condition	
d	Dead oil	
i, j	Component i and j	
mix	Mixture property	
n	Number-averaged	
o	Reference condition	
r	Reduced conditions	
w	Weight-averaged	

Glossary of Abbreviations

AAD	Average Absolute Deviation
ANS	Alaska North Slope
API	American Petroleum Institute
ASTM	American Society for Testing and Materials
BIP	Binary Interaction Parameters
CCE	Constant Composition Expansion
CMG	Computer Modeling Group Ltd.
DL	Differential Liberation
EOR	Enhanced Oil Recovery
EOS	Equation-of-State
LBC	Lohrenz-Bray-Clark
MF	Multiplying Factor
MW	Molecular Weight
OOIP	Original Oil In Place
PR	Peng-Robinson EOS
PVT	Pressure-Volume-Temperature
ROV	Relative Oil Volume
SPE	Society of Petroleum Engineers
STB	Stock Tank Barrel
UAF	University of Alaska Fairbanks

National Energy Technology Laboratory

626 Cochrans Mill Road
P.O. Box 10940
Pittsburgh, PA 15236-0940

3610 Collins Ferry Road
P.O. Box 880
Morgantown, WV 26507-0880

One West Third Street, Suite 1400
Tulsa, OK 74103-3519

1450 Queen Avenue SW
Albany, OR 97321-2198

539 Duckering Bldg./UAF Campus
P.O. Box 750172
Fairbanks, AK 99775-0172

Visit the NETL website at:
www.netl.doe.gov

Customer Service:
1-800-553-7681